Development of a human cell-based prosthesis for the repair of spinal cord injury in humans

Henry Pegram

A thesis submitted in partial fulfilment of the requirements of Nottingham Trent University for the degree of Doctor of Philosophy

This research programme was carried out in collaboration with the STFC Rutherford Appleton Laboratory, Didcot, UK

June 2019

1 Contents

2 Tables and Figures

3 Abstract

Spinal cord injury (SCI) is a devastating condition that results in a usually permanent disability. Mainstream treatments are limited to stabilisation and debris clearance, followed by early rehabilitation (Chen, Y. et al. 2013). This project investigated bio-functional aligned nanofibre scaffolds as components for personalised prostheses for SCI neural pathway repair, using an in-vitro lesion model of SCI supporting the 3Rs framework. The goal was to design an appropriate nanofibre prosthesis and establish scaffold optimisation parameters for incorporation of neural cell populations. Having a fully characterised prosthesis design, SCI patient's repair could be personalised according to the necessary requirements using lamination of engineered scaffold layers. This investigation built evidence to achieve:

1. Testing of a spectrum of prosthesis designs, engineered to maximise potential neuronal migration and elongation into and within a scaffold.
2. Advances in in-vitro SCI modelling in the form of a fibre-based SCI lesion which may be used as a platform for testing a wide spectrum of treatment materials and conditions.

In this investigation, scaffold parameters were optimised to neuronal (SH-SY5Y) and glial (U87-MG) cells representing human neural cell populations. Evidence suggested that PAN best supported neuronal populations and PAN-Jeffamine® best supported glial populations in terms of long-term viability and neuronal axonal length over a period of differentiation. A multi-layered design hosting neural cell populations on discrete layers, suggested that indirect co-culture improved axon length and long-term viability, as much as direct co-culture. To limit inter-layer migration (but maintain the beneficial effects of indirect co-culture), a porous barrier was introduced between these layers. Welded nanofibre showed promise in maintaining long term cell viability and maximising neuronal axon length. To encourage neuronal migration (from the injury sight) into a supportive structure, a collagen gel incorporating cryo-fractured nanofibre interface showed promise in promoting neuronal migration whilst limiting glial migration. This approach could 'plug' the ends of any developed prosthesis and mediate entry of neurones into the structure. A nanofibre-based model was also developed using the same principles developed in prosthesis development which showed multiple hallmarks of SCI.

Evidence obtained allowed development of a potential prosthesis structure, constructed of repeating units of nanofibre suited to neuronal recovery and resident supportive cells, separated by physical barriers. In the future, in place of resident supportive clonal astroglial U87-MG cells, the investigation aims to integrate human Mesenchymal Stem cells (MSC's) and Olfactory Ensheathing Cells (OEC's) as feeder cellularised layers. A diagrammatic summary of the proposed prosthesis is shown in figure 1.

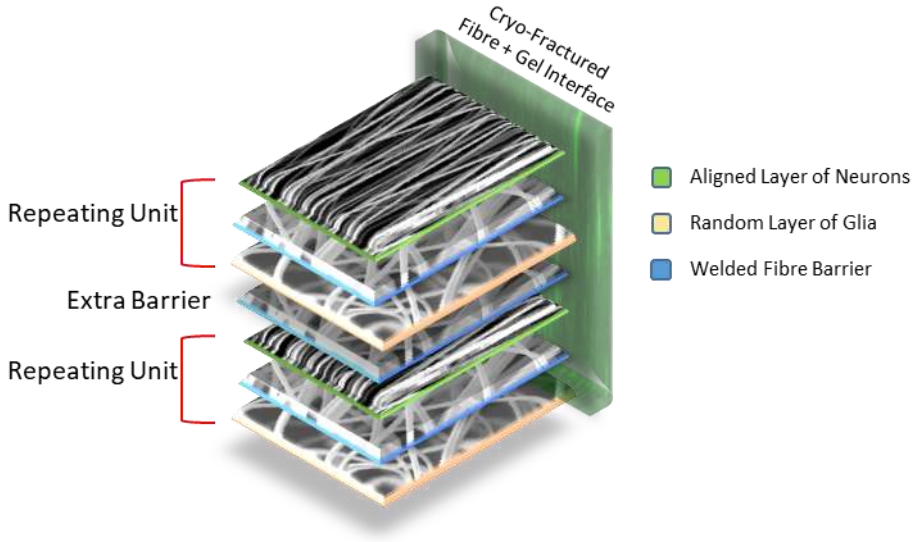

Figure 1: Diagrammatic summary of the proposed prosthesis design based on evidence generated in this investigation.

4 Introduction

4.1 The Spinal Cord

Spinal cord injury in humans is a complex subject and thus an initial understanding as to the nature of spinal cord anatomy had to be established. Both tissue and finer cellular structure were considered in this section as both would play a role in the design of the desired prosthesis.

The spinal cord is a delicate part of the central nervous system (CNS) running from the brain stem down the back to the first lumbar vertebra (Adigun, Varacallo 2018, Silva et al. 2014). It is protected by the vertebral column and is covered by three membranes of the CNS; dura mater, arachnoid and pia mater (Silva et al. 2014) as shown below in figure 2. The central canal consists of cerebral spinal fluid (CSF) which is thought to play a role in protection (shock absorption), delivery of nutrients and removal of waste to the spinal tissue (Huff, Varacallo 2018). The spinal cord is split into four main regions; cervical, thoracic, lumbar and sacral, on either side of which are the anterior lateral and posterior lateral fissures which the dorsal and ventral roots emerge from to form spinal nerves (Adigun, Varacallo 2018). There are thirty one spinal nerves; eight cervical - responsible for glands and muscles in the upper body and receive sensory input, twelve thoracic nerves – innervating the abdominal wall and chest, five lumbar – innervating the legs and hips, five sacral nerves – feeding the lower digestive tract and genitals, and one coccygeal nerve – running to the skin over the coccyx (Silva et al. 2014).

Figure 2: Depiction of the various layers of the spinal cord (Dafny 2000). The dura, arachnoid and pia mater surround the spinal cord.

4.1.1 Neurones

The key cellular population resident in the spinal cord is made up of neurones. These vary in shape and size and are classified based on morphology and function (Nógrádi, Vrbová 2000). Neurones may either be unipolar (harbouring a single process), bipolar (having one axon and one dendrite) or multipolar (having one axon and two or more dendrites) (Nógrádi, Vrbová 2000). Multipolar neurones are either type I Golgi neurones and have long axons, transmitting signals over long distances into the white matter, or they are Type II Golgi neurones which are much shorter and do not extend beyond the grey matter (Abdel-Maguid, Bowsher 1984). Type I Golgi neuronal cells include Pyramidal cells, Anterior Horn cells and Purkinje cells for example (Caddy, Herrup 1991, Safronov et al. 2000). Type II Golgi neuronal cell include granule cells for example (Dafny 2000).

4.1.2 Spinal Structure

The spinal cord is split into grey matter and white matter, the latter of which surrounds the grey matter (Silva et al. 2014). White matter consists of highly myelinated neurones which insulate and conduct electrical signals (Fields 2008). There is a relatively high proportion of myelinated neurones and low proportion of cell bodies. Made up of the dorsolateral, dorsal, ventral, ventrolateral and lateral funiculi, the spinal cord incorporates those neurones that translate signals up and down the spinal cord (Chung, Coggeshall 1983, Fields 2008, Walhovd et al. 2014).

The white matter can be split into the lateral column, dorsal column and ventral columns. It largely consists of highly myelinated neurones which conduct signals via ascending and descending tracts (Dafny 2000). Descending tracts are only found in the ventral and lateral columns, and transmit signals associated with motor activities – muscle tone, balance, posture, voluntary movement and reflex activity. Ascending tracts are found in all the white matter columns and communicate sensory information from the sensory receptors to the CNS (Dafny 2000). Three nerve fibre types can be identified in the white matter; long ascending nerve fibres originating from the column cells, long descending nerve fibres originating from the cerebral cortex entering the grey matter, and shorter nerve fibres interconnecting at numerous levels of the spinal cord which are involved in reflex coordination (Dafny 2000). Figure 3 presents the ascending and descending tracts and the components that make up each (Dafny 2000). Some regions of note in the ascending tracts include; lateral and anterior spinothalamic tracts – these carry temperature, touch and pain information, and the ventral and dorsal cerebellar tracts – which carry unconscious information from the lower extremities (Dafny 2000). Within the descending tracts, the Lissauers tract regulates incoming pain signals, and the reticulospinal, vestibulospinal and anterior corticospinal tracts mediate posture and

balance movements (Dafny 2000). The diagram below summarises the white matter anatomy and mentioned regions.

Figure 3: Ascending (top) and Descending (bottom) tracts of the spinal cord white matter *(Dafny 2000).*

Table 1 below summarises the roles that the major white matter tracts (ascending and descending) carry out in transmitting sensory and motor signals up and down the spinal cord. When considering the recovery of SCI, the corticospinal tract was highlighted as a major target for repair on account of it's role in voluntary movement mediation, though in repairing one tract it was considered likely that others may be effected too.

Table 1: Summary of white matter tracts and their roles in signal transmission in humans (Kenhub 2019).

The grey matter is roughly butterfly shaped and is made up of layers of neurones of various type. Grey matter neurones are distinguished from those of the white matter as they consist of relatively few myelinated axons and numerous cell bodies (Nógrádi, Vrbová 2000). This region mediates the flow of signals into and out of the spinal cord via the dorsal and ventral roots. Specifically, the grey matter is split into the intermediate grey, ventral horn, the centromedial region and the dorsal horn. From the dorsal horn and dorsolateral white matter, dorsal roots exit the spinal cord and converge into two bundles. From there they enter the dorsal root ganglion. In the dorsal root ganglion, the dorsal and ventral roots form a trunk and form the spinal nerves which may go onto the peripheral nervous system (Nógrádi, Vrbová 2000). In short, the dorsal root transmits sensory information and the ventral root carries motor information as shown in the figure 4.

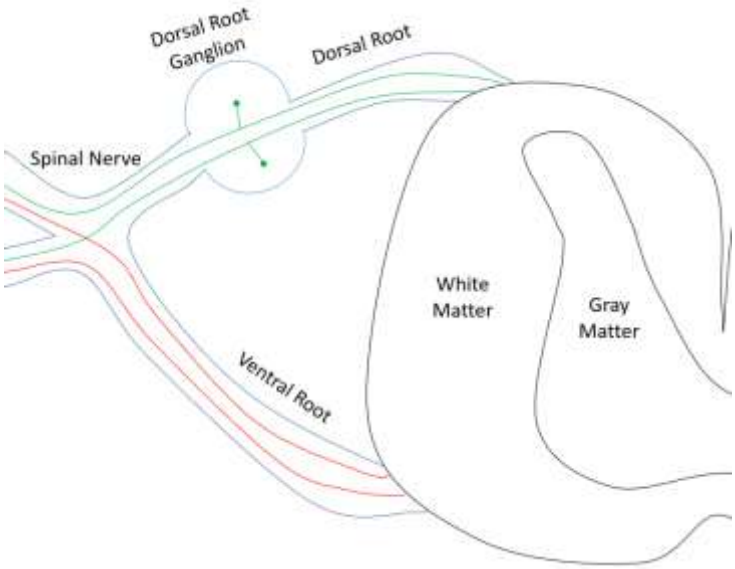

Figure 4: Diagrammatic description of the dorsal and ventral roots exiting the spinal cord.

The grey matter structure is described as laminar in that neurones are arranged in 9 layers (Todd, Spike 1993) as shown in figure 5. Within these layers, a variety of type I and II Golgi neuronal cell types can be found. The dorsal-most lamina is lamina I, this covers the dorsal horn tip. The neuronal density is low with a loosely packed neuropil and includes neurones of various sizes (Nógrádi, Vrbová 2000, Lima, Coimbra 1986). The Waldeyer cell makes up most of the neurones in this layer (Puskar et al. 2001). Lamina II has a comparably high neuronal density consisting largely of small fusiform neurones (type II Golgi Neurones); the two main types are islet and stalked cells (Nógrádi, Vrbová 2000, Todd, Lewis 1986). There is a prevalence of interneurones in lamina II and lamina III. Lamina III has a lower neuronal density once more and consists largely of intermediate sized (still largely type II Golgi Neurones) antenna-like and radial neurones (Todd, Spike 1993). Lamina IV is the thickest of the first four lamina and consists also of antenna-like and transverse cells, spreading towards the lamina II and III layers (Nógrádi, Vrbová 2000, Ralston 1982). Lamina V consists of a variety of neuronal (some Golgi Type I and II) types (and some evident interneurones) with extensions in lamina II, it is thick and thus split into medial and lateral zones (Ralston 1982). Neurones are largely fusiform and triangular in the medial section and multi-polar in the lateral zone. Lamina VI is developed mostly in the cervical and lumbar regions, it is also composed of a medial and lateral zone with a similar composition to lamina V (Ralston 1982, Nógrádi, Vrbová 2000). Lamina VII occupies much of the intermediate zone for the grey matter, consisting of a homogenous population of multipolar neurones (Nógrádi, Vrbová 2000). Lamina VIII has a dorsoventral extension unlike the previous seven and consists largely of multipolar neurones and some motor neurones (Szucs et al. 2003, Nógrádi, Vrbová 2000). Lamina IX is unique in that it consists of motoneurones which exist largely within the peripheral nervous system (Nógrádi, Vrbová 2000). Interneurones within the spinal cord are worth a

mention given their importance in relaying signals from the sensory to the motor neuronal systems (Puskar et al. 2001, Jankowska 2001). The grey matter can also be split into the marginal zone, substantia gelatinosa, nucleus proprious, dorsal nucleus of clarke, intermediolateral nucleus, lateral motor neurones and medial motor neurones as shown in the diagram below (Dafny 2000, Abdel-Maguid, Bowsher 1985).

Figure 5: Schematic of the Lamina arrangement in the spinal cord grey matter (Dafny 2000).

Figure 6 below presents how the white and grey matter fit together, and how the ratio of distribution varies down the spinal cord. The grey matter contribution at each level is dependent upon the tissue requirements at the given level. The ventral and dorsal horns supply different muscle types; the ventral horn for example consists of cell bodies responsible for supplying skeletal muscle, and the dorsal horns receive sensory information from this muscle (Purves et al. 2001). In the lumbar region, the ventral horns are relatively large as the requirement for supplying skeletal muscle is greater (Purves et al. 2001). The lateral horns contain cell bodies of neurones controlling cardiac and smooth muscle (Purves et al. 2001). Typically, further down the spinal cord, the white matter contribution is lower as there is less requirement for transmission of signals (sensory input and motor output) (Dafny 2000). The diagram also depicts how signals may flow between the grey matter and ventral/dorsal horns.

Figure 6: Diagrammatic representation of spinal cord structure. a. Depiction of the changing ratio of grey to white matter depending on the location down the spinal cord. b. Schematic diagram of the major structures of the spinal cord and how signals may be communicated through it (Ali, Dublin 2018).

4.1.3 Neuroglia

In addition to neurones, the other major cell group present in the spinal cord is neuroglia; these are made up of astrocytes, oligodendrocytes, ependyma and microglia. Glia as a population outnumber neurones five to one (Sofroniew, Vinters 2010). Astrocytes exist as protoplasmic astrocytes in the grey matter and fibrous astrocytes in the white matter (Vasile et al. 2017). Protoplasmic astrocytes consist of many finely branching extensions that form a globoid arrangement. They enwrap blood vessels to form the glial limiting membrane, which in turn forms the outermost wall of the blood brain barrier (BBB) (Tabata 2015). They are also known to modulate synaptic function (Tabata 2015). By comparison, the fibrous astrocytes have longer fibrous extensions and express comparatively higher levels of glial fibrillary acidic protein (Sofroniew, Vinters 2010). They are thought also to interact with vasculature to help form the BBB (Tabata 2015). In the mature CNS, astrocytes help to provide a structural scaffolding for the neuronal residents and help to establish perivascular cuffs in the formation of the blood brain barrier (Gray, Patel 1992). Otherwise, these cells act as transporters, carrying fluid and ions from the extracellular space into vessels. It is thought that these cells release neurotrophic factors to aid in axonal health and growth, potentially NGF (nerve growth factor – mostly in peripheral tissues), bFGF (basic fibroblast growth factor) ciliary neurotrophic factor (CNTF) and s100B (particularly for serotonergic neurones), GDNF (glia cell line-derived neurotrophic factor), BDNF (brain derived neurotrophic factor), NT-3 (neurotrophin-3) (Hansebout et al. 2012). Evidence of GDNF aiding in the recovery of neuronal outgrowth post SCI has been captured (Zhang, L. et al. 2009). NT-3 is homologous to BDNF and has been shown to enhance axonal regrowth after a dorsal root crush (Hanna-Mitchell et al. 2008). Research in this area is ongoing, so it is likely in this investigation that functional effects of astrocytic co-culture will be examined.

Glial precursors differentiate into astrocytes and oligodendrocytes. Oligodendrocyte progenitors (OPCs) are also a source of these cells, largely in the developing brain (seen in rat models) (Tabata 2015). Oligodendrocytes are amongst the most vulnerable cell types in the spinal cord because of the long and complex differentiation pathway they must endure to become functional (Bradl, Lassmann 2010). Oligodendrocytes eventually form large myelin sheaths as extensions of their cell membrane. These cells myelinate neuronal axons (typically axons over 0.2µm in diameter) - each can myelinate an average of 30 axons each. Oligodendrocyte precursors are present in the adult CNS and can remyelinate and regenerate mature oligodendrocytes. As the white matter requires myelination in the insulation of signal transfer, these cells reside largely there (Bradl, Lassmann 2010). Astrocytes have been shown to regulate oligodendrocyte behaviour in the white matter (Li, J. et al. 2016).

Microglia are unique residential macrophages of the CNS (Lannes et al. 2017). Their functions include phagocytosis of developing neurones, monitoring synapses and even phagocytosis of synapses during normal synaptic development (Wake, Fields 2011). The cells play an important role in maintenance of the BBB and fight infectious agents in the CNS (Lannes et al. 2017, da Fonseca et al. 2014). In response to stress or aging, these cells have the capacity to release reactive oxygen species and inflammatory cytokines (Wake, Fields 2011). Overall, they contribute to the structure and function of the nerve tissue (Lannes et al. 2017, Salter, Beggs 2014). In response to injury they have been shown to become activated and try to enclose the damage, followed by cleaning away debris and forming non-functional scar tissue in an effort to repair damaged tissue (Lannes et al. 2017, Loane, Kumar 2016).

In summary, the spinal cord has a complex physiological structure. Re-creating this tissue is complex, though a level of simplicity can be added when developing a treatment. Depending on the location of the injury, damage to the white matter is what effects the transmission of signals up and down the spinal cord. Encouraging regeneration of this slightly more plastic, linear tissue could potentially be done with a scaffold with alignment cues – such as aligned nanofibre. To begin assessing the validity of this hypothesis, the nature of spinal cord injury must first be understood.

4.2 Spinal Cord Injury

Spinal Cord Injury (SCI) is characterised by a damage to the spinal cord resulting in complete or incomplete cutting of neuronal signal communication through the spinal region. SCI occurs at an estimated incidence of 250,000-500,000 SCIs annually across the globe. Up to 90% of these injuries are traumatic with road traffic accidents and falls forming the bulk of incidences as displayed in figure 7 (WHO 2019).

Figure 7: Diagrammatic representation as to the proportionate contribution of certain SCI causes (WHO 2019).

4.2.1 Forms of Spinal Injury

Primary spinal cord injury refers to the physical injury that occurs to the neural tissue which is categorised as transection, compression, laceration, contraction or contusion (Ju et al. 2014). Injuries can be complete or incomplete depending on the maintenance of sensory and motor functions at the distal level of injury (Nas et al. 2015). A contusion is caused by the crushing of the cord (Bradbury et al. 2002). By comparison, a transection injury is caused by the cutting of the cord, for example by a knife stab wound. Severity of the injury depends upon how much of the tissue is spared and the physiological state of surviving tissue/nerve fibres (Ju et al. 2014). By comparison, a transection injury, caused for example by a knife stab wound will vary in severity depending on how much of the tissue is spared.

4.2.2 Pathology

Pathology is often severe and may be split into primary (mechanical) and secondary (biological) mechanisms (Webb et al. 2010). Primary damage occurs immediately (within the first two hours) and involves initial impact damage, widespread cellular death, haemorrhaging and oedema (Varma et al. 2013). The grey matter is subjected to most of the haemorrhaging given its vascularity (Rowland et al. 2008). The vast majority of SCI does not involve complete cord transection (Bunge et al. 1993). The severity of this primary injury is linked to the force of the initial damage, the longer term sustained cord compression if present, cord displacement and energy absorbed in the impact (Stokes 1992).

Secondary damage occurs subsequently and can be split into acute, sub-acute, intermediate and chronic phases based on the time post injury. The (early) acute phase occurs within the first forty-eight hours post injury and alongside the primary mechanical damage. This phase includes breaking of the blood-brain barrier, cellular death, neurotransmitter accumulation (for example glutamate and aspartate) and further

influx of inflammatory cells (Varma et al. 2013). Excitatory neurotransmitters have been described as pivotal mediators of both neuronal and glial cell death, for example by activating the N-methyl-D-aspartate (NMDA) receptor (Choi, Rothman 1990). Specifically, the rupture of blood vessels (largely in the grey matter) can lead to leakage and influx of immune mediators such as neutrophils, which in addition to resident microglia can be activated and begin to apoptose resident neuronal and oligodendrocyte populations (Ding et al. 2005). There is a release of reactive oxygen species (ROS), axon and myelin degradation, and systemic events such as shock, hypotension and hypoxia (Rowland et al. 2008). The disruption of the autoregulation of blood flow to the spinal cord as a result of systemic vascular problems leads to the spinal cord being perfused by residual arterial pressure - this exaggerates the ischaemic environment (Kobrine et al. 1975).

The sub-acute phase follows this period within the first fourteen days and encompasses further biological damage, including myelin destruction, free radical release and the onset of inflammation (Ahuja et al. 2017). The influx of macrophages leads to prolonged apoptosis of neuronal and glial cells, with oligodendrocytes particularly at risk. The BBB repair begins to occur, and oedema is localised (Kobrine et al. 1975). It is during this phase that the astroglial scar begins to form as a result of reactive astrogliosis. Calcium-activated neural proteases (calpains) are responsible for the degradation of the cytoskeleton and mediation of necrotic cell death (Chan, Mattson 1999). These are formed in repose to calcium influx and oxidative stress within the injury. The free radical release within the injury can be damaging in axonal conduction failure, spinal cord hypoperfusion and energy metabolism breakdown (Hall, Braughler 1993).

The intermediate phase is a description of the first 6 months post injury before the chronic phase takes effect (Rowland et al. 2008). During this phase, the glial scar continues to form as a result of astrogliosis and the fluid-filled cyst begins to take shape. The lesion is stabilised by the natural healing process and in doing so potential neuronal recovery is limited.

The chronic phase occurs after 6 months and continues over years. Most crucially this phase involves the astroglial cell mediated scar formation (Yuan, He 2013). The fluid-filled cyst will become fully formed in response to injury, harbouring mostly excess cerebral spinal fluid (Rene Hudson et al. 2008). There is persistence of function in spared axons, and potential plasticity in these cells (Fehlings et al. 2012).

Table 2 summarises the key events that occur during the primary and secondary events of a spinal cord injury in addition to the recommended therapeutic aims at each time point (Fehlings et al. 2012, Rowland et al. 2008).

TABLE 2

Table 2: Table summarising the events that take place in primary and secondary SCI (Rowland et al. 2008).

The location and neural tissue that remains in the chronic injury will determine the prognosis for the given patient (Varma et al. 2013). Figure 8 summarises the worsening symptoms as the injury site progresses up the spinal cord towards the cervical region in addition to a schematic of SCI (McDonald 1999).

Figure 8: a. Diagram presenting the prognosis resulting from spinal injury and damage to the spinal cord (McDonald 1999). b. Diagrammatic summary of the acute-chronic onset of SCI (McDonald 1999).

Damage can be split further into grey and white matter pathologies. White matter-based axons can grow to over a metre in length (Vogelaar 2016). Damage to these highly myelinated white matter 'tracts' can be devastating as communication is lost between the brain and that level of the periphery. However crucially, cell body incidence is relatively low compared to that in the grey matter and if the cell bodies still survive an injury and remain healthy, they are capable of re-growing and slowly repairing their axonal extensions (Vogelaar 2016). Functional recovery is also possible in the white matter where information may be communicated through an alternative, surviving route – or by creating a new route with a scaffold.

The grey matter neuronal population has greater metabolism and blood-flow requirements (greatest in the thoracolumbar region) largely owing to the high density of cell bodies (Losey, Anthony 2014). Following injury, these vessels can bleed and become leaky, leaving the grey matter particularly susceptible to hypoxia and cell death. It is for this reason that in a lot of cases, spinal cord injury is focussed on the inside of the cord. The vascularity of the grey matter means that in addition to the blood-based elements that escape from broken vessels, immune mediator recruitment may occur quickly (Safronov et al. 2000). As a result, macrophages may become present in addition to resident activated microglia to further add to the apoptotic death of resident oligodendrocytes and other cells (Ding et al. 2005).

Notably, neuronal survival (particularly in the grey matter) is linked to the connections they make. It must be considered that the grey and white matters are connected and thus death in neighbouring neurones can cause a cascade of death in connected neurones. However, it became clear from the basic SCI pathology that a therapeutic scaffold would be best suited to repairing the slightly more plastic white matter regions where surviving axons are able to re-extend (with the help of the scaffold) over the damaged regions of the cord (Zorner et al. 2014). It was for this reason also that it was decided that no resident neuronal population would be externally introduced into the cord, only supportive cells to aid this recovery of existing neurones.

4.2.3 Glial Scar Formation

One of the key hallmarks of SCI and indeed one of the most devastating symptoms is the formation of the astroglial scar as described in figure 9. Here, astrocytes become 'activated', hypertrophic and change molecular expression (Toy, Namgung 2013). One such change is the up-regulation of Glial Fibrillary Acidic Protein (GFAP) in resident astrocytes, leading to the formation of a dense web of misaligned plasma extensions (Yuan, He 2013). GFAP is an intermediate filament protein that mediates synthesis of increased cytoskeletal structures and extends pseudopodia (Yang, Z., Wang 2015). Proliferation of astrocytes in response to injury in combination with upregulated ECM protein release (laminin, fibronectin and proteoglycans (eg, chondroitin sulfate proteoglycans)) and noted plasma extension misalignment leads to the formation of a scar that cannot be penetrated by neurones (Wiese et al. 2012). It should be noted that proliferation of astrocytes in a healthy system is at a relatively low level, with reports that proliferation in

response to injury often only occurs if the injury is severe (Sofroniew, Vinters 2010). Chondroitin Sulfate Proteoglycans inhibit axonal regeneration and neurogenesis (Yuan, He 2013). The net product of this natural response to injury is limited axonal recovery through the injury site – this scarring becomes more developed with time and so early rehabilitation is encouraged.

Figure 9: Graphical description of reactive gliosis and formation of the glial scar (In Vivo 2019).

4.2.4 Functional Recovery

Surprisingly, around 40% of patients (and animal models) will see some form of functional recovery following spinal cord injury, despite the axonal growth-inhibitory molecules at the lesion site (Ding et al. 2005). This is a testament to the potential plasticity of the CNS and spinal cord in particular in altering the strength of existing connections and establishing new connections (Ding et al. 2005). This plasticity is present throughout the nervous system as depicted in figure 10 (Ding et al. 2005).

Figure 10: Depiction of the plasticity that can occur throughout the nervous system and in particular in the spinal cord (Wall et al. 2002).

As shown in the diagram, the spinal cord shows notable potential for regeneration through structural, functional and molecular changes. Given the right treatment to facilitate this recovery (a scaffold for example), it is hypothesised that this plasticity can be boosted. It should be noted however that though functional regeneration is possible, it is still limited and the prognosis following a spinal cord injury is usually severe.

4.3 Therapeutic Strategies for Spinal Cord Injury

Mainstream SCI treatments currently provided by the NHS in the UK and recreated globally involves following several basic steps. In the short term; the injury is immobilized as fast as possible, there is surgical intervention if needed in order to stabilise and reduce neuronal compression as well as removing bone fragments if necessary, corticosteroids are administered to combat inflammation and then physiotherapy and rehabilitation is given in an effort to optimise function of remaining muscle (Burns et al. 2017, Ushiku et al. 2017, Evaniew, Dvorak 2016). Treatments are focussed primarily on stabilisation and minimising further damage as opposed to direct functional repair (Nas et al. 2015).

Treatment for SCI is being widely researched across the globe. Broadly, research can be categorised into pharmacotherapy, biological, technological and physical treatments. Some of these are described below. Literature review suggested that the most promising functional recovery from a treatment targeting boosting of existing neuronal populations was in those that see motor supraspinal fibre recovery in the

corticospinal tract in the descending tract of the white matter (Kenhub 2019). These are derived from the brainstem nuclei and regulate locomotion (Bradbury et al. 2002).

Treatments of SCI are targeting both primary and secondary injuries, largely addressing the cascading mechanism that occurs after primary injury that leads into this secondary injury. Specifically, groups are developing means of treating free radical damage, neuro-inflammation, blood flow, excitotoxic damage, free Ca^{2+} levels, myelin degradation, proteolytic activity, axon degradation, myelin vesiculation and scar tissue formation (Varma et al. 2013).

4.3.1 Pharmacotherapy

Treating SCI pharmaceutically may entail an array of approaches; introducing neuroprotection, reducing inflammation, breaking down the scar tissue or preventing it forming in the first place.

Methylprednisolone (MP) is the only pharmacotherapy approved for SCI, though the clinical effects have not shown to be significant. Intravenous delivery of this drug leads to numerous unwanted side effects such as immunosuppression and muscle catabolism (Varma et al. 2013, Miekisiak et al. 2019). The drug can be delivered instead using a localised nanofibre based delivery mechanism. The Chvatal et al. group encapsulated active MP in PLGA (poly(lactic-co-glycolic acid)) nanoparticles and delivered them locally to an adult rat spinal cord contusion. The nanoparticles were embedded in agarose hydrogel to allow localization at the injury site for 1 week – functional outcomes in rat models were reported as good, although the recovery with MP is somewhat limited even when delivered locally (Chvatal et al. 2008). Clinical trials have been carried out using MP, largely comparing dose response – high dose (1000mg IV bolus daily for ten days) versus standard dose (100mg IV bolus daily for ten days). In NASCIS I (National Acute Spinal Cord Injury Study I), the first randomized multi-center trial, no significant difference was seen after six weeks or six months (Bracken et al. 1992). Revisions to this national experiment showed that the dose was not high enough, not achieving the recommended dose per kg. Instead, in NASCIS II, 30mg/kg dose was given over the first hour, followed by an infusion of 5.4mg/kg/hour for the next twenty-three hours. In this study, patients had better neurological function after six months than those who maintained the standard dose (Bracken et al. 1992). A final study (NASCIS III) compared efficacy of MP administered for twenty-four hours and forty-eight hours with Tirilazad mesylate (TM) (Bracken et al. 1992). Results showed that earlier treatment after three hours of injury showed equivalent functional recovery across all groups. But eight hours after injury, the 48-hour group did better (Coleman et al. 2000). In summary, MP or other corticosteroid options could form a supplementary feature of a treatment design, though functional repair even if provided early is still limited.

Oestrogen and associated analogues (e.g. 17β-oestradiol) has been shown to reduce oligodendrocyte apoptosis in rat models (Lee, J. Y. et al. 2012). Studies by other groups have shown oestrogen to provide

protection to microglial and neuronal populations (Samantaray et al. 2011) in addition to contributing to the attenuation of vascular endothelial growth factor (VEGF) and aquaporin up-regulation (Wang, Y. F. et al. 2011).

Melatonin has shown anti-inflammatory, free oxygen radical scavenging capabilities in SCI (Wu, U. I. et al. 2011, Bonnefont-Rousselot et al. 2011). It has also been associated with intracellular Ca^{2+} influx attenuation and cysteine protease activation (Ray et al. 2011) in rat models.

Certain factors identified in myelin such as Nogo, myelin-associated glycoprotein (MAG), oligodendrocyte-myelin glycoprotein (OMGP), semaphorins, ephrins, netrins and repulsive guidance molecule (RGM) have been targeted in an effort to promote functional regeneration of axons in emerging but early-stage therapies (Borisoff et al. 2003, Yiu, He 2006). One such target is Rho-Kinase which has been shown to promote axonal outgrowth from dorsal root ganglia on aggrecan substrates (Borisoff et al. 2003).

The Bradbury et al group has experimented with the delivery of Chondroitinase ABC (ChABC) as a strategy to reduce Chondroitin Sulphate Proteoglycan (ChSP) molecules present within the astroglial scar in the chronic phase of SCI (Bradbury et al. 2002). These ChSPs are extracellular matrix proteins which have been shown in vitro to inhibit axonal elongation, and in vivo have been shown to stop axonal elongation where they are in high concentration (Davies et al. 1999). The group have achieved some functional recovery in adult rat crush injury models using electrophysical and behavioural tests, though noted that anatomical recovery was limited (Bradbury et al. 2002). This was perhaps because the enzyme treatment promoted recovery of surviving axons only. The same group has experimented with delivery of neurotrophins as a direct treatment of the SCI conditions (Bradbury et al. 1999). Specifically, the group looked at BDNF and NT-3 for their neuroprotective qualities, finding that NT-3 reversed atrophy, likely reaching the cell bodies themselves of surviving axons (Bradbury et al. 1999).

This concept has also been analysed by other groups such as Jones et al. This group recognised the potentially chemotropic qualities of neurotrophic factor administration in influencing axonal regeneration across a lesion site (Jones et al. 2001). The group targeted neuronal growth factor (NGF) for example and showed axonal recruitment from a peripheral nerve graft into the white matter dorsal column in rat models (Oudega, Hagg 1996). The group furthered this work by genetically modifying fibroblasts to secrete NGF in a graft inserted directly into an acute injury in rat models. Though axons from coerulospinal and ventral motor axons were detected, axons did not then exit the graft and so functional recovery was limited (Oudega, Hagg 1996). A parallel experiment in which BDNF was delivered to the lesion site showed some axonal recovery. However, genetically modifying fibroblasts to secrete BDNF showed significant growth of motor axon, dorsal root sensory axons and supraspinal coerulospinal axons once more, suggesting localised high dose BDNF could be useful (Oudega, Hagg 1996).

One of the major issues associated with treating SCI chemically is in maintaining the appropriate concentration of active ingredients of the drug in question (Vawda et al. 2012, Sharma 2008). Nanoparticles provide one potential solution for the delivery of said treatments, they can; reduce concentration-related toxicity, enhance drug delivery to target and increase duration of exposure (Torchilin 2000). One such example is poly (butyl cyanoacrylate) (PBCA) in combination with polysorbate-80 which has been shown to penetrate the BBB and shows little toxicity in delivering NGF in mouse models (Kreuter et al. 2003, Kurakhmaeva et al. 2009).

Nimodipine is a calcium channel blocker and have been shown to enhance blood flow to an injured spinal cord in a lab setting (Fehlings et al. 1989). In a double blinded study, no significant difference was seen in treatment with this or just with MP other than an increased incidence of infections once more (Varma et al. 2013).

G-acyclidine is a N-methyl-D-aspartate (NMDA) antagonist which has been shown to target secondary SCI pathology in rat models by blocking glutamate-induced Ca^{2+} influx (Gaviria et al. 2000). Unfortunately, one year after the trial took place, there was no clinical benefit shown from using the compound in acute SCI even within two hours of injury (Varma et al. 2013).

Thyrotropin releasing hormone (TRH) regulates the pituitary-thyroid axis (part of the neuroendocrine system which regulates metabolism) as well as playing a role in numerous neurological processes (Monga et al. 2008). Some potential was shown in patients with incomplete injury treated with TRH after 4 months, though none was seen in patients with complete injury, and no follow up study was thus planned (Varma et al. 2013).

GM1 Gangliosides are membrane-bound lipids which are typically found in high concentration in the CNS (Ledeen 1978) and have been shown to encourage neuronal sprouting and regeneration following CNS trauma in animal trials (Cuello et al. 1986). Two studies carried out years apart suggested conflicting results and ultimately it was shown that though promising, GM-1 therapy did not adequately show improved neurological recovery in human patients (Chinnock, Roberts 2005).

One potent inhibitor of axonal regeneration is the myelin associated protein Nogo-A (Gonzenbach, Schwab 2008). Phase I human trials have been conducted testing anti-Nogo IgG antibodies which target this myelin associated protein (Zorner, Schwab 2010). The drugs were administered intrathecally to patients within four to fourteen days of injury with no obvious adverse effects – the efficacy of the trial indicated that at one year, some electrophysiological tests indicated promising outcomes which could lead to further trials (https://clinicaltrials.gov/ct2/show/NCT00406016).

Acidic Fibroblast growth factor (aFGF) is a well-known cell signalling protein which has been tested in humans in Taiwan (Wu, J. C. et al. 2011). In all cases, injuries were greater than 10 weeks old. The aFGF

was applied in combination with fibrin glue and then re-administered via lumbar puncture 3- and 6-months post-surgery. Significant improvement has been seen in patients using ASIA motor, sensory and impairment scores (Varma et al. 2013).

Cethrin is a recombinant engineered variant of C3 transferase which targets Rho - a GTPase involved in cell signalling and which has been shown to promote neuronal, oligodendroglial and astrocytic apoptosis as well as inhibiting neuronal regeneration (Dubreuil et al. 2003). Cethrin blocks signalling from myelin debris at the injury site. A clinical trial involving Cethrin was carried out in which the drug was administered extradurally over a range of 5 doses (0.3mg-9mg) and tracked over a year. Results showed no serious adverse effects and an improvement in 6% of thoracic and 66% of cervical patients – more trials are being planned to continue testing (Varma et al. 2013).

Certain groups including the Pritchard et al group are developing electrospun nanofibre technology as a delivery system for bioactive compounds (Pritchard, E. M., Kaplan 2011). Hydrogels are a major field of study with which applications are numerous and SCI is no exception. The Donoghue et al group is working on developing a hydrogel system that slowly releases NT-3 neurotrophic factors among other compounds directly into the lesion (Elliott Donaghue et al. 2016).

4.3.2 Biological

Treating SCI with biological remediation may entail a spectrum of different cell types and techniques to target the injury site damaged state or to directly repair it. Each cell type offers certain merits and drawbacks in the context of SCI treatment.

Following SCI, a local immune response is activated, which can lead to widespread neuronal death. Using rat models, one group introduced autologous macrophages to the injury site having incubated them with autologous skin (Bomstein et al. 2003). It was shown that incubation with skin leads macrophages to build a tolerance to neuronal populations and increase release of IL-1β, BDNF expression and reduces release of TNFα (tumour necrosis factor) – the result is an environment that is supportive of axonal regeneration. In humans, the treatment was trialled in patients fourteen days post injury caudal to the injury site. No adverse effects were seen and just less than half showed notable improvement on the ASIA impairment scale (Bomstein et al. 2003).

One group used multiple intercostal nerve grafts aimed at redirecting pathways from the white matter proximal to the grey matter. This led to corticospinal tract regeneration – which is associated with locomotive function (Cheng et al. 1996). This was carried out in rat models and showed the power of peripheral nerve grafting.

Another group made use of human foetal spinal cord tissue in rat model SCI models (Giovanini et al. 1997). In their study, significant neurite outgrowth and survival of the graft was shown in both acute and chronic lesions (Carlson, Gorden 2002). Functional recovery was shown to be evident in said rat models, though on account of the ethical issues surrounding foetal tissue, most groups made use of stem-cell based alternatives, such as embryonic stem cells (Carlson, Gorden 2002).

Embryonic stem cells (ESCs) are obtained from human preimplantation embryos and are not without their ethical issues given their origin, however, they have tremendous differentiation potential (Semb 2005). Transplantation of embryonic stem cell-derived precursors indicated efficient neuronal myelination in one group's study in rat models (Brustle et al. 1999). In another, the group transplanted ESCs into rat SCI 9 days post injury and showed differentiation into astrocytes, oligodendrocytes and neurones – indicating the differentiation power of these cells (McDonald et al. 1999). One limitation of this cell type is the teratoma risk associated with a long differentiation pathway (Zhang, W. Y. et al. 2008).

Neural stem cells are multipotent, self-renewing cells that can differentiate into both neuronal and glial cells. They are formed during embryonic development and reside in the ventricular zone, and some have suggested that they continue to be generated in the adult brain in restricted regions such as the adult subventricular zone and the dentate gyrus of the hippocampus (Curtis et al. 2018, Paspala et al. 2011). The Curtis et al group carried out a human trial using neural stem cells (NSCs) on chronic spinal cord injuries using microinjections. In 50% of the subjects, neurological improvement was seen (1 or 2 levels using the ISNCSCI motor and sensory scores). Though data was encouraging and showed little adverse effects, a larger population was required (n=4) in addition to a control group (Curtis et al. 2018).

In 2006, the Yamanaka et al group first reprogrammed mouse embryonic fibroblasts into ES-like cells. Around one year later, in collaboration with the Thomson et al, the Yamanaka et al group reprogrammed human somatic cells into these induced pluripotent stem cells (iPS cells) using four factors (oct4, Sox2, Klf2 and c-Myc) in a lentiviral vector (Zhao et al. 2013, Khazaei et al. 2017). It is now possible to generate iPS cells from a variety of mature cells like blood and skin, making them attractive options for research as they can be autologous and easily obtained with few ethical issues. One of the limitations of using iPS cells is the potentially lengthy reprogramming process – particularly when treating SCI (Khazaei et al. 2017). Skin fibroblasts are a commonly used source, though the process is lengthy in reprogramming these cells. Other options include cord blood cells, adipose tissue derived stem cells, CD34+ cells and melanocytes (Khazaei et al. 2017).

Figure 11 presents some of the SCI treatment targets available when using iPS cells.

Figure 11: Diagrammatic demonstration of the treatment options when using iPS cells as SCI treatment (Khazaei et al. 2017).

Several protocols have been developed to generate NSCs from iPSCs. This presents a potentially fruitful source of SCI treatment cells given NSC's ability to remyelinate axons as glia, replace neurones and provide trophic support (Tsuji et al. 2010). In 2016, the Tuszynski et al group generated NSCs from iPSCs and showed enhanced corticospinal tract regeneration compared to NSCs derived from normal sources (Kadoya et al. 2016). The Fuhrmann et al group made use of iPS cells in combination with hydrogels to deliver pluripotent stem cell-derived neuroepithelial cells in rat models (Fuhrmann et al. 2016). The group showed that using chondroitinase ABC alongside, they were able to maintain a high progenitor cell population and also noted neurones, astrocytes and oligodendrocytes (Fuhrmann et al. 2016).

Mesenchymal stem cells (MSCs) are multipotent stromal cells derived from the bone marrow (potentially autologous) which have the ability to mature into fat, cartilage and bone cells naturally (Varma et al. 2013). Another interesting finding was that in an immature state, these cells can elute bioactive compounds which can form an environment encouraging of neuronal regeneration in an injury site (Caplan 2007). In one human trial, these cells were obtained from patients own bone marrow and introduced systemically via intra-venous or intra-arterial routes between ten and four hundred and seventy six days post injury (Sykova et al. 2006). Results were encouraging in arterially introduced cells when introduced within thirty days of injury. No adverse reactions were seen in any patients. Another human study delivered the cells directly though microinjection into the spinal cord (Deda et al. 2008). Significant improvement was seen in all patients, which was particularly encouraging given that all patients were at least six months post-injury. The encouraging results prompted a study by Kumar et al in which two hundred and ninety seven patients

were administered MSCs though lumbar puncture, all at least seven days post injury (Kumar et al. 2009). In one third of patients, neurological improvement was seen, prompting further studies.

MSCs have also been combined with scaffolds which act as delivery systems for this cell type. One such contribution was the combination of a PLGA scaffold with immature MSCs, which in rat models was shown to encourage the natural neuronal repair within a SCI (Ropper et al. 2017). In fact, the group showed that scaffold-based MSCs performed better than those introduced without structural support, largely as those cells-maintained survival, stemness and function over a longer period (Ropper et al. 2017).

Within the olfactory mucosa, one group of sensory neurones are replaced throughout life. These replaced neuronal axons re-enter the CNS (Varma et al. 2013). The re-entry of said olfactory axons into the olfactory bulb is mediated by a macroglial population called olfactory ensheathing cells. It is possible to obtain a part of the olfactory mucosa, which includes some progenitor cells and it will regenerate (Huard et al. 1998). Olfactory ensheathing cells have been seen to bridge damaged myelin tract of the spinal cord and mediate the extension of axons across lesions in rat models (Li, Y. et al. 1998). The Raisman/Tabakow group in UCL (one of our collaborators) have begun human trials in which they are introducing olfactory ensheathing cells into SCI lesions by microinjection, they have shown promising results with one patient regaining significant locomotive ability (Tabakow et al. 2013).

Figure 12: image of the successfully treated patient 2 years post-op during rehabilitation – photo given by Li et al group from UCL.

The Xu et al group used PAN/PVC polymer tubes loaded with Schwann cells (peripheral myelinating cells) to show recruitment of (around 25% myelinated) axons across a rat thoracic spinal cord injury gap (Xu, X. M. et al. 1995). This bridge-like structure showed the capacity for axonal recovery in vivo if the 'bridge' is engineered properly with effective resident support cells (Xu, X. M. et al. 1995). Functional recovery was

shown to be boosted in PAN/PVC constructed by adding corticosteroids at the lesion edges to minimize loss of neural tissue (Chen, A. et al. 1996).

4.3.3 Technological

Alongside cellular treatments, technological answers to the SCI problem are also being developed. Here, technology and biology are being interfaced to bridge broken neural connections. One such example is the Capogrosso et al group who artificially stimulated locomotion first in rats and then in Macaca mulatta monkeys (Capogrosso et al. 2016, Wilcox et al. 2017, Wenger et al. 2014). In rats, the group implanted an epidural electrical stimulation device in the lumbar spinal cord to replicate a complex sequence of individual muscle activation patterns (Capogrosso et al. 2016). Though results were encouraging; rats were making 1000 successive steps without failure and even navigating staircases, the technology is currently more limited than it may seem. The electrical stimulation parameters are tuned manually, and they remained constant during movement – this meant that during stimulation, the movement was repetitive. The scope of potential for this technology however is great and therefore the same group were given permission to carry out a primate study. In this study, the group developed an intracortical microelectrode array in the leg area of the motor cortex and a spatially selective epidural implant. Following thoracic unilateral corticospinal lesioning, the brain-spinal interface was activated and showed restoration of weight-bearing locomotion on a treadmill (Capogrosso et al. 2016). Muscle activation patterns were basic but stimulated from motor cortex activity. This investigation demonstrated the potential that this study has and the group seeks to work towards human trials in the future. Figure 13 summarises how the primate study functioned.

Figure 13: Summary of the brain-spinal technological interface manufactured for a primate study (Capogrosso et al. 2016).

4.3.4 Physical

4.3.4.1 Hydrogels

Hydrogels provide a dynamic treatment option for a variety of pathologies. Their properties can be changed depending on requirement and purpose (Perale, Rossi et al. 2011). Essentially, their chemical, physical and mechanical properties are designed such that they define the cellular microenvironment of the cell types in question (Yu, L., Ding 2008). These 3D structures are held together by covalent bonds or other cohesive forces (Khazaei et al. 2017). These hydrogels can be natural or synthetic in their construction. A synthetic gel could be polyacrylamide, polyethylene glycol or polyethylene oxide as examples (Khazaei et al. 2017). Synthetic polymers offer more versatility and dynamicity in the design and formulation of their properties (Perale, Rossi et al. 2011). Natural gels such as collagen, hyaluronic acid or polysaccharides like agarose or cellulose are derived from molecules present in living tissues (Perale, Rossi et al. 2011). Natural polymers offer certain advantages for example in the provision of a biocompatible, enzymatically degradable material that can act as a physical bridge or means of controlled drug delivery (Perale, Rossi et al. 2011). It is also possible to combine synthetic and natural polymers into composites in order to combine the biocompatibility properties of the natural polymers with the mechanical and physical tuning capabilities of

synthetic ones, by adding poly-L-lysine to PEG channels for example (Wang, C. Y. et al. 2011, Perale, Giordano et al. 2011).

In practice, hydrogels can serve to carry cells in a matrix form, protect a delivered cellular population from a cytotoxic environment for example in a SCI lesion, act as a support in the regeneration of resident host cells or even carry insoluble drugs within the gel network, delivering them at a controlled rate over time (Mallett, Korbutt 2009). The gel can be engineered to degrade over time or remain present as required (Perale, Rossi et al. 2011).

Some examples of their versatility include the use of alginate gels in supporting linear axonal regeneration in rat models (Stokols et al. 2006). This group showed integration of gels into spinal structure and even pre-loaded the gels with genetically modified bone marrow stromal cells which secreted BDNF. This significantly enhanced axonal penetration. Another group loaded chondroitinase ABC (ChABC) into a trehalose gel (Lee, H. et al. 2010). The group showed that ChABC rapidly loses its activity at 37 degrees centigrade and so embedding it in a trehalose gel prolonged its activity and reduced the requirement for repeated injections. The gel was engineered such that it was combined with lipid microtubes and was also combined with NT-3, showing sustained local delivery of both compounds. The NT-3 delivery was shown to enhance axonal growth, sprouting and functional recovery in rat models with T-10 hemisection injuries (Lee, H. et al. 2010). Interestingly, multiple groups chose to use gels to target controlled axonal elongation and deliver supportive factors such as ChABC, corticosteroids or BDNF (Chvatal et al. 2008, Park et al. 2010).

4.3.4.2 Electrospinning

Electrospinning is a relatively simple technique dating back to 1934 (Chew et al. 2006, Valizadeh, Mussa Farkhani 2014, Garg, Bowlin 2011). The process allows creation of nano-scale fibre, the dimensions of which can be manufactured to requirement (Chew et al. 2006). Over the years its applications have been focussed largely on filtration and it was not until the 1980s that cell culture was originally experimented with (Valizadeh, Mussa Farkhani 2014, Vasita, Katti 2006). Specifically, in 1988 that Eric M. Simon began seeding nanofibre with a variety of cell types (human foreskin fibroblasts, turkey embryo fibroblasts, Mink Lung Epithelia and HEP-2 cells) (Ifkovits et al. 2009). There is an abundance of variations in electrospinning techniques, including coaxial, emulsion and melt electrospinning – useful when embedding compounds in polymers (McClellan, Landis 2016). In its simplest form, electrospinning works by passing high voltage (typically at least 5kV, though not always) through a polymer as it is fed through a 'spinneret' or syringe. As the repulsive forces, caused by charging the fluid of interest exceed its surface tension, it erupts as a jet. Initially, this is stable, though as the solvent evaporates, it becomes unstable (bending instability stage) and stretches. The material is directed towards a grounded collector (Teo, Ramakrishna 2006). Figure 14 below summarises this process.

Figure 14: Typical electrospinning set-up in it's simplest form (Teo, Ramakrishna 2006).

In order to create aligned nanofibre – which groups have shown has an influence on cellular proliferation and growth direction (Xu, C. Y. et al. 2004) – some groups utilised a high speed rotating drum technique (Matthews et al. 2002). This group suggested that rotating the collector at speeds of 4500 rpm allowed significant alignment to be formed. Another group made use of parallel electrodes as collectors, the distance between which could be varied according to requirements (Teo, Ramakrishna 2006). The Bhattarai et al group took both concepts and combined them by creating a rotating drum system with parallel wire extensions running along it either horizontally or vertically, creating aligned nanofibre at slower speeds (Teo, Ramakrishna 2006, Bhattarai et al. 2004). One group (Teo et al) used negatively charged knife edge blades beneath the rotating collector in order to create this aligned fibre (Teo, Ramakrishna 2006). More recently, one group proposed using a moving belt to collect long lengths of aligned fibre in an aligned fashion as shown in figure 15 below (Teo et al. 2011, Zheng et al. 2015). Finally, one group used a disk collector to create aligned nanofibre in which a disk is rotated vertically at high speed without the need of large drum – though issues arise with fibre alignment in thicker deposition volumes (Xu, C. Y. et al. 2004). Mass production of fibre can be generated with multiple spinnerets if the interference between jets can be avoided (Kidoaki et al. 2005).

Figure 15: Belt nanofibre deposition as used developed by the Rafique et al group (Teo et al. 2011).

Many groups are using biodegradable electrospun nanofibre as either physical bridges or as methods for controlled drug delivery. Groups focussing on physically bridging the gap include for example the Chen et al group (Chen, B. K. et al. 2011), who are using PLGA (poly lactic co-glycolic acid), PCLF (poly ε-caprolactone fumarate) and OPF (oligo polyethylene glycol) fibres and even incorporating hydrogels in rat models. By comparison groups such as the Chew et al group have focussed on delivering GDNF with aligned nanofibre (made of caprolactone and ethyl ethylene phosphate) with some success in rat models (Chew et al. 2007). Some are blending synthetic nanofibre with natural materials, for example gelatin, such as the Alverez-Perez group who combined poly ε-caprolactone enhanced with gelatin and compared neurite outgrowth in vitro to PCL scaffolds (Alvarez-Perez et al. 2010). Other groups are modifying nanofibre structures with ECM proteins and other bio-functional compounds such as Laminin – the Cheng et al group for example have doped their chitosan scaffolds with laminin, showing improved behavioural results in rat models (Cheng et al. 2007).

4.3.4.3 3D printing

Three-dimensional printing is a growing research discipline in the context of spinal cord injury treatment and surgery (Wilcox et al. 2017). This additive layer manufacturing technique allows the printing of a multitude of materials, from plastics, metallic powders, rubber, glass, sand, carbon fibres and organic materials, even cells (Dodziuk 2016). The technique is advantageous in its enablement of construction of complex geometries with porosities and other physical properties engineered to purpose (Jammalamadaka, Tappa 2018). Once again, both natural and synthetic materials can be chosen with which to print, with natural polymers offering biocompatibility, but synthetic offering engineerable faculties (Jammalamadaka, Tappa 2018). Stereolithography, continuous projection printing, bioprinting, fused deposition modelling, electron beam melting, polyjet, extrusion-based and inkjet-based methods are commonly used to create either acellular scaffolds containing biological components, or to print cellular tissue (Deng et al. 2017, Jammalamadaka, Tappa 2018). It is possible to use patient data (CT/MRI) to generate a 3D printable scaffold which has potential in SCI treatment.

This method of treating SCI is relatively novel, though one group recently used microscale continuous projection printing to print biomimetic polyethylene glycol-gelatin methacrylate hydrogel scaffolds loaded with neural progenitor cells to support axonal regeneration and boost functional recovery in rat models (Koffler et al. 2019). The group found that resident surviving neurones grew into the printed scaffold and synapsed with resident NPCs and that significant improvement in functional recovery was seen compared to controls (Koffler et al. 2019). Specifically, corticospinal recovery was noted. Interestingly, the 3D printed structure was designed such that activated astrocytes could not penetrate its walls.

4.4 The Problem

To date, there have been no well documented treatments for SCI in human beings (Ju et al. 2014). A few groups have experimented with varying success though the issues remain in the complexity of the 'messy' injuries and the natural scaring that occurs in response to injury. Figure 16 summarises several of the research themes described above in SCI treatment.

Figure 16: Diagrammatic representation of numerous potential physical, biological and chemical treatment methods for SCI (Pires, Pego 2015).

Overall, there are some promising research themes being developed, however in man success is limited, perhaps due to the approach to treatment. It is known that stem cells and other such biological treatments have shown success in other medical challenges, but this unique challenge requires an engineered solution that has been developed from the ground up, not one which seeks to blindly point and shoot. Interestingly, several groups are beginning to use multiple themes together, for example 3D printing hydrogels in combination with bioactive molecules of resident cells (Koffler et al. 2019). This project also aims to eventually fulfil several of the described roles in the figure above in a step-wise fashion. It is hypothesised that of the treatment options available, a simple aligned nanofibre treatment may provide both a physical and cellular solution. The fibre core can be built and optimised, introducing resident supportive populations and then perhaps hydrogel interfaces gradually. This gradual development is what is needed to ensure that white matter corticospinal tracts can be targeted.

4.5 This Project

A physical treatment may provide the structural stimuli needed for efficient long-term repair of SCI. Initially, a non-biodegradable, aligned, electrospun scaffold was designed and optimised to encourage neuronal migration into the structure. This concept was then developed to include a supportive cellular population as the literature recommends (Varma et al. 2013). The treatment was developed to include multiple stacked layers of nanofibre, each engineered to offer optimal conditions to the cell types of interest. In future work it will be wrapped in a semi-porous membrane to provide mechanical support and protect from cellular infiltration and will bypass the lesion as shown in one group who excluded activated astrocytes. The ends of this 'safe-haven' tunnel will be plugged with a gel interface capable of secreting high concentrations of neurotrophic factors, corticosteroids and anti-scar enzyme, but also selectively mediating neuronal migration only. (Koffler et al. 2019). It is hoped that it could be implanted at the time of injury during standard SCI stabilising surgery as described in section 3.6.3.

4.5.1 Electrospinning in this Project

Spinning aligned nanofibre is a more complex electrospinning process than random fibre manufacture, though achieving alignment is possible through numerous techniques, including parallel electrospinning, sharp edge electrospinning and using patterned electrodes (Beachley, Wen 2009, Yang, F. et al. 2005, Li, D. et al. 2005). Specifically, in this project, a rotating drum technique developed in-house (described below) was employed. This dynamic technique allowed manufacture of random, radially aligned and aligned fibre from a variety of both synthetic and natural polymers by changing the polyester sheet 'stencil' design wrapped around the rotating collector (Jahani et al. 2012). In this way, nanofibre provided a unique opportunity to manufacture a prosthesis bespoke to requirement (Vasita, Katti 2006). In this case, the fibre

diameter, material type, pore size and scaffold thickness were all optimised to create an aligned or random system in which cellular integration of cell types of interest could be optimised.

Broadly speaking, the technique chosen conforms with the basic electrospinning process described above. A high voltage is applied to the polymer of interest until as above, the fluid of interest erupts as a jet towards the grounded collector (Teo, Ramakrishna 2006). Wrapped around the grounded collector are two thin polyester sheets, cut to mediate aligned or random nanofibre manufacture. To manufacture random fibre, an array of simple circles are cut in both layered sheets. For aligned fibre, the bottom sheet consists of two parallel rectangles, and the top sheet the same with an elliptical region in between as shown in figure 17.

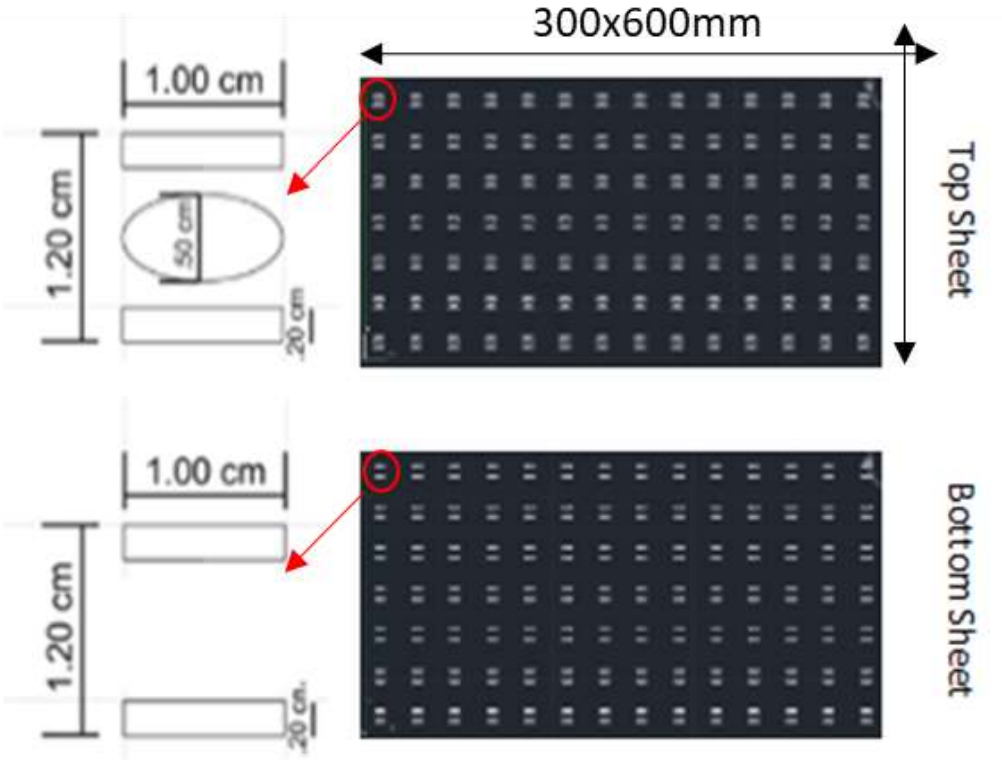

Figure 17: Apertures cut into polyester sheets for electrospinning aligned nanofibre.

The two sheets are ultra-sonically-welded together and nanofibre collected on the top sheet. Removal of the bottom sheet and addition of a second top sheet upon the original top sheet 'sandwiches' the fibre between the sheets and allows the fibre to be removed and handled. Though the process parameters for

rotating drum electrospinning will be described in detail later, figure 18 below summarises the rotating drum technique.

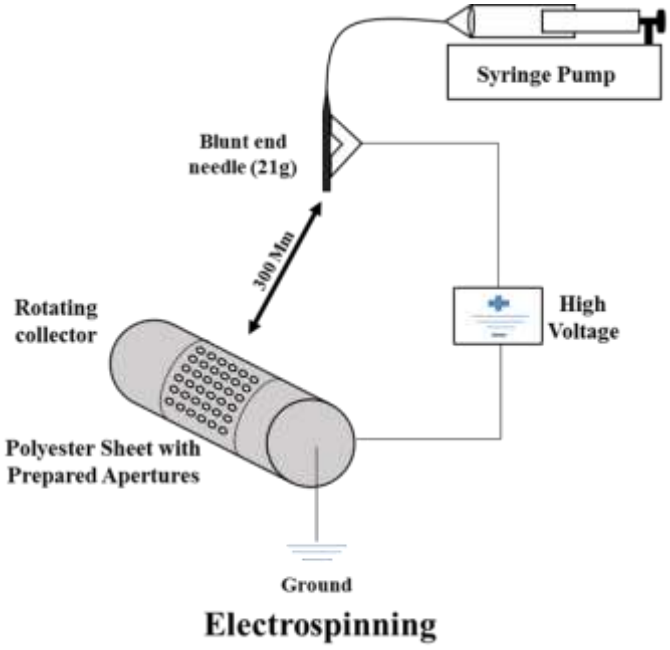

Figure 18: Electrospinning process described diagrammatically. Using a spinning drum technique, aligned and random nanofibre can be manufactured in sheets, composed of the polymer of choice. Diagram by Joseph Chemmarappally.

4.5.2 Cell Lines

The project sought to optimise the nanofibre system using clonal SH-SY5Y neuroblastoma and U-87 MG glioblastoma cells (Buira et al. 2010), representing human neuronal and human glial cell types, respectively. These cells offered an easily sourced, robust, in vitro culture option that possesses the capacity for large scale expansion prior to differentiation into more mature, neuron-like and glial-like cell types (Kovalevich, Langford 2013). The cells have been used in research into multiple disease states including spinal cord injury (Cai et al. 2017, Won et al. 2018), Parkinson's studies (Wang, F. et al. 2015) and Alzheimer's (Wang, H. et al. 2010).

SH-SY5Y cells are a subclone of the parent cell line SK-N-SH (Biedler et al. 1973), first deposited to ATCC in 1970 By JL Biedler (Biedler et al. 1978). Early studies indicated that this differentiated cell line contained two distinct phenotypes; epithelial and neuroblast-like cells (Ross et al. 1983). Removal of the un-wanted epithelial-like population is achieved through serum starvation (shown to induce apoptosis in epithelial cells (Allsopp et al. 2000)) and the use of retinoic-acid during differentiation (Shipley et al. 2017). Retinoic acid has been shown to activate tyrosine receptor kinase B (Trk) in neuronal cells, leading to neurotrophin-dependant cellular survival only (Encinas et al. 2000). The resultant homogenous population then begins to exhibit long processes, forming a network of neurites (Shipley et al. 2016). With retinoic acid treatment,

the cells are driven primarily towards a cholinergic phenotype (Lopes et al. 2010), with some evidence that cells can become dopaminergic also (Presgraves et al. 2004). SH-SY5Y cell culture has been investigated in combination with various aligned nanofibre materials, including Poly(lactic Acid) (PLLA) (Yu, Y. et al. 2016) and poly-ϵ-caprolacton (PCL) (Innala et al. 2014), showing that alignment can be created, in addition to enhanced viability and neurite outgrowth compared to 2D culture conditions (Innala et al. 2014). Using the documented differentiation procedure, mature SH-SY5Y cells were deemed an appropriate cell line to investigate neuronal interaction with a spinal cord injury prosthesis.

U-87 MG cells are (likely) of CNS glioblastoma origin with epithelial morphology (Allen et al. 2016), first deposited to ATCC in 1966 by J Ponten (Ponten, Macintyre 1968). When subject to retinoic acid treatment (Das et al. 2008), they have been evidenced to undergo differentiation towards an astrocytic phenotype (Karmakar et al. 2008), forming long extended processes (Mita et al. 2007). Astrocyte co-culture with neuronal cells in the white and grey matter is a natural phenomenon (Vasile et al. 2017). Using the described retinoic acid-based differentiation protocol, it was hoped that long astrocytic processes could be created, to recreate white matter fibrous-like astrocytes with which to co-culture with elongated neurons. Notably, it was accepted that these cells were of glioblastoma origin and so limitations would exist on this recreation. Astrocyte support has been shown to help mediate neuronal recovery in the white matter in rat models, thus introducing a resident astrocytic population in a designed prosthesis could potentially enhance performance of said prosthesis (Joosten, Gribnau 1989). As such, in combination with the SH-SY5Y cell line, this glial cell line was identified as a suitable candidate with which to investigate a prosthesis design. It was not considered essential to elongate glial U-87 MG cells, though some evidence has been shown in which some U-87 MG cell elongation (Agudelo-Garcia et al. 2011a) and migration is influenced by aligned PCL nanofibre structures (Jain et al. 2014). This suggested that nanofibre would influence the glial population too, so it was deemed reasonable to consider both aligned and randomly arranged nanofibre for this population.

The limitations of clonal cell lines were known. Notably, neuroblastoma SH-SY5Y and glioblastoma U-87 MG cells have cancerous properties which influence viability, differentiation fate and growth performance for example (Xicoy et al. 2017, Lenting et al. 2017). It was hoped however that using clonal cells, an optimal prosthesis design may be hypothesised for later primary cell and stem cell work. Cells were kept under 30 passages to ensure cellular phenotype was maintained.

4.5.3 Making the Treatment Mainstream

The project contributes to an overall goal of developing a multi-faceted strategy capable of treating a specific patient on multiple fronts, and which importantly fits within the current time frame and treatment

pathway utilised by the health service. This concept is crucial in developing a treatment that may be realistically adopted in the future. Currently, the framework presented below in figure 19 summarises how a physical treatment may be incorporated into existing pathways, but also includes an additional added pathway that may permit the addition of a supportive resident cellular population (like autologous MSCs for example). The chosen cellular populations (MSC's for example) could be harvested from the patient in question at the time of standard debris-clearance surgery. These cells could then be re-introduced once they had been purified and expanded into the inserted nanofibre system (labelled a 'safe-haven bridge' as it could be cellularly isolated from the damaged region).

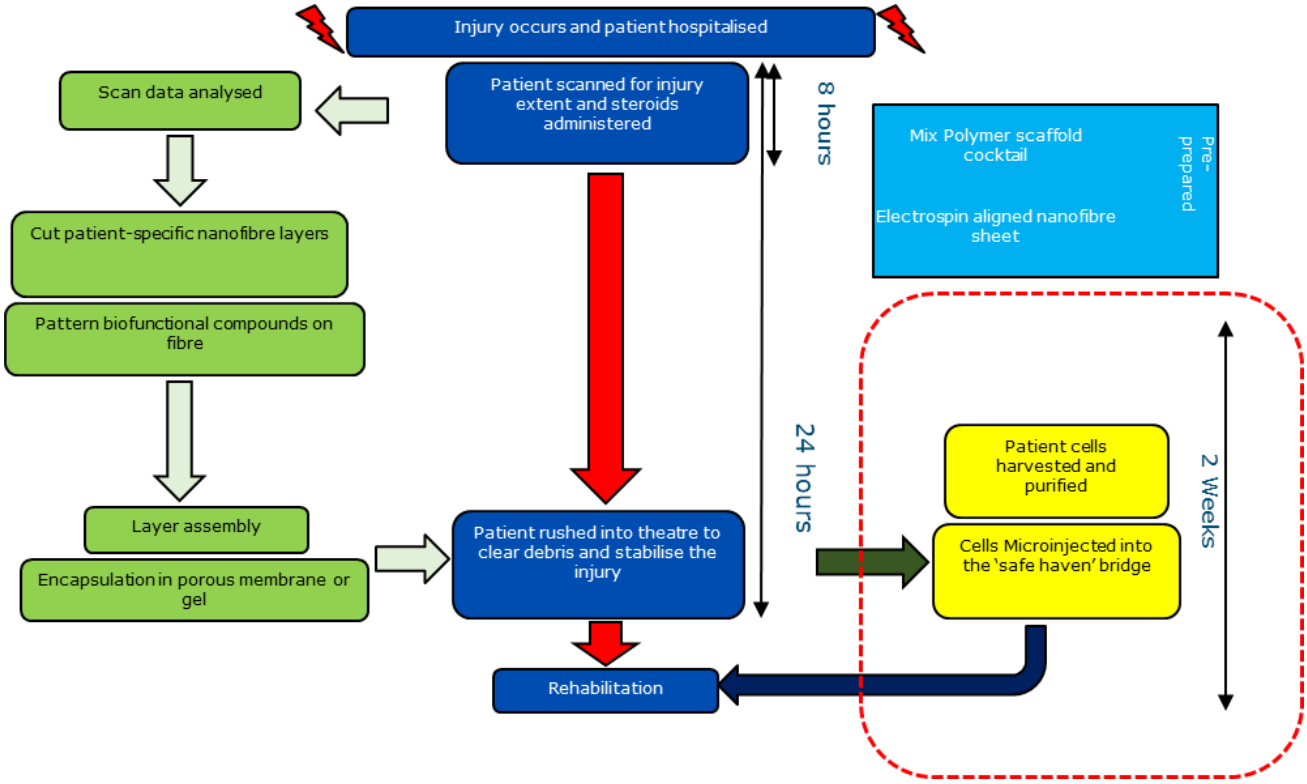

Figure 19: Flow diagram describing the standardised mainstream emergency care currently carried out for SCI in the UK and internationally (in dark blue). Surrounding this standard process is the suggested treatment process, using nanofibre based technology to introduce a more effective SCI treatment within the standard treatment time-frame.

Understanding how this prosthesis could fit into the current health system on a large scale is important to consider early in the research project. It was hoped that keeping this target a priority would allow the project to evolve in such a way that it could be adopted one day on a large scale – something that many research pathways could not be.

4.5.4 Modelling

As described, several treatments are being researched globally. As part of development, trials must first occur in vitro before any animal testing may be trialled (Weightman et al. 2014). Having a physiologically

relevant and robust model for SCI would be a useful tool in early stage development and would reduce the cost-time burden to development groups in academic and commercial settings (Pritchard, C. D. et al. 2010).

Though some basic neurite outgrowth modelling is carried out purely on 2D culture plastic (Kwon et al. 2002), the majority of spinal cord injury modelling is done in animals; they are split into contusion, compression, distraction, dislocation, transection or chemical models (Cheriyan et al. 2014, Vismara et al. 2017). Contusion involves usually dropping a weight or applying an electromagnetic force to push a metal ferrous object onto the spinal cord. Compression crushes the spinal cord with a given force. Distraction is a controlled stretching of the cord, dislocation is separation of the vertebrae and transection is a useful technique involving partial or complete surgical cutting and chemical makes use of a range of chemical interventions (Cheriyan et al. 2014). Rodents are the most commonly used animal models, though are not as relevant as non-human primates or large animals (Cheriyan et al. 2014). Though animals are useful tools, they are not human and therefore will always have some limitations physiologically and ethically. Similarly, some groups have made use of tissue slices and triggered injury in said slices before subsequently attempting to treat the injury with physical nanofibre, though these tissue slices had to be initially harvested from animals (Weightman et al. 2014). Others have used dissociated rat glia and overlaid spinal neurones on top with good results (Weightman et al. 2014, Vismara et al. 2017). The limitations seen in both cases is in the use of animals, and further the injury caused in dissection of animal tissue before the injury model is even carried out. Though there are limitations to using simple clonal cell lines, it would seem logical that using human cells and avoiding dissection in early stage studies would be beneficial before then carrying out a more minimised animal model-based investigation if necessary.

It is possible that this concept has certain commercial value, and this will be explored as part of this project. The nature of this project in the potentially large-scale production of nanofibre and optimisation to cell types of interest enables the project to be directed towards a commercialisation route if the opportunity did arise. Models are being developed in multiple disciplines, for example in 3D printing, though the scalability of these options is often limited. This project sought to address those issues.

To summarise, the study aims to build evidence to achieve:

1. Testing of a spectrum of prosthesis designs, engineered to maximise potential neuronal migration and elongation into and within a scaffold.
    a. Consider the use of a resident support population
    b. Consider an interface by which neuronal cells could selectively be navigated into the prosthesis
2. Advances in in-vitro SCI modelling in the form of a fibre-based SCI lesion which may be used as a platform for testing a wide spectrum of treatment materials and conditions.

a. Show certain hallmarks of SCI can be recreated in-vitro
b. Show the model can be treated

5 Materials and Methods

5.1 Materials

5.1.1 Cell Culture

Accutase, (A6964), Sigma-Aldrich, UK

DMEM Media 199 (10X), (11825-015), Fisher Scientific, UK

DMEM F-12 (1:1) mix with 15mM Hepes, L- Glutamine, (L2020-1MG), Lonza, UK

Foetal Bovine Serum, (11573397), Invitrogen Gibco

Hybridmax filter sterilised Dimethylsulfoxide (DMSO), (D2650), Sigma-Aldrich, UK

Laminin from mouse Engelbreth-Holm-Swarm (EHS), (11243217001), Sigma-Aldrich, UK

MEM non-essential amino acid solution, (M7145), Sigma-Aldrich, UK

Penicillin-Streptomycin, (DE17-603E), Lonza, UK

Phosphate Buffered Saline without Ca2+ and Mg2+, (BE17-516F), Lonza, UK

Sodium Pyruvate Solution 100 mM, (BE13-115E), Lonza, UK

Tris Buffered Saline (10x), (T5912-1L), Sigma-Aldrich, UK

Trypan blue solution (0.4% solution), (T8154), Sigma-Aldrich, UK

Trypsin-EDTA, (BE02-007E), Lonza, UK

5.1.2 Plastic, Glassware and Other Materials

Silanized 9" Pasteur pipette to an opening of ~0.5 mm, BrainBits, UK

10 ml syringe tube luer-lok tip, Becton and Dickindon, UK

15 ml and 50 ml red capped tubes, Sarstedt, UK

21-gauge tube grade 304 cut to length 100mm with back point one end, Stainless Tube and Needle Company, UK

3M 425 Conductive Aluminium Tape, (R06933), RS Components

6 well, 12well, 24well and 96 well sterile, adherent tissue culture microplates, Sarstedt, Leicester, UK

Cell culture flasks (T25, T75 and T175), Sarstedt, UK

Cell Scraper, Fisher Scientific, UK

Corona discharged Polyester Sheets 600mm X 300mm clear polyester 75microns thick, Nano Products, UK

Cryovials, Sarstedt, UK

Leit Adhesive Carbon Tabs 12mm, (AGG3347N), Agar Scientific, UK

Leit Adhesive Carbon Tabs 25mm, (AGG3348N), Agar Scientific, UK

Nalgene Syringe Filter (199-2020), Fisher Scientific, UK

Pipette filter tips (10 µl, 200 µl and 1000 µl), Dutscher Scientific, France

Polypropylene sterilin tubes, Sarstedt, UK

PTFE tubing 1/31 inch bore size, Altec, UK

RS Pro scalpel blade, Swann Morton, UK

SEM Specimen Stubs, 12.5mm dia, (AGG301), Agar Scientific, UK

SEM Specimen Stubs, 25mm dia, (AGG399), Agar Scientific, UK

SLS Coverslips No 0 15mm Dia, (MIC3278), Scientific laboratory supply, UK

Sterile serological pipettes, (5ml, 10ml and 25ml), Sarstedt, UK

5.1.3 Chemicals and reagents

3-(4,5-dimethylthiaol-2-yl)-2,5-diphenyltetrazoulium bromide (MTT), (M2128), Sigma-Aldrich, UK

Accugel 29:1 (40% solution) acrylamide, (A20068), GeneFlow Ltd UK

Acetone, natural ≥97%, (W332615), Sigma-Aldrich, UK

Acrylamide, (A9099-25G), Sigma-Aldrich, UK

Adenosine 5'-triphosphate, ATP, (A3377), Sigma-Aldrich, UK

Ammonium persulfate, (A3678), Sigma-Aldrich, UK

B27 Supplement 50X, (17504001), Fisher Scientific, UK

Bicinchoninic Acid (BCA) kit, (BCA1-1KT), Sigma-Aldrich, UK

Bovine serum albumin, (A2153), Sigma-Aldrich, UK

Cell Counting Slides for TC10™/TC20™ Cell Counter, Dual-Chamber, (1450015), BioRad, UK

CellTiter-Glo® 3D cell viability assay kit, (G9681), Promega, UK

Collagen I, Rat Tail, (A10483-01), Gibco, UK

CooBlue MAX protein gel stain, (R2034A), Interchim Ltd, UK

Copper phthalocyanine 3, 4', 4", 4" tetrasulphonic acid tetrasodium salt, (245356), Sigma-Aldrich, UK

Copper(II) Sulphate, (451657), Sigma-Aldrich, UK

DCDFDA Cellular ROS Detection Assay Kit, (ab113851), Abcam, UK

Dibutyryl-cAMP, (D0627), Sigma-Aldrich, UK

Dimethylformamide, (D1331), Fisher Scientific, UK

SC250 Solvent Cement, (14295), ScrewFix, UK

Fluocinolone Acetonide, (F8880), Sigma-Aldrich UK

Folin & Ciocalteu's phenol reagent, (F9252), Sigma-Aldrich, UK

Glycine, (410225-50G), Sigma-Aldrich, UK

Hexafluoro-2-propanol, (105228), Sigma-Aldrich, UK

InstantBlueTM protein stain, (ISB1L), Expedeon Ltd, UK

Jeffamine®® ED-2003 Polyetheramine M_w2000, Huntsman, USA

L-Buthionine-sulfoximine, (B2515), Sigma-Aldrich, UK

Marvel milk powder, Marvel, UK

Methanol, (34860), Sigma-Aldrich, UK

MG132 Proteasome Inhibitor, (M8699), Sigma-Aldrich, UK

NEAA 100x, (BE13-114E), Sigma-Aldrich, UK

Nitrocellulose 0.22 µm pore size, (WP2HY00010), Labtech Ltd, UK

Phalloidin conjugates with TRITC, (P2141), Sigma-Aldrich, UK

Polyacrylonitrile M_w150,000, (181315), Sigma-Aldrich, UK

Polycaprolactone M_n80,000, (440744), Sigma-Aldrich, UK

Poly-L-lysine solution, (P4707), Sigma-Aldrich, UK

Potassium Sodium Tartrate Tetrahydrate, (217255-100G), Sigma-Aldrich, UK

Precision Plus protein all blue standards, (161-0376), Bio-Rad Laboratories Ltd, UK

Protease inhibitor cocktail, (P8340), Sigma-Aldrich, UK

Retinoic acid, (R2625), Sigma-Aldrich, UK

RIPA Buffer, (R0278), Sigma-Aldrich, UK

SDS PAGE Tank Buffer (10 X) Tris-Glycine SDS, (9-0032), Geneflow Ltd, UK

Sodium bicarbonate, (S5761), Sigma-Aldrich, UK

Sodium butyrate, (B5887), Sigma-Aldrich, UK

Sodium dodecyl sulfate, (L3771), Sigma-Aldrich, UK

Sodium hydroxide, (S8045), Sigma-Aldric, UK

Sodium Chloride, (S7653), Sigma-Aldrich, UK

Tetramethylethylenediamine, (TEMED) (T9281), Sigma-Aldrich UK

Tris Base (Tris-Ro), Sigma-Aldrich, UK

Tris-Glycine Electroblotting Buffer (10X), (B9-0056), Geneflow Ltd, UK

TritonX (X100), Sigma-Aldrich, UK

Tween 20 (P1379), Sigma-Aldrich, UK

VECTASHIELD® mounting medium with DAPI, (H-1500), VECTOR Laboratories, UK

VECTASHIELD® mounting medium with propidium iodide, (H-1300), VECTOR Laboratories, UK

5.1.4 Equipment

Aida image analyser software (version 4.03), Raytek Scientific Ltd, Germany

Automated Cell Counter (TC20™), BioRad, UK.

BioRad model 680 microplate reader, Bio-Rad Laboratories Ltd, UK

HAAKE™ CaBER™ 1 Capillary Breakup Extensional Rheometer, Thermo Fisher Scientific, UK

CBS isothermal liquid nitrogen storage system 2300 series, Sanyo medical division, UK

CO2 laser cutter, (SP500), Trotec, UK

Eppendorf research pipettes (P10, P100 and P1000), Eppendorf, UK

ES sputter coater, (Q150R), Quorum Technologies, UK

Euromex camera, (CMEX 5), Euromex microscopes, Holland

Farnell L3OB stabilised power supply, Farnell, UK

FLUOStar OPTIMA, BMG Labtech, UK

FujiFilm FLA-5100 gel scanner, Fujifilm Life Sciences Products, Sheffield, UK

Fujifilm intelligent dark box, Fujifilm Life Sciences Products, Sheffield, UK

Glassman high voltage power supply, Glassman Europe Ltd, UK

Iblot, Invitrogen Lifesciences Ltd, UK

iMark microplate reader spectrophotometer, BioRad, UK

Leica CLSM laser confocal scanning microscope, Leica, Germany

MIKRO 22R microcentrifuge, Hettich Ltd, Germany

Mini wet blotting apparatus, Geneflow, UK

MiniClima humidity control EBC 11, MiniClima, Austria

Mini-Protean III, Bio-Rad Laboratories Ltd, UK

Mini-Protean tetra, Bio-Rad Laboratories Ltd, UK

Nanodrop 8000, Labtech International Ltd, UK

NE-1002X Syringe pump, New Era Syringe Pump Systems Inc, USA

Nikon digital net camera (DN100), Nikon Ltd, Japan

Nikon Eclipse TS 100 inverted microscope, Nikon Ltd, Japan

Ohaus Scout Pro balance, Fisher Scientific Ltd, UK

Olympus BX51 fluorescence microscope, Olympus, Japan

Olympus CK ULWCD light microscope, Olympus Ltd, Japan

Olympus microscope (CKX31), Olympus, UK

Phenom™ G2 Pro desktop Scanning Electron Microscope, Lambda Photometrics, UK

Philips pH meter model PW9409, Pye-Unicam, UK

Power Pac 3000 power supply, Bio-Rad Laboratories Ltd, UK

Power Pac mini power supply, Bio-Rad Laboratories Ltd, UK

Protean IEF cell, Bio-Rad Laboratories Ltd, UK

QSonica 125V Sonicator, QSonica, USA

REVCO Ultima II -80 °C Freezer, Biocold Laboratories, UK

Rotor-gene 3000 Thermal cycler, Corbett Research Ltd, Germany

Sanyo CO2 incubator (MCO-17AIC), Sanyo Gallenkamp PCL, Leicestershire, UK

Sanyo Harrier 18/80 refrigerated centrifuge, Sanyo Gallenkamp PCL, Leicestershire, UK

Scanning Electron Microscope from (JSM – 7100F), JEOL, UK

SM1 magnetic stirrer, Stuart Scientific Ltd, UK

Soniprep 150, MSE Scientific instruments, UK

SamplePrep 6770 Freezer/Mill, SPEX, Germany

Stuart Heating block model (SBH10D), Geneflow Ltd, UK

Stuart orbital shaker model (SSL1), Geneflow Ltd, UK

Stuart vortex mix (SA7), Geneflow Ltd, UK

Tlesto II OCT, Thor Labs, UK

Ultrasonic welder, Altrasonic, China

Ultra flex III TOF/TOF mass spectrophotometer, Brucker Daltonics Ltd, UK

UV Light Box 8W, Hug Flight Co, Ltd. UK

Virtis Sentry 2.0 Freeze Dryer, SP Scentific, USA

Walker class II safety cabinet, Walker safety cabinets Ltd, UK

Water bath 20 -90 °C, Grant Ltd, UK

Water purification system, Millipore Ltd, UK

5.1.5 Antibodies

5.1.5.1 Primary antibodies

Antibody Name	Specificity	Host Species	Application	Supplier
Monoclonal anti GAPDH – 36 KDa	C-terminal region of human GAPDH	Mouse	W-B- 1:2000	Source Bioscience (GX627408)
Monoclonal anti α-Tubulin – 50 KDa	C-terminal end of the αtubulin isoform	Mouse	IF- 1:200 WB – 1:5000	Sigma-Aldrich (T6074)
Monoclonal anti BIII Tubulin 50 - kDa	C-Terminal end of human βTubulin	Mouse	IF- 1:300 WB- 1:1000	Abcam (ab78078)
Monoclonal anti GFAP – 50 kDa	C-Terminal end human GFAP	Rabbit	IF- 1:500 WB- 1:1000	Genetex (GTX108711)
Monoclonal anti s100B – 24 kDa	C-Terminal	Mouse	IF- 1:100 WB- 1:100	Thermo Fisher Scientific (MA5-12969)
Monoclonal anti Viniculin – 124 kDa	C-Terminal	Rabbit	WB- 1:1000	Abcam (ab129002)
Monoclonal anti Neurofilament – 200 kDa	C-terminal segment pig neurofilament	Mouse	IF- 1:400 WB- 1:1000	Sigma-Aldrich (N0142-100UL)
Monoclonal Synaptophysin – 33.8 kDa	C-Terminus of Human synaptophysin	Rabbit	IF- 1:100 WB- 1:1000	Abcam (EPR1097-2)

Table 3. Table describing all used primary antibodies. IF = Immunofluorescence. WB = Western Blot.

5.1.5.2 Secondary Antibodies

UK Polyclonal goat anti-rabbit IgG HRP conjugated antibody (#7074) – Cell Signalling Technology, UK

UK Polyclonal horse anti-mouse IgG HRP conjugated antibody (#7076S) – Cell Signalling Technology, UK
UK Alexa Fluor® 488 donkey anti-mouse IgG (A21202) - Invitrogen Ltd, UK
UK Alexa Fluor® 568 goat anti-mouse IgG (A11004) - Invitrogen Ltd, UK
UK Alexa Fluor® 568 conjugate Goat anti-Mouse IgG (H+L) (A11004) – Thermo Fisher Scientific, UK
UK Alexa Fluor® 488 conjugate Donkey anti-Mouse IgG (H+L) (A21202) – Thermo Fisher Scientific, UK
UK Zenon™ Alexa Fluor™ 532 Rabbit IgG (Z25303) – Thermo Fisher Scientific, UK

5.1.5.3 Live-cell Immunofluorescence Imaging Antibodies

CellBrite™ Orange (30022) - Biotium, US, 1:1000
Laurdan (D250) – ThermoFisher Scientific, UK, 1:1000

5.2 Methods

5.2.1 Electrospinning

Electrospinning is the technique employed to manufacture all nanofibre scaffolds in this investigation. Their manufacture involves multiple steps. Namely, preparing of dissolved polymer mixtures, laser cutting of the polyester sheets onto which the polymer nanofibre are electrospun. Post spinning, the nanofibre coated sheet is laminated with an additional polyester sheet and cut to size for cell culture.

5.2.1.1 Preparing the Polymer mixtures

In this investigation two synthetic polymers were chosen; Polyacrylonitrile M_w150, 000 (PAN) (Sigma-Aldrich, UK) was dissolved in N, N-Dimethylformamide 944 kg/m^3 (Fisher Scientific, UK) to prepare 10wt% PAN/DMF. The other was Jeffamine®® ED-2003 (Jeffamine®)(Huntsman, USA) which was prepared in combination with PAN dissolved in DMF. Using a heated stirrer, the PAN (and Jeffamine® if required) was mixed with DMF and left at 50^{o}C overnight with constant magnetic stirring. Polymer preparations were prepared as follows.

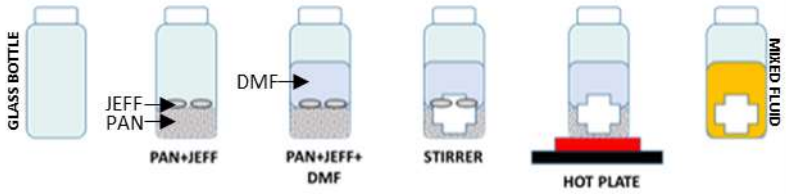

Figure 20. Cartoon depiction of the mixing process when manufacturing polymers for electrospinning (PAN and Jeffamine®) – Figure by Berenice Pic.

Weight percent of PAN was calculated either by percentage or mass. However, density was also considered. The density of DMF (Fisher Scientific, UK) is 0.9445g.mL^{-1}. If the total volume (V_T) wanted is 20ml, then then mass of DMF (m_{DMF}) needed is 18.89g. This remains standard for the calculation of the mass of PAN required.

DMF Calculation:

$m_{DMF} = d_{DMF} \times V_T$

m_{DMF}= Mass of DMF
d_{DMF}= Density of DMF
V_T= Total Volume

PAN Calculation:

$$m_{PAN} = \frac{\%_{PAN}}{\%_{DMF}} \times m_{DMF}$$

m_{PAN}= Mass of PAN
$\%_{PAN}$= Weight Percentage of PAN
m_{DMF}= Mass of DMF
$\%_{DMF}$= Weight Percentage of DMF

Jeffamine® Calculation:

$$m_{JEFF} = \frac{\%_{JEFF}}{1-\%_{JEFF}} \times m_{PAN}$$

m_{JEFF}= Mass of Jeffamine®
$\%_{JEFF}$= Weight Percentage of Jeffamine®

For example, to calculate mass of PAN for 10wt%, the calculation would require (10(%)/90(%))*18.89 = 2.099g

For Pan-Jeffamine®, percentage of Jeffamine® is calculated as a percentage of the mass of PAN. To calculate the mass of Jeffamine® for 10wt%PAN and 1% Jeffamine®, the calculation would give 0.0022g. Weight percent was varied between 6wt% and 12wt% in PAN. Then with 10wt% PAN as standard, Jeffamine® was varied between 1 and 5%.

Weight Percentage	DMF/g	PAN/g	Jeffamine®/g
6wt% PAN	18.89	1.206	--
8wt% PAN	18.89	1.642	--
10wt% PAN	18.89	2.099	--
12wt% PAN	18.89	2.576	--
10wt% PAN 1% Jeff	18.89	2.122	0.022
10wt% PAN 5% Jeff	18.89	2.222	0.117

Table 4. Summary table describing recipe for manufacture of PAN and PAN + Jeffamine® polymers for electrospinning.

5.2.1.2 Cutting Polyester Sheets

Two 600 x 300mm polyester sheets were laser cut using a Trotec laser system. Here, power and speed of cutting was optimised as shown below to ensure that the shapes were cut as clean and controlled as possible. Two sheet formats were designed; a top sheet consisting of an array of 1cm (in length) ellipses and a bottom sheet including an array of just the rectangles as shown in figure 21. Power was varied from 40%-100% and speed was either 50% or 100%. Optimisation was judged by visually assessing the edges of the cuts for consistency, un-wanted melting and similarity to digital design. Candidate 2 with power 100% and speed 50% was deemed visually the most suitable specification. Figure 21 describes this optimisation process. For random fibre, both top and bottom sheets simple had a circle with a 10mm diameter in the same array size with the same laser power and speed specification.

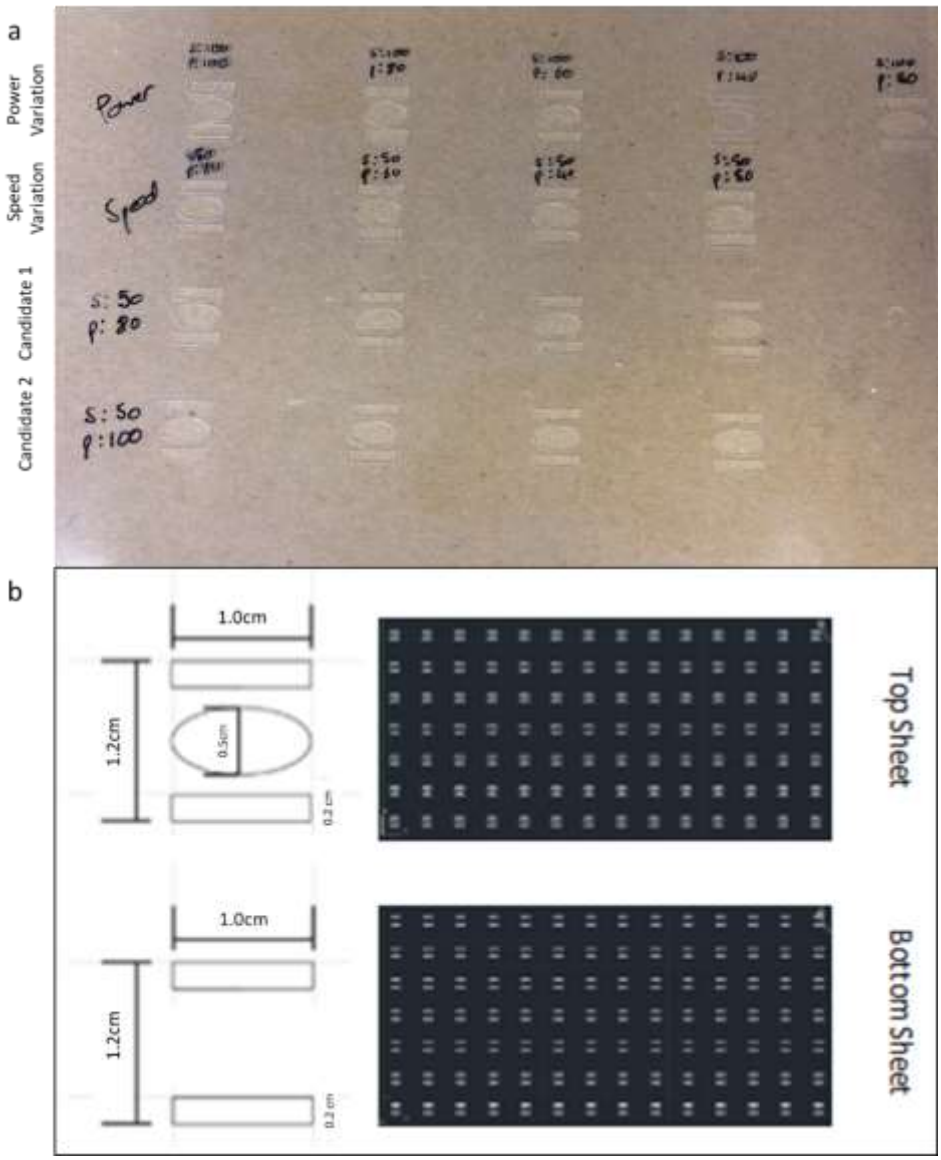

Figure 21. a. Aperture design examples with the power and speed optimisation process carried out using the CO2 laser (Trotec, UK). Candidates 1 and 2 were picked as visually optimised cutting specifications. b. dimensions plus AutoCAD array display for both top and bottom sheet designs.

5.2.1.3 Running a Spin

The sheets were cleaned with de-ionised water and sterilised using 70% ethanol and ultrasonically welded together and adhered to a rotating drum using conductive aluminium tape (RS components, UK) at a distance of 30cm from the 21-gauge 100mm needle (The Needle Company, UK) in a humidity-controlled environment (45% humidity maintained). The polymer was fed into a 10ml syringe tube (luer-lock tip) (Dickindon, UK) attached to a 0.5mm blunt-end needle (spinneret, UK) and a length (estimated 100 cm) of PTFE tubing 1/31 inch bore size (Altec, UK), leading to the 21-guage 100 mm needle. A high voltage of 19-24kV (polymer dependant) was applied to the needle and the system left to deposit at a flow rate of 1ml/hr. This set-up is described below in figure 22. Once the cycle had completed the fibre and the sheets were

removed and the bottom sheet peeled away. On top of the freshly spun sheet, a fresh top sheet (see figure 21) was ultrasonically welded (Altrasonic, China). This process allowed the manufacture of aligned nanofibre membranes which were sandwiched between the two sheets but spanned the open elliptical window. The alignment of the nanofibre being parallel to the minor of the ellipse and both sides of the aligned nanofibre membrane being accessible in cell culture.

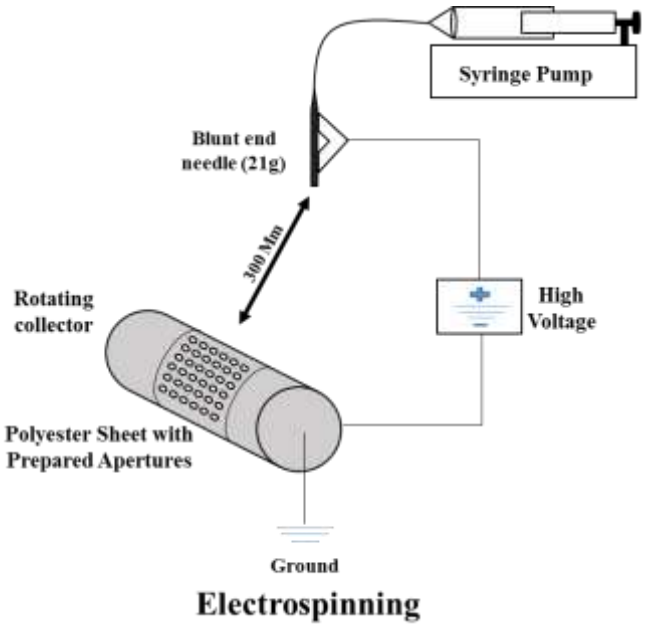

Figure 22. Cartoon representation of the electrospinning process carried out in-house. Figure by Joseph Chemmarappally.

Electrospinning was possible because a potential difference is applied between the needle (positive terminal) and the collector drum (negative terminal). This allowed for polarization of the solution and formation of a Taylor cone. This cone in turn leads to the formation of a jet (firing towards the grounded collector below) and then production of nanofibre in plume formation. In the absence of a voltage, no Taylor cone is formed, the fluid leaks out of the needle and forms a pendant drop. This then simply drops out of the end of the needle. This is described in figure 23.

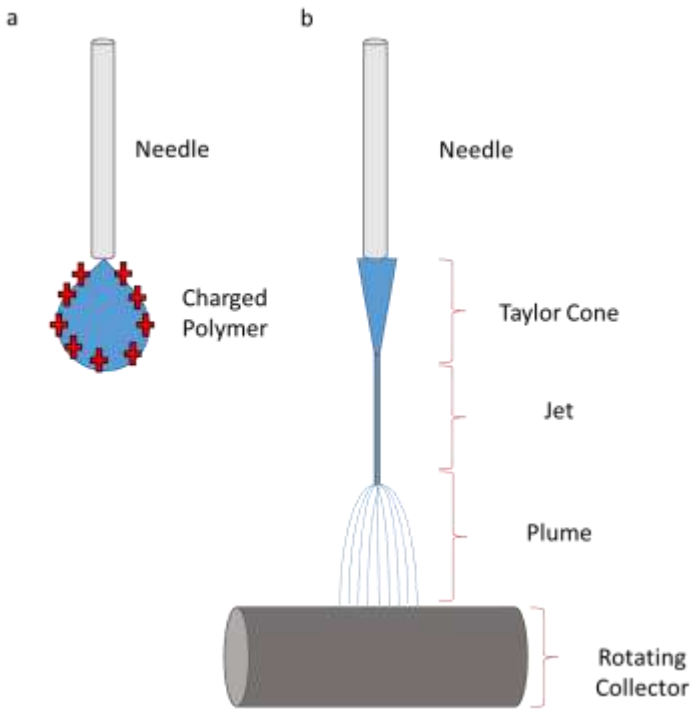

Figure 23: a. Depiction of a bead of polymer without charging - the polymer builds at the end of the needle. b. With charging, the polymer forms a Taylor cone, and jets towards the grounded collector, forming a plume before impact, forming nanofibre.

5.2.1.4 Preparing the Fibre for Cell Culture

After laminating the sheet so that the nanofibre is sandwiched between two top sheets, the sheet is taken back to the laser cutter to be cut into disks suitable for culture in 12 well microplates. The dimensions of which are shown in figure 24. The power and speed of laser cutting was adjusted to 50% power and 30% speed as required to cut through all layers present. The laser cutting process welds all sheets together securely.

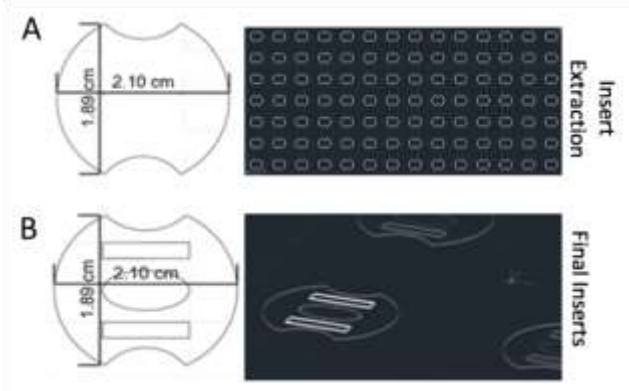

Figure 24. Depiction of the design cut-out using the CO_2 laser (Trotec, UK) once the sheets had been spun. A. design specifications of the final cut before cell culture is possible. B. Final product from the electrospinning process.

5.2.1.5 Analysis of Fibre Properties

5.2.1.5.1 Extensional Rheometry

Using the HAAKE™ CaBER™ 1 Capillary Breakup Extensional Rheometer, it was possible to measure viscosity of prepared polymers solutions. Here, a small volume of less than 200 µl was loaded between the pistons to visually fill the space neatly, forming a liquid bridge of around 500±50µm in length connecting the two ends of the rod. The pistons were then pulled apart at a controlled rate and the diameter of the filament tracked over time until it breaks from over-stretching. This process allows calculation of strain rate, sheer viscosity and calculated breakup time. Figure 25 demonstrates the set-up of the extensional rheometer in use. This technique was used in place of extensional rheometry as the viscosity of the fluids in use deemed it most appropriate.

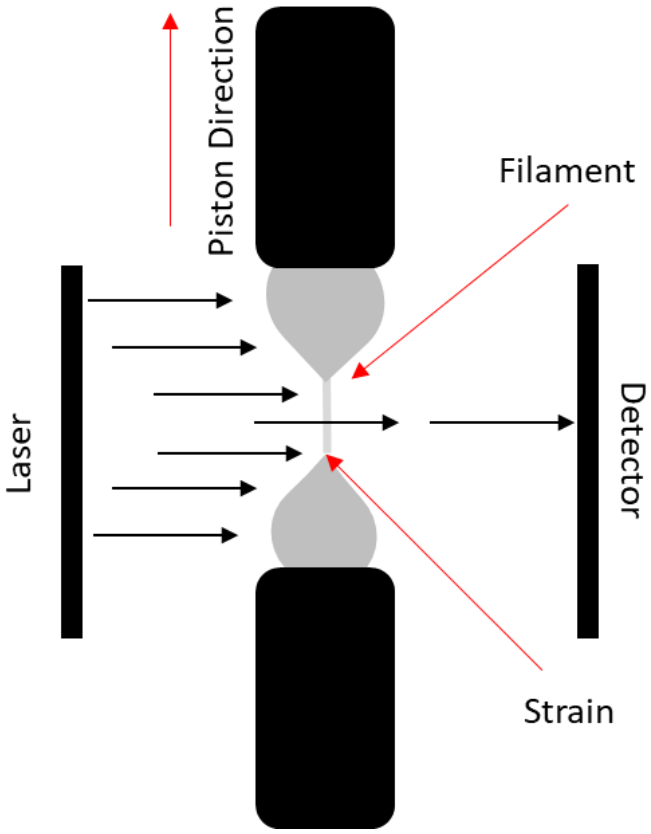

Figure 25: Pictorial demonstration of how extensional rheometry establishes fluid properties in the HAAKE™ CaBER™ 1 Capillary Breakup Extensional Rheometer.

5.2.1.5.2 Drop Shape Analysis (DSA) of Contact Angle

Contact angle is measured by looking at the angle between a water droplet edge and the nanofibre surface it is on two seconds after placement. An angle over 90° indicates hydrophobicity and under 90° hydrophilicity (Villa et al. 2018, Tran, Webster 2013). Figure 26 demonstrates this process.

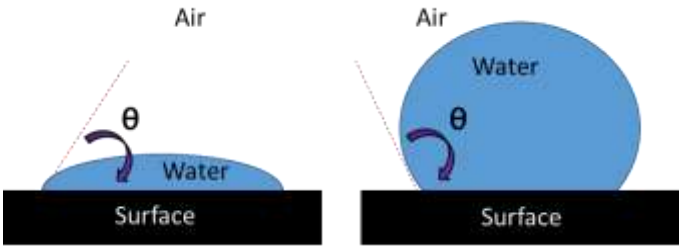

Figure 26: Demonstration of method used to calculate hydrophobicity using DSA.

5.2.1.5.3 OCT Analysis of Nanofibre Membrane Thickness

Optical coherence tomography (OCT) was used to assess the matt thickness of fibre disks after spinning different volumes of polymers and different weight percentages. The technique relies on low-coherence, light interferometry, a process analogous to ultrasound, to create cross-sectional images of the object of interest (Fujimoto et al. 2000). The sample was placed in the beam path of the OCT machine in use and light passed through a beam splitter, redirecting the light either to an adjacent mirror or towards the sample. Reflecting the light from both sources towards a detector allowed creation of low-coherence – detection of which can be used to create an image. ImageJ software was used to analyse thickness by taking 10 random points and calculating the mean in triplicate images - as shown in the example in figure 27.

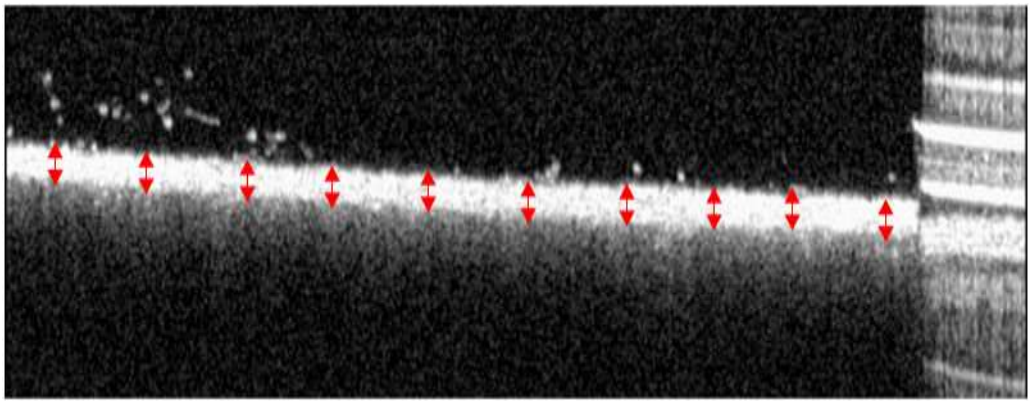

Figure 27: Example of OCT image taken of cross-sectional area of nanofibre. Ten random locations are chosen, and mean thickness calculated in triplicate images.

5.2.1.5.4 SEM Analysis of nanofibre diameter and pore size

The Phenom™ ProX SEM (Lambda Photometrics, UK) was used to analyse nanofibre properties at an accelerating voltage of 10kV. Prior to analysis, fibre was coated with 10nm of gold using a gold splutter (Edwards S150B). Post imaging analysis of said fibre diameter and pore size was analysed using Phenom Fibremetric ® software. Specifically, a selection of 100 fibre examples (in one image) were randomly selected to be included in an average measurement at 5000X magnification. Overlapping fibre was discounted from the results as they were considered misleading.

5.2.1.5.5 FFT (Fast Fourier Transform) Analysis

FFT is an algorithm that may be used to assess spatial patterns. This process is accessible using ImageJ software and may be used to assess alignment of nanofibre and cellular populations. Figure 28 presents the outcome of inputting the top row into an FFT algorithm.

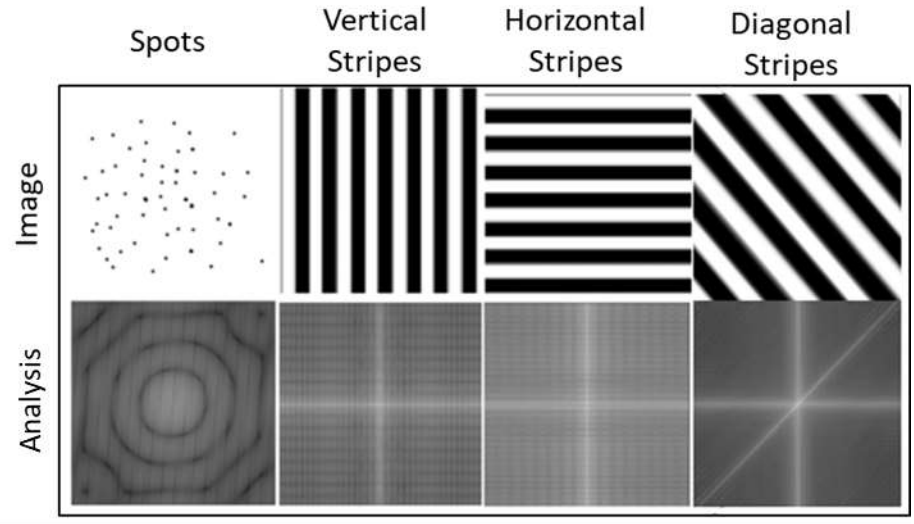

Figure 28: Examples of how certain patterns would be displayed using FFT pattern analysis.

5.2.1.6 Electrospray Modification

Solution for spray was first prepared (Collagen 6mg/ml is pre-prepared by 'Collagen Solutions') and loaded into a 1ml syringe. A standard 21-gauge needle was attached to the end before sealing the needle to a finer glass needle with a heat-seal. The syringe-needles construct was inserted into the syringe holder with the 21-guage needle in contact with the metal high-voltage elastomeric contact in place before screwing said syringe holder shut. The sample/target was positioned on the sample holder microplate below, exposing

only the regions of interest by covering additional areas with a custom-cut polypropylene sheet, and metal grounding aluminium sheet positioned below the sample. The syringe pump was started at the appropriate (ultra-low, experiment-dependant) flow rate and high voltage switched on. The syringe pump was separated from the high voltage supply with an extended plunger 'pusher' to ensure that no damage was done to the high value syringe pump. Figure 29 below describes this set-up.

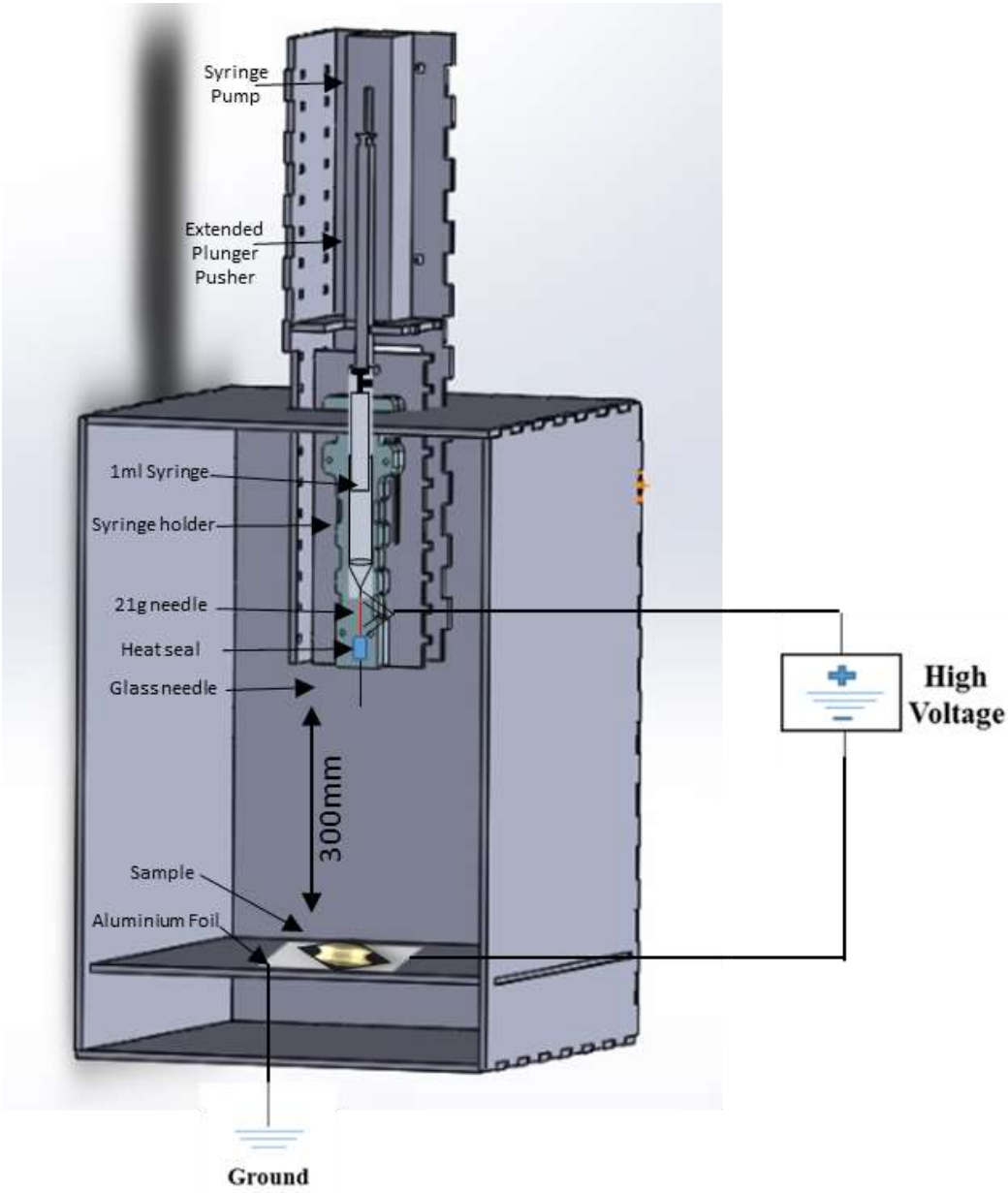

Figure 29: Electrospray apparatus designed and assembled in-house.

5.2.2 Manufacture of Additional Cell Culture Tools

5.2.2.1 Stacker design and manufacture

Using the in-house Trotec laser and the AutoCAD design presented in figure 30, 5mm Acrylic was cut, producing the required number of 'stackers', storing them in a sealed container post-cut.

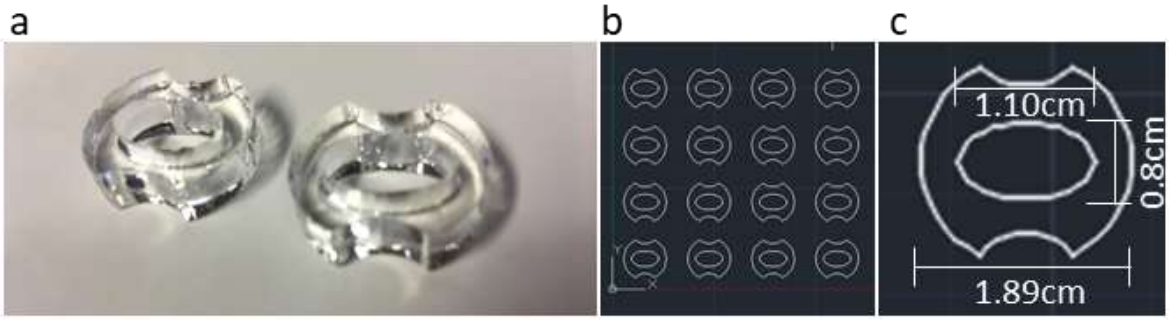

Figure 30: a. Example 5mm acrylic stacker design (MARK III). b. AutoCAD demonstration of an array of stackers ready for laser cutting. c. Dimensions of a single stacker on AutoCAD.

5.2.2.2 Pre-Culture Sterilisation

One hour prior to any cell culture, all nanofibre inserts and stackers were subject to 70% ethanol sterilisation within a laminar flow hood for 30 mins before first washing 3 times in phosphate buffered saline (PBS) (Lonza, UK) and then equilibrating in Dulbecco's Modified Eagle Medium (DMEM) F12 culture medium (Lonza, UK). Inserts and stackers were left in media until ready to seed/use.

5.2.3 Tissue Culture Protocols

5.2.3.1 Stock Preparations

A 10x stock (10x more concentrated than required) of Tris-Buffered Saline (TBS) was prepared by dissolving 24g Tris Base and 88 g NaCl in 900 mL of distilled H_2O. The pH was adjusted to 7.6 with 1M HCl before making the volume up to 1L with more distilled H_2O. A 10x stock of Phosphate Buffered Saline (PBS) was made up by mixing 800g of NaCl, 20g of KCl and 144g of Na_2PO_4 with 8L of distilled H_2O. Ph was adjusted to 7.4 with 1M HCl. These could later be diluted to 1x by diluting in distilled H_2O. Penicillin-Streptomycin 100x mix contained 5000 units of potassium penicillin and 5000µg of Streptomycin Sulfate per ml in 0.85% saline. This was diluted from 100x with 1x PBS to 1x concentration prior to use.

5.2.3.2 Media Preparation

Both human neuroblastoma SH-SY5Y and human glioblastoma U-87MG (American Type Culture Collection, Manassas, VA) cells were grown at 37°C and 5% (v/v) CO_2 supply in either T25 or T75 flasks (Sarstedt, UK) depending on cell number. In both cases, cells were maintained in a DMEM-F12 (Lonza, UK) medium, supplemented with 10% heat inactivated Foetal ovine Serum (FBS) (Invitrogen, UK), 2mM L-Glutamine (Lonza, UK), 1% Non-essential Amino Acids (NEAA) (Lonza, UK) and 1X concentration (stock is 10x) Penicillin-Streptomycin (Pen Strep)(Lonza, UK). Differentiation media consisted of the same preparation with 1% heat inactivated FBS (Invitrogen, UK) rather than 10%.

5.2.3.3 Differentiation Protocol

All media and other reagents were pre-warmed. Differentiation was carried out using DMEM-F12 (Lonza, UK) media, supplemented with 1% heat inactivated FBS (Invitrogen, UK), 2mM L-Glutamine (Lonza, UK), 1% Non-essential Amino Acids (Lonza, UK) and Penicillin-Streptomycin (Lonza, UK), 1% FBS low serum DMEM F12 with Pen Strep (Thermo Fisher Scientific, UK) and NEAA (Thermo Fisher Scientific, UK). 100 mM Retinoic acid was added at 1µl in 10ml of low serum media for SH-SY5Y and U-87 MG differentiation. All culture was carried out at 37°C, 5% CO_2 and 95% relative humidity.

5.2.3.4 Cell Passage

All fresh media and other reagents were pre-warmed. Media was removed and 5ml of PBS (Lonza UK) added and left for 3 minutes, this was repeated 3 times. Subsequently, 3ml of Trypsin-EDTA (Lonza UK) (T25 flask, 5ml for a T75 flask) was added and left for 5 minutes at 37°C. Media was quenched with fresh 10% FBS culture media (Lonza, UK) and triturated to release all cells from base of flask before centrifuging supernatant at 300g for 5 minutes and re-suspending in an appropriate volume of media. Cells were kept under 30 passages to ensure cellular phenotype was maintained. All culture was carried out at 37°C, 5% CO_2 and 95% relative humidity.

5.2.3.5 Cell Counting

Protocol was the same as 'Cell passage', however post centrifuge, cells were re-suspended in 2ml 10% DMEM media before removing 20µl of suspension and adding to 80µl of 10% DMEM media (Lonza, UK) in a 15ml Eppendorf tube. 10µl of this was added to a haemocytometer and an average count taken – multiplying this by 100 revealed cell count per microlitre of suspension.

5.2.3.6 Cell Seeding on Nanofibre

The volume required to seed 50,000 cells was calculated and said volume was pipetted carefully onto the centre of the pre-sterilised ellipse section of the nanofibre disk – typically a 2-20 µl tip was used to ensure accuracy. The fibre should be washed in DMEM F-12 immediately prior to seeding. This was left for at least 30 minutes (no more than 45 minutes) before filling the well with 2ml of media (DMEM F-12 10% serum at least for twenty-four hours (Lonza, UK)) carefully down the side of the fibre disk, not on top – this volume excluded any air bubbles. Any bubbles were removed carefully with a pipette tip, carefully lifting one side of the fibre to remove the bubble – bubbles trapped beneath the fibre could limit cell access to media.

5.2.3.7 2D scratch assay

A population of 50,000 undifferentiated SH-SY5Y cells was seeded on glass slides and cultured for forty-eight hours. Here a 'scratch' was introduced out using a jig made in-house, directing a pipette tip (100µl) across the centre of the confluent layer of SH-SY5Y cells on each glass slide in a straight and repeated line. Cells were subject to 1% differentiation media containing retinoic acid and fixed at various time points by adding 95% methanol (5% 1xTBS (Sigma-Aldrich)) and storing in freezer for 20 minutes before transferring to a fridge for storage prior to immunofluorescence staining.

5.2.3.8 Immunofluorescence staining

Culture technique is the same for 2D glass slides or nanofibre disks, 2ml of media was suitable to ensure coverage of nanofibre disks. Fixed cells were permeabilised in 1x TBS with 1% Triton (Sigma-Aldrich, UK) at room temperature (21°C) for 10 minutes before washing slides in 1x TBS for 10 minutes. The slides were incubated in blocking solution (3% BSA (Sigma-Aldrich, UK)) for at least 1 hour at room temperature with gentle agitation (at least 1ml per 12 well microplate well) and subsequently incubated with primary antibody in 3% BSA/TBS (Sigma-Aldrich, UK) overnight in a 95% humidified chamber. The following day, four repeated 15-minute washes in 1x TBS were carried out with 0.1% Triton (Sigma-Aldrich, UK) for 1 hour each at room temperature before incubating for at least 2 hours with secondary antibody made up in 3%BSA in 1xTBS – sample was covered up from light exposure using aluminium foil. Following this, a further four repeated 15-minute washes in 1xTBS with 0.1% Triton were carried out at room temperature, again keeping the sample covered up from light exposure. Lastly, glass slides were prepared with 1 small drop of VectaShield (Vector Laboratories, UK) mountant with DAPI (as prepared by supplier) and samples added face down on-top of said droplet, applying light pressure to remove excess mountant. Samples were stored in a dark-box.

5.2.3.9 Protein Extraction

Technique here varies more widely for 2D glass slides and 3D nanofibre scaffolds. In the case of 2D flasks, media was removed, and flasks were washed with ice cold PBS before adding 1ml of ice-cold RIPA Lysis and Extraction buffer (T75 flask) (Sigma-Aldrich, UK). The flask was incubated for fifteen minutes and a cell scraper (Fisher Scientific, UK) was used to thoroughly scrape the entire surface of flask. The supernatant was centrifuged at 14,000g for fifteen minutes to pellet debris and supernatant transferred to a fresh tube where it was frozen. For 3D scaffolds, all media was removed, and disks were washed with pre-warmed PBS (37 Degrees Celsius). Following this, nanofibre disks were trimmed as shown in the diagram below (figure 31) and placed in a 2ml Eppendorf tubes where 0.5ml of 0.5% SDS (Sigma-Aldrich, UK) in TRIS buffer (Geneflow Ltd, UK) was added (these were pre-heated to 95°C). Inside said tubes, using a pipette tip, nanofibre was extracted from the plastic as best possible and physically 'mashed' in the bottom of the tube. Tubes were heated in a heat block at 95°C for five minutes and pulse spun to remove the plastic debris left. Samples were then placed on ice for five minutes, vortexed for thirty seconds and placed once more in the heat block for five minutes – this process was repeated at least three times. Samples were pulse spun once more before placing in -20°C freezer.

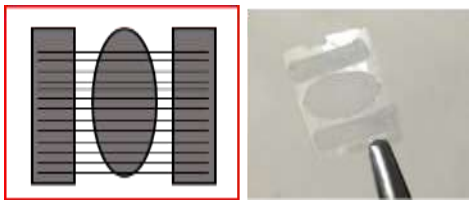

Figure 31: Demonstration of process used to trim un-needed random regions of aligned fibre disks prior to protein extraction on nanofibre – random fibre was carried out with identical technique.

5.2.3.10 Protein Estimation

Working Lowry Reagent was prepared using Sodium Carbonate (2g)/Sodium Hydroxide(0.04g), made up to 100ml with distilled water, 1.0% (w/v) Copper Sulphate solution (Cupric Sulfate) (1g in 100ml) (Sigma-Aldrich, UK) and 2.7% (w/v) NAK-tartrate (2.7g in 100ml) (Sigma-Aldrich, UK). A stock solution of 1mg/ml of BSA was prepared and used to assemble a standard curve (0, 5, 10, 15, 20, 25, 30, 35, 40, 45, 50, 60, 80 µg of protein was made up to 100ul with distilled water and extraction buffer (Sigma-Aldrich, UK) in triplicate). All samples were taken for protein estimation, removing 25µl and adding to an Eppendorf before making up to 100µl with distilled water. To this, 1.0ml of Working-Lowry Reagent was added to samples and standard curve tubes. Tubes were incubated for fifteen minutes and 100µl of diluted Folin-Ciocalteau reagent (Sigma-Aldrich, UK) was added. Said tubes were subsequently capped and vortexed (1:1 with distilled water) and then incubated for thirty minutes – a blue colour becomes evident. 100µl was taken from all tubes and placed into a 96 well microplate, measuring absorbance at 750nm. Readings were

recorded on an Excel Spreadsheet. For the 3D nanofibre scaffolds low levels of protein could be extracted so concentration was required by precipitation in acetone. Here, nine volumes of ice-cold acetone (Sigma-Aldrich, UK) per volume of sample were mixed. Samples were vortexed and left in the freezer overnight. The next day they were spun at 13,000g for 15 minutes before removing supernatant, air drying the pellet for 5-10 minutes and re-suspending in 50µl of buffer. Protein estimation was then carried out.

5.2.3.11 Gel Electrophoresis and Western Blot

The western blot is a commonly used technique used to detect and quantify protein expression in cellular populations. This blot was carried out by first defrosting prepared protein isolates. The required equipment was assembled, including both top and bottom glass microplates (recommend 1.5mm spaced microplate and obtain 1.5mm combs). Microplates were layered together and clicked into the holder, ensuring there was no leakage. A 10% resolving gel (7.5ml was sufficient) was prepared by combining 2.5ml 40% (w/v) acrylamide (Sigma-Aldrich, UK), 2.5ml 1.5M Tris pH 8.8 (Sigma-Aldrich, UK), 100ul 10% (w/v) SDS (Sigma-Aldrich, UK) and 4.9ml distilled water per gel. To each 10ml of resolving gel mix, 5ul of TEMED (Tetramethylethylenediamine) (Sigma-Aldrich, UK) and 50ul ammonium persulphate (APS) 10% (w/v) (Sigma-Aldrich, UK) was added before allowing to set. A layer of water was added on top to break bubbles and physically straighten the gel. A 4% stacking gel was subsequently prepared by adding 5ml 40% (w/v) acrylamide, 12.5ml 0.5M Tris pH 6.8 (Sigma-Aldrich, UK), 500ul 10% (w/v) SDS and 32ml of distilled water. This was polymerised by mixing with 20ul of TEMED and 50ul of ammonium persulphate (APS) 10% (w/v). The stacking gel was added, filling the construct up to the top. Subsequently, the combs were added at a 45 degrees angle to avoid air bubbles and the system could set. Following setting, the chamber was set up and running buffer prepared by mixing one litre of 10x concentrate is 0.0256M (31g) of Tris base, 0.192M (144g) Glycine (Sigma-Aldrich, UK) and 0.1% (10g) SDS, making the mix up to 1000 ml with distilled water. Gels were added to the chamber and locked in place before adding the running buffer to fill central cavity and then the outside of the chamber. The ladder was added into left hand side of gel before loading all samples and running the system at 200 milliamps (150 milliamps for 5 minutes and then up it to 200 milliamps) for 45 minutes.

To transfer the protein, gels were removed and transferred into a boat containing distilled water. Gels were then trimmed to remove combs sections and transfer construct components were gathered. A black sponge mat was added first, followed by 2 filter papers and nitrocellulose membrane, then gel, then 2 filter papers and a sponge - all components were all pre-soaked in transfer buffer. These were locked together within the construct before adding it into the transfer chamber and adding 1 litre of transfer buffer (pre-mixed from Bio-Rad). The transfer buffer was comprised of 25mM Tris, 192mM glycine and 0.1% SDS at a pH of 8.3, with 20% methanol (vol/vol). This was run for 960 minutes at 30 volts. Staining was subsequently carried out by removing the nitrocellulose and washing in TBS, before copper staining (if bands are close)

if necessary (Copper Phthalocyanin, Sigma-Aldrich, UK). The nitrocellulose (Labtech, UK) was then cut above 75kDa and below 25kDa, marking in pencil which nitrocellulose belongs to which blot. All cuts were blocked in 5% marvel (Marvel, UK) in TBS TWEEN for at least 2 hours before soaking in primary (in 5% marvel) in addition to the housekeeping primary and rocking overnight. The following day four repeats of fifteen-minute washes were carried out in 1xTBS TWEEN before adding the secondary HRP conjugated antibody in 5% milk and incubating for two hours. A further three repeats of ten-minute washes in TBS TWEEN were carried out before imaging. Here, 2ml of a 1:1 mixture of ECL reagents A and B was added to the nitrocellulose and the blots re-assembled before adding to the Fujifilm intelligent dark box (Fujifilm, UK) and exposing for 20-30 seconds. An image of the ladder was also taken for comparison.

5.2.3.12 MTT Reduction Assay

MTT assays were carried out by culturing cells in well microplates (12 well adherent microplates for this work) in accordance with the experiment purpose. The glass coverslip or nanofibre disks were transferred into a fresh 12 well microplate along with 2ml of media. 200ul of MTT stock (5mg/ml) (Sigma-Aldrich, UK) was added to each well before incubating for two hours. Carefully, all media was removed and 500ul of DMSO was added, leaving the microplate(s) shaking for ten minutes. 100ul of solution from each well was transferred to a 96 well microplate and read in microplate reader (iMARK, Biorad, UK).

5.2.3.13 CellTiter-Glo® Assay

This assay was carried out by first defrosting the reagent completely. An equal volume of reagent (Promega, UK) was added to a volume of media in a 12 well microplate well – 250ul of media was preferred with 250ul of reagent through optimisation for both glass slides and nanofibre disks. The combination was shaken vigorously for 5 minutes minimum and read once every 5 minutes for luminescence on the microplate reader.

5.2.3.14 DAPI Cell Count

Protocol was the same for glass coverslips or nanofibre disks. Cells were first fixed by adding 95% methanol (5% 1xTBS) and storing in the -20°C freezer for 20 minutes and then replacing volume (all 2ml) with PBS and transferring to the 4°C fridge. Cells were permeabilised in 1xTBS with 1% at room temperature (21°C) for 10 minutes before washing samples in 1x TBS for 10 minutes. Subsequently, glass slides were prepared with 1 small drop of VectaShield with DAPI (as provided by the supplier) and samples added face down onto each slide DAPI droplet, applying light pressure to remove excess DAPI. A cover slide and/or nail varnish to cement the sample in place was optional. Samples were subsequently stored in a 'dark box' in the fridge, ready for imaging. Said imaging was carried out on an immunofluorescence microscope and five

random areas per sample assessed for DAPI count with ImageJ software. Counts were averaged and at least three samples were taken per condition for significance. Alternatively, a fluorescence microplate reader was used on the same samples, measuring fluorescence intensity at an absorbance of 720nm.

5.2.4 Specialised Nanofibre Culture Protocols

5.2.4.1 Lesion Assay

This assay was developed in-house. Nanofibre disks were first seeded with 50,000 cells per disk; 25,000 SH-SY5Y and 25,000 U-87 MG (not pre-mixed). These were incubated for two hours before adding 2ml of media and leaving in the incubator for forty-eight hours. Seven days of retinoic acid-mediated, low serum differentiation was carried out on all samples. Separately, a scalpel-mediated lesion 'Jig' was prepared by assembling five layers of laser-cut clear 4mm Perspex as shown below in Figure 32. The lower two layers were adhered with plastic 'cement' (SC250 Solvent Cement, FloPlast, UK) and pins permanently attached to these layers with the same adhesive. The top three layers were fed sequentially onto the pins, allowing the loading of a sample between the two-hollow circle-containing layers. The layer with the scalpel slit was added last. A fresh Jig was assembled for each experiment. Nanofibre disks were removed from their 12 well microplates and placed into the central cavity of the 'jig' and nanofibre was lesioned with one careful and slow insertion of a fresh, sterilised RS Pro scalpel blade through the custom-made aperture. Injured nanofibre was inserted into fresh 12 well microplates (with a fresh stacker) with fresh (low serum) media (and retinoic acid) and cultured. For an indication of short-term events, the first sample was analysed at three hours post injury, by fixing for staining or protein extraction for western blot analysis. An un-lesioned, mature (seven days of differentiation) control was always included alongside lesioned disks.

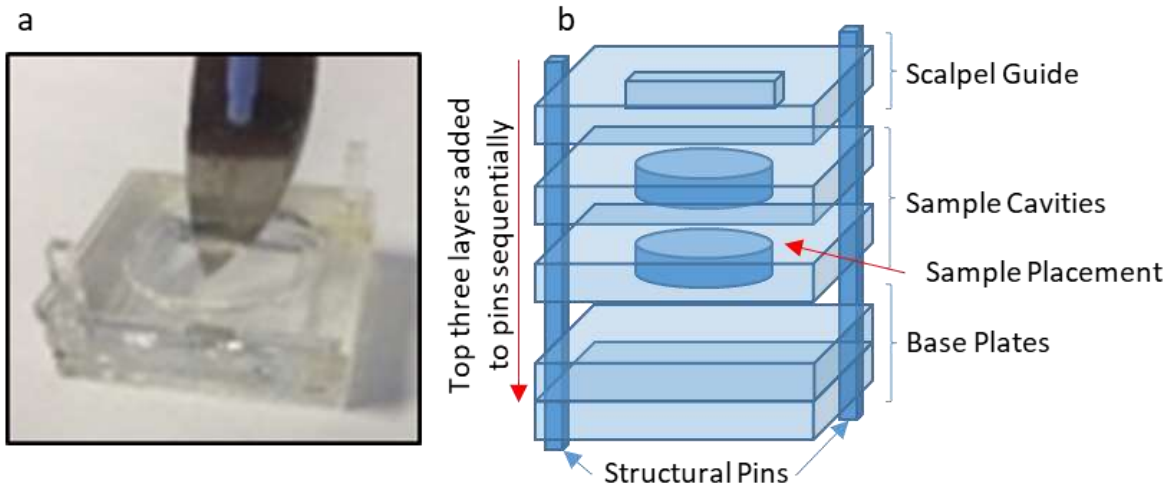

Figure 32: a. Photograph of scalpel jig designed to hold nanofibre securely in the central cavity above which a sterilised scalpel blade may enter through a small slot, penetrating the same position and depth every time. b. Schematic of structure.

5.2.4.2 Multi-Layer Stacking

This assay also developed in-house was carried out by first sterilising two stackers per set of fibre samples (per well). All layers were initially cultured with either 50,000 SH-SY5Y cells or 50,000 U-87 MG cells per layer and left for at least one hour before filling with 2ml of DMEM F-12 media with 10% serum. All layers were incubated independently in their own 12 well microplates for seven days in differentiation media. At this point, using tweezers, the constructs were assembled in the orientation required. Often SH-SY5Y cells on PAN would be the middle layer. First a sterilised stacker would be placed in a well and then a series of nanofibre layers would be placed on the stacker. Finally, another sterilised stacker would be placed on top of the stack of nanofibre layers. The weight of the stacker was enough force the nanofibre layers close together and to keep the fibre suspended and not in contact with the base of the microplate. The layers were then analysed at various time points, assessing the layers independently.

5.2.4.3 Cryo-Fracturing Nanofibre

Following standard electrospinning procedure, a layer of randomly aligned 10wt% PAN was spun onto an un-patterned/cut 300x600mm polyester sheet. This was removed and transported to the cryo-milling facility. Fresh liquid nitrogen was brought also. 4-5L of liquid nitrogen was used to initially cool the apparatus (SPEX 6770 Freezer/Mill). A further 3-6L was needed henceforth per hour of operation. A 0.1-0.2g mass of fibre was weighed and added with 1ml of dH_2O to the cryo-vial. Into the cryo-fracturing machine, a sufficient volume of liquid nitrogen was added to fill up to 4.5cm from the lip of the tub. The cryo-vial was added, the machine closed, and the cycle length and number selected. Once the cycle(s) had

finished, the sample was carefully removed and left in a freeze dryer (Virtis Sentry 2.0, SP Scentific, USA) could be dried at a low temperature (-80°C) for 72 hours.

5.2.4.4 Collagen I, Rat Tail, Gel Polymerisation

All components were kept on ice and pushed through a 0.2µm Nalgene Syringe Filter (Fisher, UK) to ensure sterility. For 10ml of gel, first 1ml of 10x DMEM M199 media (Fisher Scientific, UK) was mixed with 2.13ml of dH_2O. At this point, cryo-fractured nanofibre was added if required and mixed using a sonicator (QSonicca, 125W), pulsing for 10 seconds with a 50% duty cycle. Where cryo-milled fibre was added, extra sterilisation was carried out using the Hug Flight company Ltd. Light box (UV tube 26cm long, 1cm wide, 35V, 256nm, 3cm distance from sample, 30 minutes). This sterilisation source was proven suitable and optimised by a colleague (Joseph Chemmarappally). Subsequently, 6.7ml of Collagen I Rat Tail was mixed in. Finally, 0.17ml of 1M NaOH was added (Sigma-Aldrich, UK). Once the mixture turned pink it indicated that polymerisation had started. The mixture was mixed using a 1ml pipette and then deposited at the volume required onto the nanofibre of interest (even dispersion across the area). Polymerisation was typically left to occur for two hours at 37°C.

5.2.4.5 Dichlorofluorescin Diacetate (DCFDA) Dye Staining

Wash cells in 1x buffer (diluted from 10x buffer with dH_2O – buffer provided in the kit). Defrost the DCDFDA dye and incubate at 20µM with cells of interest for 30 minutes in the dark. Wash cells once more in 1X buffer and read signal at a 485nm excitation.

5.2.5 Statistical Tests

Data was presented generally as mean ± standard deviation (SD) at a 95% confidence limit. Statistical analysis was performed as per experiments.

- Where comparison of two groups was required over multiple time points, significance was indicated using a two-way ANOVA with Sidak's multiple comparisons test with $P<0.05$ indicating significance (* in all cases).
- Comparing multiple groups such as nanofibre material deposition volume or mix specifications, a one-way ANOVA with Sidak's multiple comparisons test was used. Significance was indicated with P-values <0.05 (* in all cases).

- Comparing just two groups like in random nanofibre properties analysis, significance was assessed using a two-tailed, parametric, unpaired t-test with Welch's correction with a P-value of <0.05 (* in all cases).
- Comparing multiple means such as visual GFAP expression in one time point, Significance was assessed using a one-way ANOVA with Tukey's multiple comparisons test with P<0.05 indicating significance (* in all cases), ensuring all confidence intervals were computed for every comparison.
- Presenting multiple pairs of data that can't be directly compared, significance was indicated using multiple unpaired, parametric, two tailed T-tests, using the Holm-Sidak method with a P-value of <0.05 (* in all cases). For example, visual GFAP expression on three conduits.

Statistical significance was accepted for the tests where $p < 0.05$ (* for all).

6 Results – Scaffold Engineering

6.1 Introduction and Aims

Due to the physiological nature of the white matter of the spinal cord, an aligned nanofibre design was chosen. This white matter consists of long lengths of axons with relatively few cell bodies and provides a relatively simple tissue segment to target in repair. It was hypothesised that providing aligned nanofibre may present surviving axons with the physical cues needed to boost natural regeneration and reorganisation that can occur in this tissue segment.

The nanofibre scaffolds utilised in this project were manufactured using 'electrospinning'. The process is highly dynamic in that multiple process parameters can be altered, giving nanofibre tuneable properties. It was possible to modify fibre diameter, orientation, membrane thickness, pore size, material type and surface properties. In this case, aligned nanofibre was needed in almost all cases owing to the physiological nature of the white matter in the spinal cord. However, in later parts of this study, some randomly aligned fibre was utilised where direct neuronal guidance was not necessary.

Non-biodegradable Polyacrylonitrile was chosen to form the basis of the fibre scaffolds in this study. This synthetic polymer has ideal biologically inert faculties (Zhang, X. et al. 2018) and long-term stability (Zhang, X. et al. 2018, Al-Enizi et al. 2018) – some polymers can be engineered to degrade but in this study stability was favoured. This is because it was hypothesised that maintaining the physical guidance cues provided by the scaffold would be useful. Further, no bi-products of degradation would need to be considered. The molecular structure of PAN is shown in figure 33.

Figure 33: Molecular structure of Polyacrylonitrile (PAN) (Rianjanu et al. 2018).

PAN is innately hydrophobic and so Jeffamine® ED-2003 was chosen to be mixed in with the chosen solvent (N, N-Dimethylformamide 944 kg/m^3 (Fisher scientific, UK)) at either 1% or 5% (w/v) to vary hydrophobicity from hydrophobic to hydrophilic and an intermediate level. Jeffamine® ED-2003 (Huntsman, Holland BV) is a water-soluble aliphatic diamine which has been derived from propylene oxide capped polyethylene glycol (Huntsman 2019). The molecular weight is around 2000 and the molecular structure is shown in figure 34. The presence of amine groups (and perhaps also the abundance of oxygen) on this molecule means that when introduced to PAN with the relevant solvent, it changes the hydrophobicity of the resultant polymer and spun fibre.

Figure 34: Molecular structure of Jeffamine®-ED-2003 (Huntsman, Holland, BV) (Huntsman 2019).

The aim of this section of the study was to identify a candidate nanofibre scaffold specification that was likely to perform well in cell culture. This should have robust faculties but should not be too thick to allow high resolution imaging and other analytical procedures. Further, the nanofibre scaffold should have reproducible fibre diameter and pore size, and crucially modification with Jeffamine® should have a minimal effect upon fibre diameter, pore size and membrane thickness – the single modified attribute should be hydrophobicity whilst maintaining a consistent manufacturing process and cell environment. Results indicated that 10wt% PAN with or without Jeffamine® would most likely be suitable for cell culture for these reasons.

In this investigation, certain electrospinning conditions were kept constant. Specifically, the polymer was always spun with a syringe pump injection rate of 1ml/hour. The distance between the needle and the rotating drum was always 30cm. Temperature was maintained at 18°C and humidity at 65% Relative Humidity (RH). The voltage passed through the needle was maintained between 19 and 24kV dependant on the weight percent of the polymer in question – though 10wt% PAN was always spun at 19kV.

6.2 Characterising Polymer Pre-spin

Once dissolved overnight (see materials and methods for specific recipes), electrospinning formulations existed in liquid form. These were characterised using a HAAKE™ CaBER™ 1 Capillary Breakup Extensional Rheometer as shown in figure 35 below. From this investigation, shear viscosity and calculated breakup time could be established with changing weight percentage of PAN and Jeffamine®. In this experiment, weight percent of PAN was varied between 8-12wt%. Having initially calculated shear viscosity of PAN, Jeffamine® of 1 and 5% was added to 10wt% PAN which showed a predictable intermediate viscosity of the weight percentages tested.

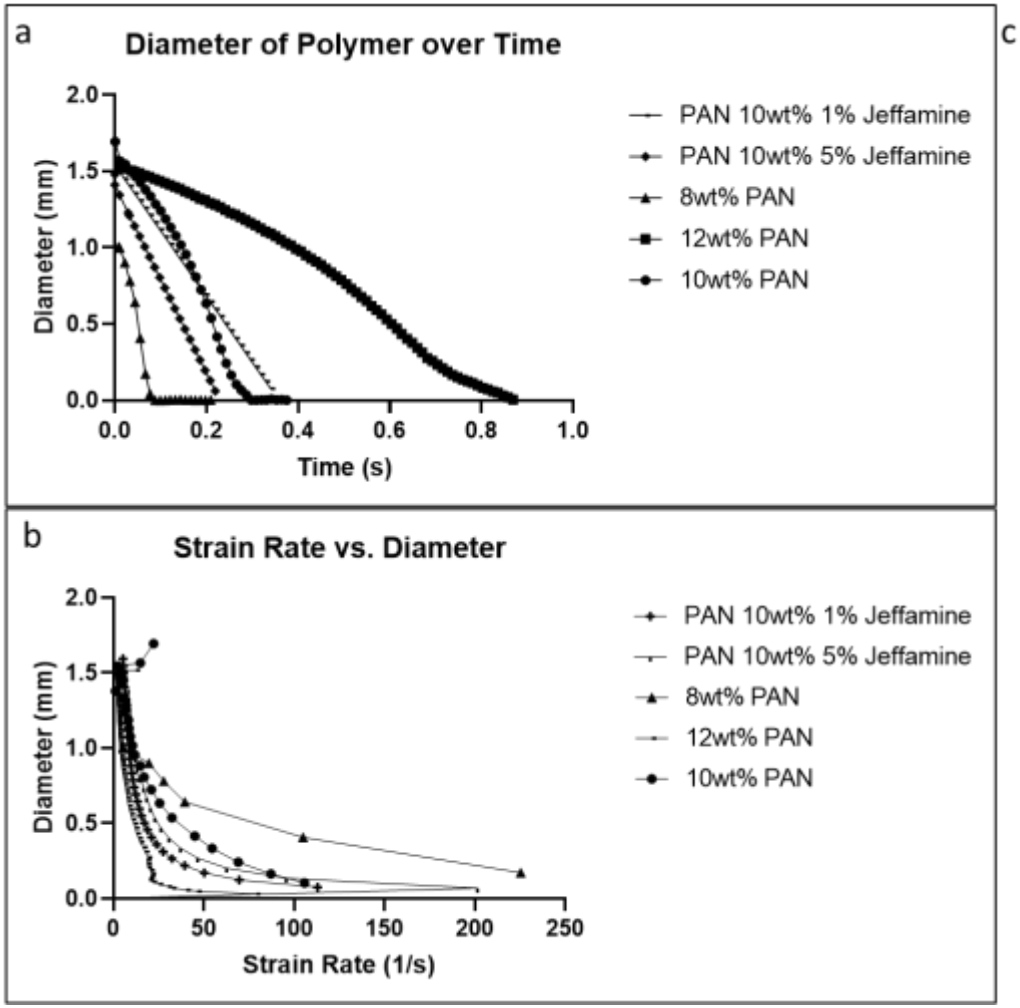

c

Polymer Mix	Shear Viscocity/ Pa.S	Calculated Breakup Time/ Seconds
8wt% PAN	2.60E-01	7.86E-02
10wt% PAN	6.80E-01	2.98E-01
12wt% PAN	2.17E-00	8.61E-01
10wt% PAN+ 1% Jeffamine	9.87E-01	3.58E-01
10wt% PAN+ 5% Jeffamine	7.03E-01	2.29E-01

Figure 35: Physical properties of polymer solutions. a. Change in diameter of the polymer columns within the 'HAAKE™ CaBER™ 1 Capillary Breakup Extensional Rheometer' over time. b. Change in strain rate in the same polymers plotted against diameter. c. Table presenting the shear velocity and calculated breakup times in investigated polymers.

Results showed an increasing shear viscosity as the weight percent of PAN increases. The calculated breakup time follows a similar pattern. The 12wt% PAN presented challenges, in that viscosity and break up time was particularly high, meaning maintaining a constant flow rate was difficult.

In all electrospinning runs, a standardized flow rate was maintained for manufacturing consistency. Further, all formulations were run through a 1/31 inch bore size PTFE tubing (Altec, UK) and 21-guage tube grade 304 needle (Stainless Tube and Needle, UK). To ensure a consistent flow rate was maintained despite the viscosity differences, a robust NE-1002X Syringe pump (New Era Syringe Pump Systems Inc, USA) was utilised, and the system run for a short time prior to the application of voltage to ensure the required flow rate was achieved. Voltage applied to these weight percentages had to be adjusted to ensure a consistent flow and spread of polymer onto the grounded drum. 19kV was sufficient to spread 8wt%, though an increased voltage of 24kV was required to achieve the same spread with 12wt% (Judged visually).

PAN 10wt% showed an intermediate viscosity that was deemed most suitable for electrospinning given that the polymer would have to be pushed from a syringe pump, through tubing and out of a needle at a steady rate. The shear viscosity of 10wt% PAN does not notably change with the doping of 1 or 5% Jeffamine® as intended.

6.3 Aligned Nanofibre

Aligned nanofibre scaffolds may be manufactured using the laser-cut sheet method shown in the materials and methods section 5.2.1. This design was perfected historically prior to the start of this investigation and allows efficient manufacture of unidirectionally aligned nanofibre within a handleable, central elliptical region.

Using PAN and Jeffamine® in combination, aligned fibres were spun with varied weight percentage and using a varied polymer deposition volume to assess properties. Having initially investigated PAN without Jeffamine®, it became clear that 10wt% provided a highly reproducible fibre diameter. It was for this reason that when the investigation moved to characterise doping with Jeffamine® that 10wt% PAN was chosen as a stable and unchanging mix.

The first investigation carried out analysed changing fibre diameter as weight percentage of PAN-DMF was varied from 8wt% to 12wt%. In this study, 1ml/hour and 1ml total deposition were maintained throughout. Fibre diameter and pore size were ascertained by imaging gold coated samples using Scanning Electron Microscopy (Phenom ProX SEM). In-built Phenom FiberMetric software defined fibre diameter from 100 fibre regions in each sample. Outliers were generated where the software picked up two fibres instead of one for example. Outliers were removed where necessary within reasonable limits. Figure 36 presents this

data in the form of raw SEM images (5000x magnification) and the spread of fibre diameters (including error bars, indicative of reproducibility).

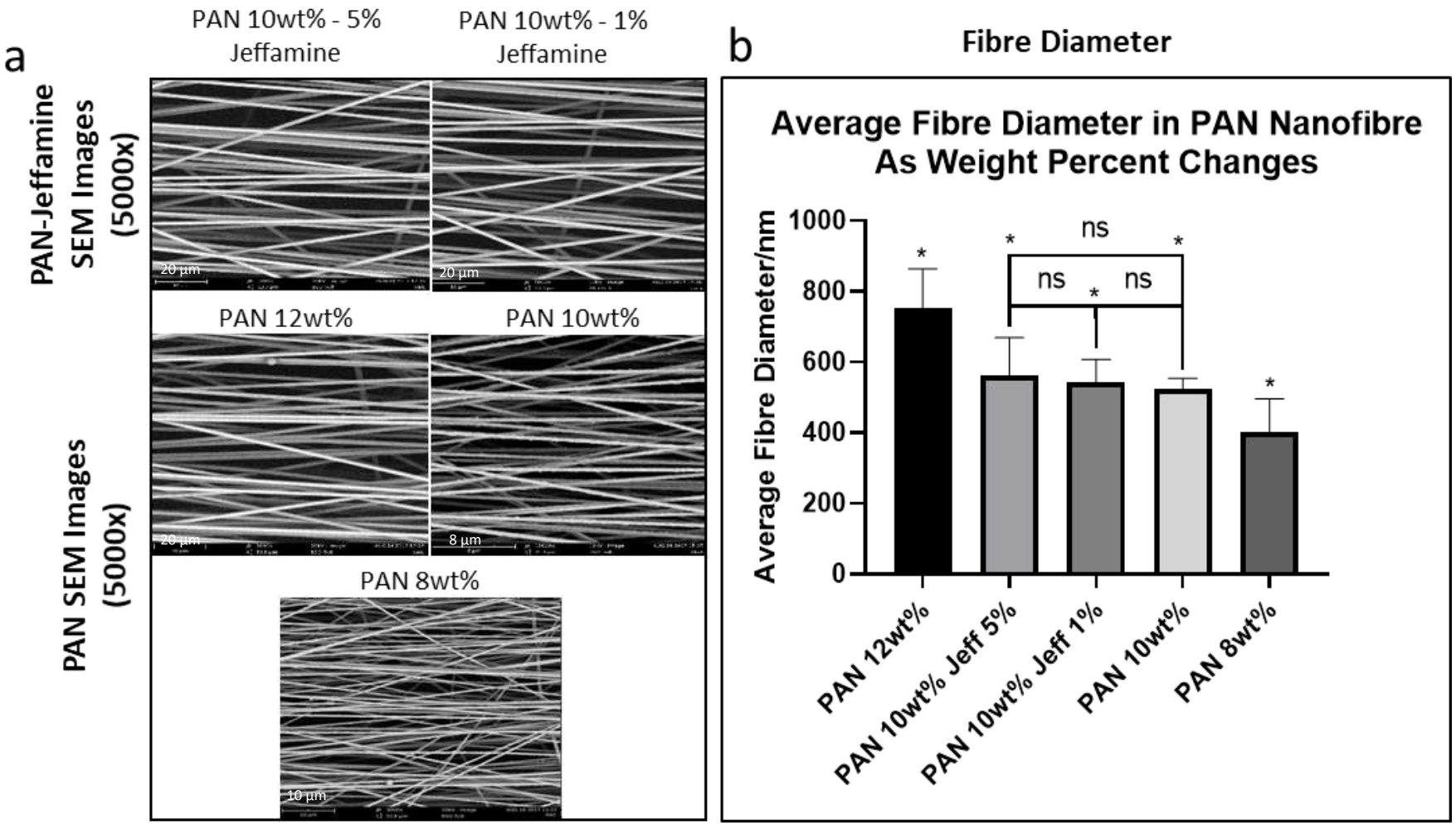

Figure 36: Change in fibre diameter with weight percentage of PAN and addition of Jeffamine. a. SEM images obtained from a Phenom ProX Desktop SEM at 10kV. Images were taken at 5000x magnification. b. Fibre diameter as calculated by taking an average of 100 sites per sample in each case and analysing using the onboard Phenom Fibremetric Software. Significance was assessed using a one-way ANOVA with Sidak's multiple comparisons test comparing all values against each other, with a P value of <0.05 (*), 'ns' indicates a relationship without significance.

Results showed an increase in weight percentage of PAN leads to a steady average increase in fibre diameter. The only insignificant differences in fibre diameter as a product of spinning varying weight percentage of PAN was between 10wt% PAN, 10wt% PAN + 1% Jeffamine® and 10wt% PAN + 5% Jeffamine®. Introducing 1 and 5% Jeffamine® into 10wt% PAN increases fibre diameter slightly on average but not significantly. Spinning PAN at 10wt% showed aligned, reproducible manufacture of nanofibre of a mid-range fibre diameter.

OCT analysis was used to define the membrane thickness of aligned fibre sections. Once again, PAN weight percent was varied between 8 and 12wt% and deposition volume between 1 and 2ml. Jeffamine® was added at 1% and 5% of total PAN mass (see materials and methods section) when mixing with the chosen solvent (N, N-Dimethylformamide 944 kg/m^3 (Fisher scientific, UK)). It was decided that Jeffamine® was to be added to 10wt% PAN where fibre diameter had been deemed reproducible and intermediate in the study above. Nanofibre was imaged and later analysed using ImageJ by measuring 10 random points along the aligned section of the membranes and generating an average. Figure 37 presents the spread of membrane thicknesses as both weight percent and deposition volume changes.

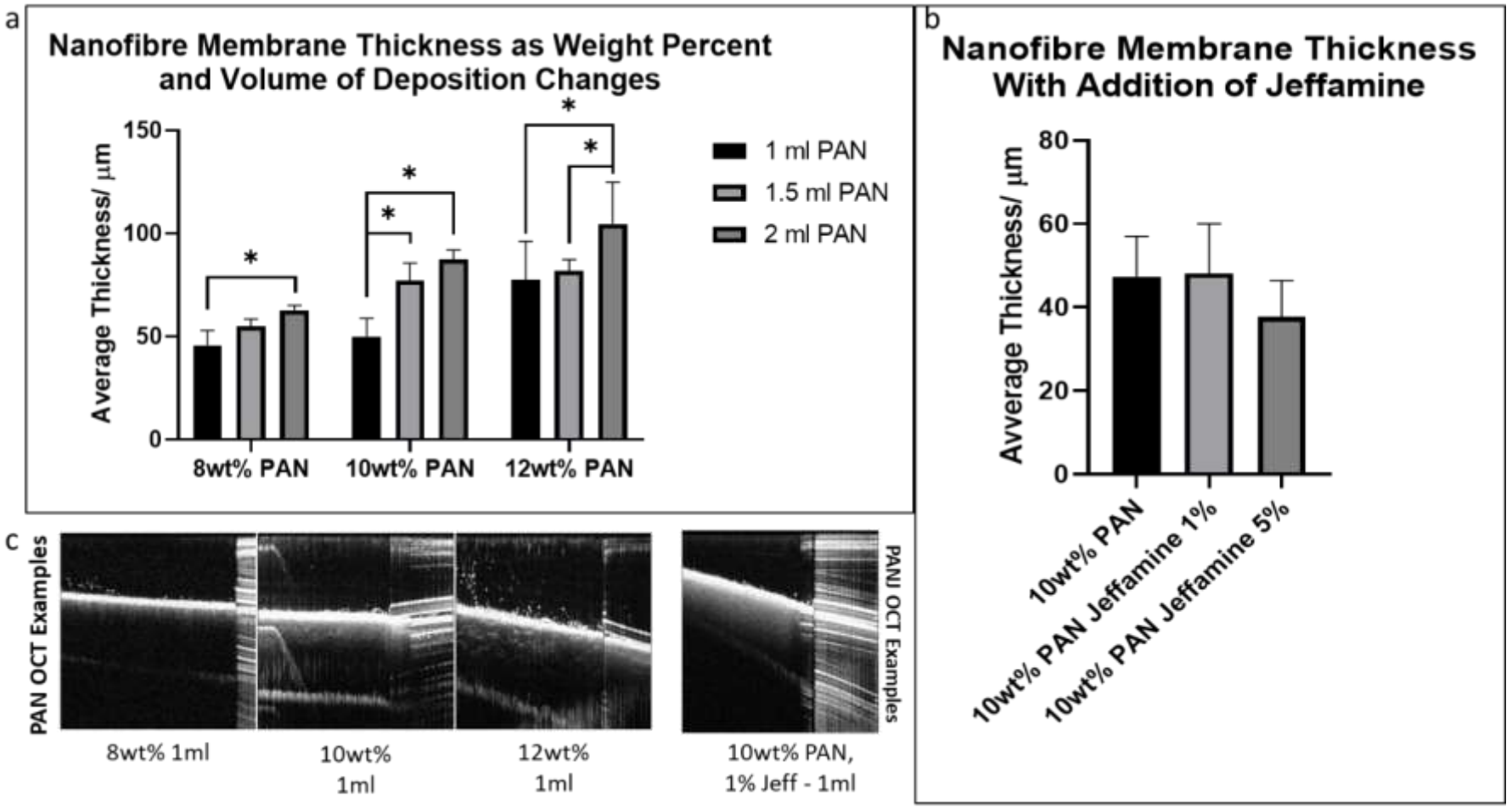

Figure 37: Membrane thickness changes with deposition volume modification. a. Measure of nanofibre membrane thickness in 1-2ml deposition runs using OCT analysis in 8-12wt% PAN. b. Nanofibre membrane thickness in 1ml deposition runs using OCT analysis in PAN 10wt% + Jeffamine®. c. Images of membranes as viewed on the OCT - ImageJ was used to measure average membrane thickness using said image examples (see materials an methods section 5.2.1). In 'a', Significance was assessed using a two-way ANOVA with Sidak's multiple comparisons test with P<0.05 indicating significance (*). In 'b', Significance was assessed using a one-way ANOVA with Sidak's multiple comparisons test comparing all values against each other, with P<0.05 indicating significance (*).

Data suggested that increasing deposition volume from 1ml to 2ml significantly increased matt thickness in each case, though this increase was non-linear and perhaps not as much as was expected. Seemingly ~80% of deposition occurred after 1ml and the following 1ml accounts for comparably less. It is possible that this was because as deposition occurred, the grounded detector became increasingly covered in nanofibre and the product was a reduced leakage path to ground and charge repulsion causing fibre to be deflected further from the centre line defined by the needle. This occurrence could be investigated in future work if time and finances allowed. The 10wt% specification provided a reliable mid-point in matt thickness of the variables analysed, with a distinct increase in matt thickness where 12wt% PAN was used even at 1ml deposition. The limit for high resolution imaging across a 3D fibre matrix was later defined to be ~40µm and as such, to ensure both imaging capability and structural integrity of the nanofibre, this reproducible mid-point was chosen to be taken forward for Jeffamine® doping. Results indicated that increasing deposition volume of 10wt% PAN even to 1.5ml from 1ml would have a significant effect upon membrane thickness and so care was taken going forward to ensure the deposition volume was kept consistent. Doping 10wt% PAN with 1% and 5% Jeffamine® at 1ml deposition did not significantly change the membrane thickness from the baseline as intended.

Having identified 10wt% PAN as a likely suitable candidate for beginning cell culture, a brief investigation into the effect of changing deposition on pore size (and fibre diameter) was carried out. Specifically, deposition of 0.5ml (30-minute spin), 1ml (1 hour) and 2ml (2 hours) were examined. Figure 38 presents the spread in fibre diameter and pore size as these parameters were changed. The data was obtained using Phenom Fibremetric software from SEM images of gold coated samples. The software automatically identified 100 pore regions (regions where a black background was detected) and 100 fibre regions. In both cases, some outliers were created, for example where two fibres ran parallel but were counted as one. Outliers were removed where necessary within reasonable limits. This investigation also allowed assessment of the reproducibility of fibre diameter with changing deposition volume.

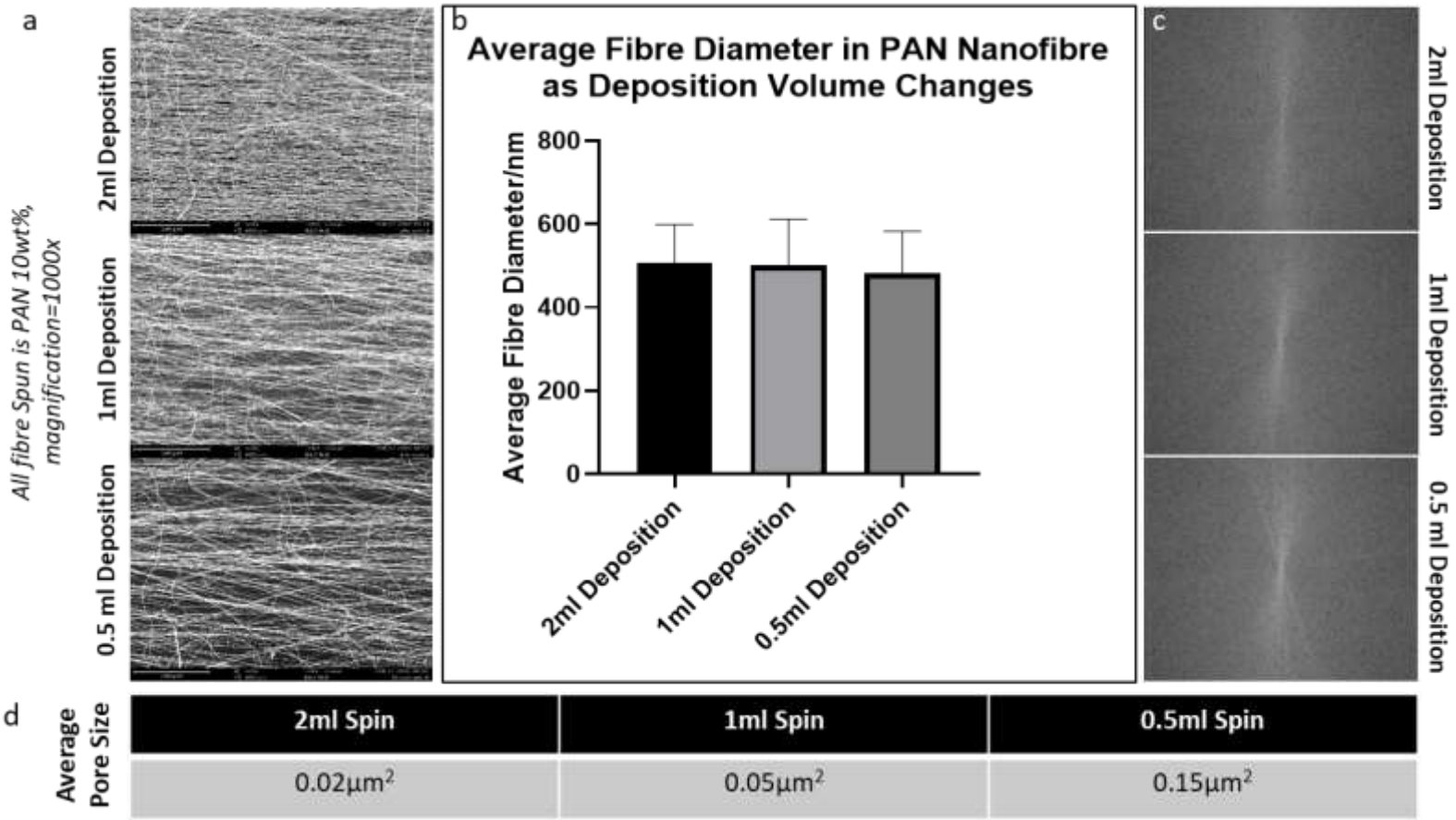

Figure 38: Changes in fibre diameter, pore size, and alignment with changing deposition volume. a. SEM images of gold coated (10nm thickness) nanofibre scaffolds (of various deposition volumes) with images acquired using a Phenom ProX Desktop SEM. b. Using the images, in-built Phenom Fibremetric Software was used to analyse fibre diameter from 100 random regions per sample. c. FFT analysis of nanofibre alignment using ImageJ analysis on the shown SEM images. d. Phenom Fibremetric Software was also used to calculate average pore size. Significance was assessed using a one-way ANOVA with Sidak's multiple comparisons test showing no significance between compared variables $P<0.05$ (*).

Results confirmed that indeed, changing deposition volume had no significant effect upon fibre diameter where 10wt% PAN was maintained in all cases. However, reducing deposition volume led to an increase in pore size. This can likely be attributed to both alignment and membrane thickness – at low deposition volumes, alignment was visually less efficient. FFT analysis showed that alignment was visually superior at 1ml and 2ml compared to 0.5ml deposition where spread was greater.

It was known that PAN is hydrophobic but doping with 1 and 5% Jeffamine® changes this quality. Figure 39 presents the changing water contact angle on the surface of 8-12wt% PAN and 10wt% PAN+1/5% Jeffamine®. A drop shape analyser was used to assess contact angle in each case as shown in the example images at the bottom of figure 40. An angle over 90° indicates hydrophobicity and under 90° hydrophilicity (Villa et al. 2018, Tran, Webster 2013). Measurements were taken (as close as possible to) 2 seconds post water droplet deposition.

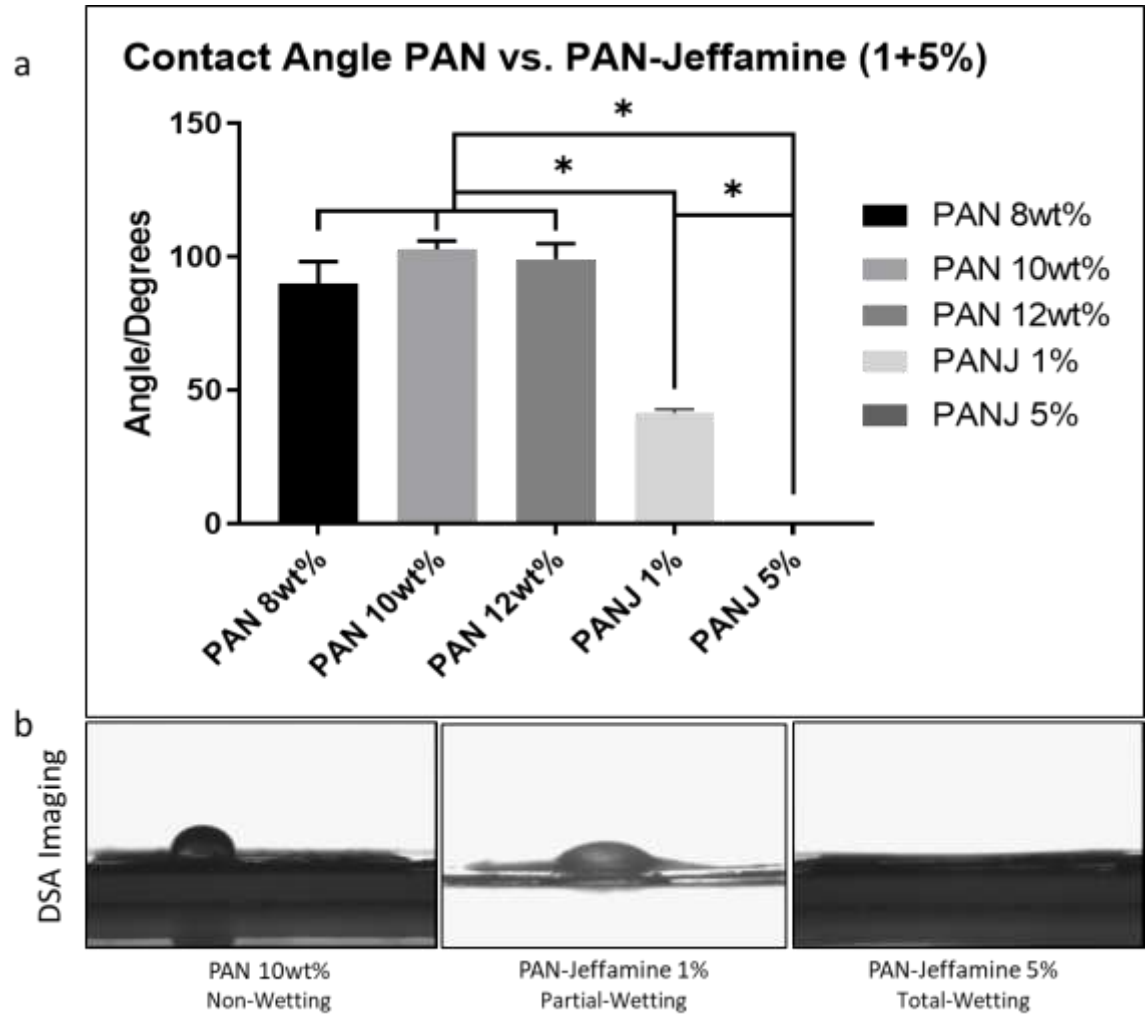

Figure 39: Contact angle analysis with PAN and Jeffamine mixes. a. Analysis of contact angle in 8-12wt% PAN and 10wt%PAN+Jeffamine® – said contact angle is indicative of hydrophobicity. b. Example DSA Images from which contact angle is derived. Fibre always ran into the camera angle (in and out of the page). Significance was assessed using a one-way ANOVA with Sidak's multiple comparisons test with P<0.05 (*).

Results indicated that PAN remains consistently hydrophobic irrespective of weight percentage (no significant change was seen). Introducing Jeffamine® lead to a significantly reduced contact angle in both cases. Adding 1% Jeffamine® lead to a contact angle of around 50° and 5% Jeffamine® lead to a totally hydrophilic (total wetting), contact angle. Introducing more amine groups onto the surface of PAN (the result of doping PAN with Jeffamine®) changed its interaction with water (and it was hypothesised that this would also change interaction with cells – this was explored later in chapter 7). It was decided that either a completely hydrophobic or completely hydrophilic surface was most likely to be useful within this study, though some investigation was carried out into the mid-range alternative.

In the case of aligned fibre, it was concluded that 10wt% PAN +/- Jeffamine® was to be taken forward for cellular testing as a most likely candidate.

6.4 Random Nanofibre

As mentioned earlier, aligned fibre formed the basis of most of experiments carried out within this investigation, however in a few cases, random nanofibre was used (largely where alignment of glia was not necessary). Having chosen 10wt% PAN and a 1ml deposition as a good candidate to take forward into cell culture (due to reproducibility, suitable 3D scaffold thickness, a robust nature and having hydrophilic and hydrophobic alternatives), these conditions were recreated in random nanofibre also. No mid-range 1% Jeffamine® was investigated as it was not deemed necessary. Instead, 1ml 10wt% PAN was compared only to 1ml 10% PAN+5% Jeffamine®. Figure 40 presents a summary of this data. Included are gold coated SEM images of random 10wt% PAN and 10wt% PAN + 5% Jeffamine®. These were analysed using the Phenom Fibremetric * Software as above for fibre diameter. Random fibre arrangement (cross-over) lead to a greater incidence of outlier generation and as such here, 20 samples were selected per sample of the original 100, ensuring each was of good quality and an average taken. Using a combination of OCT imaging and ImageJ analysis, fibre membrane thickness was ascertained. Finally, contact angle (hydrophobicity) of both fibre types was obtained using DSA analysis.

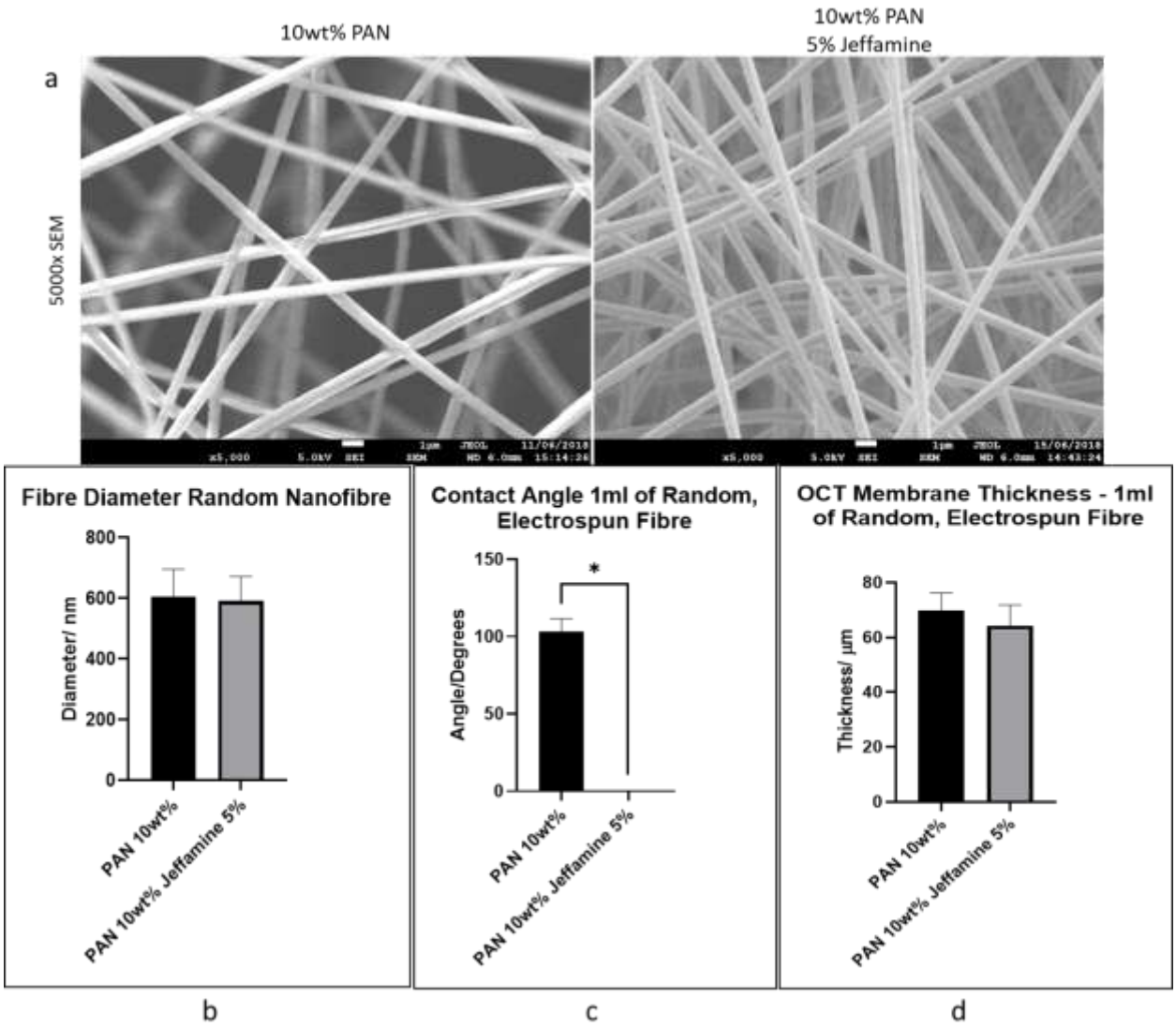

Figure 40: Random nanofibre analysis. a. SEM images obtained of randomly aligned 10wt% PAN and 10wt% PAN+5% Jeffamine® nanofibre using the Phenom ProX Desktop SEM on gold coated microplate samples. b. Comparison of fibre diameter as calculated using the in-built Phenom Fibremetric software on 100 random fibre regions and taking an average per sample. c. An assessment of contact angle using the DSA on 10wt% PAN with and without 5% Jeffamine®. d. An assessment of membrane thickness using OCT analysis and analysing the images using ImageJ and taking 10 random regions. Significance was assessed using a two-tailed, parametric, unpaired t-test with Welch's correction with a P-value of <0.05 (*).*

Results showed no significant difference in fibre diameter when 5% Jeffamine® was introduced to the random fibre. A significant contact angle difference was intended when 5% Jeffamine® was introduced. The contact angles seen were consistent with those seen in aligned fibre. There was no significant difference in OCT membrane thickness when depositing 1ml of 10wt% PAN versus 1ml 10wt% PAN+5% Jeffamine® in random conformation. The trend seen was comparable to that observed when adding Jeffamine® to aligned fibre also.

Manufacturing randomly aligned nanofibre with the same specification with comparable fibre diameter, membrane thickness and contact angle was important in ensuring later cellular optimisation was applicable in this scaffold alignment also.

6.5 Electrospray Modification

Electrospraying is a technique that works in much the same was as electrospinning (see methods). In this project, an electrospray chamber was developed in-house, designed in AutoCAD and manufactured from Perspex cut to size with the SP500 CO_2 Trotec laser. Applying a high voltage to a needle attached to a syringe pump allows deposition of nanodroplets of material onto a sample placed above a grounded microplate. This sample can be deposited for example with bioactive proteins such as collagen as shown in figure 41. It was theorised that this patterning could be made highly specific and adds a level of control to this bio-engineering process.

Figure 41 presents the design process from AutoCAD through to manufacture. The device was then tested as is detailed below.

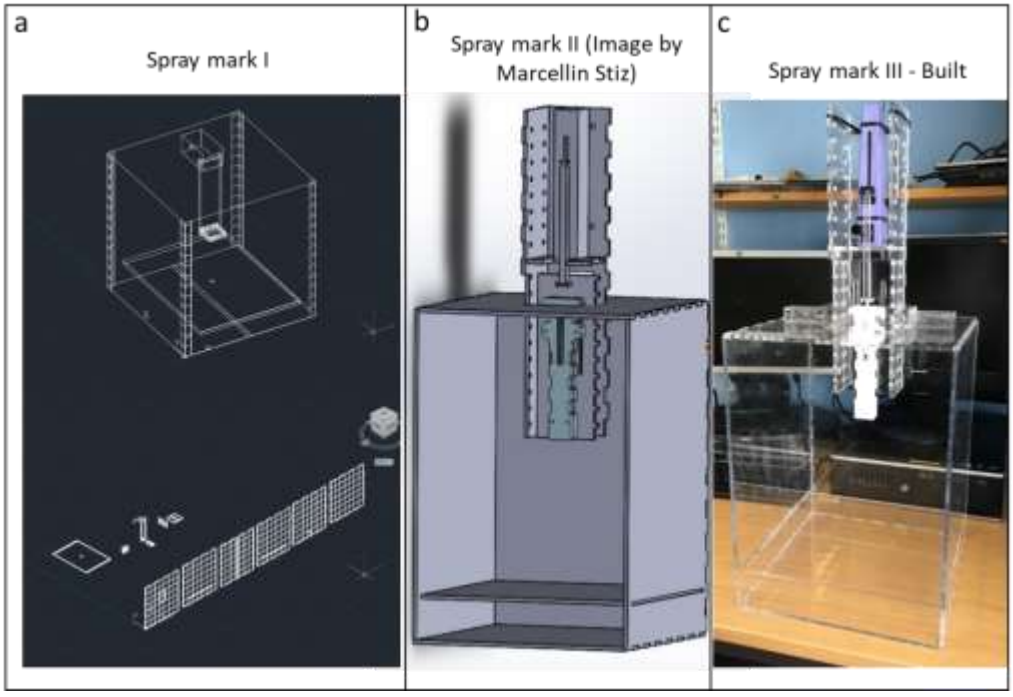

Figure 41: Panel of images depicting the development of Electrospray technology from design through to manufacture. a. AutoCAD screenshot depicting the initial build design. b. SolidWorks image depicting a later design in collaboration with Marcellin Stiz. c. The finished product ready for testing.

In this investigation, unpolymerised collagen (6mg/ml) was sprayed for 40 minutes on 10wt% PAN (1ml deposition). The design process is presented in figure 42 along with SEM images and fibre diameter obtained using Phenom Fibremetric * Software as before. Fibre diameter was compared to that of unsprayed 10wt% PAN fibre as a control.

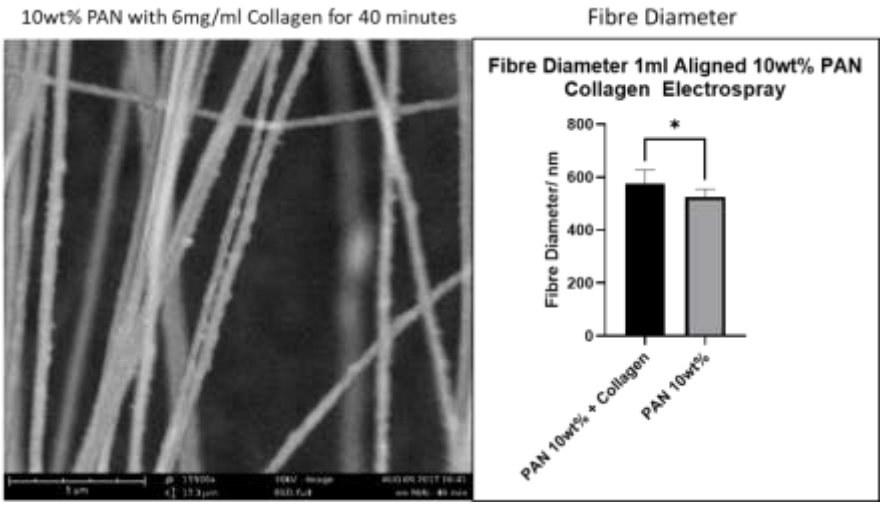

Figure 42: Electrospray testing using Collagen on 10wt% PAN nanofibre. SEM image obtained and analysed for fibre diameter using Phenom Fibremetric software and analysis of an average of 85 readings per sample. Significance was assessed using a two-tailed, parametric, unpaired t-test with Welch's correction with a P-value of <0.05 (*).*

Results showed what appeared to be visible deposition of collagen on the surface of PAN. This was evidenced further by a significantly increased average fibre diameter compared to control. The experiment provided preliminary evidence to suggest that electrospray may be a useful tool in future experimentation – perhaps in coating nanofibre with protein that may boost cell viability or attachment for example. Further experimentation, perhaps with mass spectrometry would be required to confirm the presence and functionality of this protein, though no more trials were carried out due to time and financial limitation.

6.6 Sterilisation Techniques

Prior to cell culture, the scaffolds had to be sterilised - they were not spun in a totally sterile environment. Various techniques were tested to achieve sterility – these were either wet or dry. This investigation had already been carried out by colleagues in the development of best practise protocols and so only a basic investigation was executed. An Autoclave (Ambassador, Serial no #1989, UK) was run at 121°C and 100kPa above atmospheric pressure for one complete 90-minute cycle. A 254nm 4.9W UVC lamp was used for 1 hour at 50cm distance. Lastly, a 70% Ethanol (with distilled water) soak was carried out for 30 minutes before washing with fresh PBS and DMEM F-12 media (Lonza, UK). A control was used in the form of unsterilized nanofibre straight from the production line. Sterility assessments were carried out in microplate and broth cultures. In each case nanofibre was left for three days to cultivate and then assessment of colony forming unit (CFU) number (on petri-dishes) and broth colour was carried out. Figure 43 presents images of both the broth and microplate cultures carried out in addition to a table summarising results.

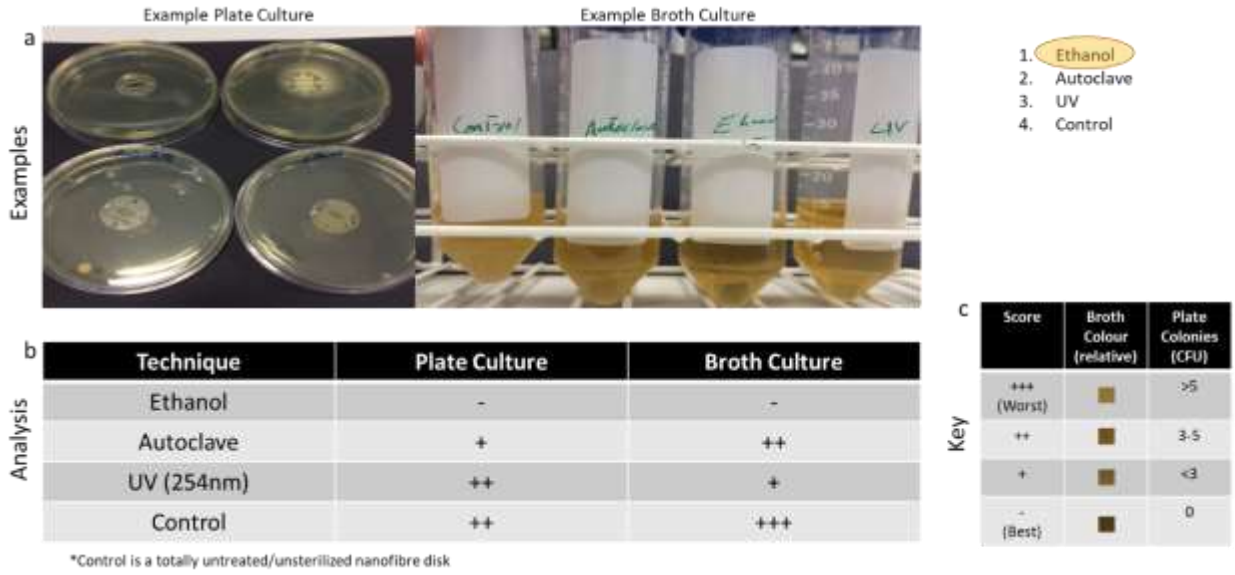

Figure 43: Sterilisation techniques trialled on PAN nanofibre. a. Images depict both microplate and broth culture examples carried out to assess sterilisation efficiency. b. The table below breaks down the results with the accompanying key (c).

Results suggested ethanol (a wet sterilisation) performed the best, producing the clearest broth cultures and microplate cultures with the fewest CFU (after three days). The fact that this sterilisation technique was wet was deemed useful; as when fibre is wet, depositing cells in a small suspension droplet could mean that because of water tension, the said droplet may spread within the central aligned fibre ellipse and stay there, limiting cell attachment in this region of interest only. This was covered in more depth in chapter 7. Autoclave sterilisation proved too damaging in most cases to be a viable technique. UV sterilisation in most cases proved to be a viable option second to ethanol sterilisation, though in the image in figure 43 showed a large plate CFU. The effects of each sterilisation technique upon nanofibre properties was covered by Joseph Chemmarappally (Joseph Chemmarappally Thesis, submitted March 2019) who is a colleague in the same group whose results suggested that the best practise was a 70% ethanol soak. As such, a 70% Ethanol soak was used as the staple nanofibre sterilisation technique in all experimentation going forward. This technique was both simple and reliable.

6.7 Discussion

Prior to carrying out electrospinning it was possible to define the viscosity of the polymers of interest in their liquid form. Increasing weight percent of PAN from 8-12wt% correlated with an increasing shear viscosity and breakup time as was expected. It was noted that a shear viscosity of 9.51E-02 (6wt% PAN) created a fragile fibre that was difficulty to handle and so this specification was eliminated from the investigation. There was a notable difference in shear viscosity between 10 and 12wt% PAN which was seen in the viscous and difficult to spin 12wt% PAN. These data points correlated to tangible differences in

the electrospinning process. Data suggested that 10wt% provided a manageable viscosity for reliable electrospinning.

Aligned nanofibre can be successfully manufactured using the parameters employed in this investigation. These aligned fibres were deemed good candidates for recreating spinal cord tissue structure given the physiological nature of the spinal cord white matter.

Through experimentation it was possible to show that PAN nanofibre could be electrospun at 8-12wt%. Spinning at 10wt% PAN reliably produced aligned nanofibre with a reproducible fibre diameter. This weight percentage could be doped with 1% or 5% Jeffamine® with no effect upon pore size and a minimal effect upon fibre diameter. This doping also led to manufacture of either hydrophobic or highly hydrophilic nanofibre - or indeed (in the case of 1% Jeffamine®) a middle point nanofibre specification with reduced surface energy. 10wt% PAN was physically robust, handleable for cell culture and the manufacturing process was unproblematic –12wt% often clogged in the syringe due to viscosity and had at times unreliable flow rate during spinning as a result. A 1 ml deposition was appropriate in forming robust fibre that did not easily break at all weight percentages. This volume generated fibre membranes that were thin and following testing in later chapters (Chapter 7), permitted clear high-resolution cellular imaging and analysis. Crucially, changing deposition volume had no effect upon fibre diameter, only pore size. Particularly low volumes of deposition led to the degradation of alignment (as shown in 0.5ml 10wt% PAN deposition FFT analysis – figure 38). In the case of 10wt% PAN, using 1ml deposition, no significant difference in membrane thickness or fibre diameter was seen with the addition of Jeffamine®. In summary, a 1ml deposition of 10wt% PAN was chosen as a likely successful candidate to be trialled in cell culture.

Random nanofibre could also be manufactured using the same conditions into unaligned meshes. For cases in which aligned cellular morphology was less important in later experiments, optimisation of this fibre design was deemed appropriate. Here, using 10wt% PAN and 10wt% PAN+5% Jeffamine®, either a hydrophobic or hydrophilic scaffold could be manufactured reliably with little difference in pore size or fibre diameter (compared to one another).

Electrospray is a technique that can be carried out to potentially introduce nano-droplets of substance onto nanofibre scaffolds. It was used for example to deposit 6mg/ml collagen onto the surface of 10wt% PAN, though more experimentation is needed to assess the presence and functionality of this protein.

PAN (and Jeffamine®) nanofibre could be effectively sterilised using 70% ethanol soaking for 30 minutes, producing nanofibre that could be washed and used for cell culture. UV sterilisation was also a viable alternative. Table 5 summarises the core findings established within this line of experimentation.

Included in table 5 is pore size for the investigated weight percentages of PAN and PAN + Jeffamine investigated. This was calculated using the in-built Phenom FiberMetric software from 100 fibre regions in

each sample. Outliers were generated where the software mis-identified pores. Outliers were removed where necessary within reasonable limits. This data was included only in the summary data as it was considered preliminary and more work could be done to investigate it if time and finances allowed.

Aligned Nanofibre

Weight Percent PAN (1ml Deposition)	Average Pore Size /μm^2	Average Fibre Diameter /nm	Average Membrane Thickness /µm	Contact Angle / °
8wt%	0.1	400	45.7	90
10wt%	0.05	525	50	103
12wt%	0.03	753	78	99.1
10wt% + 1% Jeffamine	0.02	543	48.2	41.4
10wt% + 5% Jeffamine	0.02	560	41.3	0.0
PAN 10wt% Deposition Volume/ ml	**Average Pore Size /μm^2**	**Average Fibre Diameter /nm**	**Average Membrane Thickness /µm**	**Contact Angle / °**
1	0.05	525	50	103
1.5	0.03	*520	77	103
2	0.02	514	87	103

Random Nanofibre

Material	Average Pore Size/μm^2	Average Fibre Diameter/nm	Average Membrane Thickness/µm	Contact Angle / °
10wt% PAN	0.21	599.8	69.8	103.4
10wt% PAN 5% Jeffamine	0.19	569.6	61.7	0

*Table 5: Summary of aligned and randomly aligned nanofibre properties as defined during this investigation. * – Indicative of a predicted result, it wasn't deemed necessary to calculate this as 0.5ml 10wt% PAN was calculated for a wider understanding showing no significant difference.*

In this section the dynamicity of electrospinning using the rotating drum technique was highlighted. By changing certain system and process parameters, it was shown that the desired properties of nanofibre scaffolds could be produced consistently. This was an important feature and was essential in designing a nanofibre based implant which could be catered towards the cell types of interest. Having understood this optimisation process it could be applied to a multitude of other materials in future research.

Other groups, such as the Orr et all group (Orr et al. 2015) showed that aligned, electrospun scaffolds could be engineered using electrospinning with varying technique – this group used parallel copper electrodes. The group determined ethanol sterilisation to be a good technique and quantified fibre diameter using the same technique employed here. This evidence suggested that rotating drum electrospinning was just one

method that could be suitable for generating aligned nanofibre reproducibly. Indeed, assessment of the characteristics analysed in this chapter were comparable to those analysed by other groups. For example, the Ifkovits et al group (Ifkovits et al. 2009), the Yu et al group (Yu, L. et al. 2017), the Garg et al group (Garg, Bowlin 2011) and the Beilke et al group (Beilke et al. 2013) employed various electrospinning techniques including the rotating drum and air gap electrospinning methods to manufacture fibre materials with varying properties as shown by contact angle, fibre diameter, matt thickness and alignment analysis. In general, electrospinning provided a highly dynamic technique that could be utilised in various conformations to produce nanofibre of various materials with tuneable properties – the analysis of said properties is consistent in this study as by others.

7 Results - Cellular Integration

7.1 Introduction and Aims

Having established a viable protocol for the manufacture of a cellular scaffold, it was possible to begin testing the scaffold designs with cell populations of interest. The cell lines chosen for this investigation included the human neuroblastoma SH-SY5Y cell line and the human glioblastoma U-87 MG cell line top represent neuronal and glial populations respectively. Including both cell populations allowed development of a prosthesis design that could have the potential to support both key cell types. In this way, it was possible to optimise their interaction with nanofibre scaffolds.

The immortalised cell lines chosen have been widely used in literature (Zablocka et al. 2015, Yang, Z., Wang 2015). Human neuroblastoma SH-SY5Y is a cell line which may be differentiated to form long, functional axons – some groups have shown cells to be electrically active (Tosetti et al. 1998). Human glioblastoma U-87MG can be differentiated to produce an astrocytic lineage (Shi et al. 2013). In both cases, the cells derived are human, which provided certain species-specific relevance advantages over animal tissue slices for example. The limitations of utilising cell lines were known – these cells were immortalised and thus genetically not true neurones or glia (Kovalevich, Langford 2013). However, the advantage provided by these cell lines was not only a robust source of cells, but also clarity in the simplicity of single cell populations. Many groups attempt to engineer scaffolds with complex populations of stem-cell derived or primary tissue for example. This was considered to be a complex and unclear optimisation process. Instead, this investigation aimed at developing knowledge and design parameters from individual cell populations initially, before later building up complexity in a multiple-cell system. It was hypothesised that different cell populations may perform differently on different scaffold materials (and designs) and this hypothesis derived the novel approach to prosthesis design seen here. This approach involved engineering different 3D scaffold designs to cater for the cellular requirements of different populations brought together through layering of cellularised and acellular scaffolds as required.

Optimisation was needed for both cell lines to begin to understand the cell-material interaction in an implant that harbours multiple cell types. Initially, the cellular behaviour had to be understood on 2D plasticware. In figure 44, the two cell lines used in this study were imaged using an immunofluorescence microscope to highlight basic undifferentiated morphology - 50,000 of each cell line were seeded in DMEM F-12 and left to attach to the base of an adherent tissue culture microplate overnight before staining and imaging.

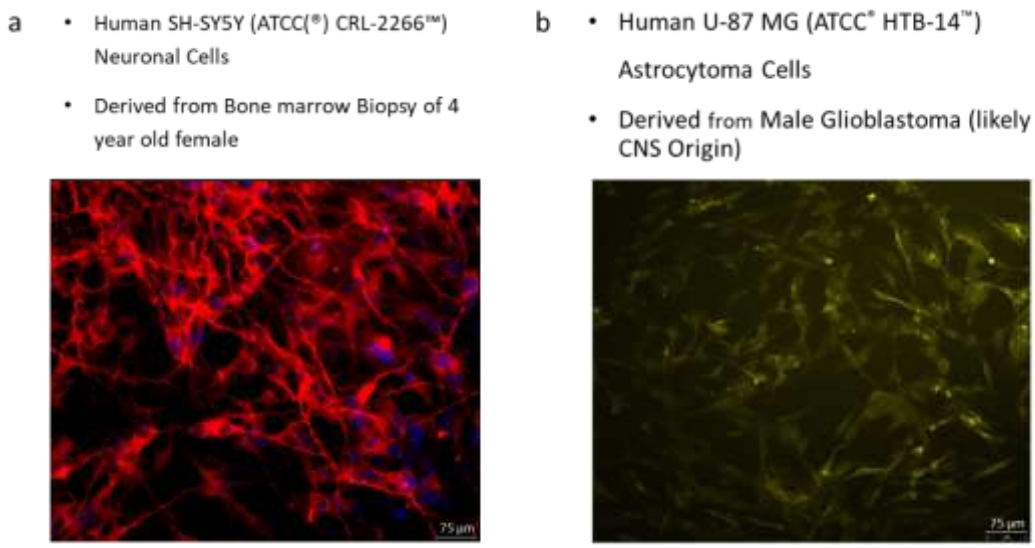

Figure 44: Immunofluorescence images showing undifferentiated cells. a. SH-SY5Y cells stained with anti-Beta-III (βIII) Tubulin primary antibody (and Alexa Fluor 568 secondary antibody - red) and DAPI nuclear stain (blue). b. U-87 MG cells stained with anti-GFAP primary antibody (and yellow Alexa Fluor 532 secondary antibody).

7.2 Cell Population Size

Having designed the scaffold's physical parameters including size and shape (see chapter 6), it was important to understand the best population sizes or cell density to start experiments. Determining the sensible cell capacity for these structures was a key point to establish in defining prosthesis specifications and understanding how it would perform in vivo.

First, a calculation was required to establish the comparable well microplate size required when experimenting with 1ml 10wt% PAN nanofibre. Certain assumptions were made in this calculation for the brief 2D comparisons that took place in this investigation. The top surface area of an aligned ellipse was 0.39cm^2 – in a given cross-sectional area, cells grew both on and between fibre strands and roughly traversed the surface of the structure, so this cross-sectional area was assumed constant throughout the structure. It was also known that cells migrated and elongated through the depth of the structure (see figure 45), making the entire depth functionally accessible. Nanofibre diameter was characterised as being small enough to be negated in terms of capacity of the structure. The thickness of 1ml 10wt% PAN was approximately 50±5µm. The surface area of the ellipse of aligned nanofibre is 0.39cm^2. By day seven, average differentiated SH-SY5Y axon diameter was calculated to be ≈5µm (4.6µm)**. It was assumed therefore that 10 axons diameters could fit side-by side within the depth of the nanofibre structure in use. Therefore, the equivalent functional surface area available to cells was calculated to be approximately 3.9 cm^2 (0.39cm^2 x 10 axon diameter sections). This was considered equivalent to a 12 well microplate (4cm^2 surface area). For consistency, the same plates were used for glial populations too.

** This was calculated based on SH-SY5Y cells that had been seeded at a density of 50,000 cells in adherent, 12 well microplates and left to adhere for twenty-four hours in supplemented DMEM F-12 media. They were then subject to differentiation using the DMEM F-12-based differentiation media detailed in chapter 5.2.3 for seven days before staining with anti-βIII Tubulin primary antibody and imaging using a Leica CLSM confocal microscope. Using ImageJ analysis, 10 random points along the axon length were measured in triplicate immunofluorescent images and an average axon diameter obtained. Notably, in vivo, axons can become much narrower as they elongate, however here, the clonal cells were given a minimum of seven-fourteen days of maturation time.

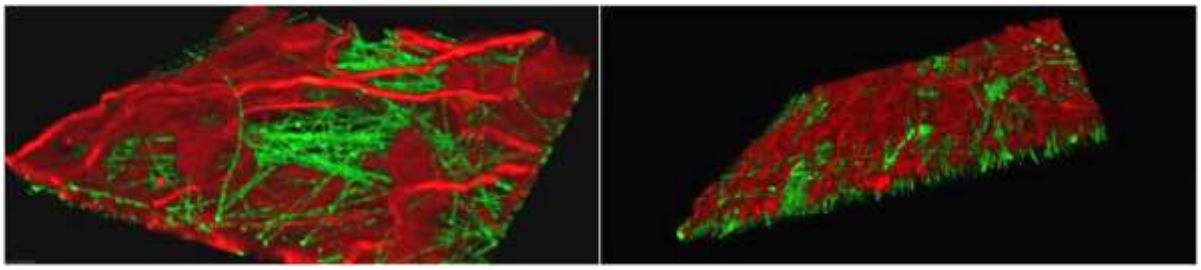

Figure 45: Image showing SH-SY5Y cells following a 7-day differentiation growing into aligned (right) and random (left) 1ml 10wt% PAN scaffold onto which it was seeded. SH-SY5Y were stained with primary βIII Tubulin antibody (and Alexa Fluor 568 secondary antibody - red) and imaged with a confocal (SP8) (Leica, UK) system at the Laser for Science Octopus Facility at STFC, Rutherford Appleton Laboratory. PAN auto-fluoresced green.

Having determined that the use of 12 well adherent microplates was acceptable, 50,000, 10,000 and 5000 cells per well were trialled in 2D tissue culture plasticware initially, to establish ideal population seeding size. Specifically, each trialled population size was seeded with SH-SY5Y cells in 12 well microplates and incubated for twenty-four hours for all cells to adhere (this was always the case in 2D or 3D). Cells were then subject to differentiation and images at day zero, one, two and three (of differentiation) taken using Light microscopy. Following this, using the population size deemed visually most appropriate (based on over-crowding), light microscopy was carried out after a further three days of differentiation in both SH-SY5Y and U-87 MG cells individually and in co-culture on 1ml 10wt% PAN aligned nanofibre. This time-period was chosen as evidence (Khwanraj et al. 2015) suggested that three days of low serum DMEM F-12 media (Lonza, UK), retinoic acid-mediated (Sigma-Aldrich, UK) differentiation was the minimum period before effects may be seen (see section 5.2.3 for culture condition details). Results are shown in figure 46.

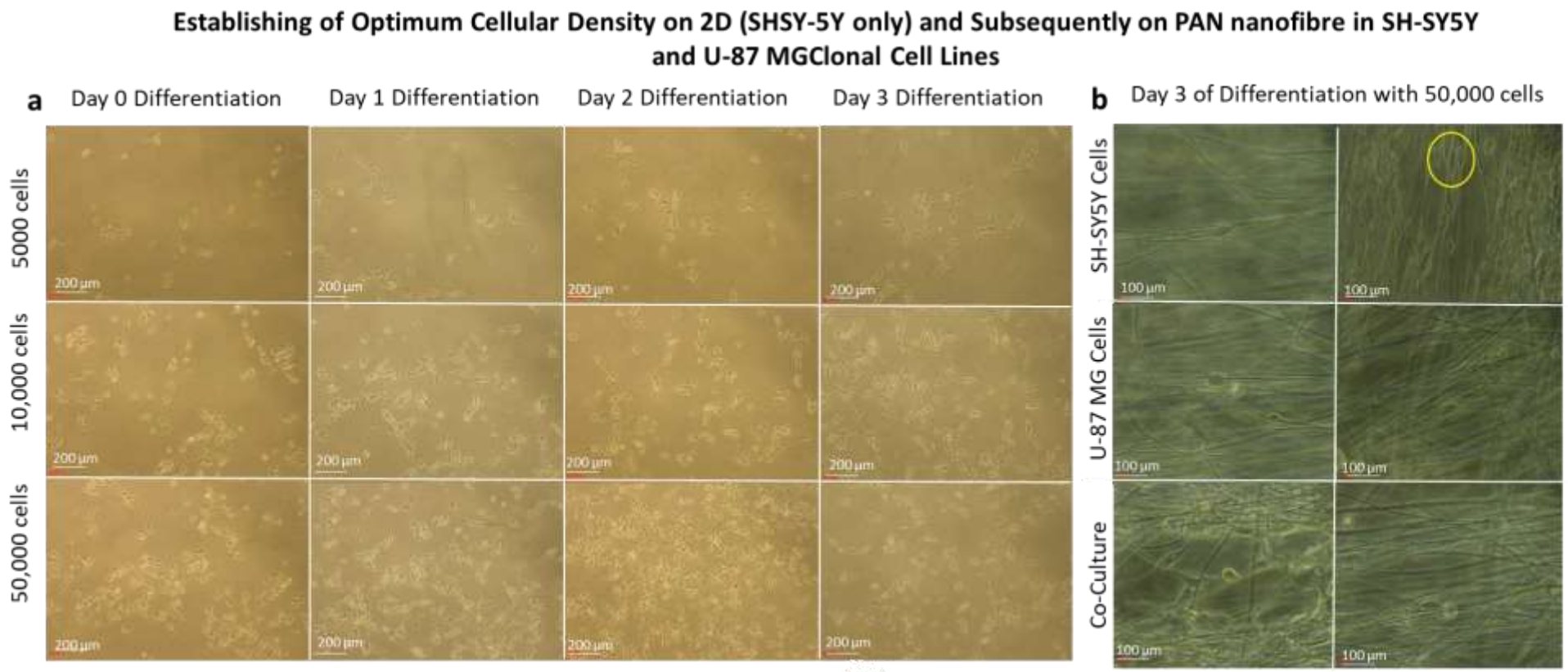

Figure 46: Assessment of optimum cellular density. a. Light microscopy images showing SH-SY5Y cells in 2D over three days of differentiation at seeding densities of 50,000, 10,000 and 5000. b. Light microscope images showing 50,000 SH-SY5Y, U-87 MG and co-cultured cells after three days of differentiation on 10wt% aligned PAN nanofibre. Yellow circle indicates some preliminary evidence of cellular navigation and possible elongation on nanofibre.

This population size study showed that using Light microscopy imaging on PAN nanofibre in both cell populations showed some basic maturation of SH-SY5Y and U-87 MG cells in that some axonal elongation was potentially observed. It was speculated that some cellular interaction of the two cell lines in co-culture was occurring, though to make any clear judgements, immunofluorescence staining was needed going forward. The 3D nature of nanofibre restricted the use of unlabelled imaging.

7.3 PAN Weight Percent Variations

In the previous chapter, aligned PAN nanofibre was manufactured in 8-12wt% (6wt% could not be made reliably). For a given deposition volume (1ml), changing the weight percentage of this nanofibre changed the fibre diameter and pore size. It was shown (in chapter 6) that 10wt% provided a scaffold that could be manufactured reliably, but these weight percentages needed testing with cells before a preferred fibre could be chosen. In the following experiment, 50,000 of both neuronal and glial cells were seeded independently on PAN nanofibre of 8-12wt%. After a twenty-four-hour incubation period in DMEM F-12 (10% serum) culture media, a seven-day differentiation using DMEM F-12 differentiation media (containing fresh retinoic acid) and low serum conditions was carried out (see section 5.2.3 for culture condition details). Cells were counted by staining with DAPI nuclear stain and analysing five random 1mm^2 fibre regions in triplicate samples using ImageJ analysis. Average counts are shown in figure 47.

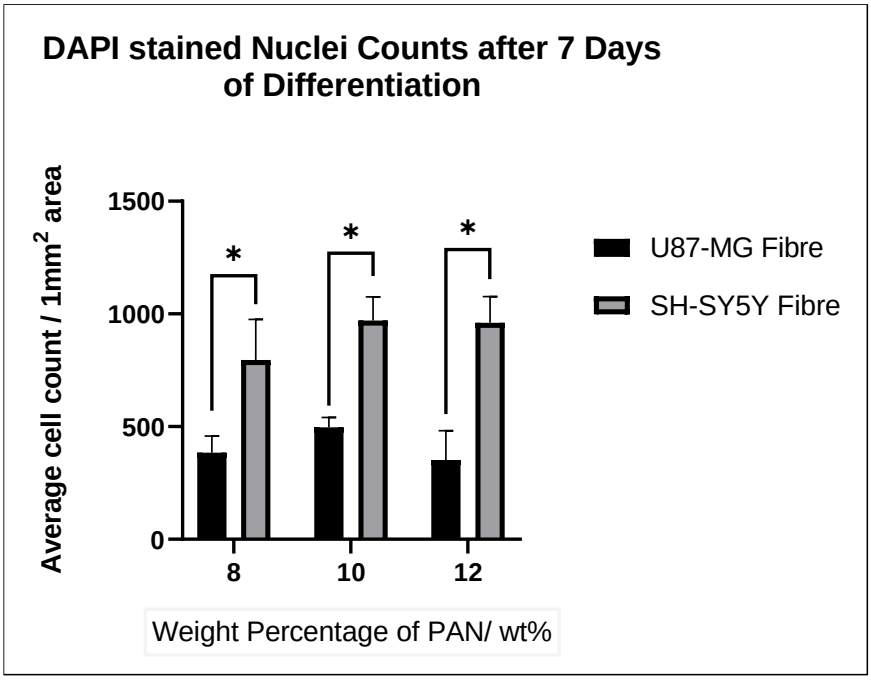

Figure 47: Cell counts of SH-SY5Y and U-87 MG cells on 8-12wt% aligned PAN nanofibre according to average DAPI-stained nuclear counts. Counting achieved using ImageJ Software, taking average counts at five random regions on three separate samples (it didn't matter which side was counted). Significance was assessed with a two-way ANOVA with Sidak's multiple comparisons test with P<0.05 (*).

Results highlighted two conclusions. The first of which was the higher cell counts (survival on fibre) of neuronal cells on PAN nanofibre over a seven-day differentiation period compared to glial cells. In both cases, cells were seeded at the same density, but neuronal attachment and maintenance appeared greater (based on nuclear presence) after seven days than their glial counterparts. This was the first piece of evidence that highlighted the potential effect of hydrophobicity on cellular viability across different cellular populations, though more experimentation was needed. The second, more pertinent finding was that both neuronal and glial cells showed reliable nuclear counts with little variation at 10wt% in particular. Neuronal nuclear count was also maintained in 8wt% and 12wt%, though variation was slightly higher (shown by standard deviation). Notably, glial population size (based on nuclear counts) remained more consistent across all weight percentages, but with the least variation in 10wt%.

This evidence was enough to identify 1ml 10wt% PAN as likely providing a suitable fibre diameter and pore size for ongoing cell culture experimentation in both cell lines. The reduced nuclear counts of glial cells was noted in this experiment and was followed up with viability and metabolic activity assays later.

7.4 Optimisation of Cell Seeding

Having investigated the change in population size with changing weight percent of PAN nanofibre, the next investigation focussed on the change in population size over a fourteen-day differentiation in the two cell lines. The initial insights into population size of the chosen clonal cell lines (SH-SY5Y and U-87 MG) on aligned, 10wt% PAN nanofibre was carried out by counting of DAPI-stained nuclei using ImageJ. In each case, five random locations were counted (1mm^2 regions) per sample (all in triplicate) and the mean taken. In addition, a complementary parallel experiment was carried out assessing DAPI expression on a microplate reader (also in triplicate). In this experiment, analysis was carried out not only on the nanofibre but also on the microplate below so that cell retention on fibre could be understood. SH-SY5Y (50,000 cells) and U-87 MG (50,000 cells) cell populations were seeded on aligned 10wt% PAN nanofibre. After twenty-four hours in a CO_2 incubator in high serum DMEM f-12 medium they were subject to fourteen days of low serum, retinoic acid mediated differentiation (see section 5.2.3 for culture condition details). Figure 48 presents the cell counts and DAPI expression in the two cell lines over a fourteen-day differentiation.

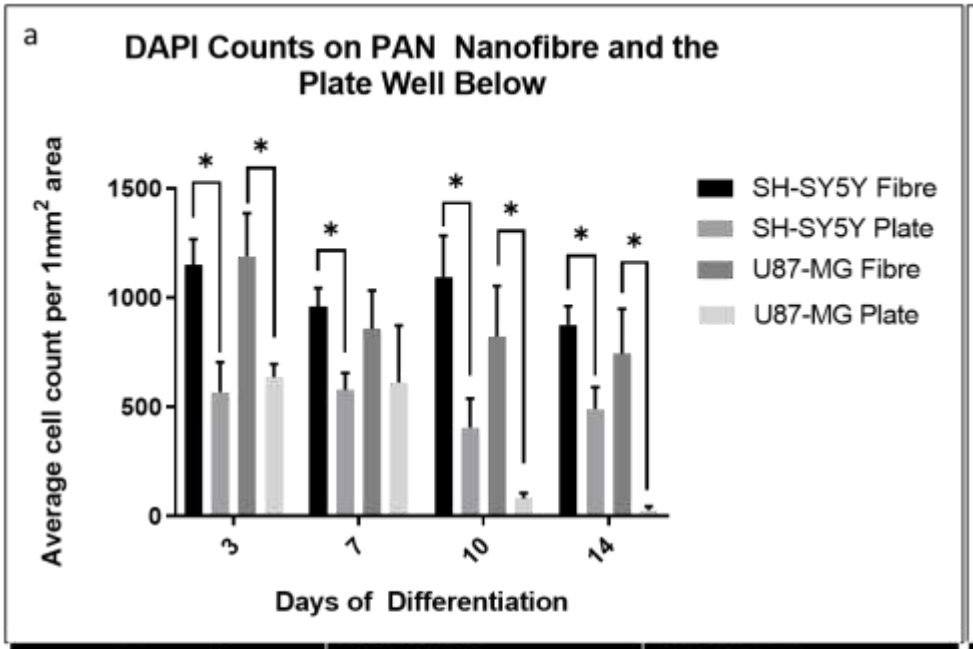

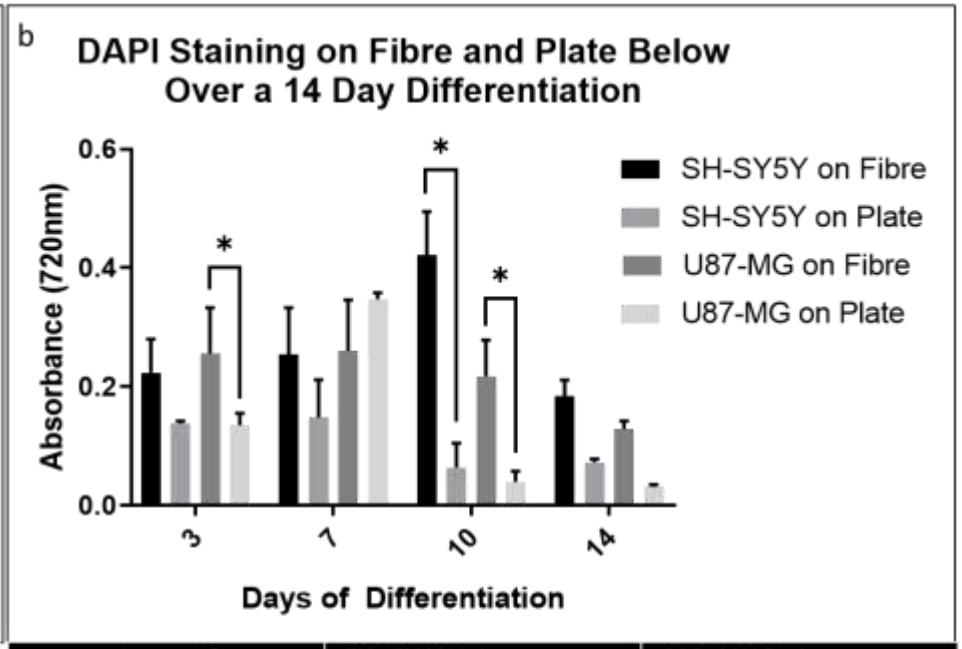

Days of Differentiation	SH-SY5Y Percentage Retention/ %	U87-MG Percentage Retention/ %
3	66.91	65.15
7	62.39	58.29
10	72.99	90.94
14	64.16	96.29

Days of Differentiation	SH-SY5Y Percentage Retention/ %	U87-MG Percentage Retention/ %
3	61.82	65.42
7	63.22	42.78
10	86.81	84.50
14	71.73	80.42

Figure 48: Measure of glial and neuronal cell counts on nanofibre and the plate below. a. Manual cell counts of SH-SY5Y and U-87 MG cells on 10wt% PAN nanofibre over 14 days of differentiation as established using DAPI-stained nuclear counts. Counting was done by taking average counts at five random regions on three separate samples. b. Comparable cell counts of SH-SY5Y and U-87 MG cells on 10wt% PAN nanofibre using instead Microplate analysis of relative intensity on DAPI stained samples. 50,000 cells were initially seeded in all cases. Significance was assessed with a two-way ANOVA with Sidak's multiple comparisons test with $P<0.05$ (*).

Using the ImageJ nuclear counting method, results obtained suggested that though not significant, neuronal cell counts seemed to remain on average higher than glial counts on PAN nanofibre over the 14 days. This finding was supported by the fluorescence intensity measurements of DAPI staining analysis carried out using a fluorescence microplate reader. Aside from this analysis, having assessed both fibre and microplate nuclear presence, the distribution of cells on the fibre and on the microplate was noticeable. In almost all cases in the nuclear counting experiment, neuronal and glial cell counts were significantly higher on the fibre than the microplate, but the population on the base of the microplate was still sizeable. This was mirrored when quantified by fluorescence intensity measurements using a microplate reader. Both data sets suggested that retention of cells on the nanofibre was poor overall in both cell types. It was hypothesised that this could be attributed to the cell seeding technique. This was initially carried out by depositing a droplet of suspended cells onto the elliptical aligned region of nanofibre with the nanofibre in direct contact with the base of the microplate. The solution to this problem was to either change seeding technique, or perhaps remove the cells seeded on nanofibre and replace them in a fresh microplate. A background level of 2D cells risked skewing the data obtained from a 3D system. The solution opted for was the former – maximising seeding efficiency would not only mean that data would not be skewed, but it also offered more control over cell counts in ongoing experimentation.

The solution to this issue was found in the design and manufacture of ‘stackers’. These structures were so called as they were originally designed to allow layering of multiple layers of fibre, but a secondary function was identified in that fibre would be suspended from the base of the microplate. Several designs were trialled, the first being a re-usable stainless-steel structure. This had promise, though frequent re-sterilisation led to rusting and damage to the structures. The second revision of the design was made to be disposable. Constructed from Perspex, these single-use structures initially held four pins for securing of nanofibre in place. A later design removed these fragile pins and introduced ‘indents’ into the side to allow easy media changes. The evolution of ‘stacker’ design is shown in figure 49.

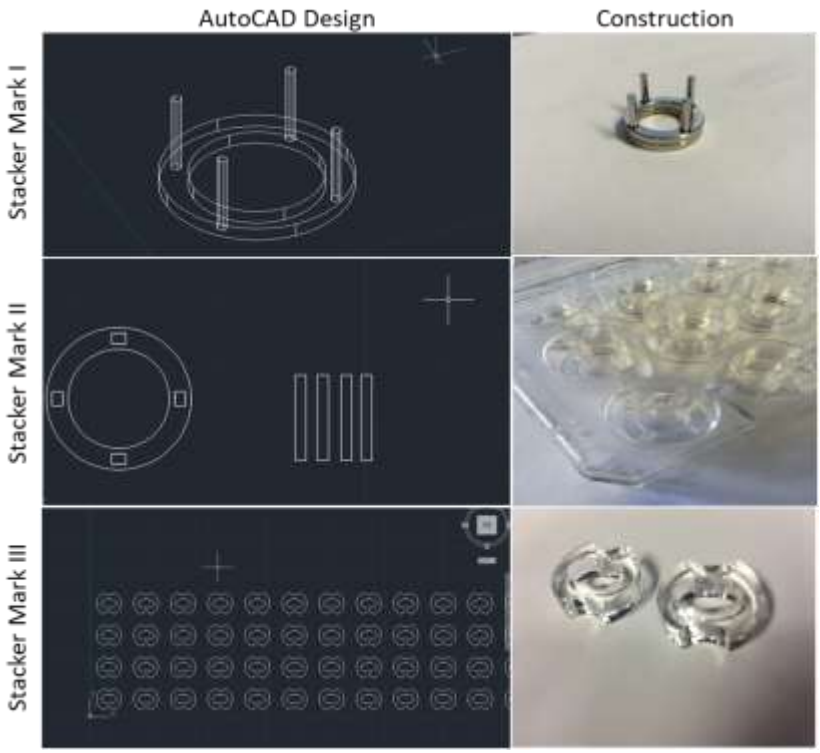

Figure 49: AutoCAD designs of MARK I-III stackers used to suspend nanofibre membranes above the base of wells microplates. Accompanying these designs are images of the products post manufacture.

To test these structures, 'Mark III' designs were used in seeding 50,000 SH-SY5Y and 50,000 U-87 MG cells separately onto aligned 10wt% PAN nanofibre. Counts were taken after three days of incubation in 10% serum DMEM F-12 on the base of the microplate to assess the cells numbers that had fallen through (see section 5.2.3 for culture condition details). Using ImageJ, six 1mm^2 regions in six wells were counted from DAPI stained nuclei and the average cell count established. Figure 50 presents these results.

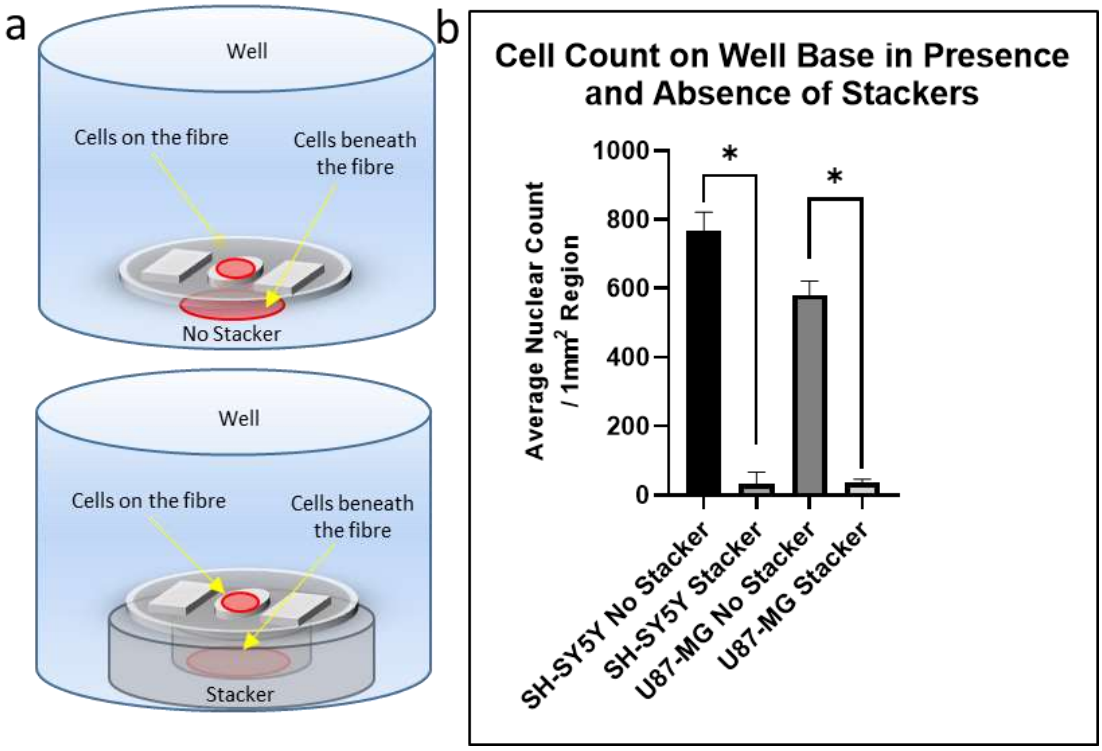

Figure 50: Cell counts of SH-SY5Y and U-87 MG cells on the base of microplate wells when Mark III 'Stackers' have been used or not. a. Schematic of use of stackers and not. b. Cells counted in six samples per condition using DAPI nuclear stains and processing in ImageJ. Cells beneath the fibre were those of interest and so only these were quantified. Significance was assessed with a two-way ANOVA with Sidak's multiple comparisons test with P<0.05 (*).

Results show a significant reduction in the cells on the base of the microplate from 769 cells/mm^2 to just 34 cells/mm^2 in SH-SY5Y cells and from 581 cells/mm^2 to just 35 cells/mm^2 in U-87 MG cells. The minimal population remaining in the base of the microplate can therefore be negated, and this was ensured by then transferring nanofibre into fresh microplates. In this way, cell number and data skew could be fully controlled.

A secondary benefit was provided by using 'stackers' to suspend nanofibre membranes above the base of the microplate. Following sterilisation and washing, nanofibre was kept wet, level and suspended until cell seeding could take place. The water tension present within the elliptical region was such that depositing a controlled droplet of cells would confine the cell population to the elliptical region of the fibre with little exception. Figure 51 presents DAPI heat-maps generated using a microplate reader reading absorbance at 720nm. 50,000 SHSY-5Y cells were seeded on 10wt% aligned PAN and cultured in low serum media with Retinoic acid for fourteen days with and without 'Mark III Stackers'.

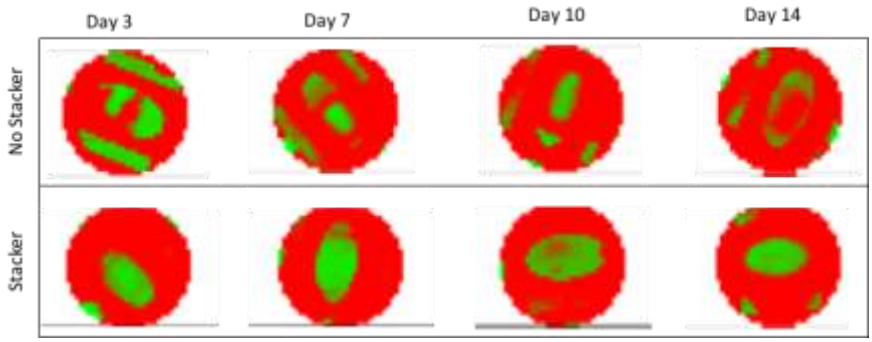

Figure 51: DAPI heatmaps created by assessing DAPI stained nuclear expression on a microplate reader at 720nm. Green indicated presence of nuclei and red the absence. DAPI expression was compared over fourteen days of differentiation in presence and absence of 'Stackers'. Using the stackers kept the cellularised elliptical regions from the base of the plate and from spreading too far from the origin of seeding.

Results indicate that most cells initially seeded remained on the elliptical region of interest. It was possible to remove the random regions present in this nanofibre design through pre-culture processing, though this effected the structural integrity of the fibre. Using stackers, the population could be largely controlled to the aligned section of the fibre, whilst maintaining maximum structural integrity of the scaffold disk and so the random regions were largely left intact.

7.5 Cell-Scaffold Interactions - SH-SY5Y Cells

It was important to fully characterise the interaction of SH-SY5Y cells on aligned nanofibre and the differentiation process. This line of investigation sought to understand the spatial alignment and axonal elongation/migration in this cell population as differentiation progresses on 10wt% aligned PAN. Initially, this was recreated on a 2D culture microplate so that comparisons may be drawn with 3D aligned PAN nanofibre. An MTT assay was used, which is an NAD(P)H-dependant cellular oxidoreductase enzyme-based colorimetric assay utilised for assessing metabolic activity in target cells (Arab-Bafrani et al. 2016).

50,000 SH-SY5Y cells were seeded either on 1ml 10wt% PAN aligned nanofibre or in a 12 well microplate well. After twenty-four hours in a CO_2 incubator in high serum DMEM f-12 medium, cells were subject to seven days of differentiation using low serum DMEM F-12 media and Retinoic Acid. Images were taken using a Confocal Microscope and MTT assay used in parallel at day zero, three, five and seven of differentiation. Figure 52 presents results. Immunofluorescence images made use of primary βIII Tubulin antibody staining (and red Alexa Fluor 568 secondary antibody staining) of SH-SY5Y axons, highlighting both axonal elongation and directionality in 2D and aligned PAN nanofibre respectively. Quantification of axon length was achieved using analysis software (ImageJ), measuring from the centre of the DAPI-stained nucleus to the tip of the longest axon in 10 random axons in triplicate samples. This 'distance from origin' technique was used henceforth. Directionality too was assessed using ImageJ in which a built in Fast Fourier Transform (FFT) analysis assessed repeating spatial patterns at day seven.

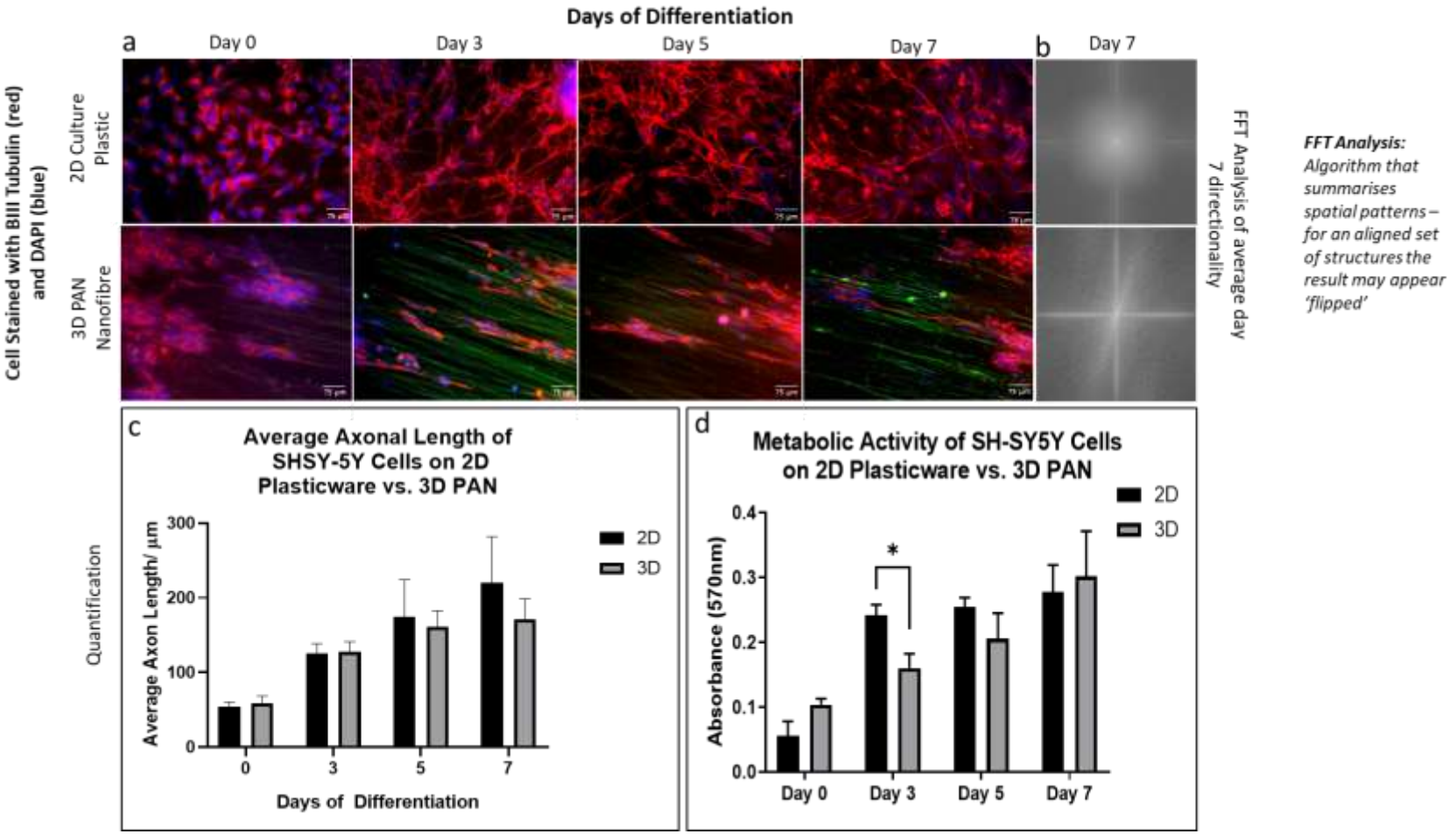

Figure 52: Assessment of neuronal cells in 2D and 3D. a. Immunofluorescence imaging depicting the differentiation of SH-SY5Y cells over seven days either on 2D plasticware or on 3D 10wt% PAN nanofibre. Staining is against βIII Tubulin protein (using red Alexa Fluor 568 secondary antibody staining), though DAPI nuclear staining (blue) and auto-fluorescent PAN nanofibre (green) are also present. b. Fast Fourier Transform (FFT) analysis of spatial patterning. This ImageJ tool enables the comparison of alignment in cells on fibre and in 2D. c. Comparison of axonal length in SH-SY5Y cells in 2D vs on 10wt% PAN. d. MTT analysis of SH-SY5Y cells metabolic activity measured in a microplate reader at 570nm over seven days of differentiation in 2D and on 10wt% PAN. Significance was assessed using a two-way ANOVA with Sidak's multiple comparisons test with $P<0.05$ indicating significance (*).

Results showed that axonal elongation appeared to be comparable in both cases. Cells were equally capable of axonal elongation in 3D on aligned 10wt% PAN scaffolds as they were in 2D. Notably, as displayed clearly in the FTT comparison and panels, spatial orientation of the nanofibre differs between 3D and 2D. Specifically, aligned 10wt% PAN nanofibre provides ample physical cues to encourage unidirectional, aligned orientation of the differentiating axons. Measurement of axon length was more challenging in 2D given their random directionality, though notably most remained 'straight'. In calculation of length, a line of best fit was used in each case and those that were particularly irregular were excluded where possible. This technique was maintained throughout this investigation, though mostly, calculations were done on unidirectional nanofibre, so assessment was simpler.

In addition to analysis of cellular orientation and axon length, a measure of metabolic activity was taken using MTT analysis. Here, comparing differentiating cells on a 2D surface and 10wt% PAN, with exception of day three, the metabolic activity showed no significant difference at any time point over the differentiation. In combination with axon length, this data provided evidence to suggest cells were equally metabolically active and capable of differentiation on 10wt% PAN as they were on 2D. However, to assess differentiation more accurately, western blot analysis of βIII Tubulin (and synaptophysin) protein expression was required. It is possible that at day three, cells in 2D were more metabolically active as they have been cultivated on a 2D surface over their life-time.

Two proteins were analysed for their up-regulation during differentiation. βIII tubulin is a microtubule protein involved in neurogenesis, axon guidance and maintenance – an active component of differentiation (Moskowitz et al. 1993). Up-regulation of synaptophysin during differentiation in SH-SY5Y cell lines is considered by many a marker of functional synapse formation (Murillo et al. 2017). In both cases, expression of these proteins was compared at day zero pre-differentiation and day seven post-differentiation. Further, the protein expression was compared in 2D and on 3D 10wt% PAN. In all cases, 50,000 SHSY-5Y cells were seeded on either 12 well microplates or 10wt% PAN nanofibre. After twenty-four hours in a CO_2 incubator to allow attachment, cells were differentiated using low serum DMEM F-12 and Retinoic Acid. Proteins were extracted and used to run Western blots. Results are shown in figure 53 along with the fold change quantification calculated using densitometry software.

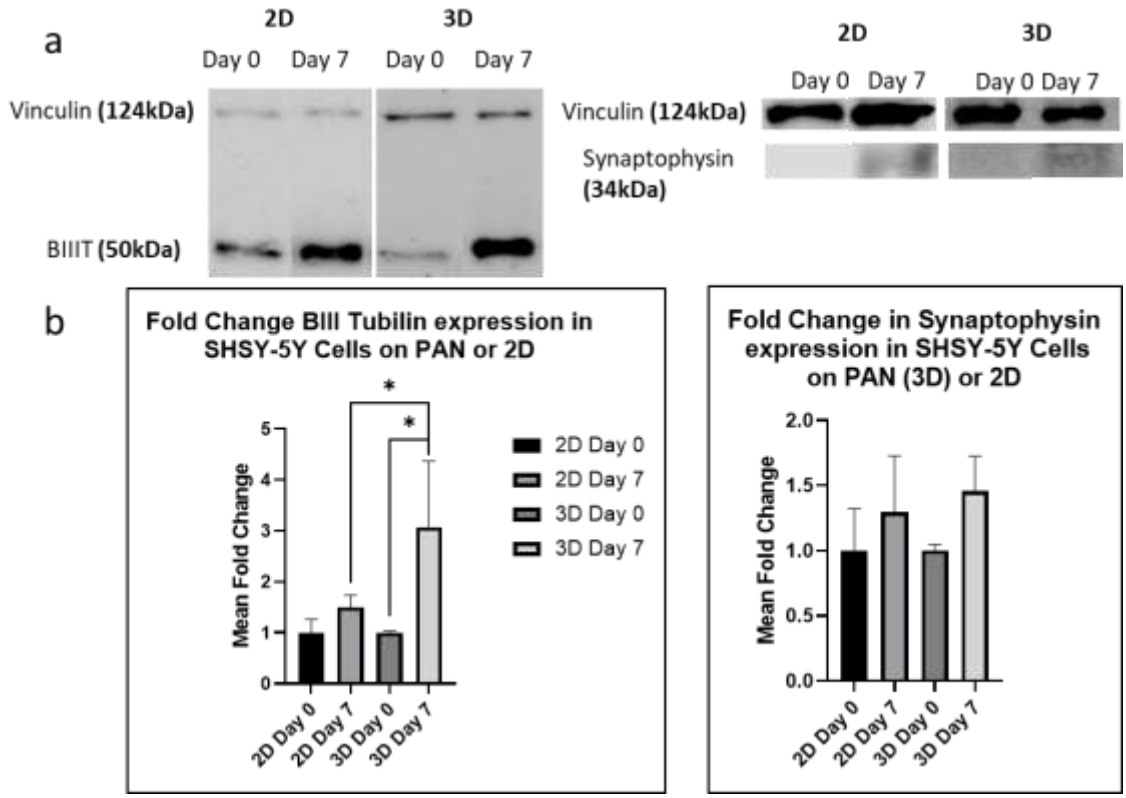

Figure 53: Western blot analysis of neuronal cells in 2D and 3D. a. Western blot comparison of βIII Tubulin and synaptophysin expression in SH-SY5Y cells at day zero and day seven of differentiation in triplicate. The housekeeping protein used was Vinculin in each case. b. Densitometry assessment of bands, allowing quantification of western blot outcomes. Significance was assessed with a one-way ANOVA with Sidak's multiple comparisons test with P<0.05 (*). A secondary statistical test was carried out to compare 2D and 3D separately, using multiple unpaired, parametric, two tailed T-tests, using the Holm Sidak method with a P-value of <0.05 (*) – not shown on the graphs but discussed in-text.

In keeping with the comparable axonal elongation seen in the previous figure 52, results showed an average up-regulation in βIII Tubulin in both 2D and 3D 10wt% PAN, significantly so in the latter case. The up-regulation of βIII Tubulin in 3D was significantly greater than that on 2D, suggesting that the nanofibre provided a suitable conduit for differentiation. In the case of synaptophysin, an average up-regulation was seen in both 2D and 3D 10wt% PAN scaffolds, though this change was not significant in either case. Notably, considering 2D and 3D separately, performing multiple, unpaired, parametric, two tailed (student) T-tests (with the Holm Sidak method) showed significant up-regulation in synaptophysin in 3D (P=0.041) and βIII Tubulin in 2D (P=0.049) where no significance was shown in the one-way ANOVA. These results suggested that in addition to the morphological axonal elongation, on PAN scaffolds, neurones were undergoing functional differentiation. More investigation would be required in future work to assess the cells electrical activity at the synapses, though this data suggested that synapse formation may be occurring.

7.5.1 Neuronal Migration on 10wt% PAN Nanofibre

Having understood the long-term differentiation process undergone by SH-SY5Y neurones, it was useful to assess shorter term migration on nanofibre. It was possible to carry out time-lapse imaging on this cell line to analyse cellular migration and active axon elongation of undifferentiated cells. Migration was the pertinent point of analysis here as differentiation does take longer to assess. 50,000 SH-SY5Y cells were seeded on aligned 10wt% PAN nanofibre and after twenty-four hours in a CO_2 incubator, were live cell imaged using confocal (SP8) (Leica, UK) microscope at the Laser for Science 'Octopus' facility at STFC-Rutherford Appleton Laboratory, near Didcot. Immunofluorescence staining carried out to highlight βIII Tubulin in SH-SY5Y cells, results are shown in figure 54 at zero and two hours, indicating the tracking of three examples of cells in the field of view.

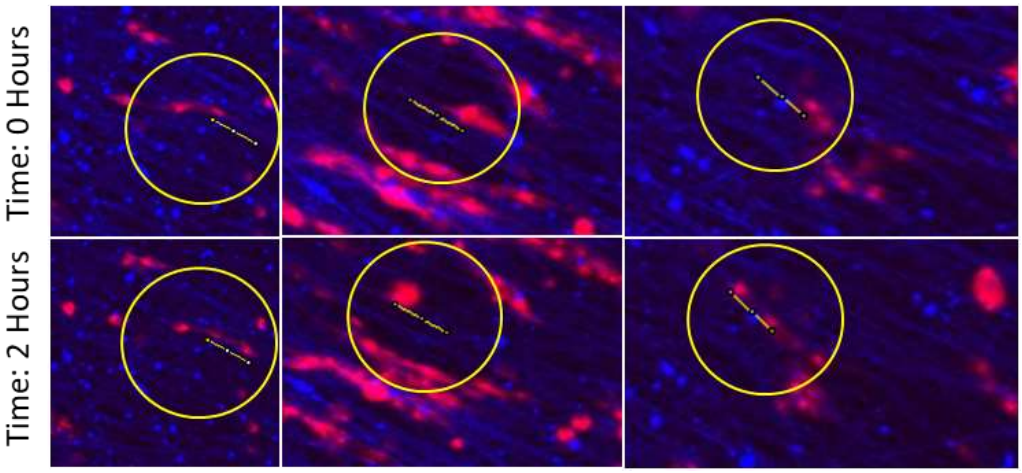

Figure 54. Assessment of immature SH-SY5Y cell migration over 2 hours. This was assessed by tracking cell body movement in triplicate samples over time in image J software. Yellow lines indicate the overall distance travelled in each case. Yellow circles highlight the region of interest. SH-SY5Y cells were stained with primary βIII Tubulin antibody and secondary red Alexa Fluor 568 secondary antibody.

By making the centre of the cell body and tracking this point in space it was possible to calculate the average migration in undifferentiated SH-SY5Y cells. This was **178±46µm** in 2 hours, or an average of **89µm** per hour. This was a faster migration than expected. A secondary finding of interest to this study was the migration of cells between fibre strands as well as along them, though mostly, cells followed the physical cues provided by the fibre they were already on. This is a finding that could be followed up in future work.

7.6 Cell-Scaffold Interactions - U-87 MG Cells

In addition to understanding the physical changes that occur during neuronal differentiation, it was also important to understand the differentiation process undergone by the chosen clonal glial population - the

U-87 MG cell line. Early investigations (section 7.3) indicated that perhaps U-87 MG cell numbers were lower than that of their neuronal counterpart on PAN nanofibre. This investigation provided an opportunity to investigate the cause. Accounting for this noted lower cell count, U-87 MG cell culture was carried out both on the hydrophobic 10wt% PAN, but also on the hydrophilic 10wt% PAN+5% Jeffamine®. It was hoped that the effect of hydrophobicity on cell number may begin to be understood.

The differentiation protocol chosen was the same as that carried out on neuronal cells. As before, Into low serum (1% FBS) DMEM F-12 media, 100mM stock Retinoic Acid was added fresh at 1µl in 10ml of low serum media (Shi et al. 2013, Liang et al. 2015).

The basis of glial cell immunofluorescent imaging and later protein expression was explored by looking at Glial Fibrillary Acidic Protein. GFAP is an intermediate filament protein responsible at least in part for provision of structural support and the tensile strength to astrocyte cytoskeleton (Restrepo et al. 2011). This protein is expressed at low levels in immature cells and is up-regulated as cells mature (Restrepo et al. 2011).

In the first investigation, the glial population was assessed morphologically on hydrophobic 10wt% PAN, hydrophilic 10wt% PAN+5% Jeffamine® and in 2D over a seven-day differentiation. 50,000 U-87 MG cells were seeded on the various surfaces and allowed to attach for twenty-four hours in a CO_2 incubator. Following this, cells were subject to low serum DMEM f-12 (Lonza, UK) and retinoic acid-based differentiation. In parallel, MTT (Sigma-Aldrich, UK) assessment of metabolic activity was used to supplement conclusions drawn from the imaging. Results are shown in figure 55.

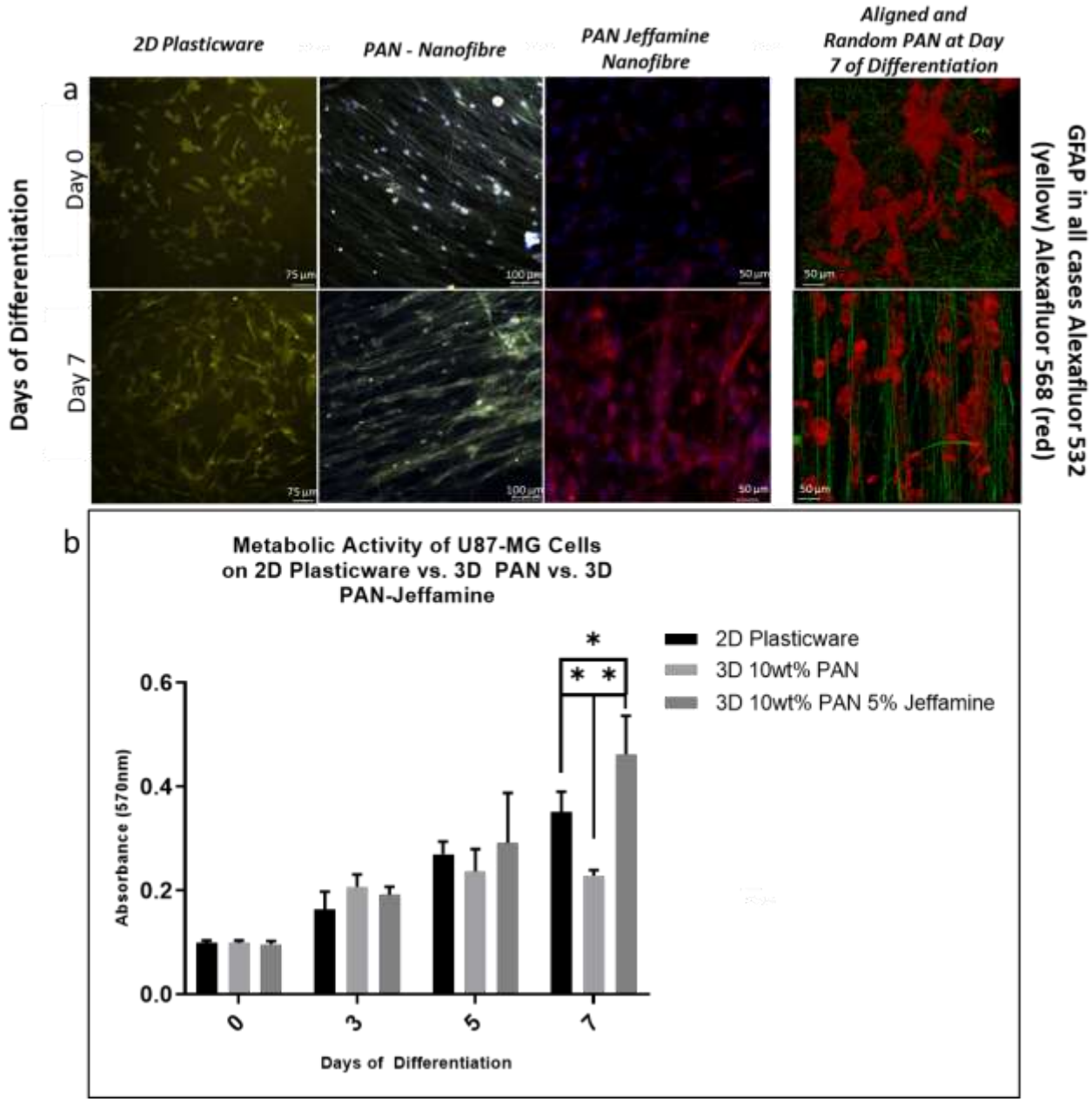

Figure 55: Assessment of U-87 MG cells in 2D and various nanofibre materials. a. Immunofluorescence imaging of U-87 MG cells in 2D on adherent plasticware, on 10wt% PAN and 10wt% PAN + 5% Jeffamine®. Cells were stained with primary anti-GFAP antibody and secondary Alexa Fluor 568 (red) or 532 (yellow) antibodies. b. Assessment of metabolic activity using MTT assay and measuring absorbance at 570nm over a 7-day differentiation either on 2D or on stated nanofibre. Significance was assessed with a two-way ANOVA with Sidak's multiple comparisons test with P<0.05 (*).

Results showed that in 2D, cells developed glial extensions and visually formed interconnected networks following differentiation. Assessment of cells on 10wt% PAN crucially showed glial extension in a unidirectional manner, following the physical cues of the aligned nanofibre. Cells appeared largely healthy, bundling as expected. However, in collaboration with the Rutherford Appleton Laboratory STFC in Didcot, high resolution imaging was carried out to confirm cellular health on 10wt% PAN (far right images in the panel of figure 55). These high-resolution images showed clear rounding of cells in sections of the aligned

fibre by day seven of differentiation. By comparison, an assessment of cell morphology on 10wt% PAN+5% Jeffamine® showed mature, visibly healthy cells forming complex, inter-connected networks. Extensions even occur between adjacent aligned fibre strands. These results provided the initial supportive evidence that glial cells underwent perhaps more extensive differentiation with longer term survival on hydrophilic PAN-5% Jeffamine®. To confirm this, functional assessment was needed.

MTT assay assessment of metabolic activity was carried out on cells over the differentiation. Up to day five of differentiation, metabolic activity was comparable across 2D, 10wt% PAN and 10wt%PAN + 5% Jeffamine®. At day seven the metabolic activity of maturing glia did appear to level-off significantly compared both the 2D and to PAN-Jeffamine® based cells populations. This evidence supported the images obtained in figure 55 in which cells maintain healthier, more mature morphologies over the seven-day differentiation period.

It was possible to quantify GFAP expression using images captured within this investigation. Optical intensity was calculated using ImageJ analysis in a given area (1.5mm x 1.5mm) and an average taken at least three samples on each case. Fold change was then calculated from the difference in average optical intensity between days zero and seven of differentiation on the various materials. Results are shown in figure 56.

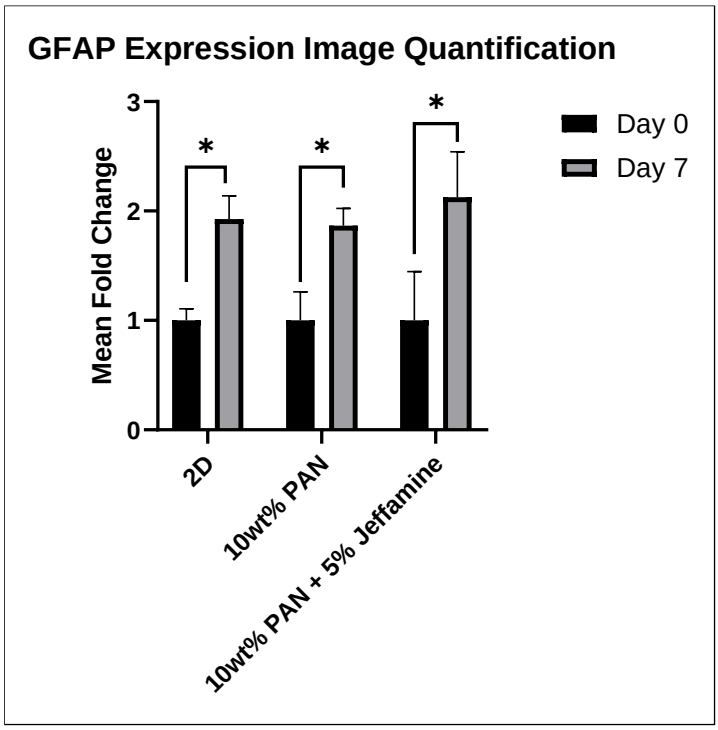

Figure 56: Mean fold change in GFAP expression using ImageJ in cells in 2D on plasticware, 10wt% PAN and 10wt% PAN + 5% Jeffamine® in triplicate samples. Optical intensity was compared between day zero and seven of differentiation. Significance was assessed using multiple unpaired, parametric, two tailed T-tests, using the Holm-Sidak method in 2D, 10wt% PAN and 10wt% PAN + 5% Jeffamine® groups separately with a P-value of <0.05 (*).

Results showed that there was a significant average fold increase in GFAP in every case. There did not appear to be a significant difference in average fold change between the different scaffolds, nor the standard 2D system using a two-way ANOVA with Sidak's multiple comparison's test, though to get a true indication as to GFAP protein expression, protein expression had to be quantified using western blot. Results did suggest that the differentiation protocol in use was effective given the GFAP up-regulation in all cases. Notably, the scaffolds were imaged in separate experiments, so to truly compare the scaffolds, they could be imaged in parallel. Comparison of individual fold change (with constant microscope settings in day zero and seven within experiments) provided the best comparable understanding that could be obtained with the time frame available. This is something that could be carried out in future work.

Western blotting provided a means of quantifying protein expression in the cells of interest over a period of differentiation either on nanofibre or in 2D. In this case, 2D (12 well microplate) was compared only to the 10wt% PAN + 5% Jeffamine® scaffold as results indicated that cells maintained better metabolic and morphological condition over seven days of differentiation. Once again, 50,000 U-87 MG cells were seeded on the various surfaces and allowed to attach for twenty-four hours in a CO_2 incubator. Following this, cells were subject to low serum DMEM f-12 (Lonza, UK) and retinoic acid-based differentiation for seven days. Figure 57 presents the blots in addition to the quantified findings calculated using densitometry software. Average fold change was calculated from the resultant bands.

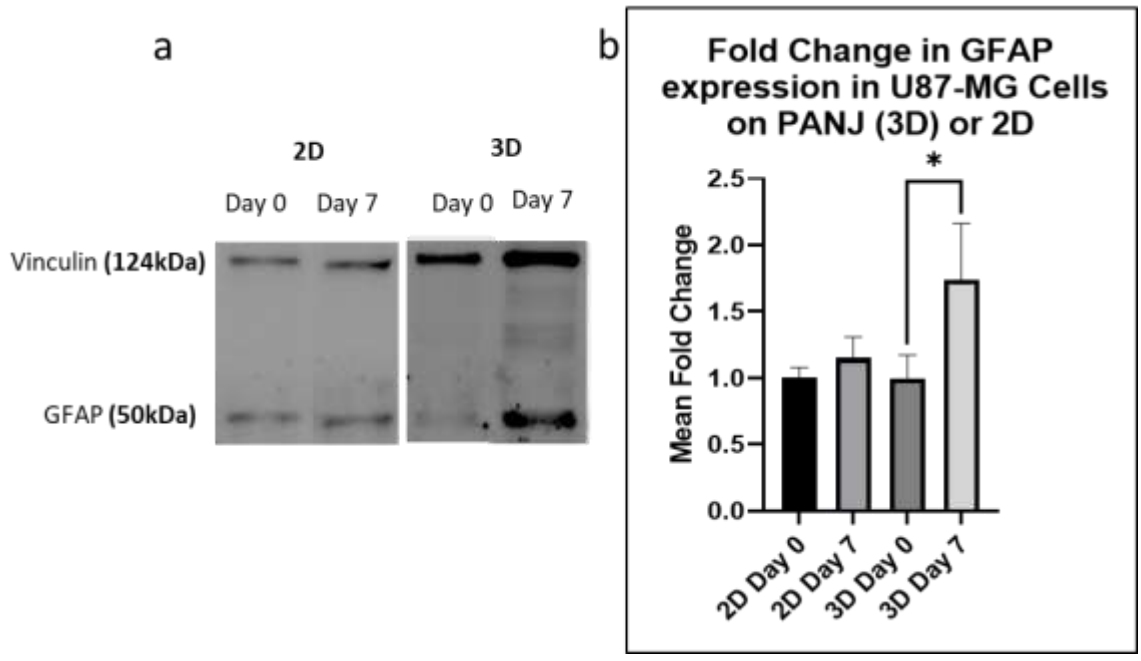

Figure 57: Western blot analysis of GFAP expression in U-87 MG cells in 2D and 3D. a. Western blot nitrocellulose image indicating bands. Analysis compared expression of GFAP at day zero and 7 of differentiation in U-87 MG cells on 2D and on 10wt5 PAN + 5% Jeffamine®. Densitometric values were normalised to the expression of vinculin (the assigned housekeeping protein). b. Densitometry quantification showing mean fold change in GFAP expression in U-87 MG cells over seven days of differentiation and on 2D and 3D 10wt% PAN + 5% Jeffamine® with triplicate samples. Significance was assessed with a one-way ANOVA with Sidak's multiple comparisons test with P<0.05 (*).

Results indicated an up-regulation of GFAP on average in both 2D and 3D, significantly so in 3D. This supports evidence obtained above (figure 56) in which GFAP up-regulation was on average highest in cells on 10wt% PAN + 5% Jeffamine®. Given that GFAP is a hallmark of maturation, results suggested that cells may undergo efficient differentiation on this scaffold. No western blot analysis was carried out on PAN alone without Jeffamine® doping as it had been established that cell viability and metabolic activity was optimum when Jeffamine® was included.

7.7 Material Preference

Results above have suggested that neuronal cells differentiate well on hydrophobic PAN and glial cells hydrophilic PAN-Jeffamine®. The study below makes use of the CellTiter-Glo® (Promega, UK) assay to assess cell viability over a seven-day differentiation period. The aim of this experiment was to identify the viability each cell line on both possible scaffolds to distinctly confirm the optimal scaffold material for each cell line based on evidence obtained above.

In addition to PAN and PAN + 5% Jeffamine®, PAN + 1% Jeffamine® was also included to gain an understanding as to how cell viability changes when a less hydrophilic material was chosen. In each case, 50,000 SH-SY5Y or 50,000 U-87 MG cells were seeded on the various surfaces independently and allowed to attach for twenty-four hours in a CO_2 incubator. Following this, cells were subject to low serum DMEM f-12 (Lonza, UK) and retinoic acid-based differentiation for seven days. Results are shown in figure 58

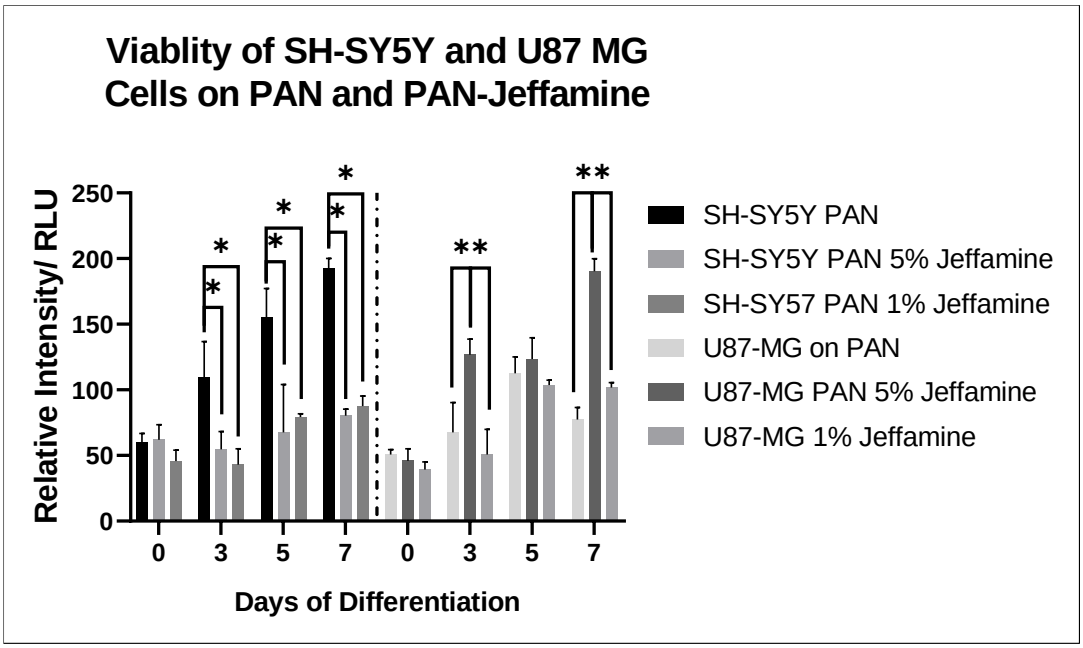

Figure 58: Assessment of viability of SH-SY5Y and U-87 MG cells on 10wt% PAN, 10wt% PAN + 5% Jeffamine® and 10wt% PAN + 1% Jeffamine® using the CellTiter-Glo® Assay. Cellular viability was compared when cells were seeded at 50,000 cells and differentiated for seven days. Significance was assessed using multiple unpaired, non-parametric, two tailed T-tests with a P-value of <0.05 (*) and supported with a two-way ANOVA with Sidak's multiple comparisons test with P<0.05 (*).

Results showed significant differences not previously seen in imaging or metabolic activity assessments. SH-SY5Y viability on PAN was significantly higher than on 1% or 5% Jeffamine® from day three. Viability of U-87 MG was significantly higher on PAN + 5% Jeffamine® than PAN + 1% Jeffamine® or PAN alone at day three and seven. This figure rounded off the study, adding more evidence to the hypothesis made earlier that different cell lines may prefer different material types. Specifically, hydrophobicity seemed to play a role in viability, morphology and differentiation. Further, the 'intermediate' hydrophobicity 1% Jeffamine® did not seem to benefit the viability of either cell line.

7.8 Cell-Scaffold Interactions - Co-cultures

Once the differentiation process had been understood in the context of individual clonal cell lines, it was important to understand how these cells performed in co-culture. It is well documented that glia perform a neuroprotective role with neurones in co-culture (Saeed et al. 2015). It was hypothesised that both cell lines would benefit from co-culture in overall viability and neuronal axon lengths. Understanding this cooperative relationship was crucial for later design of SCI treatment prostheses and in vitro models.

The first investigation carried out sought to understand morphological changes in neurones and glia in co-culture over the same seven-day differentiation period. The morphology was compared between a 2D culture surface (12 well microplate) and aligned 10wt% PAN using immunofluorescence staining. Axonal length was calculated by measuring from the nucleus to the longest axon extension in each case. 10 random cells were chosen in triplicate samples. Here, 25,000 SH-SY5Y and U-87 MG cells were seeded on the various surfaces and allowed to attach for twenty-four hours in a CO_2 incubator. Following this, cells were subject to low serum DMEM f-12 and retinoic acid-based differentiation for seven days. Staining with anti-βIII Tubulin primary antibody (and red Alexa Fluor 568 secondary antibody) and anti-GFAP primary antibody (and yellow Alexa Fluor 532 secondary antibody) was carried out prior to immunofluorescence imaging on the confocal microscope. Results are shown in figure 59.

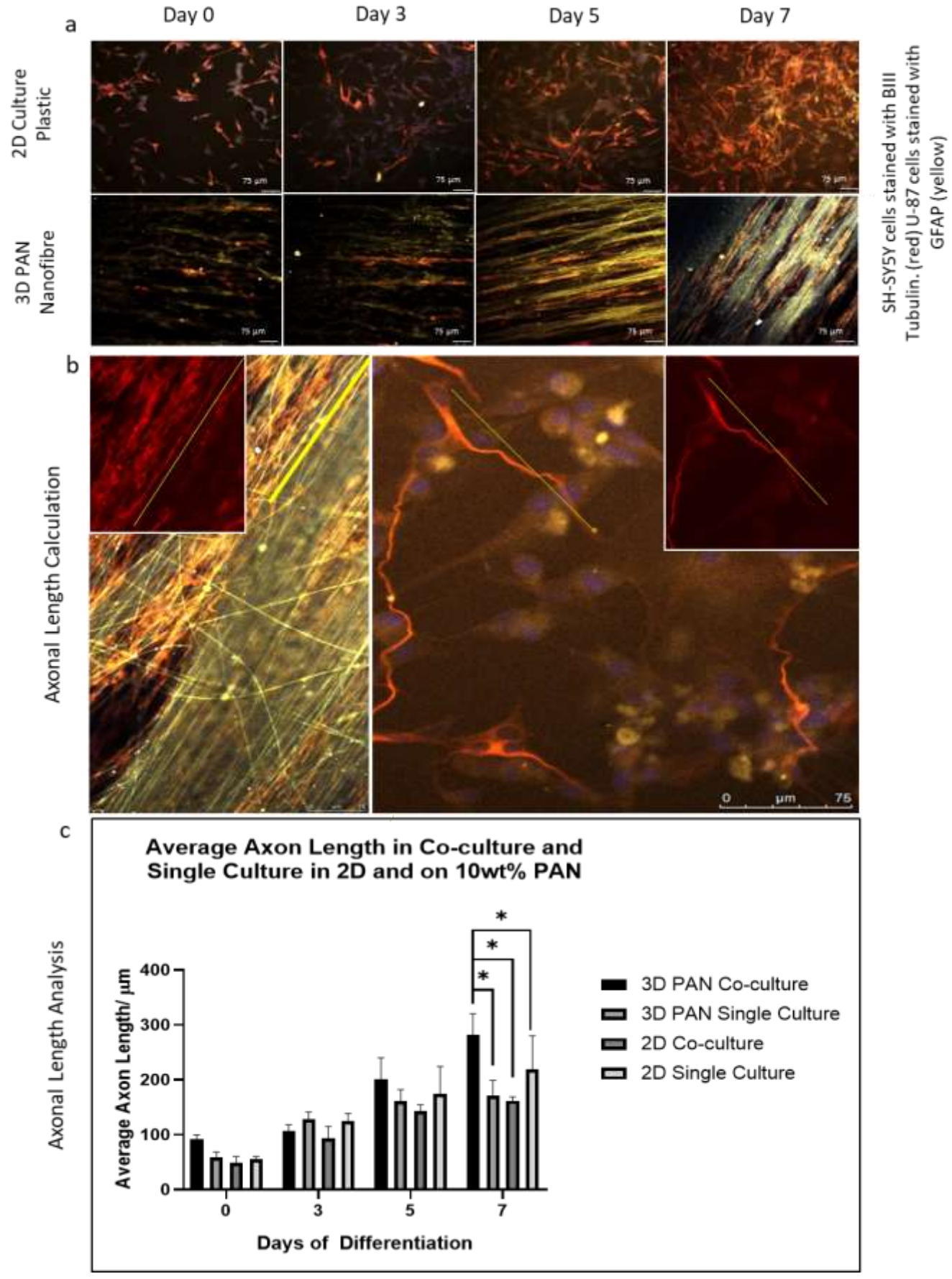
a
Day 0
Day 3
Day 5
Day 7
2D Culture Plastic
3D PAN Nanofibre
SH-SY5Y cells stained with BIII Tubulin. (red) U-87 cells stained with GFAP (yellow)
b
Axonal Length Calculation
0 µm 75
c
Axonal Length Analysis
Average Axon Length in Co-culture and Single Culture in 2D and on 10wt% PAN
Average Axon Length/ µm
400
300
200
100
0
0
3
5
7
Days of Differentiation
*
*
*
3D PAN Co-culture
3D PAN Single Culture
2D Co-culture
2D Single Culture

Figure 59: Assessment of neuronal and glial populations in co-culture. a. Immunofluorescence imaging showing differentiating SH-SY5Y and U-87 MG cells in co-culture. SH-SY5Y cells were stained with primary anti-βIII Tubulin antibody (and red Alexa Fluor 568 secondary antibody) and U-87 MG cells with primary anti-GFAP antibody (and yellow Alexa Fluor 532 antibody). Cells are either on 2D culture plastic (top row) or on 10wt% PAN (bottom row). b. High magnification image showing examples of axonal length in a 2D and 3D sample. c. Calculated average axon length of SH-SY5Y neurones on 2D culture plastic or 10wt% PAN in single culture or when cultured with U-87 MG cells over seven days of differentiation. Significance was assessed with a two-way ANOVA with Sidak's multiple comparisons test with P<0.05 (*).

Assessment of the image panels showed that in both 2D and 3D, long mature axons were formed. In 3D on 10wt% PAN, over seven days, the glial population seemed to gradually form a basement layer over which the neuronal axons extended. This was true to a lesser extent in 2D. Comparison of axonal lengths showed that on PAN in co-culture, axons were significantly longer at day seven compared to single culture on PAN and both single and co-culture in 2D. This was perhaps the product of organisational cues provided by extra cellular matrix-like nanofibre structures.

Comparing culture of individual cell lines on 1% Jeffamine® (above) indicated no improved viability. However, it was considered that given that perhaps PAN + 1% Jeffamine® would present a logical, less hydrophilic mid-point upon which co-culture may be efficiently carried out. A CellTiter-Glo® viability assay was carried out, assessing viability of SH-SY5Y, U-87 MG in co-culture on PAN - 1% Jeffamine® compared to PAN and PAN – 5% Jeffamine®. Once more, 25,000 SH-SY5Y and 25,000 U-87 MG cells were seeded on the various surfaces and allowed to attach for twenty-four hours in a CO_2 incubator. Following this, cells were subject to low serum DMEM f-12 and retinoic acid-based differentiation for seven days. Results are shown in figure 60.

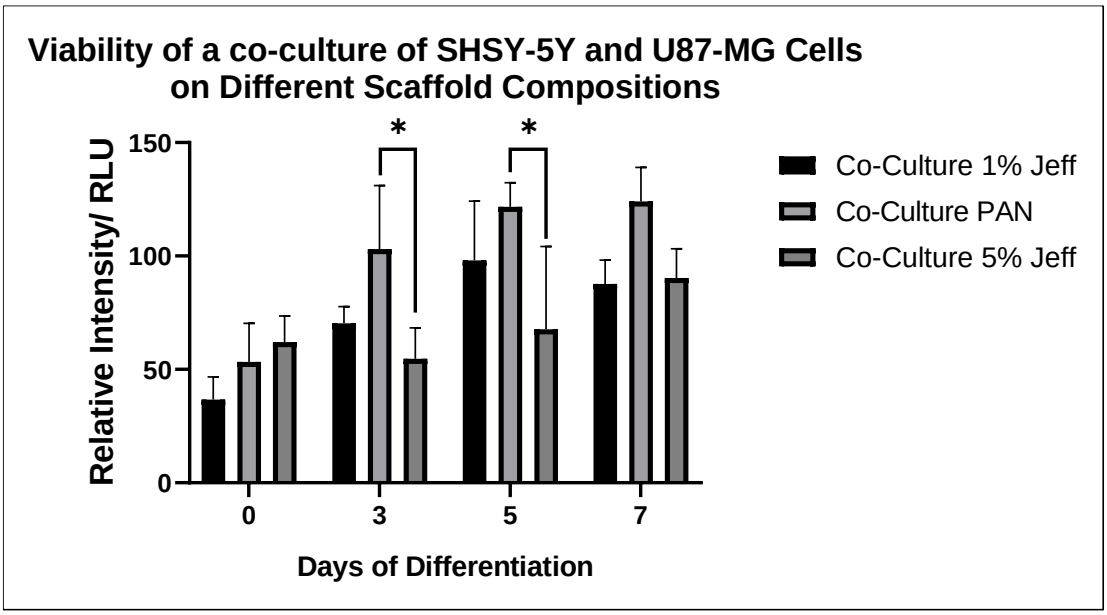

Figure 60: Assessment of viability using the CellTiter-Glo® *assay over as seven-day differentiation. A co-culture of SH-SY5Y and U-87 MG cells are analysed for viability on 10wt% PAN, 10wt% PAN + 5% Jeffamine® and 10wt% PAN - 1% Jeffamine® over the seven days. Significance was assessed with a two-way ANOVA with Sidak's multiple comparisons test with P<0.05 (*).*

Results indicated that in co-culture, using PAN without Jeffamine® established a higher than average overall viability than that of PAN 1% or 5%. There was a significant difference in viability in PAN vs. PAN+5% Jeffamine® at day three and five in co-cultured populations, though no significant difference in PAN vs. PAN+1% Jeffamine® over a seven-day differentiation. Given the boost in axonal length on PAN (investigated in chapter 7), co-culture was evidently best carried out on PAN, ensuring neuronal viability and axon length could be maintained long term. Further, this investigation posed the suggested that if two populations of cells could be kept physically on their respective preferred niches, but chemically connected, this may present the optimum system. This was investigated in later chapters.

It was possible to use time-lapse imaging to assess interactions of SH-SY5Y neurones in co-culture with other cells and with the nanofibre. Figure 62 captures the movement of lamellipodia, as cell-cell and cell-fibre interaction occurred. Using Laurdan (Thermofisher, UK) staining, it was also possible to capture active vesicle trafficking. This imaging was carried out using a TCS SP8 Confocal Microscope based at STFC Rutherford Appleton Laboratory. Once more, 25,000 SH-SY5Y and 25,000 U-87 MG cells were seeded on 10wt% PAN and allowed to attach for twenty-four hours in a CO_2 incubator. Following this, cells were subject to low serum DMEM F-12 and retinoic acid-based differentiation for three days before live imaging was carried out. Figure 61 presents a snapshot of these events. Laudon staining was used in this case.

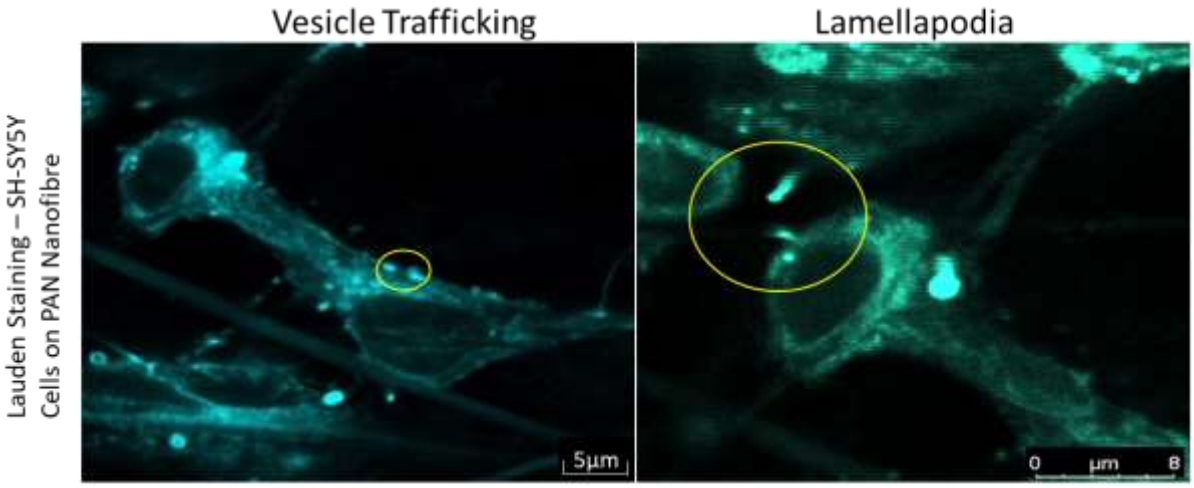

Figure 61: Immunofluorescence image obtained using live cell imaging on a Confocal Microscope (Leica TCS SP8). Laurdan staining was used in differentiated SH-SY5Y cells to show both vesicle trafficking (left) and Lamellipodia interactions (right). Images indicate one snapshot in time.

Images provided evidence as to the health of neuronal cells in co-culture on PAN and support the idea of using PAN as a suitable co-culture conduit. Results also supported the nanofibre material deposition volume (1ml) chosen in that high-resolution imaging was possible.

The aligned nanofibre sections of the elliptical scaffold design was 5mm across at the minor axis of the ellipse. It was important to understand the potential elongation of neurones across this distance to determine whether this patch of scaffold is traversable in vivo (axons would need to migrate across this

'bridge'). Indeed, using immunofluorescent staining (βIII Tubulin fluorescent antibody staining on SH-SY5Y cells specifically) on a co-culture of SH-SY5Y and U-87 MG cells, it was possible to quantify the overall axonal coverage over the central 3.5mm x 3.5mm area (imaging area). Once more, 25,000 SH-SY5Y and 25,000 U-87 MG cells were seeded on 10wt% PAN and allowed to attach for twenty-four hours in a CO_2 incubator. Following this, cells were subject to low serum DMEM f-12 and retinoic acid-based differentiation for seven days. Immunofluorescence staining, and confocal imaging was used thereafter. To calculate axonal coverage, just the βIII Tubulin channel was analysed for percentage contribution against background using ImageJ analysis on the 3.5mm x 3.5mm are in triplicate images. Figure 62 presents the results.

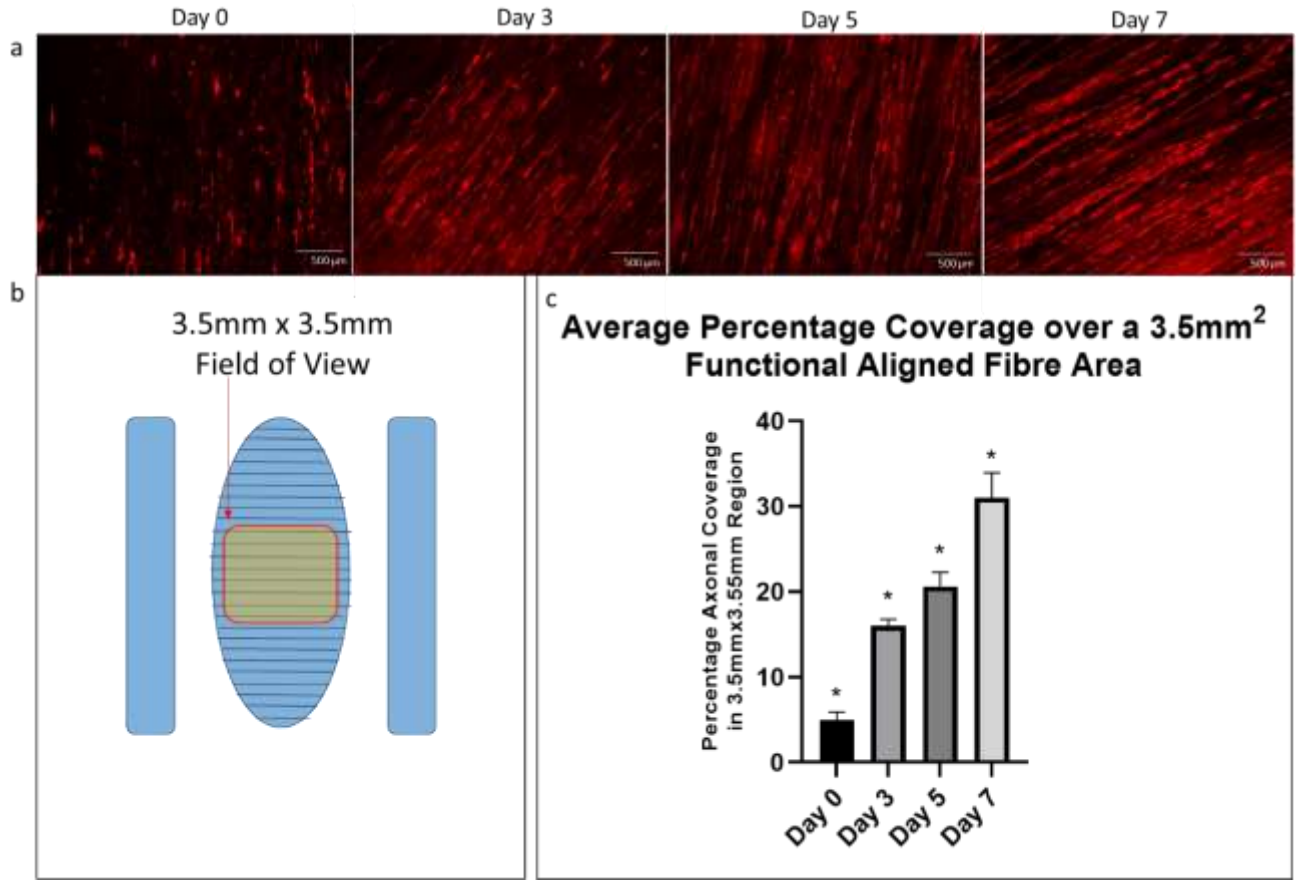

Figure 62: Assessment of neuronal capacity to traverse the nanofibre structure. a. Immunofluorescence image showing anti-βIII Tubulin primary antibody (and red Alexa Fluor 568 secondary antibody) stained differentiating SHSY-5Y cells in a co-culture with U-87 MG cells over seven days of differentiation. b. Schematic of the area being analysed in the immunofluorescence image above. c. Percentage coverage as calculated by comparing βIII Tubulin channel expression only against background. Significance was assessed with a two-way ANOVA with Sidak's multiple comparisons test with P<0.05 (*).

Results showed that long, filamentous axonal bundles traversed the 3.5mm gap successfully. The supportive glial population likely encourages maximum neuronal axon elongation as suggested earlier. The graph provides a quantified analysis of percentage neuronal coverage using ImageJ analysis. The unidirectional neuronal coverage increased over seven days of differentiation showing long neuronal bundles at the end-point. The result was indicative of the lengthening βIII Tubulin-expressing axons across

the imaged regions and thus potential functionalisation of the nanofibre. Secondary to this discovery, given that 'axonal coverage' was calculated by quantifying percentage βIII Tubulin expression against background using ImageJ analysis, it was also an indication that βIII Tubulin was significantly more expressed at each time point and thus that differentiation was effectively occurring.

7.9 Discussion

SH-SY5Y neuroblastoma and U-87 MG glioblastoma cell populations were used to assess the suitability of nanofiber scaffolds for the development of a cell prosthesis. Cell attachment was optimised using 'stackers'. It was surmised that a seeding density of 50,000 cells/ nanofibre disc was appropriate going forward. A differentiation protocol was tested and was deemed effective. This was concluded by tracking an increase in axon length over 7 days of differentiation (both in 2D and 3D) and significant up-regulation of βIII Tubulin in response to differentiation conditions (shown in western blot and immunofluorescence imaging). In 3D, βIII tubulin expression was significantly greater at day 7 of differentiation compared to cells cultivated on 2D plasticware as shown by western data. On average, synaptophysin was up-regulated in response to differentiation, though this was not significant – with more time and finance, this could be analysed further. Assessing aligned PAN nanofibre, it became clear that 1ml 10wt% PAN was appropriate for culture and differentiation of SH-SY5Y cells by comparing morphology, metabolic activity and viability to 2D over a differentiation period. However, 1ml 10wt% PAN – 5% Jeffamine® was most appropriate for U-87 MG cells using the same assessment parameters compared to PAN (and 2D). In co-culture on PAN nanofibre, neuronal axon length is significantly greater at day 7 than a neuronal single culture or either a single or co-culture on a 2D surface. No significant difference in long term viability of cells in co-culture was seen on PAN or PAN with 1 or 5% Jeffamine® was seen, though PAN alone on average boasted higher viability over seven days (not significant). Aligned nanofibre allowed directionality to be controlled in neuronal and glial populations as shown in FFT analysis. In general, providing an aligned PAN nanofibre scaffold to differentiating SH-SY5Y and U-87 MG cells enabled long, aligned axons to form and a significant up-regulation in both βIII Tubulin and GFAP in respective populations (in single culture).

Using the chosen cell lines allowed culture of neuronal and astrocytic populations distinctively. It was therefore possible to optimise and understand the cell-material interaction and thus best match the engineered scaffolds to the cells in use. Having characterised the change in cell line behaviour with the level of hydrophobicity and hydrophilicity it became clear that culturing cells on the same scaffold may not be optimal and so a more complex scaffold design was considered. This is described in Chapter 8.

Assessment of literature eludes to similar SH-SY5Y and U-87MG cell behaviour in response to culture on nanofibre conduits. Specifically, differentiating SH-SY5Y cells have been shown to demonstrate neurite outgrowth in an aligned fashion where aligned nanofibre was used (Xie et al. 2009). Another group demonstrated that neuronal cell lines such as SH-SY5Y cells can be substituted for primary cells where a

3D cell culture system was in place to drive the phenotype towards that of untransformed cells (Myers et al. 2008). The same group reported that retinoic acid-based differentiation was one that has been shown to induce neurite outgrowth in the population (Myers et al. 2008). The group reported extensive neurite outgrowth coupled with a down-regulation of both HuD and N-mcy, two prognostic markers of tumorigenicity in neuroblastoma when cultured in 3D scaffolds. Another group reported than nano-topography can play a role in differentiation of neuronal populations such as the SH-SY5Y cell line, of which increase in βIII Tubulin expression is a classic marker of neuronal differentiation (Khan et al. 2018).

Groups such as the Das et al group have shown historically that subjection of U-87 MG cells to retinoic acid treatment (Das et al. 2008) has been shown to induce differentiation towards an astrocytic phenotype (Karmakar et al. 2008), forming long extended processes (Mita et al. 2007). A marker of astrocytic differentiation is GFAP, which has been shown to increase in expression as cells mature towards an astrocytic phenotype (Restrepo et al. 2011). Interestingly, using a similar cell line (OSU2), the Grodecki et al group showed that GFAP expression was increased in glioma cell lines, and that when cultured on a nanofibre substrate designed to recapitulate the white matter, in addition to increasing GFAP levels, increased migratory behaviour was noted on the scaffolds (Grodecki et al. 2015). These findings have also been noted in U-87 MG cell lines (Agudelo-Garcia et al. 2011b).

Co-culture of SH-SY5Y and U-87MG cells on nanofibre has not been widely examined and so this aspect was considered novel. The interesting results obtained support some primary cell data obtained though it was noted that clonal data may not be directly comparable. Astrocyte support has been shown to help mediate neuronal recovery in the white matter in rat models, and as such evidence presented here showing enhanced axonal elongation and neuronal cellular viability was a logical result (Joosten, Gribnau 1989). Another group showed using nanofibre scaffolds, a resident astrocyte population supported both neuronal attachment and neurite outgrowth during maturation (Liu et al. 2015). Further, more generally in vivo, co-culture of neuronal and astrocytic populations occurs naturally (Vasile et al. 2017).

8 Results - Layering Nanofibre – 'Lamination'

8.1 Aims of Section

Having optimised the interaction of neuronal and glial populations on aligned nanofibre, it was possible to begin testing the outcome when multiple layers of nanofibre were brought together. In the previous chapter it was suggested that neuronal and glial populations maintained long term viability when on hydrophobic PAN and hydrophilic PAN+5% Jeffamine, respectively. It was logical, therefore, to suggest that when bringing together multiple cell types in a prosthesis, it may be best to initially keep these cell types in their own physical niches. The question as to whether neurons would still benefit in viability and axon elongation from the presence of glia if they were not in direct contact was pertinent to discover. A secondary aim was to investigate the cellular migratory behaviour when two nanofibre layers were brought together.

8.2 Layering with Empty Fibre

The first line of enquiry followed in this section of the investigation was to establish the effect of layering neurons and glia with an empty layer of nanofibre. In this way, it was understood the influence that the laminated layer of nanofibre had upon the cells on the bottom layer. Figure 63 presents immunofluorescence imaging of cellularised PAN, populated with undifferentiated SH-SY5Y cells stained with primary anti-βIII Tubulin antibody and red Alexa Fluor 568 secondary antibody and layered with acellular PAN (green) of the same physical specification for just three hours (Figure 63b) and twenty-four hours (Figure 63c). As shown in the schematic (Figure 63a), a plastic stacker was used both below to suspend the fibre complex away from the base of the plate but also above to keep the two layers of nanofibre in contact. Cells were initially seeded at a density of 50,000 and were subject to lamination with an additional layer twenty-four hours later.

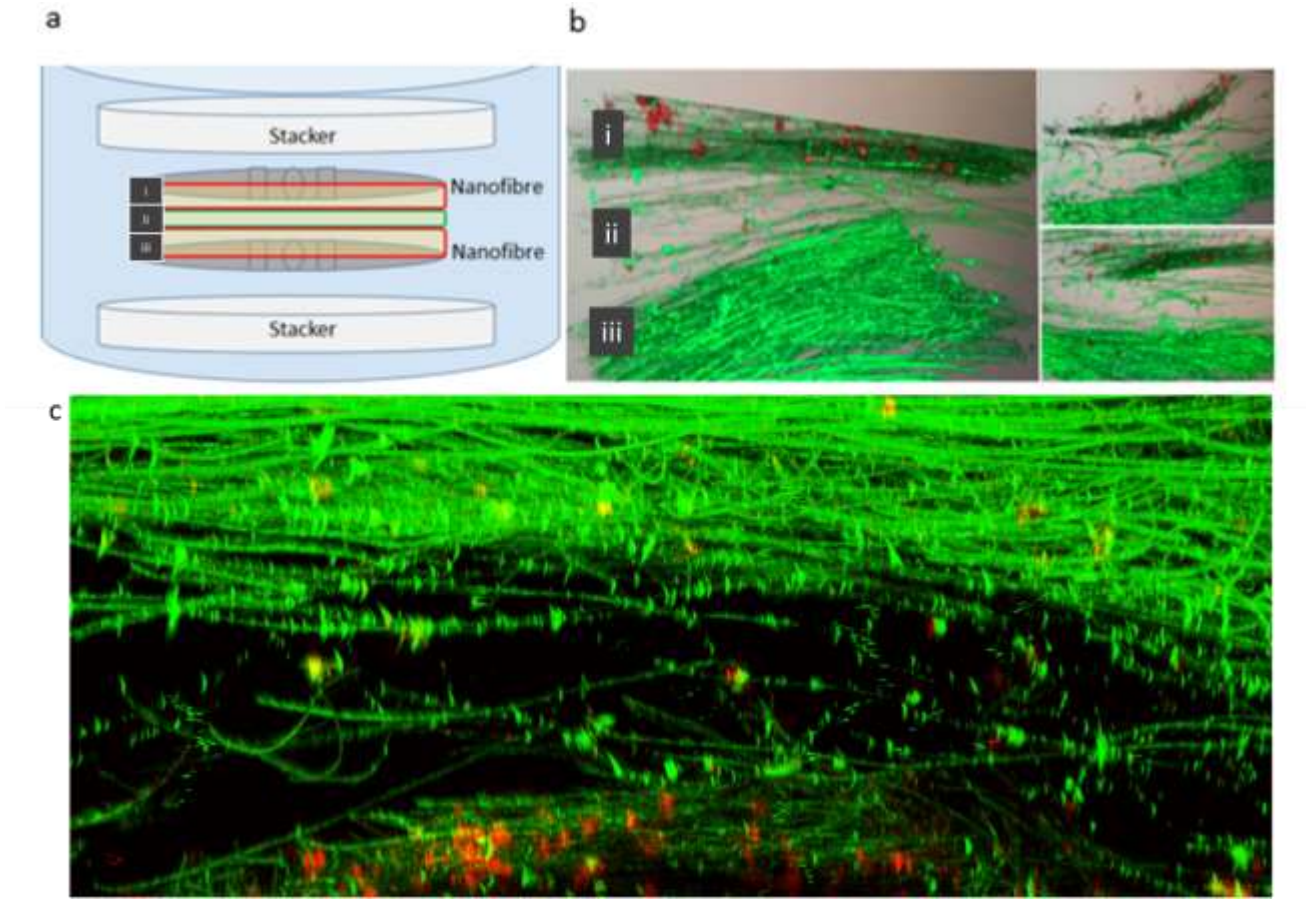

Figure 63: Diagrammatic presentation of inter-layer migration. a. Schematic drawing of the arrangement of two layers of nanofibre and how 'stackers' are used to both keeop them from the surface of the well in which culture occurs and also keep them held closely together. b. Immunofluorescence image showing green 10wt% PAN nanofibre (autofluoresces around 488nm (green)) and anti-βIII Tubulin primary antibody-(and red Alexa Fluor 568 secondary antibody) stained undifferentiated SH-SY5Y cells three hours post-layering. i, ii and iii show upper, interface and lower layers of nanofibre respectively. c. Immunofluorescence cross-sectional image of a sample showing neuronal (red – anti-βIII Tubulin primary antibody-stained) cells migrating from the bottom layer of PAN (green autofluorescence) into the top layer, through the central fibre interface - image taken twenty-four hours-post layering.

Imaging showed that bringing these two layers of hydrophobic PAN together appeared to trigger a 'laddering' effect in which the nanofibre strands formed a kind of interface. Some evidence of undifferentiated neurons (in red) migrating into this interface was seen at three-hours post layering and twenty-four hours too, which was initially unexpected. This migration provided an interesting line of investigation. It was considered that if layering nanofibre close together does trigger migration, that this phenomenon could be both useful and problematic. Specifically, if unidirectional neuronal migration and elongation were desired, lateral movement between layers could reduce efficiency of the prosthesis. Conversely, some migration could be beneficial for example in enhancing co-cultures of cells or maximising space in prosthesis designs.

To better understand the migratory behaviour of both differentiated SH-SY5Y and U-87 MG cells when brought into contact with PAN and PAN-5% Jeffamine, a basic migratory experiment was carried out. In

both cases, 50,000 SH-SY5Y or 50,000 U-87 MG cells were seeded separately on 10wt% PAN and 10wt% PAN + 5% Jeffamine respectively and allowed to attach for twenty-four hours in a CO_2 incubator. Following this, cells were subject to low serum DMEM f-12 and retinoic acid-based differentiation for seven days. At this point, layering was carried out with the same material upon which cells were initially seeded. It was hypothesised that a greater number of viable neurons would migrate into PAN and glia into PAN-5% Jeffamine. Immunofluorescence imaging shows fully mature neurons (stained with anti-βIII Tubulin primary antibody and Alexa Fluor 568 secondary antibody) and glia (stained with anti-GFAP primary antibody and Alexa Fluor 532 secondary antibody) on their respective nanofibre types. Next to these images are further images depicting days three and seven post-layering of the top-layer only. In combination with imaging, average axonal length was calculated in neurons that had migrated into either PAN or PAN-5% Jeffamine using ImageJ analysis. As before, axon length was calculated by measuring from the nucleus to the longest axonal point in 10 random examples in triplicate samples. Further, a viability assay (CellTiter-Glo® *assay*) is shown, quantifying overall viability of cells in the top layer of nanofibre in the seven days following layering. Results are shown below in Figure 64.

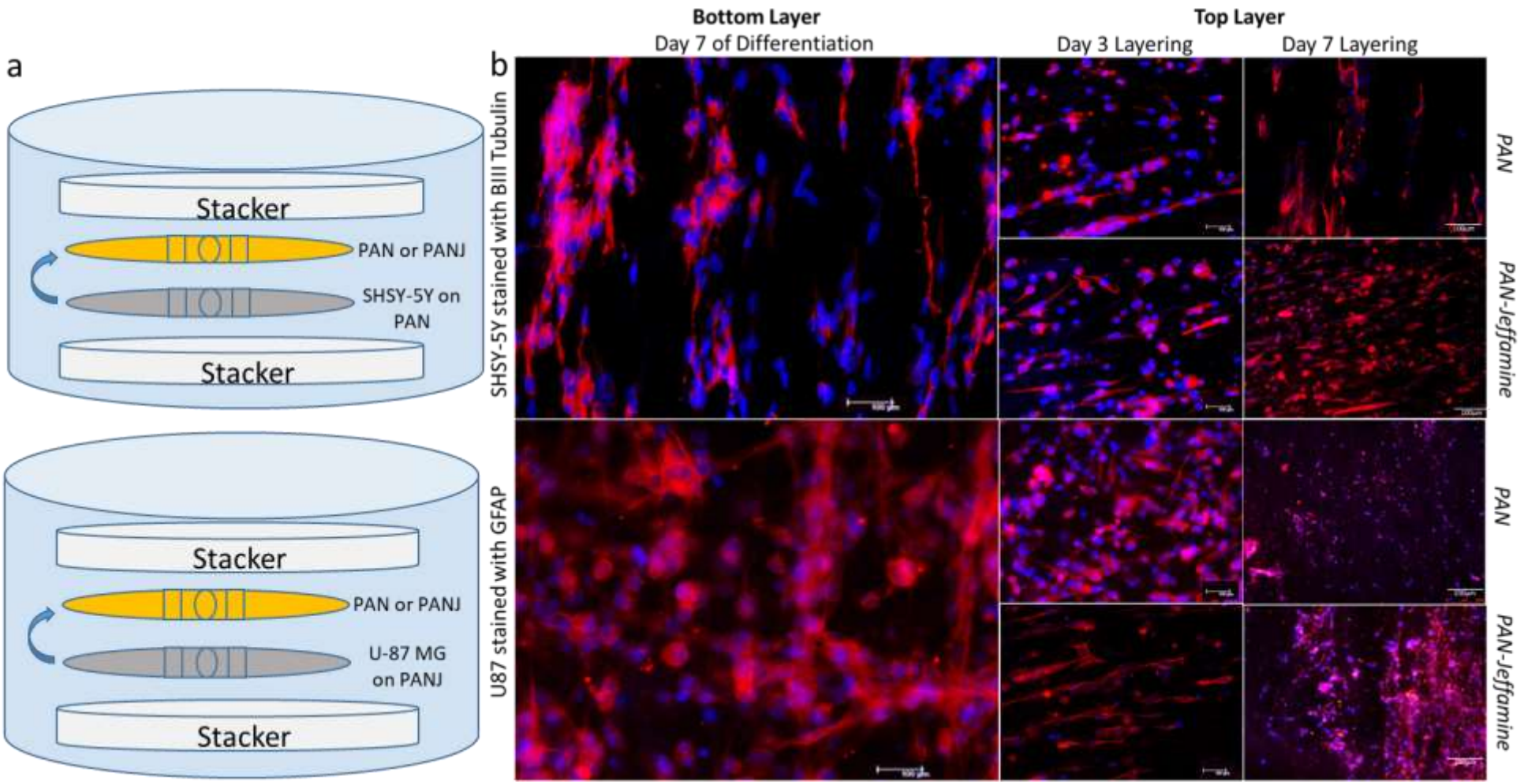
a
Stacker
PAN or PANJ
SHSY-5Y on PAN
Stacker
Stacker
PAN or PANJ
U-87 MG on PANJ
Stacker
b
Bottom Layer
Day 7 of Differentiation
Top Layer
Day 3 Layering
Day 7 Layering
SHSY-5Y stained with BIII Tubulin
U87 stained with GFAP
PAN
PAN-Jeffamine
PAN
PAN-Jeffamine

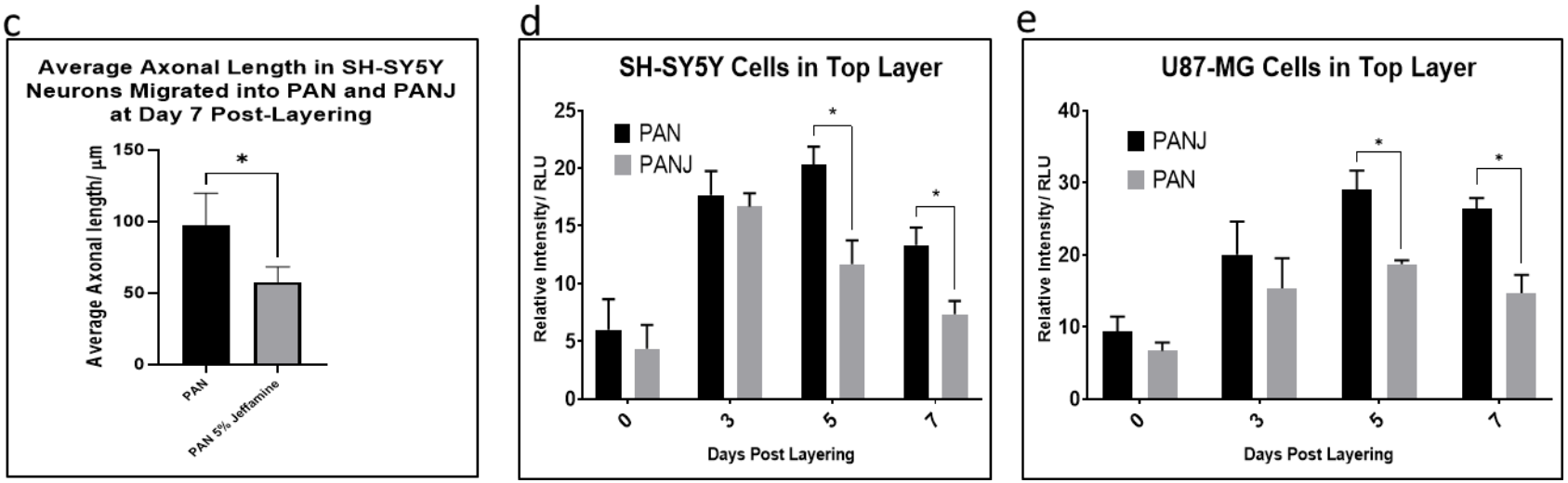

Figure 64: a. Schematic diagram displaying the experimental set-up for immunofluorescence and viability experimentation. b. Immunofluorescence imaging showing mature U-87 MG and SH-SY5Y cells (large picture on the left) stained with primary anti-βIII Tubulin and anti-GFAP antibody respectively following seven days of differentiation (both stained with Alexa Fluor 568 secondary antibody in red, in blue is DAPI-stained nuclei). On the right are images of the top layer of layered PAN or PAN + 5% Jeffamine at days 3 and 7 post layering, stained as before. c. Average axonal length calculated using ImageJ analysis on immunofluorescence images obtained. d+e. Viability assessment using the CellTiter-Glo® *assay on mature SH-SY5Y and U-87 MG cells that had migrated into the top layer on either PAN or PAN + 5% Jeffamine in each case. In 'c', Significance was assessed using an unpaired, non-parametric, two tailed T-test, using the Holm Sidak method, with a P-value of <0.05 indicating significance (*). In 'd' and 'e', Significance was assessed with a two-way ANOVA with Sidak's multiple comparisons test with P<0.05 (*).*

Results showed that neuronal migration yielded greater overall viable cell quantities into PAN top-layers over the seven days. Specifically, evidence suggested that from day five, significantly greater neuronal viability was shown in these top layers, perhaps due to a combination of the known cell preference to hydrophobic scaffolds, but also sustained migration. This was evidenced both by imaging and by viability assessment with the CellTiter-Glo® assay. Those cells that did migrate into the top layer exhibited significantly longer axons in PAN top-layers than hydrophilic PAN + 5% Jeffamine layers. Glia exhibited migration also, showing greater cell viability in PAN-Jeffamine on average that was maintained to significant levels from day five. Once again this was likely the combined effect of a preferred culture on hydrophilic scaffolds and sustained migration.

Having established an understanding as to the inter-layer migratory potential of both neurons and glia when layered with either hydrophobic or hydrophilic nanofibre, a brief investigation into the migration patterns of these cells in the presence of PAN + 1% Jeffamine was carried out. A viability (CellTiter-Glo®) assay was used to assess overall cell viability in the top layer of PAN + 1% Jeffamine only. 50,000 SH-SY5Y and 50,000 U-87 MG cells (ATCC, USA) were independently seeded on 10wt% PAN + 1% Jeffamine and allowed to attach for twenty-four hours in a CO_2 incubator. Following this, cells were subject to low serum DMEM f-12 and retinoic acid-based differentiation for seven days. At this point, fibre was layered with acellular PAN + 1% Jeffamine. It was hypothesised that migration would be relatively equal in both cell lines if neuronal migration was greater into PAN and glial migration was greater into PAN + 5% Jeffamine. Results are shown in figure 65.

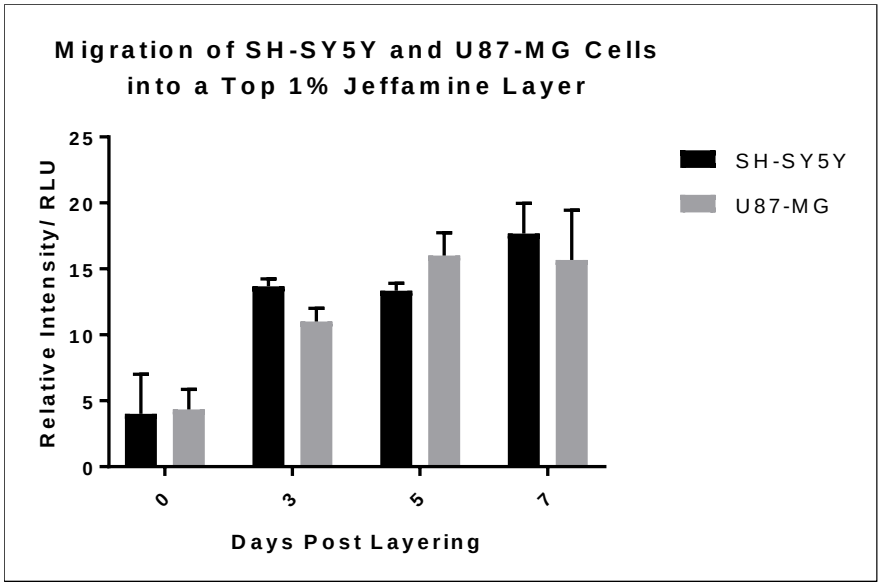

Figure 65: Assessment of viability of SH-SY5Y and U-87 MG cells in a top PAN + 1% Jeffamine layer added on top of a layer of mature SH-SY5Y cells (on PAN) or mature U-87 MG cells (on PAN + 5% Jeffamine) using the CellTiter-Glo® assay. Viability was measured over seven days post layering. Significance was assessed with a two-way ANOVA with Sidak's multiple comparisons test with P<0.05 (*).

As predicted, results showed that there was indeed no significant difference in viability of neurons and glia on layered PAN + 1% Jeffamine. These results began to highlight the potential control that engineering top-layers with specific properties could have upon cellular migration. Further, in a prosthesis in which neurons and glia were initially cultured on separate scaffold nanofibre layers and later brought together, some migration may be expected. This was considered in the design of prosthesis specifications. The property was considered potentially useful in assessment of cells that have 'migrated' into a prosthesis. In this study, it was hypothesised that in vivo, a pre-seeded glial population may be useful in a prosthesis, but resident neuronal cells would have to migrate into the system. Recreating this situation in multi-layered systems in which neurons underwent controlled migration from a central 'pool' into the nanofibre design of choice provided experimental opportunity.

8.3 Co-Culture – Direct or Indirect?

Before multiple-layers of cells were used with complex co-cultures, PAN + 1% Jeffamine nanofibre (which did not significantly change the migration of neuronal or glial cells) presented an opportunity to investigate the influence that glia had on neuronal migration and axon elongation on one layer. In the following investigation, a nanofibre design was chosen such that populations of cells could be seeded on one layer in different, connected locations as shown in figure 66. Specifically, three connected circles existed; to the first 10,000 SH-SY5Y were seeded, the second 10,000 U-87 MG were seeded and the third was left empty. The fibre was left for twenty-four hours in a CO_2 incubator in 10% serum DMEM F-12 media as before for cells to attach and then was subject to low serum DMEM F-12 and retinoic acid-based differentiation for seven days. Fixation and staining with fluorescent antibodies were carried out to allow Immunofluorescence imaging. Here, DAPI-stained nuclei and βIII Tubulin-stained axons were imaged over time from their origin either into the glia-seeded region or the empty region. As all cells were on one level, gravity could play no part in the test. Further, as all cells were on PAN + 1% Jeffamine, material type could not play a role in the migration. Immunofluorescent images show neurons and glia in each of the regions described as well as an example of the inter-region junctions from neuron-empty and neuron-glia regions. These inter-region junctions consist of aligned nanofibre created as an artefact of electrospinning three random circles in close proximity. As this experiment aimed to track neuronal cell migration, no stain for glia was used other than nuclear DAPI stain. Average axonal length was measured by taking distance between the nucleus and longest axon in ten regions on four samples.

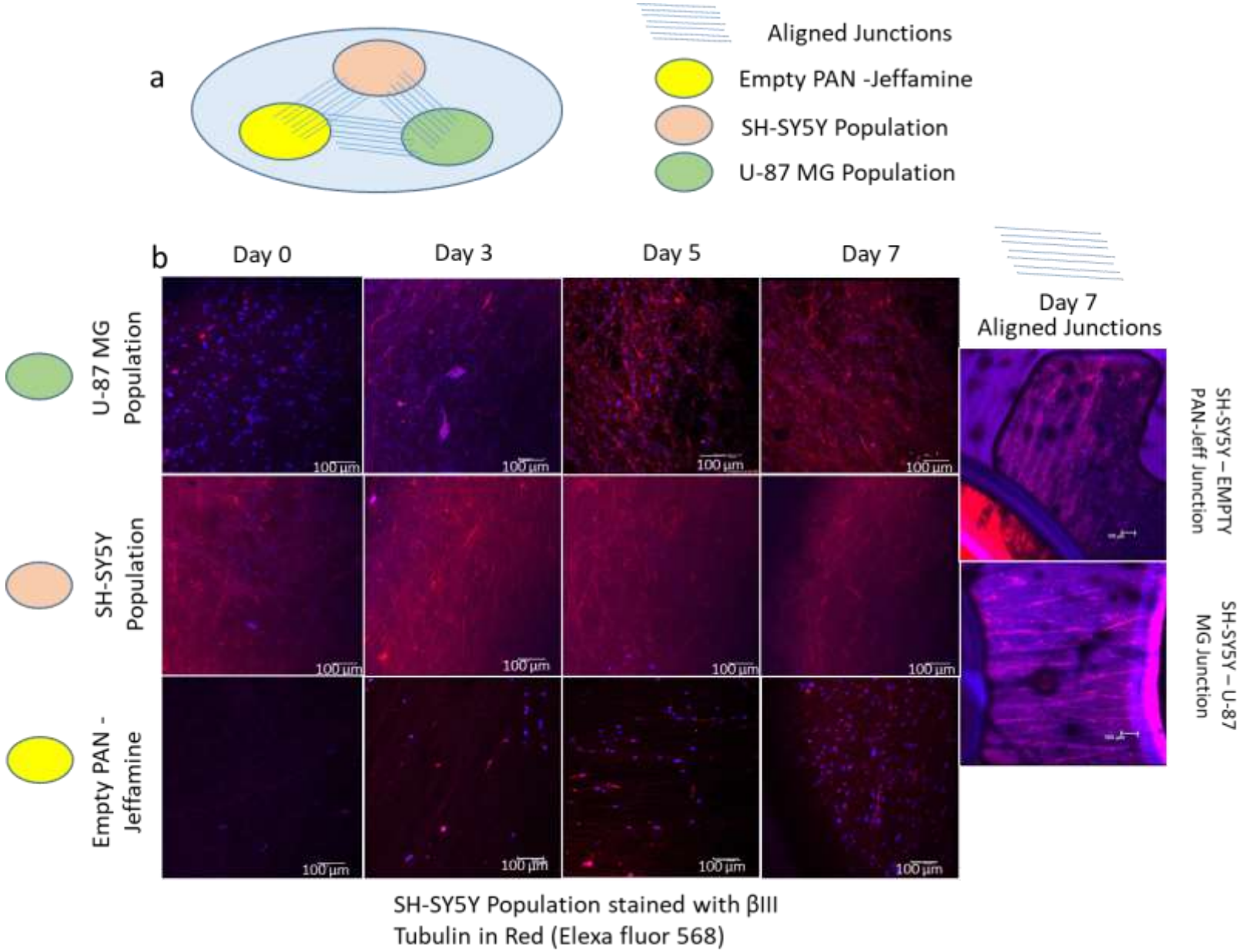

SH-SY5Y Population stained with βIII Tubulin in Red (Elexa fluor 568)

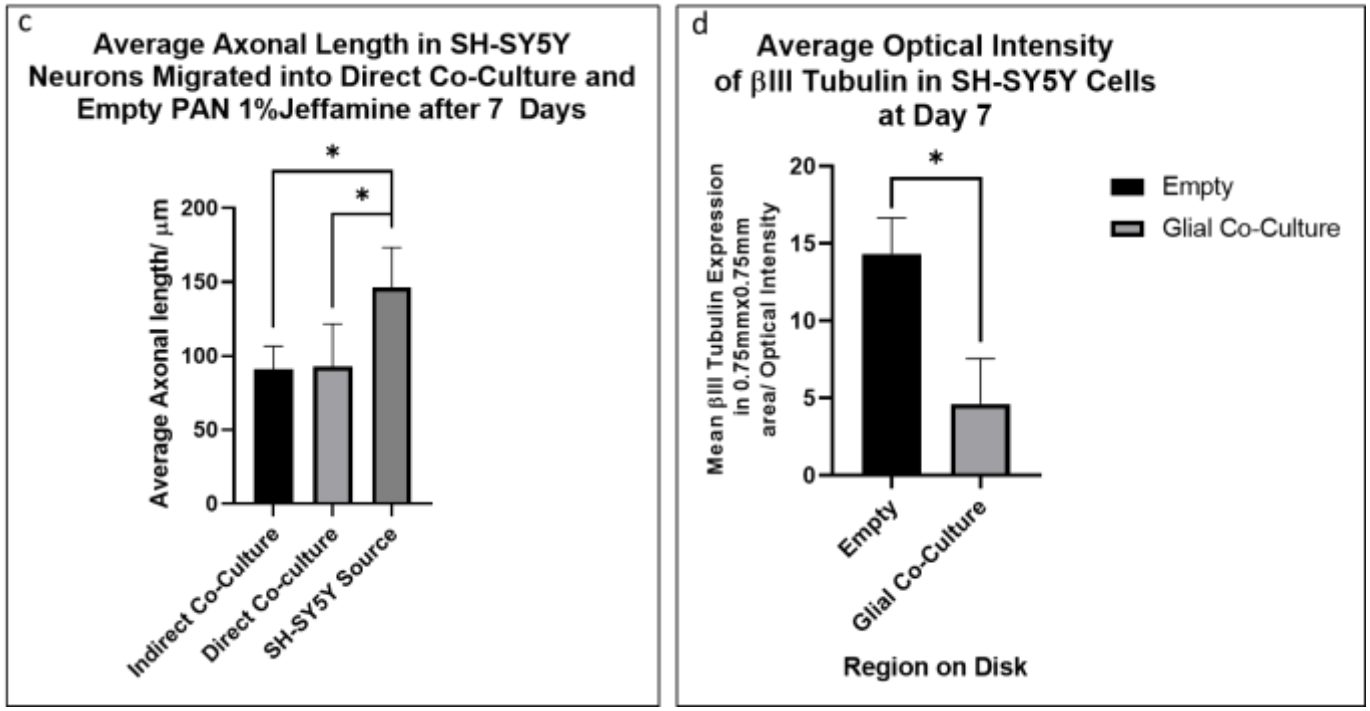

Figure 66: Neuronal Migration to direct or indirect co-culture. a. Schematic diagram describing the experimental set-up in this investigation. Three areas of random nanofibre are linked by regions of aligned nanofibre. b. Immunofluorescence imaging depicting anti-βIII Tubulin primary antibody (and red Alexa Fluor 568 secondary antibody) staining and DAPI - stained SH-SY5Y cells and DAPI-stained U-87 MG cells in all regions of the structure over seven days. c. Average axonal length of SH-SY5Y cells in direct and indirect co-culture in the structure at day seven calculated using ImageJ analysis of Immunofluorescence images on 10 axons in four samples. d. Average optical intensity of βIII Tubulin calculated using ImageJ analysis on the red channel only in triplicate samples. Significance in 'c' was assessed with a one-way ANOVA with Sidak's multiple comparisons test with P<0.05 (*). Significance in 'd' was assessed using a two-tailed, parametric, unpaired t-test with Welch's correction with a P-value of <0.05 (*).

Results showed that migration was evident both into the originally acellular region and that containing glial cells. From visual assessment and quantification by measuring optical intensity of the red βIII Tubulin channel at day 7, it appeared that a greater neuronal presence existed in regions containing glial cells. This evidence suggested that glia did play some role in mediating neuronal migration. An assessment of axon length however showed that there was no significant difference between axon length in neurons in direct coculture with glial cells and those that were not at day seven. Further, perhaps unsurprisingly, in those neurons that did not migrate, axon length was significantly greater than those that did, whether in co-culture or not. This was likely the product of migration and elongation both requiring energy, cells that did not migrate simply elongated more. Assessing the immunofluorescence images and post-imaging analysis, evidence suggested that perhaps glia had a global effect upon neuronal behaviour in axon elongation and in migration. Ensuring both migration and elongation was as efficient as possible was a key aspect for consideration in a prosthesis design (in the context of axon length and viability). This was because neurons must be recruited into and then traverse a prosthesis. It was considered that using a multi-layer system and controlled migration, it may be possible to track neuronal migration, viability and axonal length from a central pool of neurons into either direct or indirect glial co-culture. It was hypothesised that the global and local effects that glia may have in a multi-level system could be assessed. In this experiment, using seeding techniques (volumes as low as possible), local seeding of cells was carried out as best possible, though it was possible that some cells escaped into neighbouring regions, or at least the junctions – this was avoided as much as possible. This risk was addressed by using multiple layers in following experiments.

In the following investigation, 50,000 SH-SY5Y and 50,000 U-87 MG cells were seeded separately on 10wt% PAN and 10wt% PAN + 5% Jeffamine respectively and allowed to attach for twenty-four hours in a CO_2 incubator. Following this, cells were subject to low serum DMEM f-12 and retinoic acid-based differentiation for seven days. At this time, the layer of glia was placed atop the layer of neurons and an empty layer of PAN placed at the bottom of the stack. The neuronal population acted as a 'pool' of neuronal cells from which neurons could either migrate into an acellular layer of PAN (where there was unlikely to be any glial cells, confirmed with immunofluorescent staining), with indirect glial co-culture, or into a cellularised layer of PAN + 5% Jeffamine, with direct glial co-culture.

The neuronal axon length and viability was explored in cells that had migrated to form a direct co-culture and an 'indirect' co-culture. A secondary, more general analysis of migratory behaviour of cells in a co-culture system and the influence of gravity could also be carried out. Post layering, cells were subject to immunofluorescence staining (anti-βIII Tubulin primary antibody staining with red Alexa Fluor 568 secondary staining for neurons and anti-GFAP primary antibody with yellow Alexa Fluor 532 secondary antibody staining for glia) and assessment of axon length using ImageJ analysis - measuring from the cell body (nucleus) to the longest axon tip. In combination with imaging, a quantification using CellTiter-Glo® viability assay was utilised to track overall cell viability on the glial layer above and empty PAN below over

the seven days post layering – as both an (initially) empty layer of fibre and (initially) cellularised layer of fibre were being analysed a higher gain was used in analysis in this case only. In future work the gain remained low as previously done and of course data here was not directly compared to other experiments. It was understood that the PAN + 5% Jeffamine layer was already cellularised and so viability assessment was limited. This was resolved in the follow up experiment. All results are presented in figure 67.

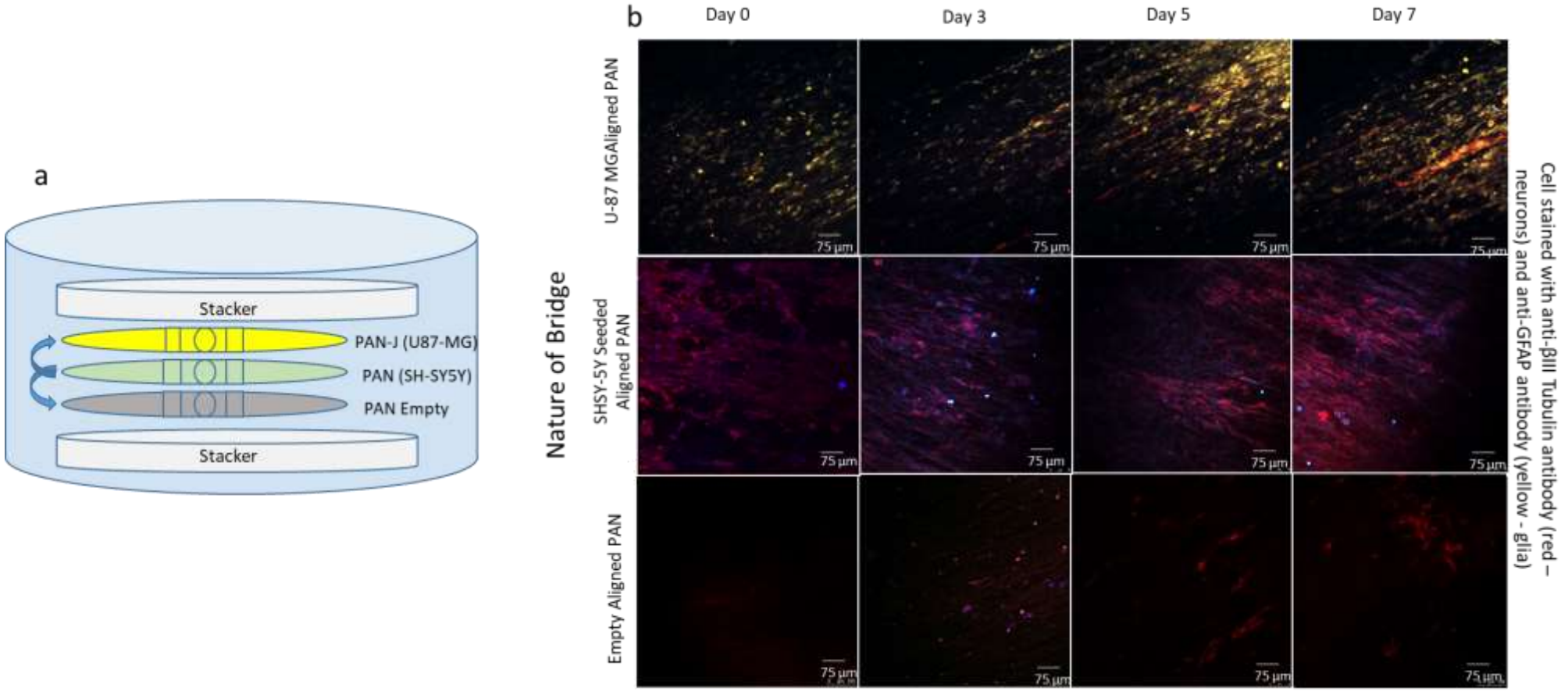
a
Stacker
PAN-J (U87-MG)
PAN (SH-SY5Y)
PAN Empty
Stacker
b
Day 0
Day 3
Day 5
Day 7
Nature of Bridge
U-87 MGAligned PAN
SHSY-5Y Seeded Aligned PAN
Empty Aligned PAN
75 µm
Cell stained with anti-βIII Tubulin antibody (red – neurons) and anti-GFAP antibody (yellow - glia)

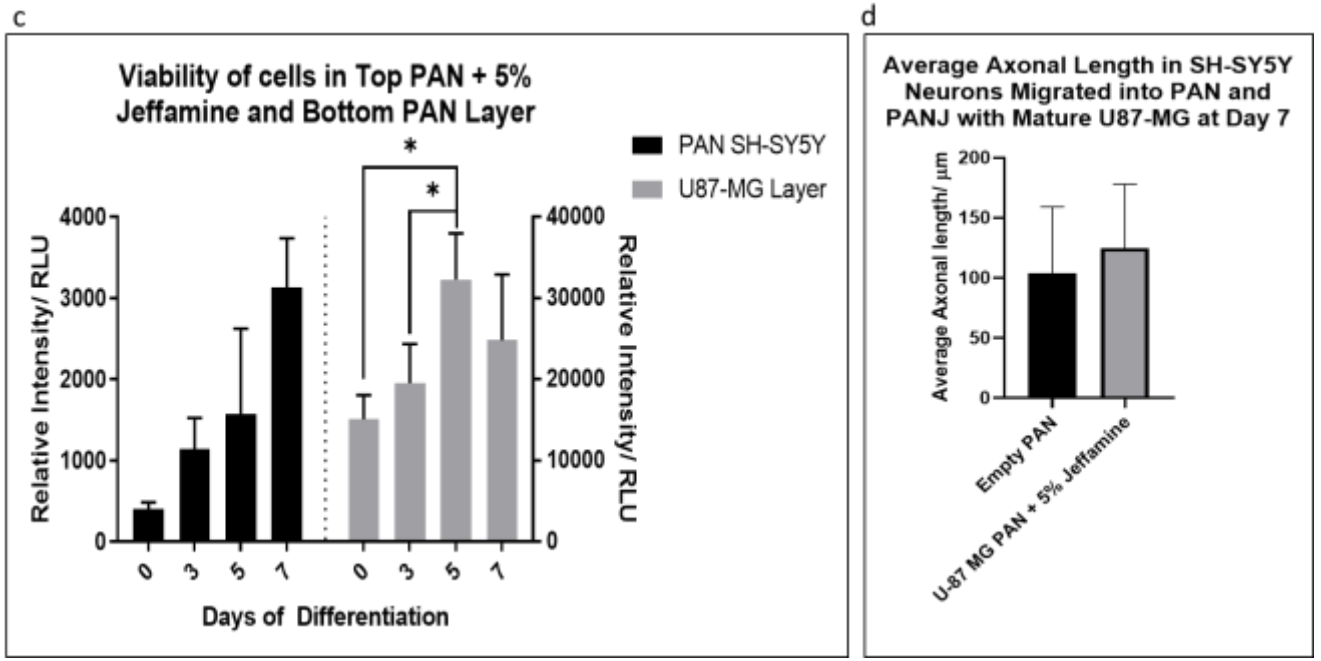

Figure 67: a. Schematic describing the experimental set up in this triple layer investigation. b. Immunofluorescence image depicting arrangement of mature SH-SY5Y and U-87 MG cells in each of the three layers. SH-SY5Y neurons are tagged with anti-βIII Tubulin primary antibody (and red Alexa Fluor 568 secondary antibody) and U-87 MG tagged with primary anti-GFAP antibody (and yellow Alexa Fluor 532 secondary antibody). c. Assessment of cellular viability in the top PAN + 5% Jeffamine and bottom PAN layers over seven days of differentiation – CellTiter-Glo® assay. d. Average axonal length as calculated using ImageJ to assess axon length at day seven post layering in the top PAN + 5% Jeffamine layer and bottom PAN layer. In 'c', Significance was assessed with a two-way ANOVA with Sidak's multiple comparisons test with P<0.05 (*). In 'd', significance was assessed using a two-tailed, parametric, unpaired t-test with Welch's correction with a P-value of <0.05 (*).

From visual assessment, results showed neuronal migration both into the acellular PAN layer and into the PAN + 5% Jeffamine layer containing mature glia cells. Immunofluorescence imaging indicated long extended axons being present in both cases with no significant difference in axon length between neuronal cells in direct co-culture on the bottom PAN + 5% Jeffamine layer, and those in indirect co-culture on the top PAN layer. Neuronal length was compared only in the top and bottom layers where direct co-culture could be considered negligible or confirmed to be present (confirmed by immunofluorescence staining). Cell viability was calculated using a CellTiter-Glo® viability assay, though this was difficult to compare directly given the presence of both neurons and glia on the top layer and only neurons on the bottom layer (evidenced by immunofluorescence imaging). As a result, despite significance at every time point, this was not marked on the graph as it would be an unfair comparison. Some suggestions can be drawn from this however – specifically in it was known that neurons do not survive well on PAN- 5% Jeffamine and so perhaps the drop to 24819(RLU) in this layer (labelled 'U-87 MG layer') in overall viability at day seven post layering is the product of neuronal presence.

In summary, results suggested that neuronal migration occurred both when PAN or PAN + 5% Jeffamine are put in close proximity – glial presence wasn't enough to override migration to an acellular layer. Glia seemed to have a global effect upon axonal length as well as local. More generally speaking, in a multi-layer prosthesis, putting layers of cells in close proximity will lead to cellular migration. Though a useful tool in testing prosthesis designs, in practise, neuronal cells should remain on one layer of fibre, traversing this layer only. Given that direct co-culture was not required for long axon formation, it was hypothesised that a multi-level design in which physically separated PAN-based neurons and PAN + 5% Jeffamine-based glia may provide the most effectual prosthesis design in which axonal elongation is maximised whilst minimising unwanted inter-layer neuronal migration. To confirm this hypothesis, a follow up experiment was designed.

In the following investigation, once more, 50,000 SH-SY5Y and U-87 MG cells were seeded separately on 10wt% PAN and 10wt% PAN + 5% Jeffamine respectively and allowed to attach for twenty-four hours in a CO_2 incubator. Following this, cells were subject to low serum DMEM f-12 and retinoic acid-based differentiation for seven days. At this time, the layer of glia was placed at the bottom as a basement 'feeder' layer. Atop this layer was placed the mature neurons and the empty PAN was placed above that. Glia were so placed as it was considered that though some migration may occur into the central neuronal layer, it was unlikely that they may end up on the initially empty top-layer, particularly against gravity. Once again, neurons from a central PAN-based 'pool' migrated either into direct co-culture or into empty PAN with indirect co-culture. This set-up was compared to an identical system in which glia were not seeded on the basement layer, only mature neurons in the central layer. It was possible therefore to compare migrated neuronal axon length and viability when subject to direct, indirect and no co-culture. Further, once again more broadly it was possible to better understand cellular migration in a multi-layer (co-culture) system.

Immunofluorescence imaging, using anti-βIII Tubulin primary antibody, red Alexa Fluor 568 secondary antibody and blue nuclear DAPI stain (for all cells) to probe cells was carried out to assess neuronal migration from this middle layer into the PAN layer above and PAN + 5% Jeffamine layer below. Using images, it was possible to quantify axon length using ImageJ analysis, measuring or the cell body to the longest axon tip. It was also possible to compare viability of cells in the top and middle layers (neuronal populations) using the CellTiter-Glo® assay.

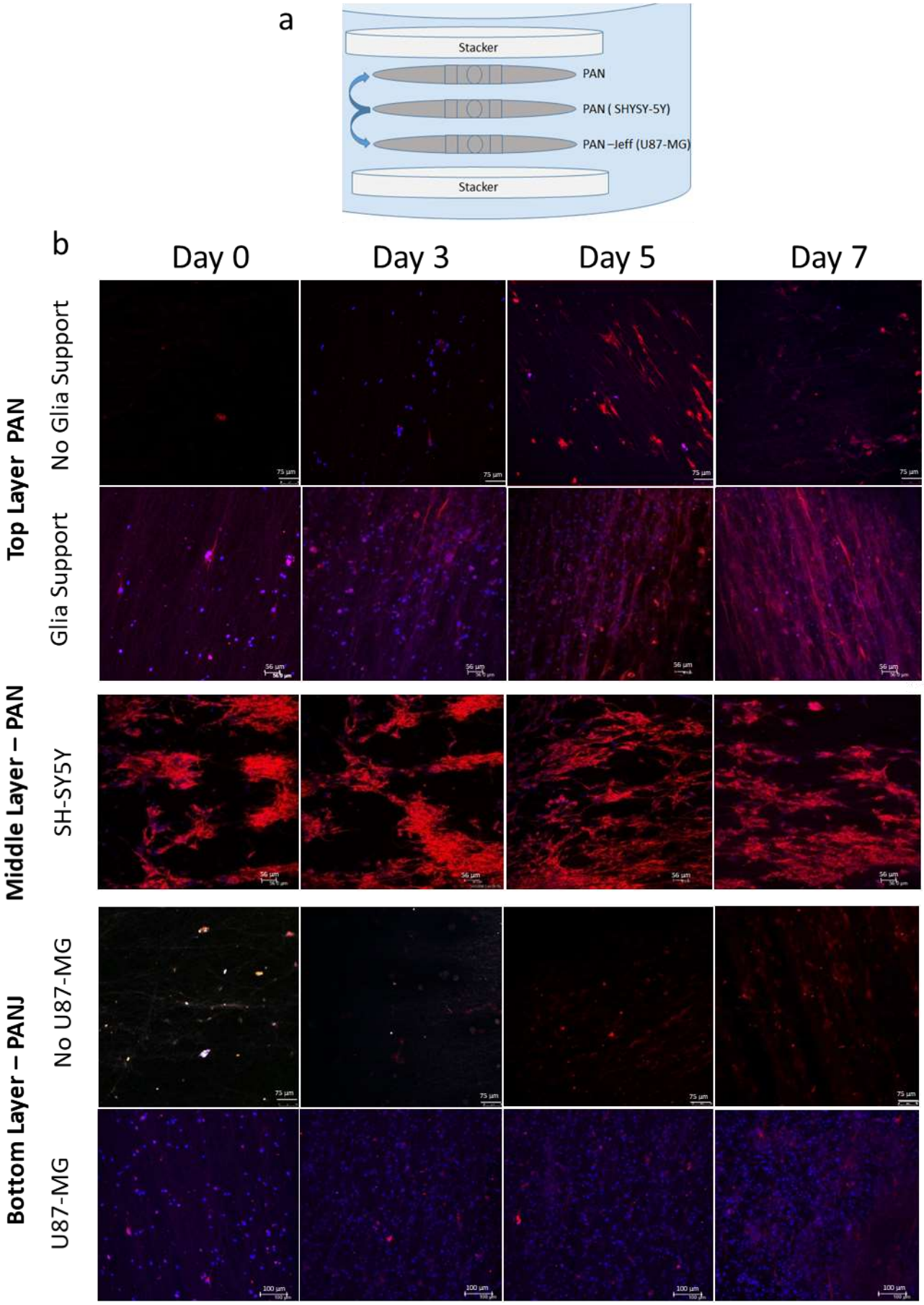
a
Stacker
PAN
PAN (SHYSY-5Y)
PAN –Jeff (U87-MG)
Stacker
b
Day 0
Day 3
Day 5
Day 7
Top Layer PAN
No Glia Support
Glia Support
Middle Layer – PAN
SH-SY5Y
Bottom Layer – PANJ
No U87-MG
U87-MG

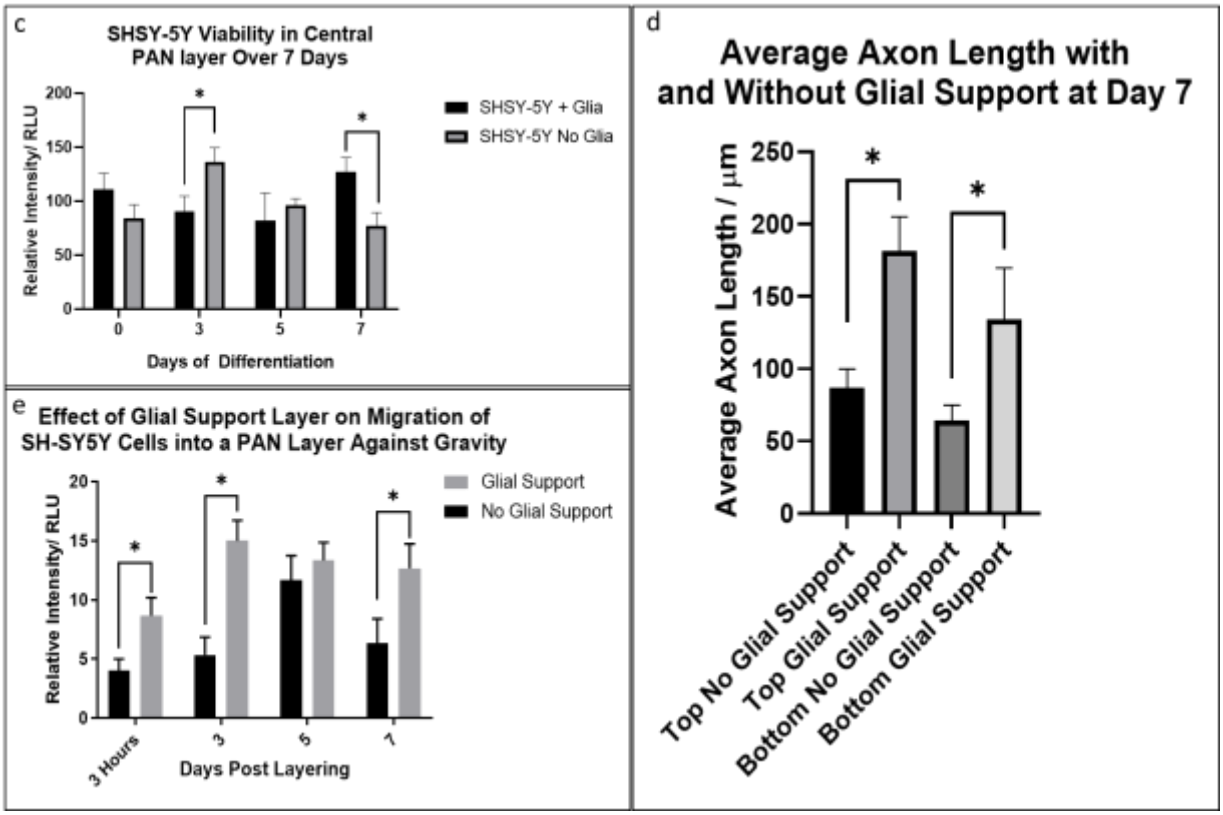

Figure 68: Impact of direct and in-direct co-culture on a multi-layer prosthesis system. a. Schematic describing the experimental set up in this triple layer investigation. b. Immunofluorescence image depicting arrangement of mature SH-SY5Y and U-87 MG cells in each of the three layers. SH-SY5Y neurons were stained with anti-βIII Tubulin primary antibody (and red Alexa Fluor 568 secondary antibody) with blue DAPI staining. U-87 MG cells were stained with DAPI only. c. Assessment of cellular viability in the middle PAN layer over the seven days of differentiation – CellTiter-Glo® *Assay. d. Average axonal length as calculated using ImageJ to assess axon length at day seven post layering in the bottom PAN + 5% Jeffamine layer and Top PAN layer. e. Viability (*CellTiter-Glo®*) assay presenting viability of SH-SY5Y cells in the top PAN layer in the presence and absence of glial support from the bottom layer. In 'd', Significance was assessed using a one-way ANOVA with Sidak's multiple comparisons test with P<0.05 (*). In 'c' and 'e', Significance was assessed with a two-way ANOVA with Sidak's multiple comparisons test with P<0.05 (*).*

This unique experimental set-up enabled tracking of long-term neuronal viability in the presence of mature U-87 MG cells (ATCC, USA) in direct, indirect and in absence of coculture. Immunofluorescence imaging in figure 68b indicated that the presence of glia as a basement layer encouraged earlier neuronal migration from the central layer into the top layer (and bottom layer from visual assessment) compared to migration in absence of glia. This was evidenced also in figure 68c in which significantly greater relative intensity was seen at day zero and three where a glial population was present compared to control (absence of glia). This was evidenced also by assessing immunofluorescence imaging. Comparing figure 68c and 68e, CellTiter-Glo® assay evidence indicated a significantly lower neuronal viability in the central layer – in figure 68c - (5.33 RLU with no glial support compared to 15 RLU with glial support) at day three is seen in line with a significantly greater viability on the top layer at the same time point – figure 68e - (90 RLU with glial support compared to 136.3 RLU without glial support). By day five, neuronal viability in the top layer is relatively equal with and without glia. However, by day seven, in absence of glia, neuronal viability is significantly reduced both in the central neuronal layer and in the top PAN layer. This evidence suggested that in the presence of glia, global neuronal migration was encouraged (both into the top PAN layer and bottom PAN + 5% Jeffamine layers). Further, the presence of glia seemed to conserve long term viability in neurons both in the top and middle layers.

ImageJ quantification (shown in figure 68d) of immunofluorescence images in the top layer indicated a significant increase in axon length where a glial feeder layer was present (around 95µm). Further, average axon length was significantly longer in the bottom layer in direct co-culture at day seven compared to axons formed in the absence of glia (average of 69µm difference). Crucially, there was no significant difference between axon length in the presence of glia in direct co-culture and indirect co-culture on the top layer. Evidence suggested co-culture did not need to be direct to significantly improve axonal length. It was not deemed necessary to image the central neuronal layer in both experimental set-ups as they were visually comparable.

In summary, co-culture of glia improved the long-term viability and axonal length of neurons both locally and globally. Migration of neurons occurred both to form direct co-culture and into acellular PAN and was up-regulated globally in the presence of glia. Therefore, as previously suggested, it was likely that a prosthesis designed with separated neuronal and glial layers may provide a system with optimum long-term neuronal viability and axon length whilst avoiding unwanted neuronal migration that may reduce efficiency of repair in vivo. This was tested in the next chapter. Comparing results to those in the previous experiment, gravity did not seem to effect inter-layer cellular migration.

8.4 Media-Based Glial Factors Only

The final experiment sought to understand whether some of the effect's glia had on neurons could be re-created in the absence of said glia but with the culture media from which the glial population was differentiated. Here, 50,000 SH-SY5Y cells were seeded on 10wt% PAN and allowed to attach for twenty-four hours in a CO_2 incubator. Following this, cells were subject to low serum DMEM f-12 and retinoic acid-based differentiation for seven days. At this time, the layer of PAN with and without glial soaking (soaked for forty-eight hours in the media of mature glia that had been in said media themselves for forty-eight hours) was placed atop the layer of neurons. Migration of mature SH-SY5Y cells was tracked using the CellTiter-Glo® assay for cell viability over the three days following layering. Results are shown in figure 69.

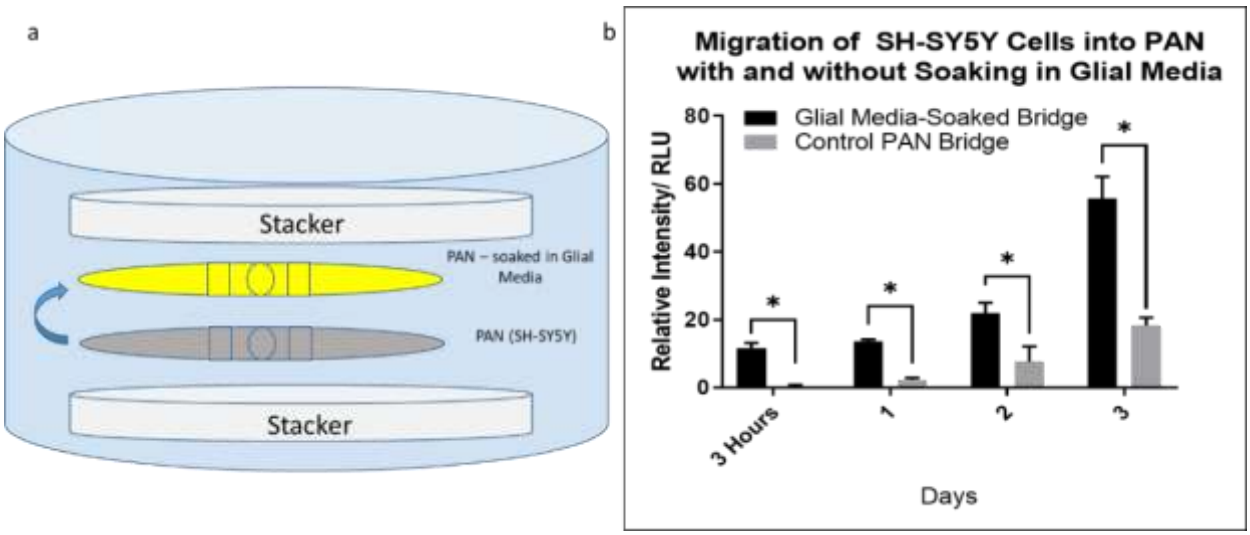

Figure 69: a. Schematic diagram depicting the experimental set up of nanofibre material types and seeded cellular populations. b. Viability assay (CellTiter-Glo® assay) showing the viability of cells in the top layer of this experiment when glial media soaking is used and when it is not. Significance was assessed with a two-way ANOVA with Sidak's multiple comparisons test with P<0.05 (*).

Results showed a significant increase in top layer neuronal viability even from three hours post layering when the top layer was soaked in glial media. This evidence suggested that some form of chemotactic or neurotrophic factor (such as NT-3 for example) released into the media during differentiation was likely responsible for this increased migratory behaviour. This evidence also supported evidence suggested above that glial cells perhaps up-regulate global neuronal migratory behaviour and that this could be conserved in an exocytosed compound in cell media.

8.5 Discussion

It was concluded that migration between layers of nanofibre was possible when nanofibre was brought into proximity using stackers. Material hydrophobicity influenced the cellular migration in glia and neurons

differently. When neurons and glia were brought together directly, glia up-regulated global neuronal migration, both to form a direct co-culture and away from direct co-culture, even against gravity. Long term viability and neuronal axon length were significantly increased in the presence of glial cells in direct and indirect co-culture. A prosthesis design which incorporated separated layers of neurons and glia may boast optimal long-term neuronal viability and axon extension whilst minimising inter-layer migration. This migration proved to be a useful tool in testing prosthesis designs and was later developed into a functioning model for SCI (chapter 10).

Considering now the overall aim of this investigation in developing a functional prosthesis, a multiple layer prosthesis was the most likely solution given the enhanced viability of neurons on PAN and glia on PAN – 5% Jeffamine. Unexpectedly, placing layers of nanofibre together led to inter-layer migration. Having understood this migration, it clearly provided some merit in that it could be used to track migration into a prosthesis in a modelling scenario. However, a multi-layer design that limited migration was deemed more appropriate. Understanding behaviour of cells within this multi-layer system helped to establish the neuronal benefits of an indirect co-culture. Further, global up-regulation of migration in the presence of glia was considered potentially beneficial in vivo if glia were resident within said prosthesis - neuronal migration into the implant could be enhanced.

Assessing the literature, little evidence of culture of SH-SY5Y or U-87 MG cells using multiple layers of nanofibre was seen. However, more broadly, the technique was being used to recreate other complex tissue types. For example, the Kim et al group showed that layers of aligned and random fibre could be used to culture maturing neuronal cells in an aligned fashion, while using double layers of random nanofibre to prevent the invasion of a glial population and to provide structural support (Kim et al. 2016). Further, the Barker et al group demonstrated that layering multiple layers of electrospun nanofibre with multiple endothelial cell sub-types pre-seeded on each led eventually to a thick layer of nanofibre with cells present throughout (Barker et al. 2013). The purpose of this study was to enhance soft tissue engineering where multiple cell types were present (similar in concept to this study on a different tissue type). Evidence that cells do migrate within their nanofibre layers to fill out the structure was encouraging (Barker et al. 2013). Similarly, the Wu et al group aimed to construct a multi-layered nanofibre structure for engineered 3D cardiac anisotropy and evidenced an enhanced overall structure capable of controlling cellular orientation and maturation using co-culture between layers (Wu, Y. et al. 2017). Given that multiple groups were utilising this technique to enhance tissue regeneration, it was ascertained that the conclusions obtained were of note and worthy of further investigation in chapter 9.

9 Results - Prosthesis Design

9.1 Aims of the study

The study thus far had surmised that a likely effective prosthesis was one that included a residential population of glia on its respective preferred material type, and which contained layers suitable for neuronal migration into the prosthesis. Crucially, these layers would be in close proximity, but not directly in contact to prevent un-wanted cellular migration. In this section, the investigation aimed to identify candidate materials that could be utilised as barriers within the proposed prosthesis design. Further, the section aimed to define the efficacy and benefits provided by the candidate barrier materials in preventing cellular migration. Finally, this section aimed to understand neuronal and glial behaviour when a suitable barrier was used between appropriate layers of nanofibre.

9.2 Adding Space Between Layers

Initially, using light sheet microscopy at the STFC, Rutherford Appleton Laboratory (STFC, RAL), experiments were carried out which introduced space between two of the layers in the three-layer stack used in the same investigation presented in figure 63. Specifically, 50,000 SH-SY5Y and 50,000 U-87 MG cells were seeded separately on 10wt% PAN and 10wt% PAN + 5% Jeffamine respectively and allowed to attach for twenty-four hours in a CO_2 incubator. Following this, cells were subject to low serum DMEM f-12 and retinoic acid-based differentiation for three days. At this time, the layer of neurons was placed atop the layer of glia and an empty layer of PAN placed at the top of the stack (in terms of sides of scaffolds that were cellularised, all were orientated 'face-up') – see figure 70. Between the layer of glia and central neurons, approximately 2mm of space was introduced unintentionally because of a deformation in the polyester frame holding the PAN + 5% Jeffamine fibre within. The result was no physical contact between the two bottom layers. Immunofluorescence imaging using Nile red staining (lipophilic stain) was carried out showing SH-SY5Y and U-87 MG cells throughout the structure below – imaging was carried out using a light sheet microscope (Leica, UK).

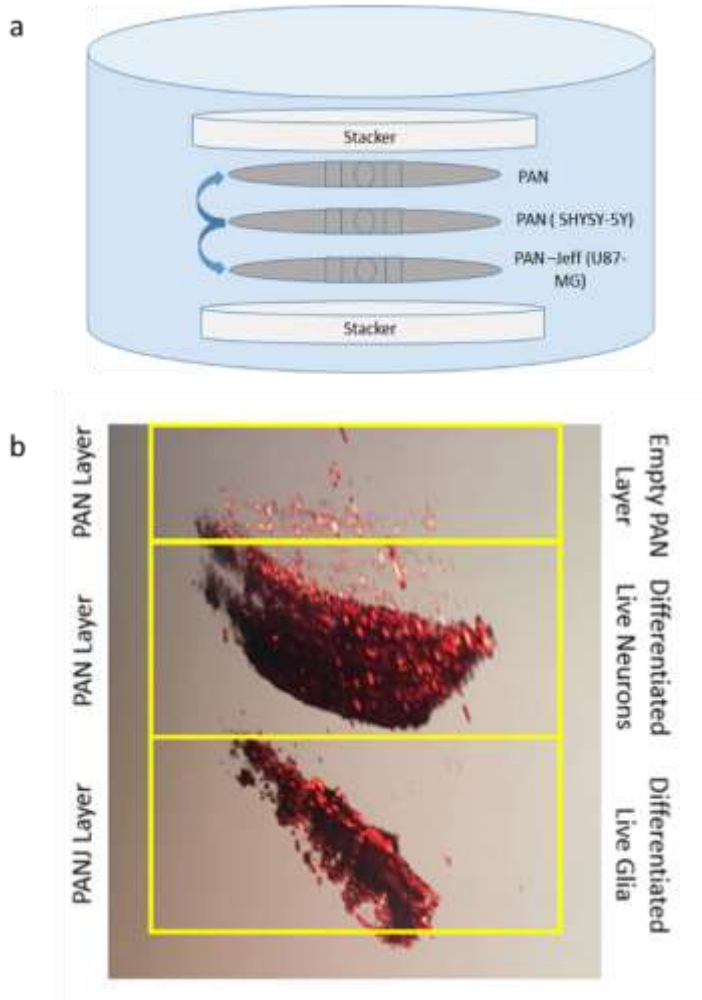

Figure 70: Triple layer construct containing physical space between layers. a. Schematic depicting the experimental set-up in the context of nanofibre layer materials in use and cellular populations seeding location. b. Light sheet image depicting Nile Red stained immature SH-SY5Y and U-87 MG cells on three layers of nanofibre at twenty-four hours post-layering. Fibre remains un-stained.

Results indicated that controlled migration was still possible between the central neuronal layer and the above PAN layer. However, no migration occurred between the bottom two layers, the glia and neuronal populations remained separate and distinct. This result demonstrates potential control that introducing space between layers could provide. It was decided however that simple space (filled with DMEM f-12 media) would be an inefficient method of controlling inter layer migration as empty space offers limited control and in vivo could even be detrimental as it could introduce air or other unwanted substances.

It was suggested that the solution to this challenge could be a thin (to allow easy passage of glial factors over a small gradient/distance), porous, 'wettable' (in aqueous solution) barrier membrane. This solution exists in vivo – for example in the Bruchs Membrane in the eye (Booij et al. 2010). This membrane acts as a molecular sieve between the retina and the general circulation, regulating exchange of biomolecules, oxygen, nutrients and waste (Booij et al. 2010). In the following investigation, four porous physical

materials were tested for their suitability in mediating/limiting cellular migration whilst maintaining the beneficial effects of glial presence.

9.3 Characterising Physical Barrier Candidates

The four materials chosen for investigation included Polypropylene (Treopore), Polyurethane, 2ml deposition of welded 10wt% PAN + 5% Jeffamine Nanofibre (referred to as welded fibre) and ePTFE (polytetrafluoroethylene). The panel of images in figure 71 presents these materials at low, medium and high magnification using SEM imaging. By analysing ten random regions of three samples using ImageJ analysis, it was possible to calculate an average pore size in each case. This data is presented in figure 71 along with contact angle calculated using DSA.

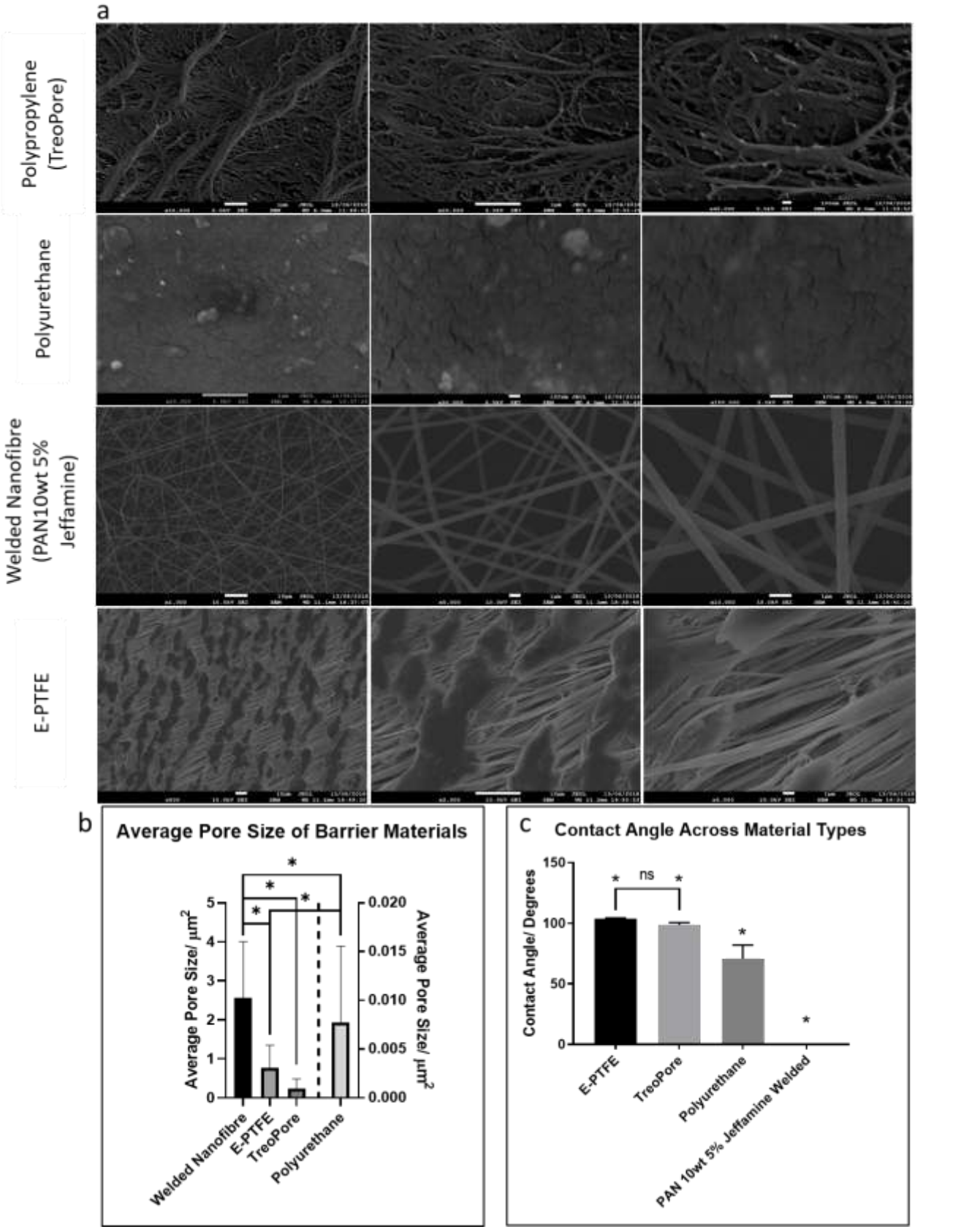

Figure 71: a. SEM imaging showing low, medium and high magnification at appropriate settings in each material. b. For comparison, these images were analysed using ImageJ for average pore size in each case. Polyurethane uses the right-hand Y axis and the others use the left-hand Y axis. c. DSA was used to assess

contact angle of each material type as part of material characterisation. Significance was assessed with a one-way ANOVA with Sidak's multiple comparisons test with P<0.05 (*), 'ns' indicates a relationship without significance – all variables were compared to each other.

Images showed that the four materials can be split into groups. Treopore and Polyurethane both exhibit comparatively low average pore size (0.229±0.256μm^{2}and 0.008±0.008μm^2) compared to welded fibre and ePTFE (2.559±1.447μm^2 and 0.760±0.586μm^2). Both ePTFE and Treopore are hydrophobic materials whereas Polyurethane and welded fibre and are hydrophilic in nature (particularly welded Jeffamine-containing fibre). It was decided that one hydrophobic material and one hydrophilic material would be selected to take forward with this investigation. Further one would have a large pore size and one would have a smaller pore size. It was decided that Polyurethane had a pore size that was too small and hydrophobicity was not distinctly hydrophobic or hydrophilic. Further, ePTFE had an elastic structure that often gave a varying pore size. Welded nanofibre and Treopore were the two materials that were selected since these fulfilled the outlined conditions.

9.4 Welded Nanofibre

The SEM images showing welded nanofibre were obtained following a manufacturing optimisation process. Typically, manufacturing welded nanofibre occurs when the needle is at a shorter distance from the grounded, rotating drum. The solvent which typically evaporates as the charged polymer reaches the drum does not completely evaporate before reaching its target. Some solvent remains which 'welds' nanofibre together, forming a more solid, inter-connected structure. The solvent then dries after nanofibre has landed. The rig available in the lab could achieve a minimum reliable distance of 7cm (literature suggests between 4 and 10cm is acceptable (Li, H. et al. 2017). To enhance the welding process, a welding kit was assembled in-house as the visual welding frequency seen from a closer needle alone was not deemed high enough – see figure 73. A schematic of apparatus is included below in figure 72.

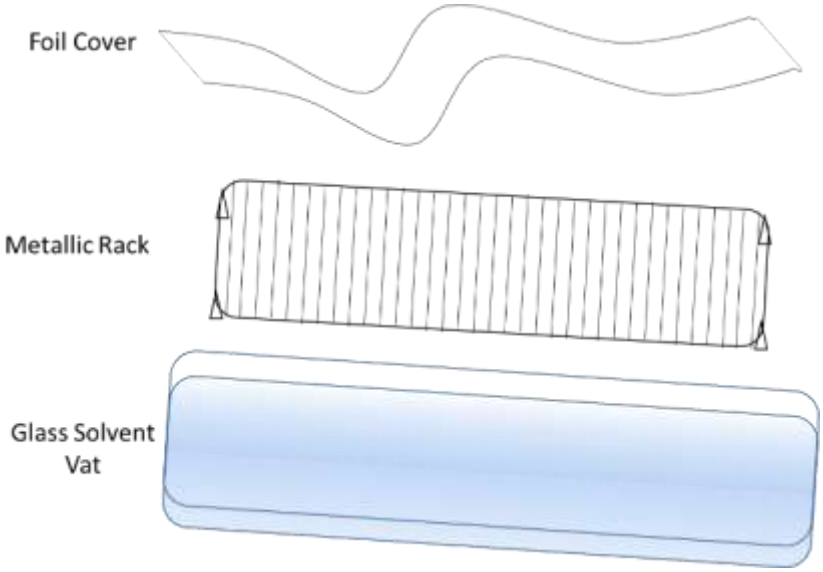

Figure 72: Design of apparatus used to conduct additional nanofibre welding. A glass Pyrex Dish/vat (40cmx27cm) held a stainless-steel metallic rack (38cmx25cm) over which tin foil was used to cover the apparatus.

Using the apparatus assembled in the diagram above, DMF (standard PAN solvent) (Fisher Scientific, UK) was poured into the glass tray (within a fume cabinet) to a depth of 2cm. The metallic rack was placed inside too such that the top surface was clear of the level of the DMF inside the vat. Post spinning, the 'pre-cut' nanofibre sheet was cut in half (200x300cm) and placed on top of the rack. Foil was used to seal the container, leaving a 1-2cm airgap above the top of the electrospinning sheet to avoid damage and to allow the solvent to reach the top surface too. The fibre was removed after a time (see figure 73) and then dried in a fan-oven at 60°C overnight typically to ensure all excess DMF was evaporated before being cut into disks using the CO_2 laser cutter (Trotec, UK) as usual.

To assess the optimum time suitable to weld nanofibre sheets in the described apparatus, SEM imaging was used to analyse weld efficiency visually over a range of time periods. Weld efficiency was analysed qualitatively by assessing relative visual frequency (compared to control) of obvious welds at 'cross-points', where fibre morphology appeared to change where two fibres had come into contact and the two fibres no longer seemed distinct. Figure 73 presents a variety of magnifications used to assess weld efficiency using welding for thirty minutes, one hour and twenty-four hours compared to control. To characterise fibre properties post-welding, average pore size and fibre diameter were quantified using ImageJ in triplicate samples manufactured using the welding spinning technique alone (control) and then fibre exposed to DMF vapour for one and twenty-four hours (where notable difference was seen). Results are displayed in figure 73.

The one-hour and twenty-four-hour exposure conditions were deemed better than the others as fusion between crossed nanofibres over cross-points was more noticeable visually than at thirty minutes or less.

Obvious morphological changes were seen at the cross points, showing that the fibres in contact were no longer individual fibres. Further, some changing in the fibre diameter occurred around the fibre contacts, which has been reported by other groups (Li, H. et al. 2017). This was comparable to other groups who for example welded PCL fibre with thirty-sixty-minute exposure to dichloromethane vapour (Li, H. et al. 2017). In future work, if finances and time allowed, computational analysis of SEM images showing likely fibre welds vs. non-welds could be done with appropriate analysis tools. Further, mechanical tests such as the tape test (sticking the fibre to a layer of tape and assessing breakage with fibre removal) could be employed to mechanically test the welding strength/welding efficiency.

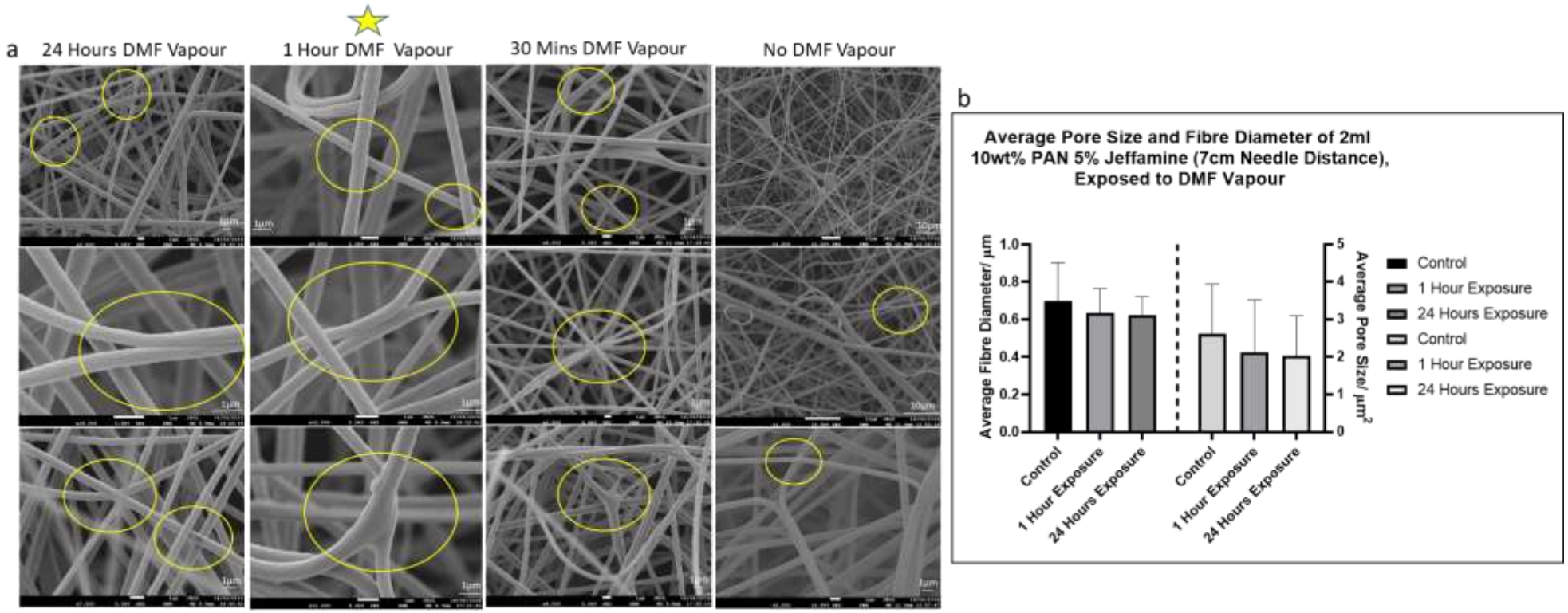

Figure 73: a. SEM panel depicting welded 10wt% PAN + 5% Jeffamine nanofibre deposited at 2ml volume and welded over a variety of times. Examples of weld points are highlighted in the varied weld-times above. The star indicates the most suitable time selected based on visual weld-point frequencies. b. Average pore size and fibre diameter in fibre exposed to DMF for 1 hour and twenty-four hours vs. control – these were the only samples with notable difference. Significance was assessed with a one-way ANOVA with Sidak's multiple comparisons test with $P<0.05$ (*).

Results indicated that notable visual difference in welding frequency could start to be seen between control and 30 minutes of DMF exposure within the constructed chamber. At 1-hour, notable improvement in visual welding evidence was seen. Assessment of cross-points indicated that fibres appeared to have become welded, showing slight morphological changes to fibre at said cross-points. No notable difference was seen between one and twenty-four hours. Therefore, considering production time-efficiency too, a one-hour weld was deemed likely to be the most effective exposure time to take forward with the investigation. These findings were seen also by other groups carrying out similar investigations (Li, H. et al. 2017). To understand any changes in fibre properties because of DMF vapour exposure, fibre diameter and pore size were assessed. Interestingly, no significant change in either fibre diameter or pore size was observed, a finding in line with other groups in the literature (Li, H. et al. 2017). Groups suggested that mechanical strength (tested by the tape test or measuring breakage with elongation for example) of welded fibre can increase dramatically, by as much as 200% (Li, H. et al. 2017). It was hypothesised that welding could strengthen the fibre network while maintaining porosity and minimising cellular traffic.

The number of welds was dependent upon the number of contacts made in the nanofibre architecture. It was important not to disrupt said nanofibre architecture whilst ensuring the fibre was welded. It was therefore decided that this 1 hour of DMF vapour exposure would be used in addition to the changed electrospinning parameters (spinning distance). To test that the nanofibre had been effectively welded, a scalpel blade (RS Pro scalpel blade (Swann Morton, UK)) was passed over the surface of the welded fibre to ensure it had gone from 'fluffy' to more 'film' like visually.

If time and finances allowed, further experimentation into mechanical strength and other means of testing weld efficiency such as crystallinity for example would have been carried out. However, it was decided that the evidence collected was enough to deem the fibre appropriate for welded fibre biological testing.

9.5 Cellular Response to Barrier Deployment

Having established that it was to be welded nanofibre and Treopore to be brought forward as candidate barriers for prosthesis design, cellular testing was commenced. The first test assessed cellular attachment and survival on the barriers in question. This was tested by seeding 50,000 SH-SY5Y and 50,000 U-87 MG cells separately on each barrier. Culture for twenty-four hours in a CO_2 incubator in 10% serum DMEM f-12 allowed attachment before layering barriers upon aligned nanofibre of the relevant type (SH-SY5Y required PAN and U-87MG cells required PAN - 5% Jeffamine). The control was 1ml un-welded, random PAN/ PAN + 5% Jeffamine. In this way it was possible to measure attachment, survival and possible migration through the barrier (relative to cells that attached). Standard cell seeding protocols were followed, though in the case of highly hydrophobic Treopore, care was taken to keep the barriers saturated with media up until the point of cell seeding, or else cells would remain in a droplet of media on top of the barrier surface. Results are shown in figure 74, described using the highly versatile CellTiter-Glo® assay.

This assay was chosen as it has been shown to accurately track cell viability in 3D scaffolds. Percentage migration is calculated for day seven only as this is the point at which cells are considered fully mature and the system considered to be stabilised. The percentages were calculated by comparing the values from figure 74c and 74d.

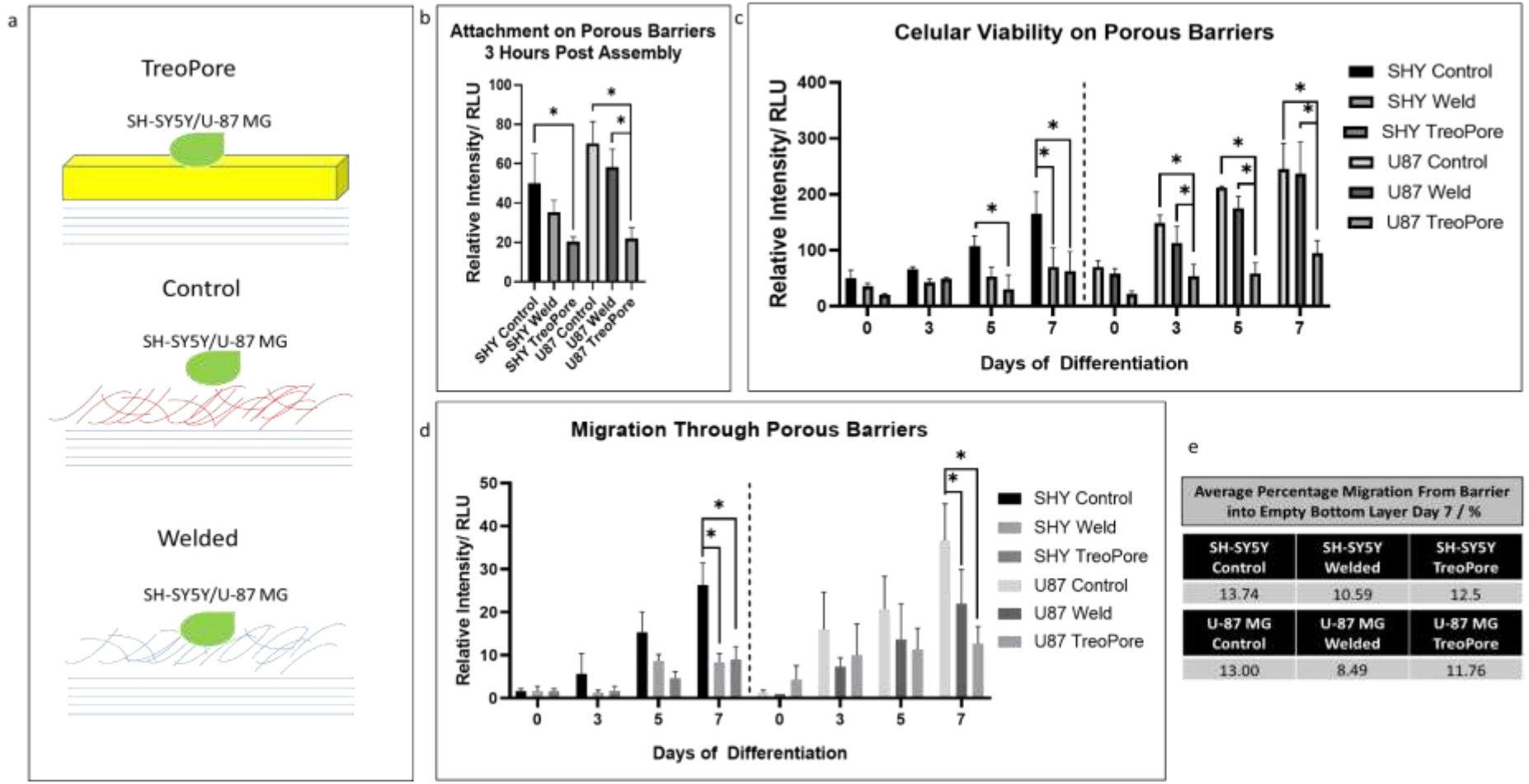

e

Average Percentage Migration From Barrier into Empty Bottom Layer Day 7 / %		
SH-SY5Y Control	SH-SY5Y Welded	SH-SY5Y TreoPore
13.74	10.59	12.5
U-87 MG Control	U-87 MG Welded	U-87 MG TreoPore
13.00	8.49	11.76

Figure 74: a. Schematic diagrams showing experimental set-up in each case including control conditions. b. Attachment as shown by tracking cell viability of SH-SY5Y and U-87 MG cells at time point 0, three hours after seeding using the CellTiter-Glo®. *c. Using the same assay, viability is tracked to day seven, indicating survival over 7-days of differentiation. d. Migration as shown by tracking viability of cells in the bottom aligned region of the experimental set-up over a 7-day differentiation (using the* CellTiter-Glo® *assay). e. Average % migration calculated at day seven from viability data. Significance was assessed with a one-way ANOVA in 'b' with Sidak's multiple comparisons test with P<0.05 (*). Significance was assessed with a two-way ANOVA in 'c' and 'd' with Sidak's multiple comparisons test with P<0.05 (*).*

Results in figure 74b indicated that attachment to barriers at three hours post assembly (having let cells attach for twenty-four hours in a CO_2 incubator) was significantly greater in control than on Treopore barriers in both SH-SY5Y and U-87 MG cells (50RLU compared to 20.333RLU in SH-SY5Y and 70RLU compared to 22RLU in U-87 MG). There was no significant difference between attachment to control barriers between cell lines. In the U-87 MG cells, attachment was also significantly higher on welded barriers compared Treopore (58.333RLU compared to 22RLU). This was unsurprising given that glial populations have shown an affinity for hydrophilic nanofibre historically.

Assessing viability over the following seven days (figure 74c) indicated that from day five, neuronal viability was significantly greater on the control barrier compared to the TreoPore barrier, and significantly greater than the welded barrier by day seven. In the glial population, there was no significant difference in viability between control and the welded barrier. This was unsurprising given their evidenced affinity (in terms of long-term viability) for PAN- 5% Jeffamine. From day three however, there was a significant difference between control and TreoPore and also welded and TreoPore barriers in these glial populations. Interestingly, glial viability was significantly greater from day three in welded barriers compared to the neuronal population on the same barrier. There was no significant drop in cell viability on any of the barriers. On the contrary, by day five, overall cellular viability was significantly greater in every case compared to day zero (with exception of neuronal cells on Treopore – which was still on average greater). This indicated cellular survival.

Evidence in figure 74d suggested that in both SH-SY5Y neuronal and U-87 MG glial populations, viable cells that penetrated the lower layer were significantly greater in control barriers compared to Treopore at day seven, though they were on average greater from day three. There was no significant difference in cellular viability in bottom layers when using welded barriers or TreoPore.

Comparing average % migration from barriers through to the bottom at day seven (figure 74e), even when cells are seeded directly on the barrier layers, migration is reduced compared to control. The migratory behaviour can be attributed to both attachment and barrier restriction. Initial attachment was lower on the barriers compared to the controls and this is mirrored with a lower migration. Taking both into account shows that neuronal migration seemed comparatively reduced compared to control with either barrier, and glial percentage migration was reduced best with the welded barrier compared to control. It was considered that this experiment presented a ‘worst-case’ scenario in which cells were directly attached to the barrier, saturating it. It was hypothesised that in a scenario in which cells were seeded on their own resident fibre that migration would be further reduced. On balance, welded barriers seemed to perform best in limiting both neuronal and glial population, though more experimentation was needed where cells were seeded on their own conduits, not the barriers. TreoPore limited migration only slightly; though this could potentially be attributed to the seeding procedure in which barriers were kept wet and saturated with media. It is possible that cells adhered directly into these pores. In the follow-up experimentation this

idea was explored, and performance of these barriers tested where cells were seeded on their own conduits (figure 77).

Therefore, in summary, evidence suggested that with exception of glia on the welded nanofibre, barriers resisted initial attachment and did not seem to adversely affect cellular viability – which may have caused global cellular problems. It was not considered an issue that glia survived well on welded nanofibre barrier as they will more likely elute useful agents to any neuronal cells that may exist in a hypothetical prosthesis on the other side of the barrier. Percentage migration indicated that even when saturated, barriers appeared to reduce migration compared to control. It was noted that deconstruction of structures to allow analysis was challenging in the presence of these barriers. This led to larger error bars than would have been liked in some cases. Though options were considered, few solutions were available to resolve this issue in the time frame and with the resources available. In future work, a control barrier of the same (2ml) deposition volume would have provided a fairer test and could be looked at.

9.6 Assembling the Prosthesis

Having tested the two candidate cellular barriers for their effects on cell attachment, cell viability and limitation of migration, it was possible to begin assembling potential prosthesis structures that included porous barriers. It was hypothesized in the previous chapter that including a co-culture of neuronal and glial cells that are not in direct contact may provide conditions that support longer term neuronal viability and increased axon length.

The manufacturing protocol employed in this case was slightly different than what was used before. Three layers were brought together as closely as possible and needed to remain together ideally as one handleable unit. Aligned 10wt% PAN nanofibre was used for neurons and random 10wt% PAN + 5% Jeffamine for glia as before. During the electrospinning process, having spun nanofibre and removed the un-necessary bottom sheets, rather than laminating (with top sheets) fibre to create suspended nanofibre membranes, this step was skipped. Just one polyester sheet was retained on each layer. In this way the sheets could be placed face down on either side of the barrier of choice, removing any un-needed polyester. In doing so, it was possible to bring sheets close together. Using the CO_2 laser (Trotec, UK), the three layers were tightly welded together during cutting and the prostheses could be handled. Figure 75 presents a schematic of how layers were brought together and then cells subsequently introduced.

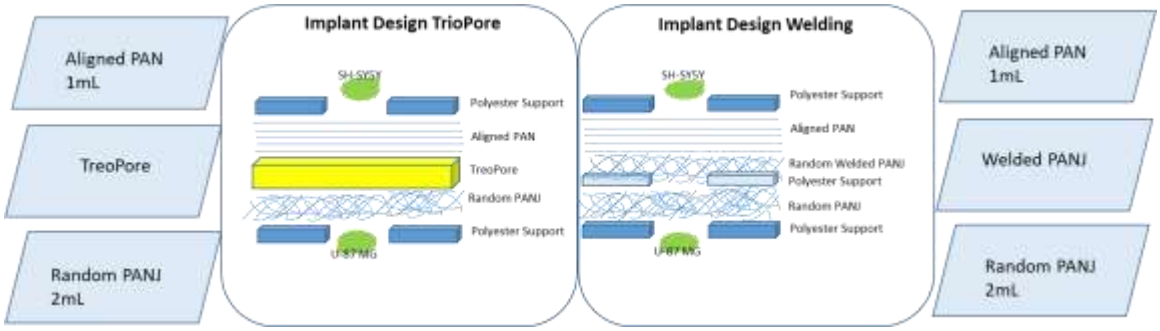

Figure 75: Schematic diagram depicting the arrangement of nanofibre, cells and barriers in each of the two prosthesis designs being tested.

Having assembled each of the two possible designs, it was important to characterise overall thickness in each case. To achieve this, OCT imaging was carried out, which enabled visualisation of each of the structures. ImageJ analysis was used to compare average overall thickness in the regions of interest. 10 random regions were selected per image (in triplicate) to calculate average thickness. The images are shown in figure 76 in addition to quantification.

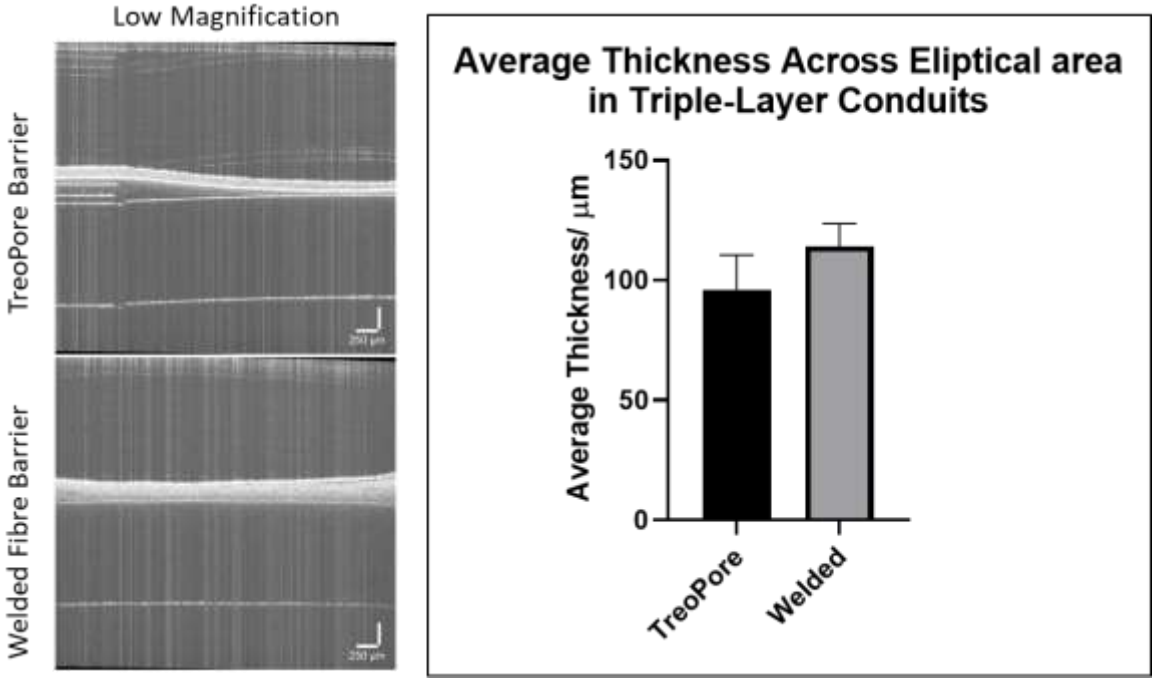

Figure 76: Average thickness of all three layers in combination in the suspended region of the constructs. Significance was assessed using a two-tailed, parametric, unpaired t-test with Welch's correction with a P-value of <0.05 (*).

Results showed no significant difference between the overall thickness of the prosthesis structures with the use of welded fibre barriers or TreoPore. The upper and lower nanofibre layers were identical (from the same batches in each case); sandwiching the two barrier types yielded a prosthesis with comparable dimensions.

In the first cellular investigation on the prosthesis inserts, an understanding as to the cellular migration through each prosthesis design was required. In line with the schematic shown the above figure, SH-SY5Y and 50,000 U-87 MG cells were seeded at a density of 50,000 cells each on the relevant insert side (SH-SY5Y cells on PAN and U-87 MG cells on PAN + 5% Jeffamine) and left to attach for twenty-four hours in a CO_2 incubator. The other side was kept empty. Following this, cells were subject to low serum DMEM f-12 and retinoic acid-based differentiation for seven days. Using the CellTiter-Glo® assay, viability of cells was tracked both on the side initially seeded and the empty side. Results are shown in figure 77.

a

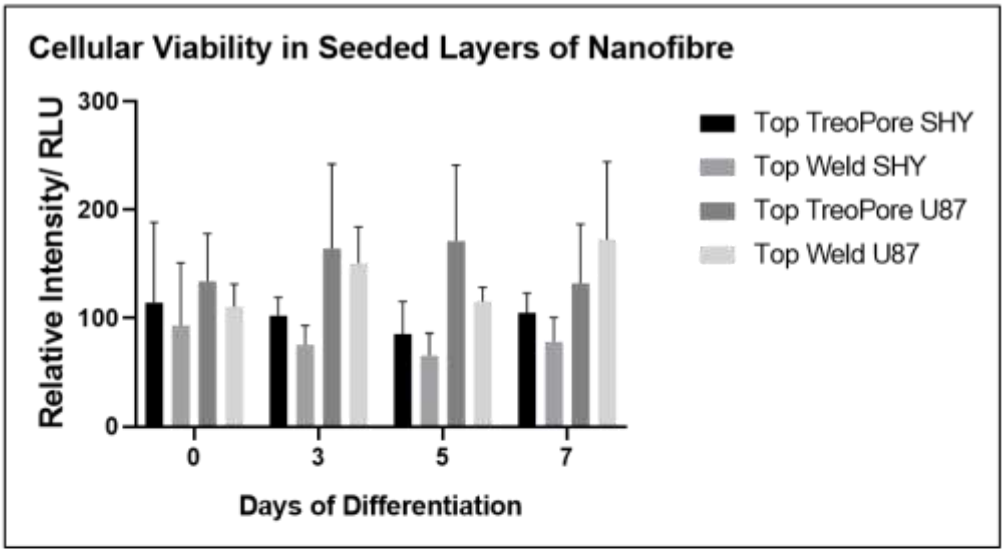

b

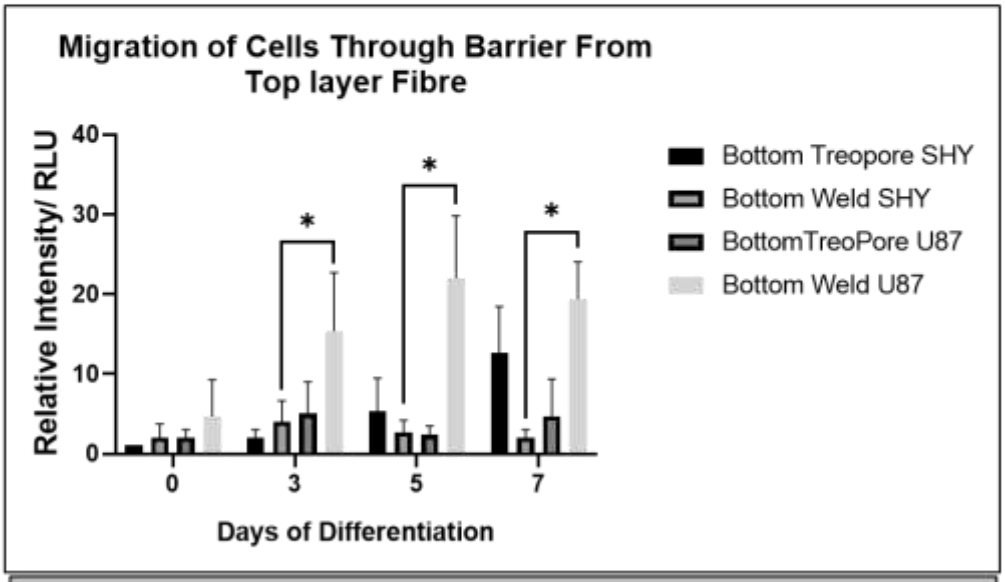

c

Average Percentage Migration From Top into Empty Bottom Layer Through Barrier Day 7 / %			
SHY Migration Through TreoPore	**SHY Migration Through 10wt% PAN 5% Jeffamine**	**U87 Migration Through TreoPore**	**U87 Migration Through 10wt% PAN 5% Jeffamine**
10.76	2.5	3.41	10.07

Figure 77: a. Average viability as quantified using the CellTiter-Glo® assay in both the top layers and the bottom layers of nanofibre. b. Using the same assay, viability of the bottom layer only over seven days of differentiation. c. Average percentage migration from the top to bottom nanofibre layers at day seven. Significance was assessed with a two-way ANOVA in 'a' and 'b' with Sidak's multiple comparisons test with P<0.05 (*).

This investigation provided insight into the migratory behaviour of neuronal and glial cells when seeded on their own nanofibre membranes with the use of a barrier, rather than seeding directly onto the barrier as done in figure 74. Assessing the product of the CellTiter-Glo® viability assay (figure 77a), results showed

that over a seven-day differentiation, cells survived well on the top seeded nanofibre in the presence of either of the barriers in question. There was a clear significant retention of cells on the top layer.

Assessing the empty layer (figure 77b), by day seven, neuronal migration was most limited when a welded barrier was in use – it was significantly lower than the glial viability with the equivalent barrier. Percentage migration reflected these results, showing an average of 2.5% migration in the case of neuronal cells with a welded barrier. This is notably less than the control experiment carried out above, showing an average of 13.74% migration in absence of any barrier (figure 74).

This evidence was encouraging and leant evidence to the finding that a 10wt% PAN + 5% Jeffamine welded nanofibre barrier may be the most appropriate for limiting neuronal migration, whilst allowing some glial penetration (though largely the population remains on the seeded layer). The percentage migration of glia through the welded barrier was comparable here to that in the previous experiment (figure 74). Glial migration with the welded barrier was on average greatest from day three, something also reflected in the previous experiment. It was considered that some glial migration into the barrier may not be a limitation, in that it would likely reduce the distance over which eluted glial supportive factors would need to travel to support neurons in indirect co-culture. Evidence also suggested that migration of a small population of glia (forming direct co-culture) into the neuronal layer would not limit neuronal axonal extension or migratory capacity (in the previous chapter). The Treopore barrier also performed well in limiting neuronal and glia migration between layers, mediating just 10.76 and 3.41% migration respectively (compared to the on average 13% migration seen in the control experiment above – figure 74). One solution could perhaps be the use of multiple barriers to limit specific cellular populations, though it is likely that one barrier shown to notably reduce neuronal migration and also limit glial migration could be the solution.

Limitations to this line of experimentation were similar those noted in figure 74. Disassembling the structures was labour-intensive and required care. Over time (and even immediately in cases), the structures become more difficult to disassemble to allow analysis. This was overcome with care and technique as much as possible, though it did cause error bars (standard deviation) to be slightly greater (slight variation) than expected. In future work, other steps could be considered to combat this, such as alternative analysis techniques that do not require disassembly.

Having shown that physical cellular migration could be limited using the investigated barriers, it was pertinent to explore whether indirect co-culture of both cell types on their relevant layers provided a boosted long-term neuronal viability and axonal length compared to single culture. To assess this, an investigation using immunofluorescence imaging and CellTiter-Glo® analysis of cell viability was used. In each case, 50,000 SH-SY5Y and 50,000 U-87 MG cells were seeded on PAN and PAN-5% Jeffamine sides and allowed to attach for twenty-four hours in a CO_2 incubator. The protocol was optimised such that both cell populations were seeded in quick succession and media added slowly so that cells would have a chance to

adhere to both sides but not dry out. Cells were then subject to low serum DMEM f-12 and retinoic acid-based differentiation for seven days. Imaging the individual layers presented a challenge in that three layers of nanofibre was difficult to image as one structure in-house on our confocal microscope (Leica, UK). Further, TreoPore was opaque in nature and so could not be directly imaged. In each case the structures needed to be deconstructed prior to imaging which required multiple attempts to ensure success in each case. As a result, when calculating axon length, nuclear socket to axon tip was averaged in ten random cells in one sample per variable. In the future, light sheet analysis could be explored as a solution perhaps in the case of welded fibre. In this investigation, the time frame chosen was from day seven of differentiation through till day fourteen to gain an insight into long term viability and axon extension. Results are shown in figure 78.

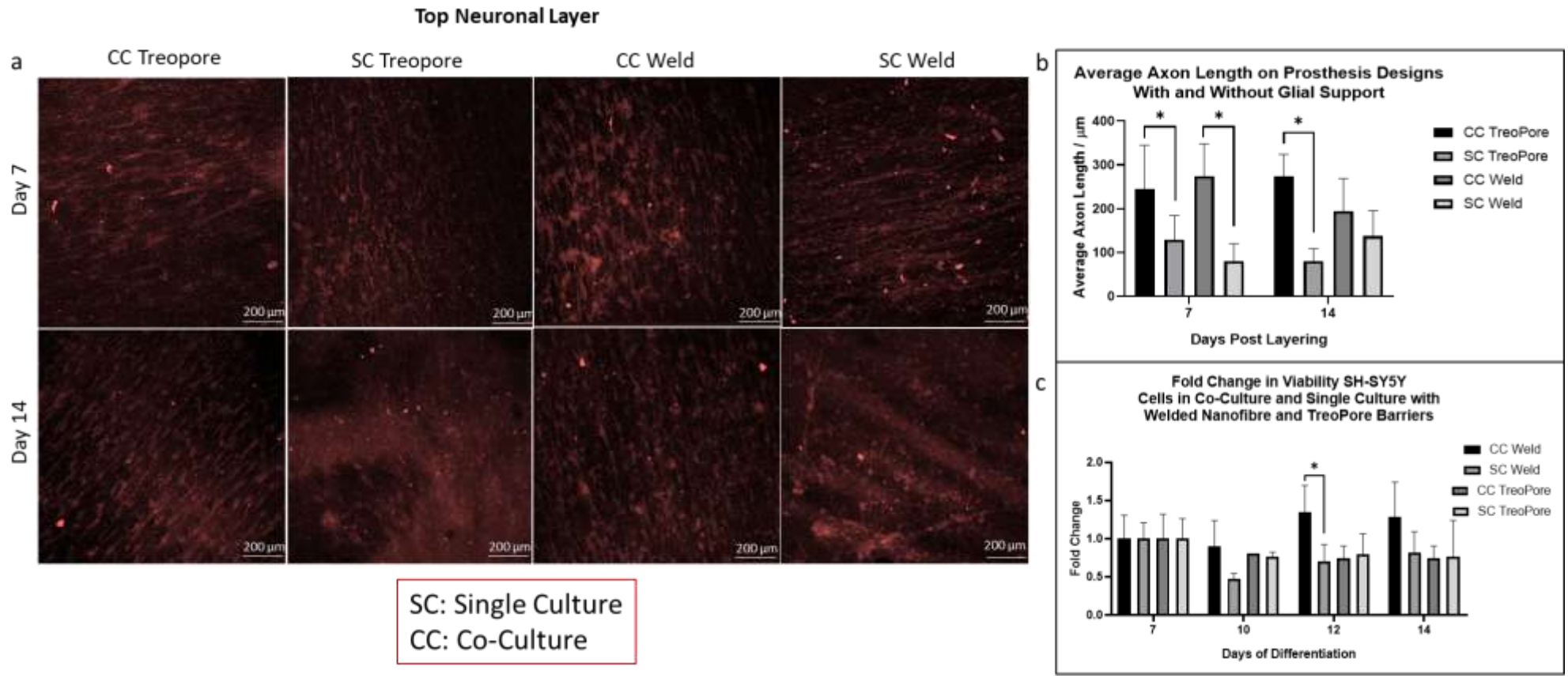

Figure 78. a. Immunofluorescence imaging displaying mature neuronal (SH-SY5Y) cells (ATCC, USA) at days 7 and 14 on the aligned PAN layer. b. Average Axon length as calculated from immunofluorescence images from 'a' using ImageJ. In each case, 10 cases were taken from 3 separate samples and used to calculate an average. c. Fold change in viability of SH-SY5Y cells between 7 and 14 days of co-culture on the prosthesis designs. viability measured using the Cell Titre Glo (Promega, UK) assay. Significance was assessed using a two-way ANOVA with Sidak's multiple comparisons test with $P<0.05$ indicating significance (*).

Looking at the immunofluorescence images taken at days seven and fourteen, visually cellular viability seemed to be retained best in co-culture compared to single culture of mature SH-SY5Y cells in the case of both barrier types. Visually, in single culture, cells seemed to undergo more cellular death by day fourteen. Using ImageJ to quantify axon length, it was possible to conclude that at day seven of differentiation, axon length was significantly greater in co-culture with the use of both TreoPore and welded nanofibre barriers (from analysing one sample per variable). This significant difference was maintained only in the case of TreoPore barriers by day fourteen. Notably, though not significant, axonal length was still on average greater using a welded barrier in co-culture of neurons than in single culture. Further, there was no significant difference between axon length in co-cultured neurons using a TreoPore or welded nanofibre barrier at day seven or fourteen.

Assessing long term viability of neurons using the CellTiter-Glo® assay and calculating fold change from day seven, a significant difference was seen in co-culture compared to single culture using a welded nanofibre barrier at day twelve. The trend does continue into day fourteen, though not significantly. There was no significant difference comparing co-culture to single culture in the case of the TreoPore barrier. The fold change in viability slightly increases over the time compared to day seven in the case of the welded fibre barriers in both single culture and co-culture (despite an initial drop in single culture), suggesting that this barrier was more conducive to long term viability. It is possible that a contribution of viability in the case of welded barriers in co-culture may be attributed to a small but acceptable amount of glial penetration into this layer – but importantly, neural migration was shown to be more limited.

It could be summarised that axons seemingly grew on average longer when a TreoPore barrier was present. It was possible that this was due to the random welded nanofibre providing physical cues for axon deviation, though more investigations into this result could be carried out in future work. Long term neuronal viability was on average better maintained using a welded nanofibre barrier in co-culture to limit cellular migration (significantly so at day twelve).

Challenges existed in the analysis of these structures both in imaging and in viability assessment because of the need to deconstruct them – this was shown clearly by day fourteen where the cells had seemingly incorporated the barriers/layers together, making disassembly difficult – this was reflected perhaps in the error bars on this day. In future work, a method of deconstructing the prostheses' or an alternative analysis technique could be trialled to best analyse these carefully assembled constructs – light sheet microscopy may provide one option.

9.7 Discussion

Adding space between layers of nanofibre appeared to limit cellular migration. Though successful, space

did not provide the most likely reproducible solution to this problem. To conserve the benefits provided in co-culture, whilst limiting cellular migration, 4 porous barriers were identified; Welded nanofibre, TreoPore, Polyurethane and EPTFE. Treopore and welded nanofibre were chosen to investigate in cellular testing as together they provided a large and small pore size and hydrophobic and hydrophilic nature. Cell attachment was comparatively low to Treopore and to welded nanofibre compared to control. Viability in the presence of both barriers was acceptable. In both cases, cellular migration through the barriers was comparatively low, with welded nanofibre showing the most effective restriction of cellular migration. Carrying out an indirect co-culture in the presence of a barrier showed that the glial population enhanced neuron axonal length compared to a control (single culture) in both Treopore and welded nanofibre (but only significantly in the former up to day fourteen). Further, long-term viability was best conserved in co-culture with a welded nanofibre barrier (significantly so at day twelve compared to single culture).

Considering the overall investigation aims, it was possible to state that evidence suggested a system which incorporated separated cellular populations cultivated on materials suited to the cellular requirements was effective. Including a barrier enhanced neuronal population viability and axon length in the presence of indirect co-culture but limited inter-layer migration which would have reduced efficiency of the prosthesis. This prosthesis design suggestion could be tested next with stem cells or primary cells to test its efficacy with a range of support cells separated with porous barriers. Using stem cells (mesenchymal for example), it could be eventually tested in vivo. Establishing these design parameters first with mature glia and neuronal populations from cell lines was an important first step in effectively designing the prosthesis in a way in which every step was optimised.

Assessment of literature showed that few groups have recreated the neuronal and glial population separation on nanofibre, making use of barriers to limit migration (particularly with SH-SY5Y and U-87 MG cells). However, interestingly, the concept has been applied in other regions of research in limiting cellular migration and in particular invasion. For example, a study in 1980 attempted to limit cellular infiltration, but maintain chemical exchange of nutrients and metabolites in transplanted islet cells using microencapsulation (Lim, Sun 1980). The concept has been advanced with groups testing nanostructures with controllable pore size to mediate cellular migration (silicone was used in combination with PCL nanofibres by one group (Fan et al. 2011)) as well as mediate maturation of cells using curated surface topographies (Tasciotti et al. 2016). As mentioned in section 8.5, the Kim et al group made us of double layers of random nanofibre to prevent the invasion of a glial population within a multi-layer nanofibre system (Kim et al. 2016). The use of welded nanofibre has been shown to have some relevant in filtration, and thus it follows that an engineered welded nanofibre membrane could have functionality in cellular filtration between layers of cellularised nanofibre (Roche, Yalcinkaya 2019, Li, H. et al. 2017). Some work has been done on examining the use of polypropylene (of which TreoPore is constructed) membranes as scaffolds owing to its porous nature. One group demonstrated the use of a polypropylene membrane in

micro- and ultra-filtration as well as a scaffold for hepG2 cells, a relatively similar concept to that explored here in that the scaffold prevents cellular infiltration but mediates chemical flow of metabolites and nutrients (Lu et al. 2015).

The conclusion of these studies was that barriers such as nanofibre have been shown to have applications in limiting cellular migration, but that porosity is an important characteristic in maintaining a dynamic system in which nutrient and metabolite exchange can be maintained. Specifically, limiting invasion of activated glial cells in a spinal cord injury prosthesis is of direct relevance. This is a concept born in diabetes research that can be applied to several other tissue targets including the spinal cord.

10.1 Aims of Study

It had been established that a viable prosthesis design is likely to be one including discrete layers of glia and neurones (with only the glia being resident in implantation). Discrete layers should likely be separated by a physical barrier (either welded nanofibre or Treopore are viable options) to avoid physical cellular migration but to encourage the non-contact benefits of co-culture. The next step was to establish how to selectively encourage local healthy, remaining neuronal axons (and cell bodies if present) into the prosthesis from a SCI. A method was required such that specific neural migration could be encouraged, whilst minimising glial migration. The presence of activated glial cells from a SCI would likely trigger negative effects within the confines of the prosthesis, such as astrogliosis or neurotoxicity (as they were in the SCI). The aim of this section was to characterise and test rat tail collagen I, (Gibco, UK) as a candidate for this role.

10.2 Collagen I Gels

Both synthetic gels such as poly-ethylene-oxide (PEO) and biological gels such as collagen exist, though collagen was chosen as a widely available, bio-compatible, functionally malleable solution. It was hypothesised that these gels could be used to coat/pattern the prosthesis such that a neuronal population could be recruited into the prosthesis. The detailed collagen polymerisation process can be found in the materials and methods section.

The first action taken was to test SH-SY5Y cell survival within 3mg/ml gel polymerised for 2 hours. Collagen I was chosen as literature suggested that it provided a gel with suitable structural integrity (with little contraction), whilst permitting long term cellular viability in investigated cell populations (Lomas et al. 2013). Further, the literature also recommended a two-hour polymerisation at 37°C using this concentration (Lomas et al. 2013). In this experiment, 50,000 SH-SY5Y cells were seeded and incubated in 10% serum DMEM f-12 media for twenty-four hours in a CO_2 incubator to allow attachment to the bottom of an adherent, 12 well microplate. Next, the collagen gel was mixed as described in methods (see 5.2.4.4) and introduced on top. Gels were polymerised over two hours, after which 1ml of high serum DMEM f-12 medium supplementation was supplied over the top of the gels. Figure 79 presents a light microscopy image of SH-SY5Y cells forty-eight hours after gel was added. The image provided basic insight into the status of morphology/visual viability of cells having left them with the gel for forty-eight hours.

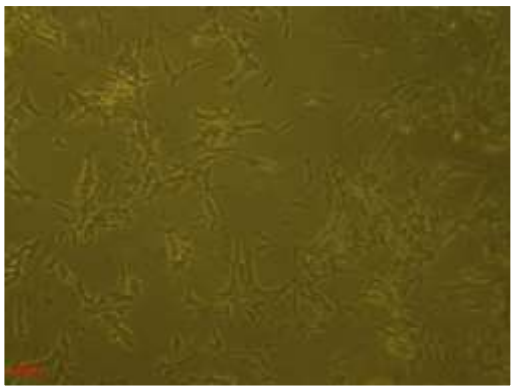

Figure 79: Light microscopy image showing immature SH-SY5Y cells left for forty-eight hours in Type I Collagen, rat tail.

Cells appeared morphologically healthy and so having established that neurons could survive within the gels (all be it on a 2D surface), the investigation moved to optimise the polymerisation process from the start point taken from literature (see chapter 10.2.1).

10.2.1 Polymerisation Optimisation

Collagen polymerisation was trialled at various temperatures to assess the changing physical properties seen both in the gels and in the cells seeded into these gels. It was well documented that collagen I (3mg/ml) polymerisation may be carried out at a cool (4°C), room temperature (21°C) or at physiological temperature (37°C) (Antoine et al. 2014). The resultant structures produced at these temperatures were reported to change and as such the gel can be adjusted to requirement. Typically, the self-assembly of molecules within the gels during polymerisation creates less bundled fibrils at a higher temperature and more at a lower temperature (Antoine et al. 2014). Some have suggested that the pore size created in gels polymerised at lower temperatures are more favourable to cell culture, and even that the channels created during this process may be utilised in tissue engineering (Chrobak et al. 2006). However, typically, the lower the temperature, the more difficult it is to control and thus a physiological temperature has its benefits also. Figure 80 presents light microscopy images of the acellular polymerised collagen I, rat tail gels created at 4, 21 and 37°C over 2 hours. Light microscopy was able to pick up the changing bundled fibre organisation.

Figure 80. Light microscopy images showing Collagen I, polymerised for 2 hours at 4, 21 and 37°C.

It was clear to see the difference in fibrous bundle formation as polymerisation temperature changes. Formation of these bundles can lead to the formation of controllable 'channel' size as suggested previously. This can be advantageous if well controlled as they have the potential to provide physical cues to migrating cells. It was decided that culture of both SH-SY5Y and U-87 MG cells in gels polymerised at these three temperatures required testing. Gels were then mixed and polymerised at 4, 21 and 37°C for 2-hours. Cells were then seeded at 10,000 cells per well into 24 well plates and were left for forty-eight hours in the 37°C incubator. In addition to the light microscopy images, the CellTiter-Glo® assay was used to assess cellular viability. It was recommended in literature to be an effective means of measuring viability in gel structures due to its penetrative capabilities (Kijanska, Kelm 2004). Both data sets are displayed in figure 81.

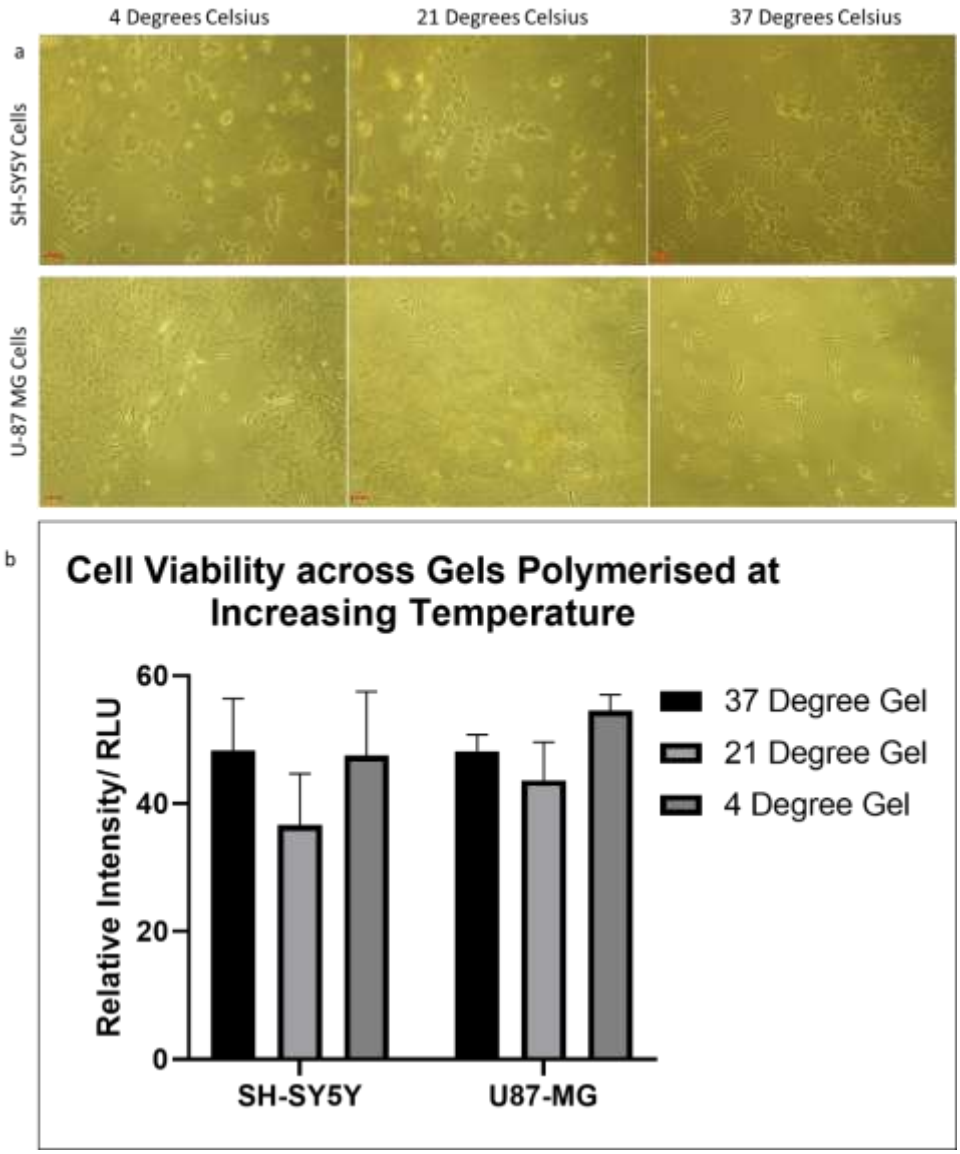

*Figure 81: a. Light microscopy images showing immature SH-SY5Y and U-87 MG cells cultured in Collagen I, for forty-eight hours in gels polymerised (for 2 hours) at 4, 21 and 37°C. b. Viability assay quantifying SH-SY5Y and U-87 MG viability over the time period on the gels in question (*CellTiter-Glo® *used). Significance would have been indicated using a two-way ANOVA with Sidak's multiple comparisons test with P<0.05 indicating significance (*) – no significance was shown.*

The images in figure 81a showed the clear difference in gel properties as seen in figure 80. As the temperature of polymerisation increases, the fibrous bundling that occurs lessens. Gels polymerised at 4°C seemed to form a less even layer at the base of the plate. This caused cells to attach to fibrous bundles over a deeper z-plane/depth. It was decided that the migratory effects that a highly fibrous gel has on neuronal and glial cells could not be controlled easily in 2D and thus perhaps it should be avoided. Further, controlling polymerisation temperature at 4°C was more challenging in that sterilised gels had to remain in the fridge before seeding and then warmed post polymerisation to physiological temperatures. Gels formed at 37°C had a smooth, uniform nature and would be immediately suitable for cell culture post polymerisation. Further, cells could even be seeded during polymerisation in complex experimentation.

Having assessed cellular viability by mixing the structures with CellTiter-Glo® assay reagent, it was established that there was no significant difference in viability of U-87 MG or SH-SY5Y cells in these structures across polymerisation temperatures - though in both cell lines, viability was on average less in gels polymerised at 21°C. It was for all these reasons that 37°C was chosen as the temperature with which to move forward.

To fully understand the properties of 3mg/ml collagen polymerised at 37°C for 2 hours, extensional rheometry was carried out on the gel, using a HAAKE™ CaBER™ 1 Capillary Breakup Extensional Rheometer (Thermofisher UK). It was possible to characterise both diameter changes over time and the changing strain rate as diameter decreases. Results are show in figure 82.

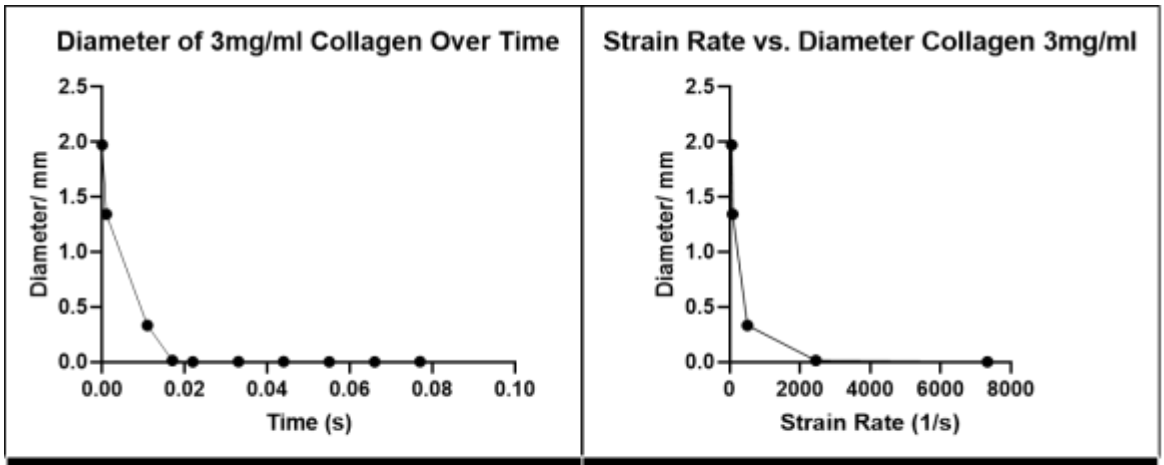

Shear Viscosity/ Pa.s	Experimental Breakup Time/ s
0.175	2.20E-2

Figure 82: Graphs depicting change in diameter with time and change in diameter with strain rate in Collagen I, Rat tail 3mg/ml – polymerised at 37°C. A summary table includes shear viscosity and experimental breakup time.

Shear viscosity of cerebral spinal fluid (CSF) is Newtonian and calculated to be around 0.001 Pa.s (Bloomfield et al. 1998). Shear Viscosity of 3mg/ml Collagen I was around 0.175 Pa.s by comparison. This was considered appropriate as structural support could be provided by this fluid that could perhaps displace but also become bathed in CSF.

Having carried out optimisation steps in 2D, the next consideration was to assess cellular behaviour when cells were seeded atop a collagen gel. What was of note was migratory behaviour through the gel and alignment cues at the gel-fibre border (aligned nanofibre was used in this case). Here, 50,000 SH-SY5Y and U-87 MG cells were separately seeded atop a 3mg/ml collagen gel that had been previously polymerised for two hours at 37°C. Cells were left for twenty-four hours in a CO_2 incubator, supplemented with 1ml 10% serum DMEM f-12 prior to visualisation. It was possible to use light microscopy to visualise this process as the gel formed a flat plane of view. Results are shown in figure 83.

In combination, over this 24-hour period, CellTiter-Glo® assay was used to compare cell viability in the gel compared to viability on the fibre – it was hoped this may give insight into cellular migration. To do this, 'scraping' using a was carried, using a scalpel blade (RS Pro scalpel blade) to remove the top gel layer as best possible and subsequently gently washing the fibre in media. The fibre alone could then be analysed. The gel alone was not subject to analysis as it was considered that physical scraping of cells could affect viability of this sub population of cells. Results of imaging and quantification are shown in figure 83.

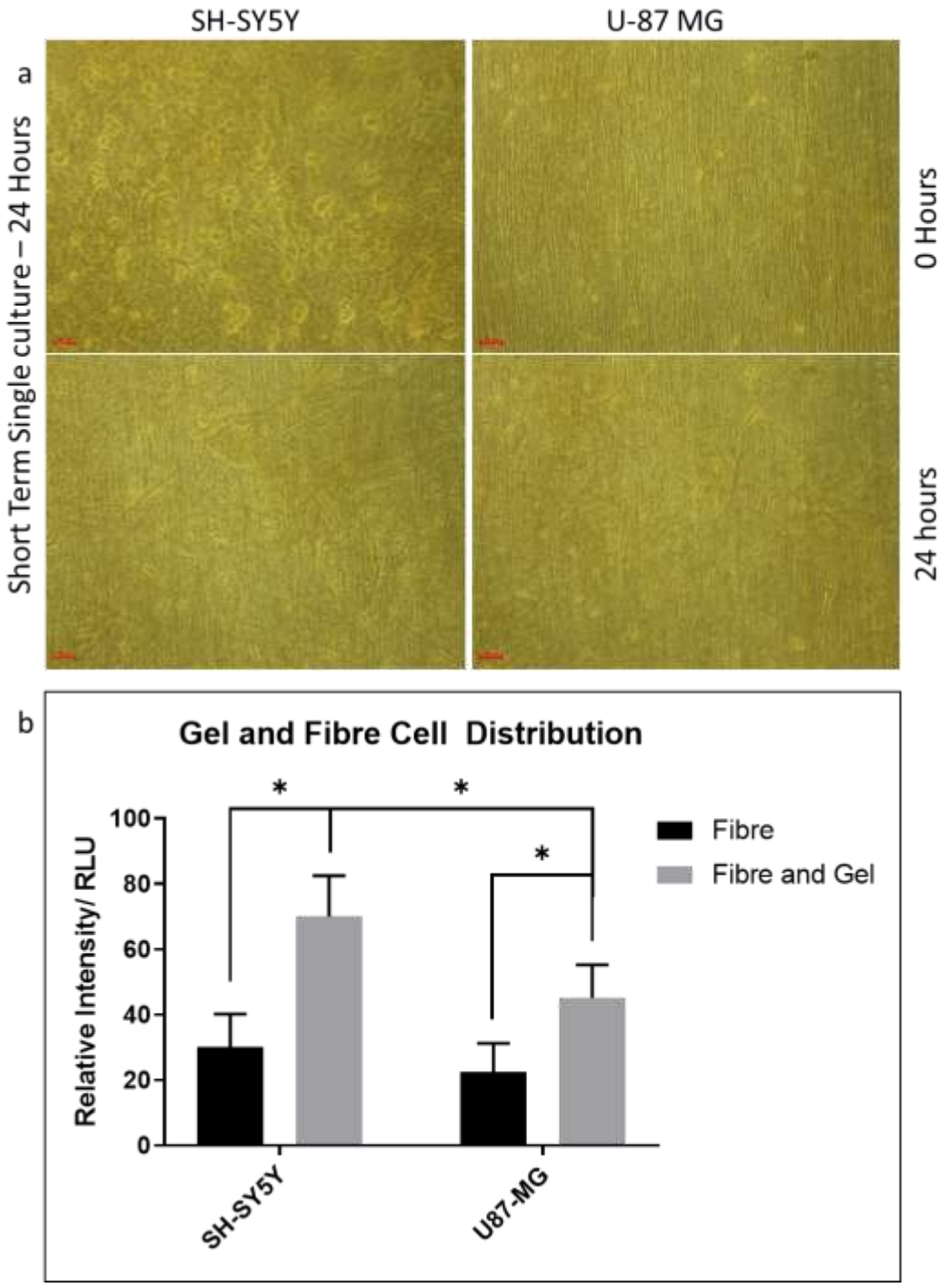

Figure 83: a. Light microscopy images depicting SH-SY5Y and U-87 MG cells having been seeded on collagen I, migrating into nanofibre below over twenty-four hours. b. Quantification of this process as described using the CellTiter-Glo® test for viability. Fibre direction top to bottom. Significance was assessed using a two-way ANOVA with Sidak's multiple comparisons test with P<0.05 indicating significance (*).

Assessing the quantification first showed that using the scraping method, it was possible to identify a population of cells within the gel and on the nanofibre below (indicated by a significant difference in total cells and cell on the fibre alone). This suggested that migration was likely to be occurring from gel into the fibre below assuming that the technique was effective in flushing out gel-bound cells from the structure (it

is possible that some cells re-attached to the fibre, though this was avoided as much as possible). A significant difference was also noted between total viability (of gel and fibre) in SH-SY5Y and U-87 MG populations, though the importance of this was considered minimal. To support quantitative evidence, light microscopy imaging of both individual cell lines was shown. What was focused on in each case was the fibre-gel interface. Here, the physical cues provided by the gel met those provided by the aligned nanofibre and the cellular orientation may change. It was interesting to note that cells at this border at twenty-four hours at least did not yet exhibit aligned orientations. However, crucially the limitation that light microscopy has with imaging nanofibre is the difficulty in distinguishing between fibre and cells. It was for this reason partially that the gel-fibre border was imaged. It was very possible that cells deeper in the fibre were aligned and this limitation was addressed later with immunofluorescence imaging.

In addition to the above experiment, some cells were seeded in co-culture (25,000 SH-SY5Y and 25,000 U-87MG cells respectively) for 25 minutes (allowing 5 minutes to prepare the gel mix) to allow initial attachment (as per the usual technique before adding medium). Collagen I gel was then added and polymerised for 2 hours before supplementing with medium. It was hoped that the effects of adding a gel to seeded cells could also be captured visually and so this experiment was left for 2 days.

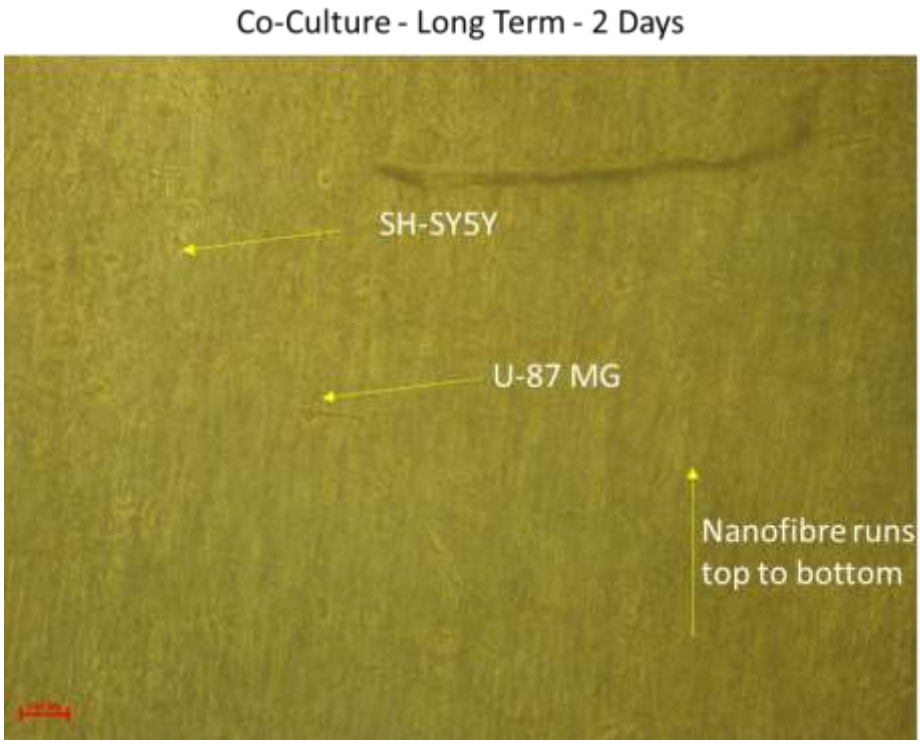

Figure 84: Light Microscopy image depicting a co-culture of both SH-SY5Y and U-87 MG cells having migrated from the PAN nanofibre (direction top to bottom) below into the gel above over forty-eight hours.

The light microscopy image in figure 84 displayed the fibre-gel border and suggested that some cellular infiltration into the gel did occur. Further, the alignment of said cells in this interface were not all consistent with the fibre direction below – which was unsurprising. These findings were pertinent as it suggested that

perhaps cells did have the capacity to move up (against gravity) into the gels in use. In future work, the cells could be left for twenty-four hours before the gel was added to more thoroughly ensure that cells had entered the gel purely through migration – this was carried out in experiments that followed. The experiment was considered an optimisation step though evidence was promising. The experiment also highlighted the need for immunofluorescence imaging in future work as the imaging quality was limited at best. This is a process that will need to be optimised for gel-work, likely with live cell imaging.

10.3 Cryo-Fracture of Nanofibre

Cryo-facture or 'cryo-milling' (see methods for protocol) is a process in which nanofibre (and other materials) can be rapidly cooled and subsequently blended into a fine powder of short length structures. It was decided that this process could be utilised to add controllable short lengths of fibre into the gels being used to offer more selective cellular migration through the gel-fibre material. It had already been seen that varying nanofibre material mediated certain cellular migratory behaviour – PAN for example elicited greater neuronal migration and long-term viability. It was hypothesised that introducing short lengths of PAN into collagen I gels could enable selective neuronal migration.

Using cryomilling, a sheet of random 10wt% PAN nanofibre was added to a small quantity of dH_2O (1ml) and the solution frozen in liquid nitrogen. This mix was then subject to 'milling' which in effect blends the fibre into short lengths. The length of this fibre could be controlled by changing the weight of fibre introduced into the machine, run time, the rate at which it worked (speed), and the number of cycles completed. Within this investigation, two sets of parameters were trialled to create one set of short lengths and one long. The first was 0.102g of fibre run for 2 minutes at 5 cycles/second for 1 run. The second was 0.208g of fibre run for 1 minute a 5 cycles/second also for 1 run. The results of this process in the form of SEM imaging and ImageJ fibre length quantification of said images is shown in figure 85. Fibre lengths were calculated by measuring 30 fibre lengths from an image in each case and taking an average.

a

	Weight /g	Pre-cool/minutes	Run-time/ minutes	Rate/ cycles per second	No. of Grinding Periods/ runs
Sample 1 1ml water	0.102	5	2	5	1
Sample 2 1ml water	0.208	5	1	5	1

b

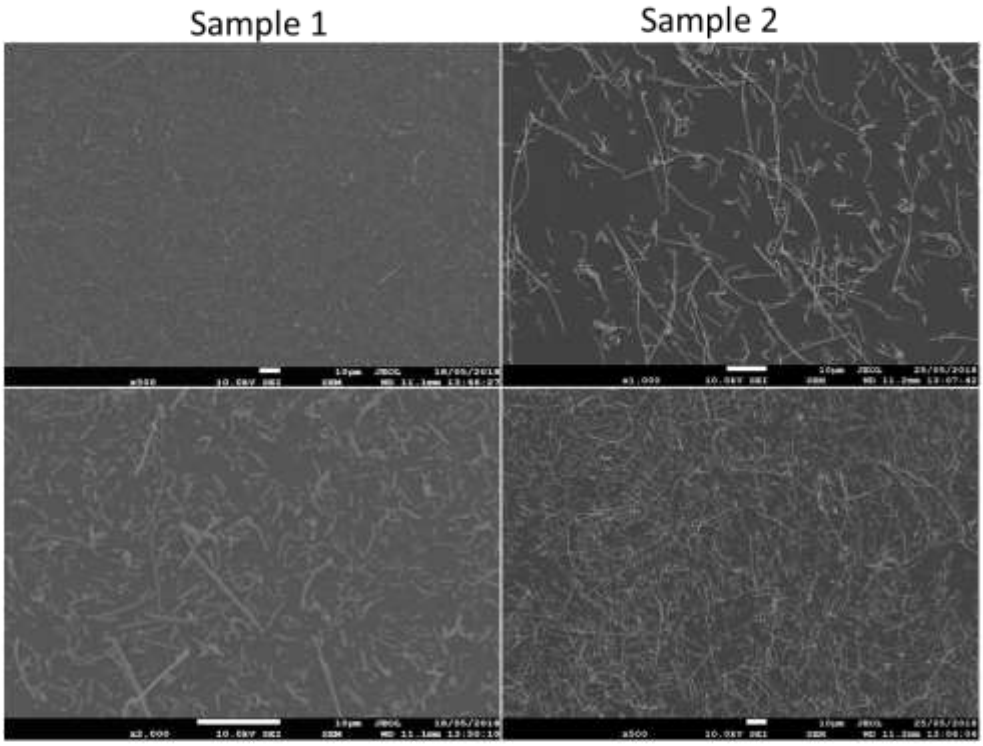

c

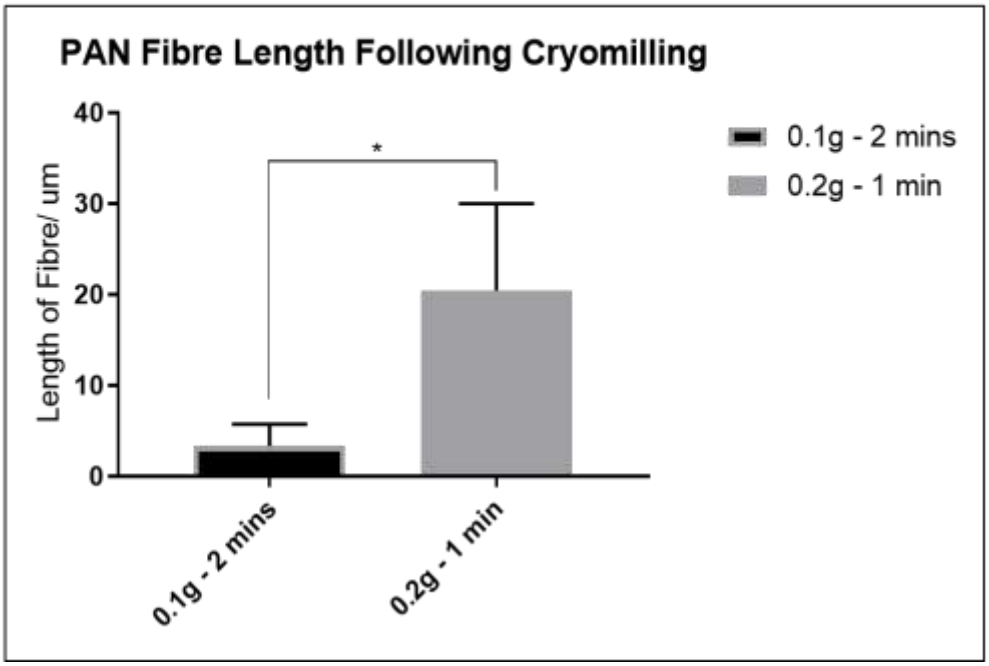

Figure 85. Manufacturing specification used to create cryo-milled nanofibre. a. Summary of the process specification on PAN nanofibre milled using the cryo-fracturing process. b. SEM images generated presenting the short lengths of fibre generated using the process specified in the table above. c. Quantification of average fibre lengths using ImageJ analysis in each case. Significance was assessed using a two-tailed, parametric, unpaired t-test with Welch's correction with a P-value of <0.05 (*).

As shown in figure 85b+c, SEM imaging and the corresponding quantification showed that changing the initial fibre input weight and cycle time significantly affected the resultant fibre length. Cryo-milling a larger input weight for less time produced a fibre length significantly longer than that of a smaller input weight spun for more time. There was variation in lengths of fibre shown and this could be resolved by filtering the lengths (with 10µm syringe filters for example) – this could be considered in future work.

Having manufactured appropriate lengths of fibre (in powder form), the powder was dried in an oven at 60°C for 48-72 hours. Each powder was then introduced into the collagen I gel polymerisation mixes. An optimisation process was required to mix the fibre with the gel well (to establish an efficient method) and to define the mass of fibre to be introduced into the collagen gels. It was decided that initially, the non-gel components would be combined with the dried fibre. Specifically, 10xDMEM 199 and dH_2O were mixed with the dried clump (pre-weighed) of cryo-milled fibre in 2ml Eppendorf tubes (Fisher Scientific, UK). Having initially trialled vortex mixing, the solution for obtaining the most even distribution was to use a sonicator (120watts, Fisherbrand Q125) for five 10 second pulses with 10 second breaks to avoid overheating. These were then sterilised in a UV sterilisation device (Hug Flight company Ltd. Light box (UV tube 26cm long, 1cm wide, 8W, 256nm)) at 3cm distance from the samples for 30 minutes. This sterilisation source was proven suitable/optimised by a colleague (Joseph Chemmarapally) for nanofibre sterilisation and as such it was also employed for nanofibre + water/media sterilisation. They were then mixed with the collagen I gel and NaOH components to start the polymerisation process. The quantity of fibre added was varied between 0.002g and 0.0001g. Confocal microscope imaging was used to assess surface and cross-sectional view of 1ml of each in 24 well plate wells. In this way the arrangement in space of fibre within each gel could be understood using the autofluorescence of PAN nanofibre.

Separately, 50,000 SH-SY5Y and 50,000 U-87 MG cells were seeded on their relevant preferred materials (SH-SY5Y cells on PAN and U-87MG on PAN + 5% Jeffamine) and left for twenty-four hours to attach in a CO_2 incubator. At this point, 100µl of each gel-fibre mix was added to the top of seeded populations and allowed to polymerise for two-hours. The volume was more than required to fill the ellipses but was then smoothed over with the edge of a scalpel blade (RS Pro scalpel blade), removing any excess material. A layer of PAN or PAN + 5% Jeffamine (cell line dependant) was added on top of the gel after 30 minutes so that polymerisation had started but could complete in contact with the top layer of gel. Migration was tracked between the bottom and top layers using the CellTiter-Glo® assay for seventy-two hours. Quantification was done by removing the gel regions from the fibre by scraping and gently washing in media as before. Each layer was then individually analysed. Results of this investigation are shown in figure 86.

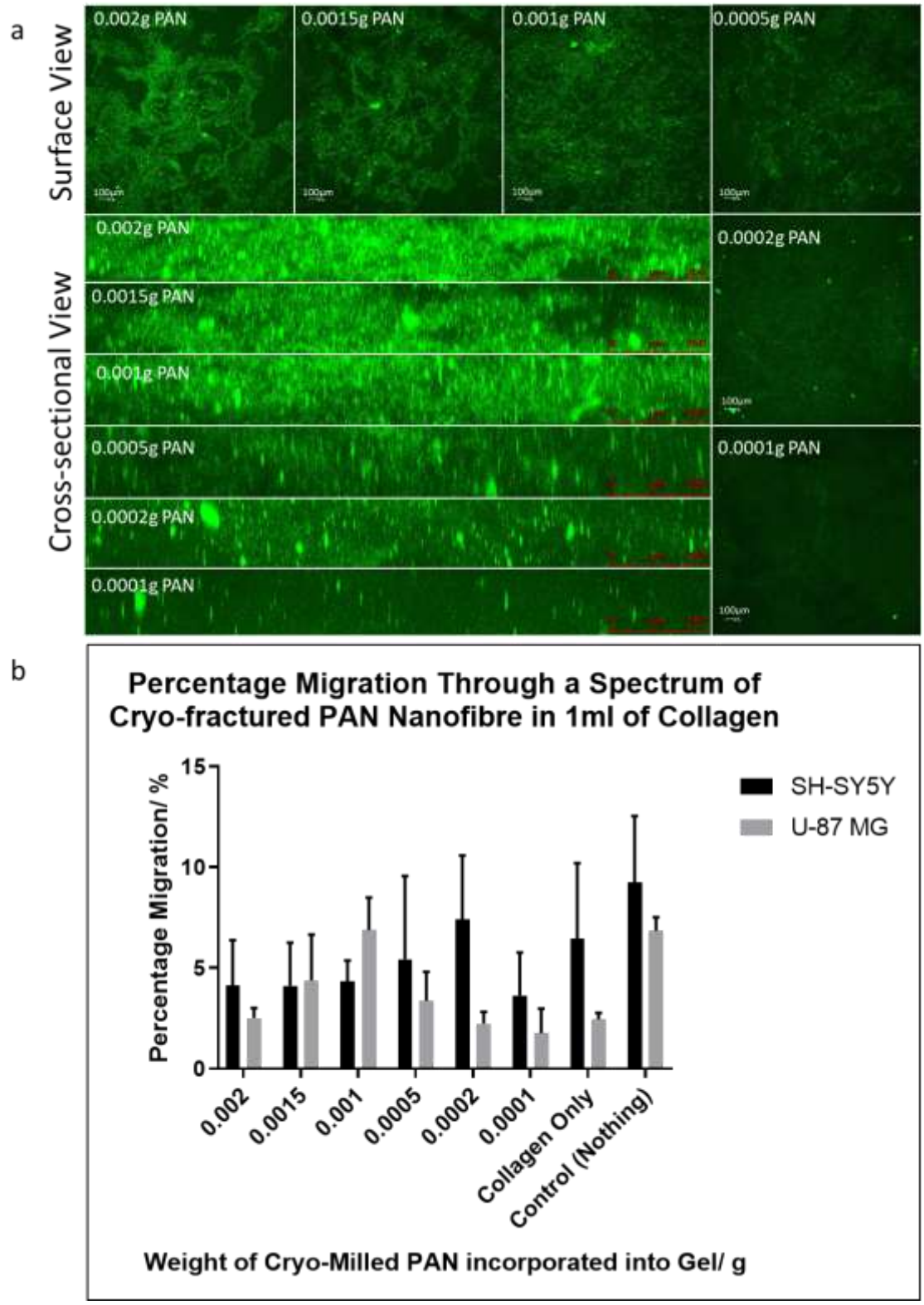

Figure 86. a. Confocal imaging of both surface (square fields) and cross-sectional areas (oblong fields) of a spectrum of cryo-milled PAN nanofibre fragment weights mixed with gel forming components and later 3mg/ml Collagen I gel. Fibres auto-fluoresced green following excitation at 488nm. b. Percentage migration of SH-SY5Y and U-87 MG cells from a bottom layer of PAN/ PAN + 5% Jeffamine into a top layer of PAN/ PAN + 5% Jeffamine over three days. The analysis was generated using viability assessment – the CellTiter-Glo® assay. Significance was assessed using a two-way ANOVA with Sidak's multiple comparisons test with P<0.05 indicating significance (*).

Assessment of confocal images indicated that sonication was a mostly successful method of mixing cryo-fractured fibre into gel-forming components based on distribution, though some clumps remained present. Images also indicated that as PAN mass added to the gels increased from 0.0001 to 0.002g, the gels became increasingly crowded and unlikely to permit the migration of cells though them at all. Percentage migration was calculated by comparing percentage viability of cells in the uppermost layer compared to that remaining in the bottom layer – disregarding any cells that may be caught in the gel interface, as they were gently washed away with media. Comparing these percentage migrations through each gel-mix into the top layer showed that on average, as the mass of PAN in the mix decreased, the passage of neurons increased down to 0.0002g. The pattern of glial migration varied slightly in that as mass of mixed PAN fibre decreased, glial migration seemed to increase down to 0.001g and then decrease again through to 0.0001g. The percentage differences seen were not statistically significant owing to the relatively large standard deviations seen, though the greatest average difference (of 5%) was seen when using 0.002g of PAN. Notably, the percentage migration through the collagen alone was also relatively high but with some variation. It is possible that this is because the top layer was more able to access the bottom layer through the unaltered gel.

Assessing the highly novel experimental design, it was difficult to control dispersion and mixing of these gels prior to introduction and assembly. Further, some clumps remained following sonication. Standard deviation was likely also increased where cells were lost in the fibre interface. These data, however, provided initial findings which can be further investigated with extra time and resources in future work. However, based on these initial data, it was decided that 0.0002g and collagen alone would be taken forward for immunofluorescence imaging. In future work, to rule out the involvement of changing metabolic activity, in addition to the CellTiter-Glo® assay, cell counts could also be carried out.

10.4 Immunofluorescence Imaging

In the following investigation, light sheet and confocal microscope (Leica, UK) live cell imaging was carried at the STFC Rutherford Appleton Laboratory in Didcot, UK. To build a picture of gel-fibre mediated migratory control, an increasingly complex cell-fibre-gel system was imaged, starting with basic one-layer imaging. Initially, 50,000 SH-SY5Y cells were applied to the random nanofibre and left to adhere for twenty-four hours in a CO_2 incubator. Using a low serum DMEM f-12 and retinoic acid, differentiation was carried out for seven days. The high-resolution confocal microscope was tested for its ability to image SH-SY5Y cells stained with anti-βIII Tubulin primary antibody, red Alexa Fluor 568 secondary antibody and blue DAPI nuclear stain on random PAN nanofibre. Images are shown in figure 87.

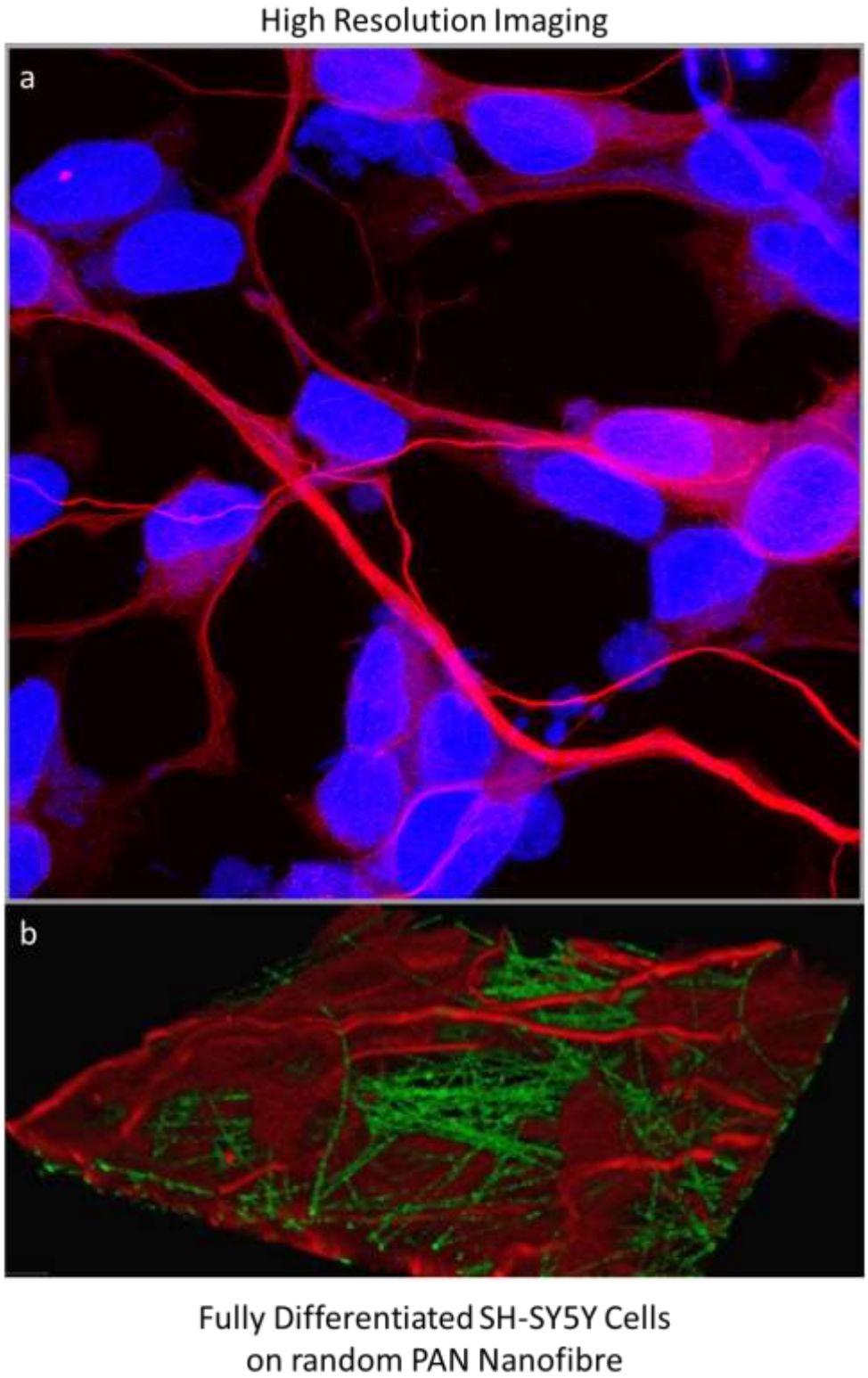

Figure 87. Imaging differentiating neurons on 3D conduits with collaborators in Didcot, UK. a. Maturing SH-SY5Y cells on randomly aligned PAN nanofibre (1ml deposition) having been differentiated for seven days. Cells stained with red with anti-βIII Tubulin primary antibody (and red Alexa Fluor 568 secondary antibody) and blue DAPI stain. b. Cells on randomly aligned PAN nanofibre as before, green colour shows auto-fluorescent PAN nanofibres. Images taken on high-resolution confocal suite a STFC Rutherford Appleton Laboratory (Leica SP8 Confocal).

Having established that imaging could be obtained in high magnification and lower magnification (in 3D constructs), 50,000 SH-SY5Y cells were applied to aligned rather than random PAN nanofibre and left to adhere for twenty-four hours in a CO_2 incubator. From this point, multiple layering designs were tested. First, the cellularised, aligned PAN was simply laminated with a second layer of PAN. Next, the cellularised PAN coated in 3mg/ml collagen I gel alone and, in some samples, a second layer of PAN was then added on top of this. Lastly, the cellularised PAN was coated with 3mg/ml collagen I gel + PAN (0.0002g/ml) and laminated with a layer of PAN (30 minutes into polymerisation) once more. In each case, cells were kept undifferentiated and labelled with CellBrite™ Orange (Biotium, US) – a cytoplasmic membrane dye. Imaging commenced after polymerisation was finished or layering was done in absence of gel. Wherever a second layer of fibre was added to a bottom layer with gel, it was added 30 minutes into polymerisation.

Experimental designs ensured migration occurred against gravity. Confocal immunofluorescence imaging was limited in that exposure to the laser light quickly triggered bleaching or cellular death. Therefore, cells were imaged for three-hour periods, two hours after layering (to allow gel polymerisation to occur). The final images shown in figure 88 show the end-point in each case. Imaging cells within the confocal microscope required optimisation steps in that action had to be taken to keep layers as close as possible together.

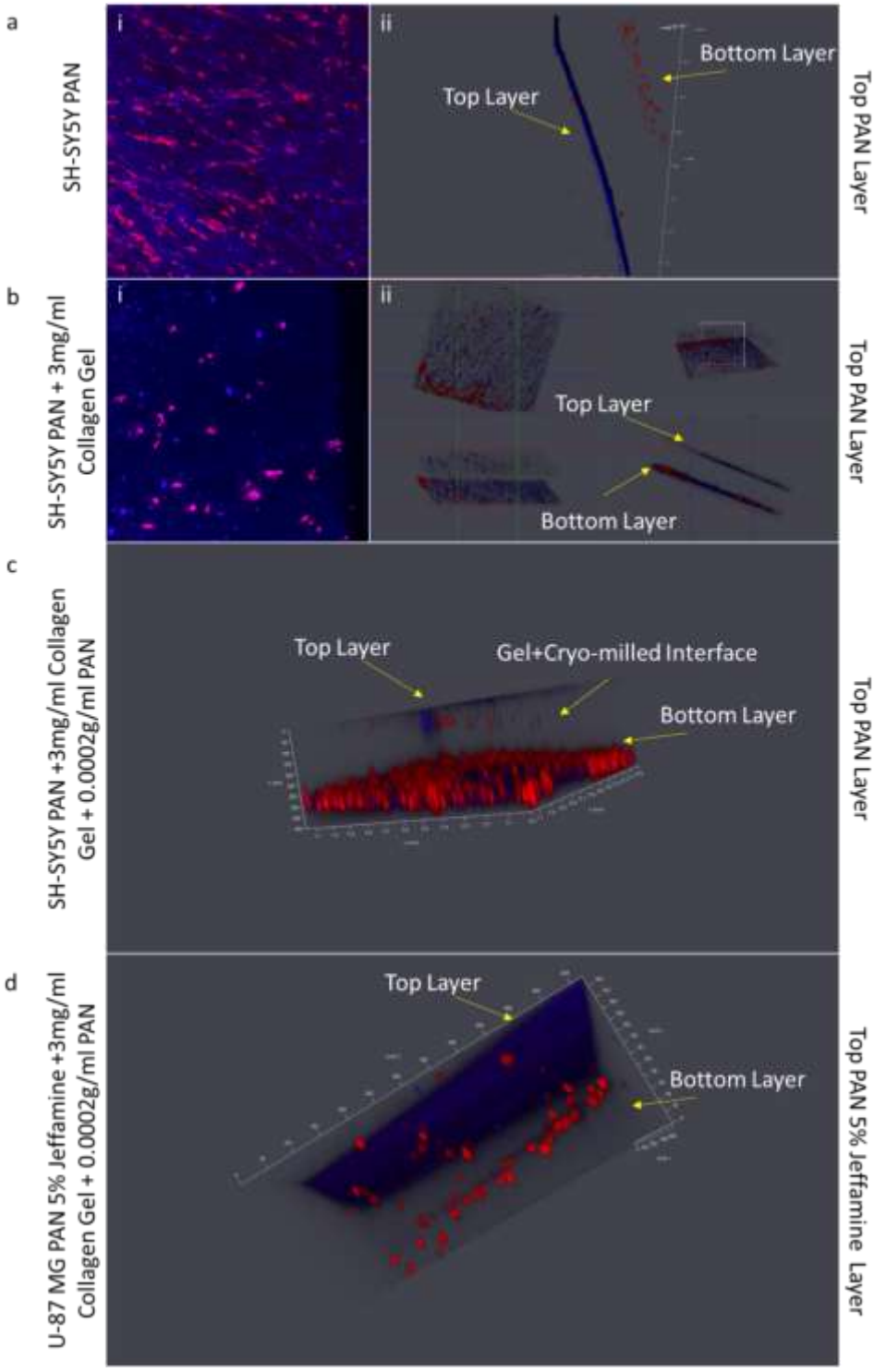

Figure 88. Confocal immunofluorescence imaging showing initially a single layer of cellularised nanofibre and later, multiple layers of nanofibre between which cellular migration was tracked. a. Immature SH-SY5Y cells on PAN nanofibre (i) and then layered with a top layer of PAN nanofibre (ii). b. Immature SH-SY5Y cells on PAN nanofibre covered with 3mg/ml Collagen I gel, polymerised for 2 hours at 37°C (i) and then layered with a top layer of PAN (ii). c. Immature SH-SY5Y cells covered with 3mg/ml Collagen I gel and 0.0002g of cryo-milled PAN nanofibre, then layered with a top PAN layer. d. Immature U-87 MG cells on PAN-5% Jeffamine, covered with 3mg/ml Collagen I gel and 0.0002g of cryo-milled PAN nanofibre, then layered with a top PAN-5% Jeffamine layer. All images taken 2 hours after layering (to allow polymerisation). All cells stained with CellBrite™ Orange.

Initial analysis of figure 88ai showed that undifferentiated SHSY-5Y cells did not form extensions as long as the control samples over the same period of time, though no differentiation media was in use in any case here (in future experiments mature cells should be analysed, time and distance restrictions limited preliminary studies). This was perhaps because the physical cues provided by the collagen distracted cells from lateral extension. Perhaps when combining the prosthesis design with a gel-based interface, it should be introduced in small sections of the fibre.

Where a second layer of PAN was introduced (figure 88aii) in the absence of collagen gel (no cryo-milled fibre), some inter-layer migration was visualised, though the limited ability to keep layers together in the microscope likely restricted this migration. In future work, this could be targeted by placing a stacker inside the microscope on top of the two layers, ensuring the layers are pushed together as they were in cell culture. This was trialled, though some difficulty was had in identifying which layer was which on the confocal microscope with its limited z-range capabilities – it was decided that with some practise this would likely be a good solution in future work. This issue was seen less in samples with a gel-only interface as the gel held the two layers together better. Several cells did make it to the top layer in each case. There was even a clear example of a cell in the interface with the use of a gel-only interface.

Keeping layers of fibre together was easier in the more structurally supportive fibre + cryo-milled gel samples (figures 88c+88d). Layers remained close and any free space was filled. It was possible that some migration was taking place largely in the SHSY-5Y population. A multitude of cells appeared to be seen dispersed on and between top and bottom layers of fibre. Some migration was seen in the U-87 MG population under the same conditions, though migration appeared more limited with relatively few cells in the top layer. As was hoped, cells seem to remain in the gel + cryo-milled interface between the two layers. As mentioned, more confocal imaging will be required in future work carried out on differentiated cell populations.

Light sheet microscopy (TCS SP8 DLS, Leica, UK) was technique available through the Octopus facility at STFC Rutherford Appleton Laboratory. This technique enabled high temporal resolution over a large working distance (with relatively low bleaching risk) which made it very useful for live cell imaging of our layered systems. The aim was to track cell migration from the bottom layer, through the interface (gel + cryo-milled fibre) and into the top layer.

To hold the sample in the light sheet, a 3D printed structure was designed and manufactured in-house at NTU. This had to hold the sample at an angle (trialled at 30°, 45° and 60°) such that the mirrors that make up the light-sheet head could be orientated around it. The CAD design model of said sample holder to presented in figure 89a+b. The holder was 3D printed (FormLabs, UK) from bio-compatible dental-grade resin. This resin was tested for biocompatibility with both SH-SY5Y and U-87MG cells in 2D cell culture. In each case, 50,000 cells were seeded into the wells of a 12 well plate and left for twenty-four hours to attach

in a CO_2 incubator. After twenty-four hours the medium was changed to fresh 10% serum DMEM f-12 and dental grade resin disks were added (2cm diameter, 0.2cm thickness) and the cells cultured for a further forty-eight hours. Light microscopy images are shown in figure 89c. Nanofibre layers were also trimmed, removing the random areas. This was done using the Trotec CO2 laser cutter so that the elliptical regions would be welded into position (cutting with scissors reduced structural integrity).

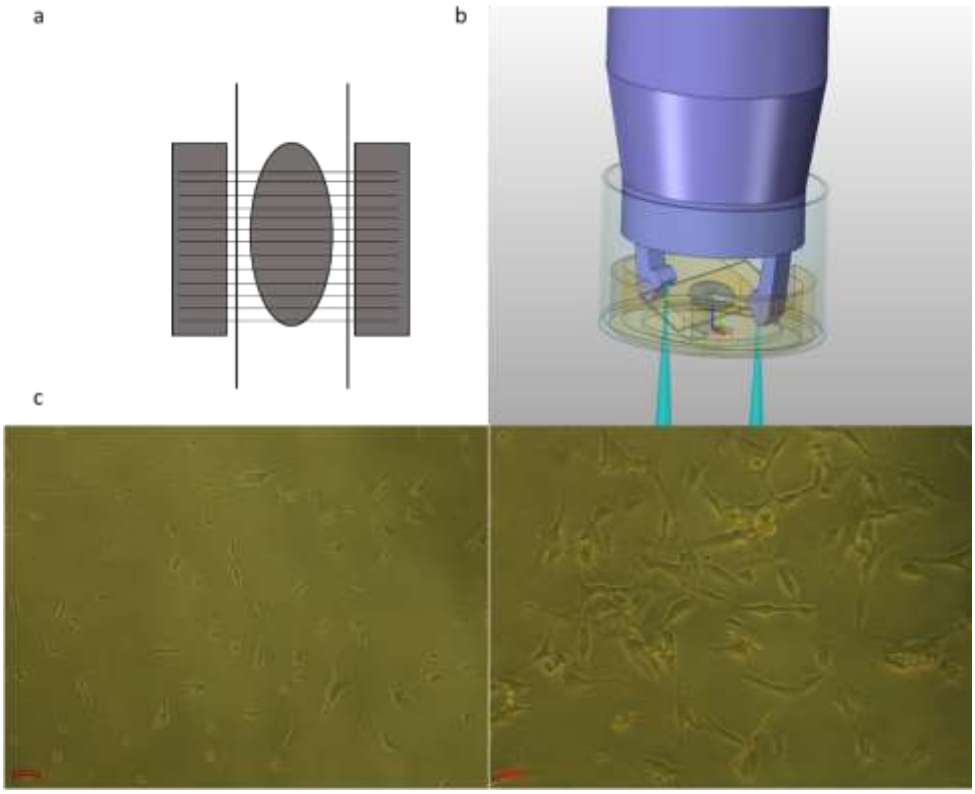

Figure 89: a Schematic showing the removed sections of randomly aligned fibre. b. Schematic (solid-works) image showing the structure of the sample holder which permits light sheet imaging of samples. c. Light microscopy images showing healthy immature SH-SY5Y (left) and U-87 MG cells (right) after twenty-four hours of exposure to dental grade, 3D printed polymer.

As depicted by the images in figure 89, the sample with removed randomly aligned regions sat at an angle such that the light sheet mirrors could redirect laser light horizontally through the region of interest. This angle was tested at 30°, 45° and 60°. The most consistent data were obtained using the 45° sample holder. Cells appeared morphologically healthy after 48-hours exposure to the dental grade material and given that the resin was sold as biocompatible this was considered an acceptable indication as to biocompatibility.

Using light sheet immunofluorescence imaging, as described it was hoped that, neuronal cells could be tracked from one layer of PAN to another through an interface constructed of gel + cryo-milled fibre. The results in figure 90 display a series of images captured over three hours. For this, 50,000 SH-SY5Y cells were seeded onto nanofibre and left to attach for twenty-four hours in a CO_2 incubator. At this point, 100µl of 0.0002g PAN – 3mg/ml Collagen I gel mix was added to the top of the seeded populations and allowed to

polymerise for 30 minutes before the top layer of PAN was added. A further 1.5 hours elapsed before imaging began. To show the progression of cells, a snapshot at the zero hours, one and a half hours and three hours points are detailed in figure 90. In addition, included is a schematic of what each region in the image represents. Immature SH-SY5Y cells were incubated for forty-eight hours before laminating with a second nanofibre layer. They were stained with CellBrite™ orange once more.

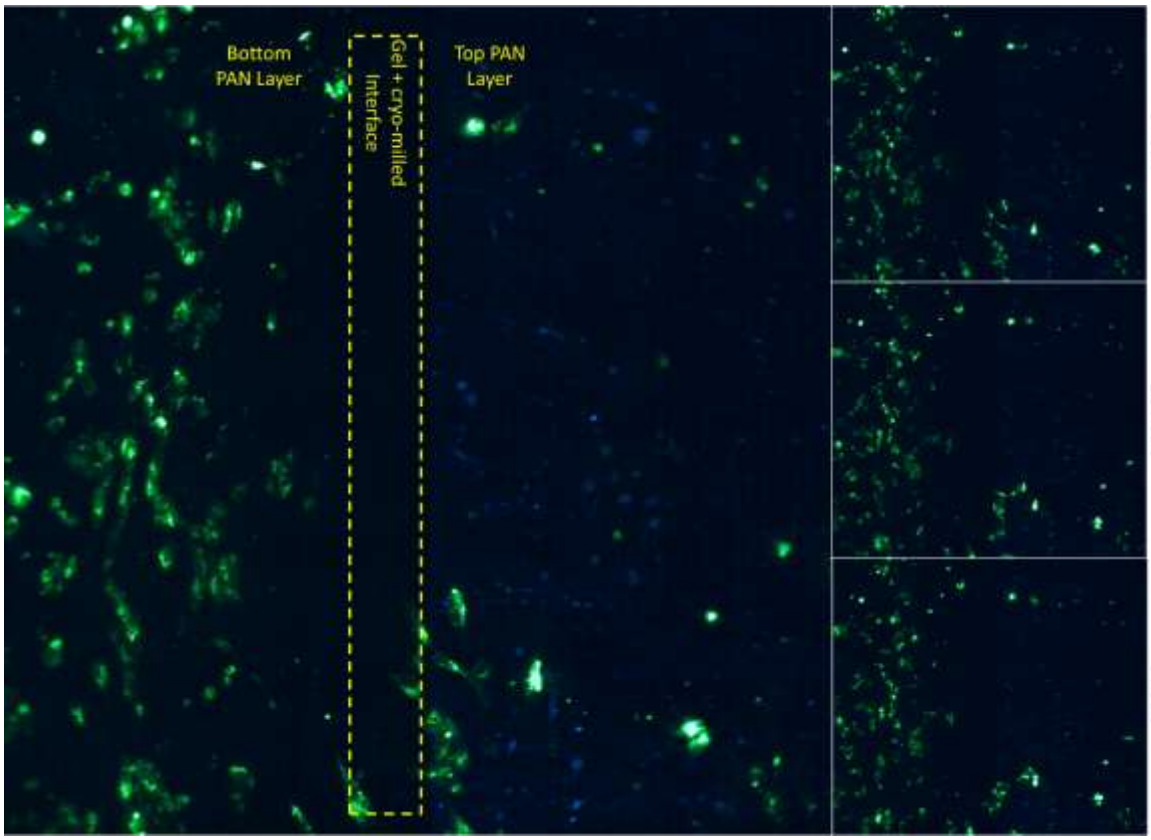

Figure 90. Immature SH-SY5Y cells stained with CellBrite™ Orange prior to seeding. Cells covered with 3mg/ml Collagen I gel + 0.0002g of cryo-milled PAN nanofibre, then layered with a top PAN layer. Following polymerisation, cells were tracked for three hours. Images depict a summary image indicating which regions depict top and bottom layers of PAN (left), and then time points 0, 1.5 and three hours (right).

Results indicated potential neuronal cell migration into the interface and up towards the second layer of nanofibre even within this short three-hour window. Notably this did seem to occur in one location in this time-frame and so this could perhaps be the product of a hole or passageway forming in the gel-cryo-fibre interface. However, these were encouraging data indicating that neuronal migration could perhaps be influenced. More experimentation was needed in future work with mature neurons (clonal cell lines and stem-cell derived neurons too), and a more developed interface. Preliminary results indicated that 3mg/ml gel + 0.0002g/ml cryo-milled PAN may provide an effective interface for filtering neuronal cells from one body of cells (modelled with neurons on PAN) into a nanofibre based implant with some further development, though much more data was needed to make any definite conclusions.

10.5 Discussion

In summary, it was possible to polymerise 3mg/ml collagen I gels in the cold (4°C), room temperature (21°C) or physiological temperatures (37°C). SH-SY5Y and U-87 MG populations survived well in gels polymerised at all three temperatures. Owing to the formation of fibrous bundles in the gels, cells formed the most consistent mat of cells at 37°C. It was possible to mix short lengths of cryo-milled PAN nanofibre into the 3mg/ml gels at a variety of concentrations. Incorporating 0.0002g/ml of cryo-milled PAN into the 3mg/ml collagen I gels delivered a material that appeared to provide a promising candidate conduit with which neuronal migration into a prosthesis structure could be perhaps mediated, whilst perhaps minimising glial migration to an extent. In future experimentation, differentiated clonal cells (and other stem-cell derived cells for example) would provide more insightful evidence to support these findings. Further, more work to improve the mixing of gel-fibre interfaces could be carried out.

Considering the overall aims of this investigation, a method with which to selectively control migration into the prosthesis will be required *in vivo* to ensure the only neuronal cells, not activated glia from the SCI enter the prosthesis. Using a gel, the prosthesis-injury interface showed early promising evidence in helping control migration, though no conclusive outcomes could be stated. Small lengths of fractured nanofibre showed potential to act like a filter to perhaps exclude glia, though again more data would be needed to say this conclusively. Crucially, the fibre was also constructed of a material shown to be catered to neuronal growth and detrimental to glial growth in the long term. This step was essential in developing a prosthesis and the concept could be applied to future work with a stem-cell based system for example, which would still require the introduction of neuronal cells from the injury. The stem cells most likely to be used would be undifferentiated mesenchymal stem cells which have shown to boost neuroprotection (Ropper et al. 2017).

Assessing the literature, nanofibre has been used in combination with collagen gels by numerous groups. One of the more relevant studies by the Nguyen et al group showed that aligned nanofibre coupled with collagen gels could mediate neuronal guidance though the gel in addition to delivering proteins and nucleic acid therapeutics in spinal cord injury research (Nguyen et al. 2017). The group provided evidence supportive of this study that nanofibre in combination with hydrogels could mediate neuronal guidance through the gel interface. Another study by the McMurtrey et al group combined aligned PCL nanofibre scaffolds with Hyaluronic Acid (HA) hydrogels. The group showed that neurite outgrowth using SH-SY5Y cells was not inhibited by the use of a gel and that the gel and nanofibre interfaces become integrated – though the group noted that the gel had low cell attachment capacity (McMurtrey 2014). Few studies have made use of cryo-fractured nanofibre in combination with gels, particularly in encouraging neuronal invasion. One group made use of cryogenically ground PCL nanofibre in combination with PGD-AlphaProA hydro-peptide-gel to mediate bone healing in dogs (Srnec et al. 2018). The group reported certain cell types

infiltrating the injury better than in control groups (higher cellularity and angiogenesis). Though using cryo-fractured fibre with gels is a relatively new concept, evidence provided here in addition to groups who used fully formed nanofibre with gels shows that some level of cellular infiltration and cellular guidance is encouraged into the gel-injury interface. This was encouraging in supporting evidence provided in this investigation.

11.1 Aim of the Investigation

Within this investigation, migration between layers of nanofibre has shown its diagnostic value. One additional use for layering populations of neurons and glia on nanofibre was uncovered within this study. A key aim of the work presented in this chapter was to prove the efficacy of a nanofibre-based *in vitro* SCI model by recreating many of the hallmarks of SCI.

11.2 Technique

To create an *in vitro* SCI model, 25,000 SH-SY5Y and 25,000 U-87 MG cells were first seeded on aligned, 10wt% PAN and left to attach for twenty-four hours in a CO_2 incubator. Cells were then differentiated using low serum DMEM f-12 and retinoic acid treatment. PAN was chosen as long-term viability of a co-cultured population was shown to be on average greater than on 1 or 5% Jeffamine doped PAN (though not significantly so). This population was then subjected to trauma to recreate the injury. There are a multitude of techniques employed by groups with which to trigger an injury, for example dropping a weight from a specific height is relatively popular (Cheriyan et al. 2014). In this investigation, 'transection' in which partial cutting of neuronal and glial co-culture (recreated spinal cord tissue) was used. A jig was designed in-house by layering 5 layers of 4mm sterilised Perspex (Plastic Company, UK) cut into 5cmx5cm squares with the CO_2 laser cutter (Trotec, UK). The bottom 4 layers were adhered using SC250 Solvent Cement (FloPlast, UK). In the centre of layers 2+3 (from the top) a cavity was (laser) cut to have the same dimensions as the nanofibre disks. The top layer included a slit the same dimensions as a RS Pro scalpel blade (Swann Morton, UK). The bottom layer had no central features (base level). The top layer was removable and the cellularised nanofibre was placed inside the cavity. After replacing the top level by guiding it through some securing pins, the injury was created by lowering a sterilised blade a fixed distance through the cellularised fibre into the base of the cavity **once**. This ensured that the lesion created was both controlled and reproducible. The jig was sterilised using 70% ethanol for 30 minutes before use. An image of the Jig is shown in figure 91a in combination with a schematic of technique in cartoon and real-world formats (figure 91b). In addition, a demonstration as to lesion size reproducibility is shown (figure 91c). This was calculated by taking an average of lesion diameters in 5 separate samples (10 separate diameter readings per sample).

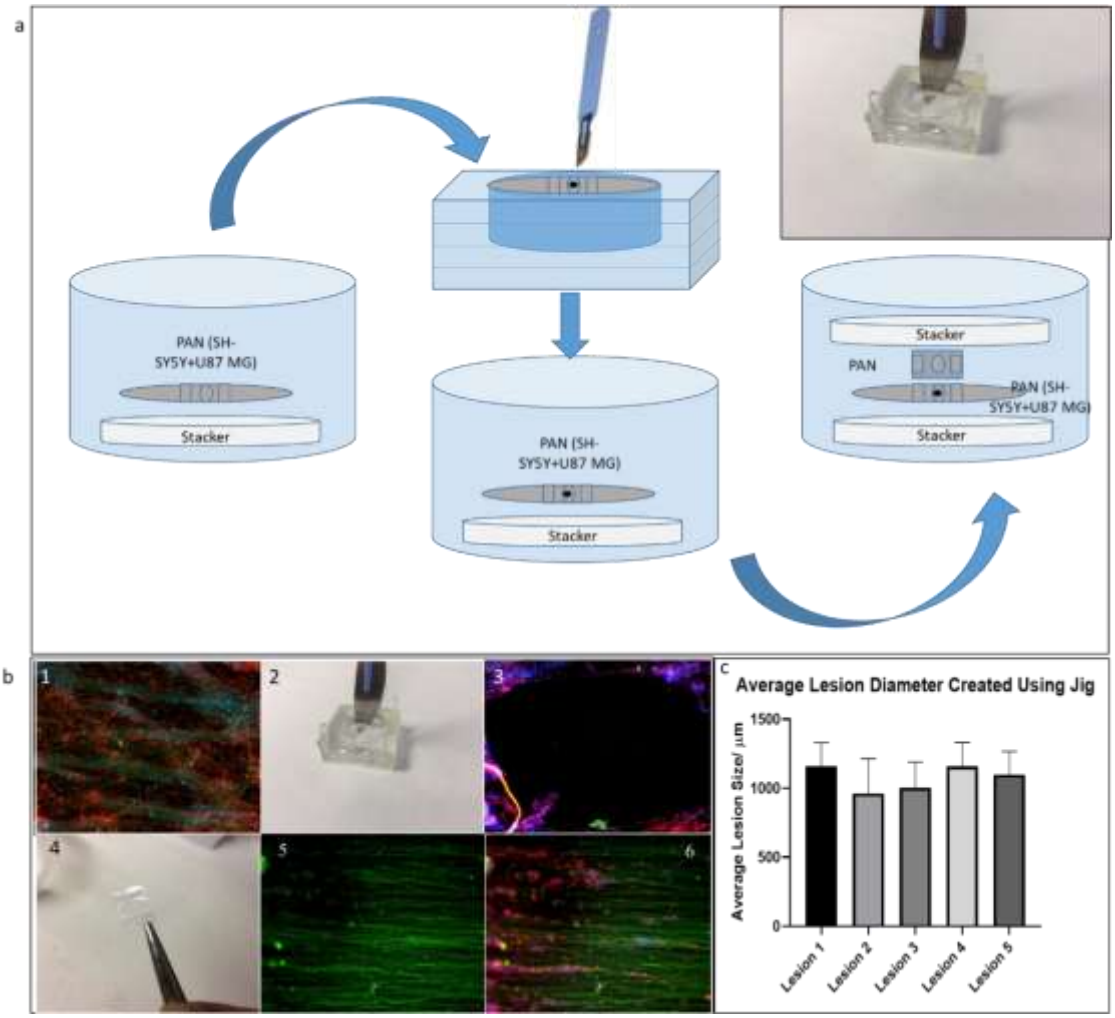

Figure 91. Diagrammatic description of SCI modelling using nanofibre. a. Cartoon depiction of the nanofibre-based lesioning process. Included is an image showing the jig design employed. b. 'Real-world' description of the lesioning process – 1. Co-culture of neuronal and glia cells. 2. Injury using a jig designed in-house. 3. Lesion created. 4. Top layer of aligned nanofibre prepared. 5. Top layer of aligned nanofibre added atop the lesion. 6. Cellular migration into the top layer of aligned nanofibre. Images are immunofluorescence images including anti-βIII Tubulin primary antibody (and red Alexa Fluor 568 secondary antibody) staining, blue for DAPI nuclear staining and green for PAN fibre autofluorescence. c. Average lesion diameter as calculated across 5 lesion samples. This was calculated using ImageJ to assess multiple diameter locations within each sample and taking an average. Significance was assessed using a one-way ANOVA with Tukey's multiple comparisons test with P<0.05 indicating significance (*).

Using this technique, it was shown that a lesion could be reproducibly (in terms of size) created within a PAN-based co-culture of neuronal and glial cells. The jig was relatively easy to construct and could be adapted to fit fibre dimensions as required.

SCI exhibits certain hallmarks *in vivo* over the acute and chronic phases of injury. For example, in the acute (and chronic) phase of SCI, widespread cellular death and release of reactive oxygen and nitrogen species (RONS) is typically seen (Zhang, N. et al. 2012). In response to injury in the acute and sub-acute phases, glial activation is often seen, which leads to astroglial scar formation in the chronic phase. To establish the model as physiologically relevant, a number of these hallmarks had to be shown to be recreated in vitro.

Though the cell lines, once mature, could not be kept for long periods of time, it was hoped that a number of these hallmarks could still be captured.

11.3 Cellular Death

Initially, the investigation sought to identify cell death in response to injury. In the following experiment, 25,000 SH-SY5Y and 25,000 U-87 MG cells (ATCC, USA) were seeded in co-culture on aligned 10wt% PAN and left to adhere for twenty-four hours in a CO_2 incubator. Cells were then differentiated using low serum DMEM f-12 and retinoic acid treatment for seven days. At this point the co-culture was subject to scalpel-mediated transection injury using the described jig. Cellular viability was measured using the *CellTiter-Glo® assay* both in individual SH-SY5Y and U-87 MG populations and in co-culture before the injury and twenty-four hours after. In this way it was hoped that the distribution of cell death could be best understood. The results are shown in figure 92.

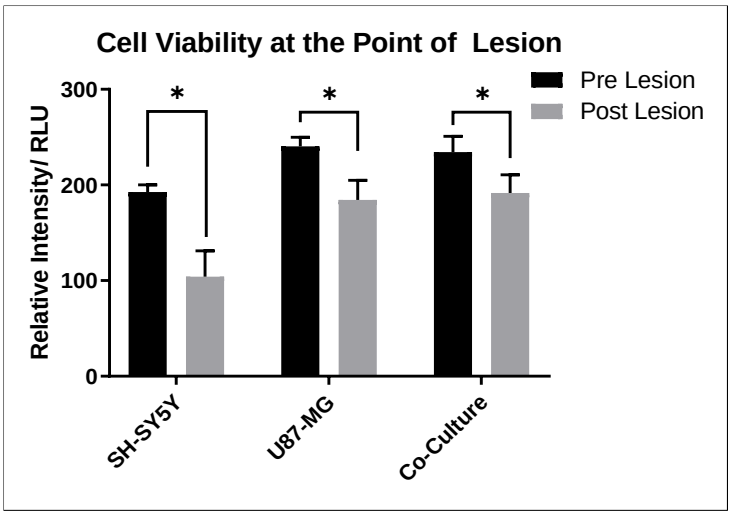

Figure 92. CellTiter-Glo® assay-based experiment in which viability was tracked in SH-SY5Y and U-87 MG populations (and in co-culture) pre and twenty-four hours post lesioning on PAN nanofibre. Significance was assessed using a two-way ANOVA with Sidak's multiple comparisons test with P<0.05 indicating significance (*).

Results indicated that significant cell death was seen in all cases. The most significant cell death occurred in the neuronal population. This was deemed logical given the length of axonal extensions after seven days of differentiation prior to injury. In co-culture, though still significant compared to the control, the cell death was more modest perhaps because of glial protection – more work needs to be done to confirm this.

11.4 Reactive Oxygen and Nitrogen Species (RONS)

RONS up-regulation is a hallmark of in vivo SCI. This is thought to be the product of Nrf2 activation in astrocytes (Xu, J. et al. 2014). To assess the up-regulation of RONS in this model, DCFDA dye staining of

injured co-cultures was carried out. Short- and longer-term release of reactive oxygen and nitrogen (RONS) species at the point of lesion could therefore be tracked. In each case, 25,000 SH-SY5Y and 25,000 U-87 MG cells were first seeded on aligned, 10wt% PAN and left to attach for twenty-four hours in a CO_2 incubator. Cells were then differentiated using low serum DMEM f-12 and retinoic acid treatment for seven days. Cells were injured, and the populations were stained with DCFDA dye (for time point 0) after three hours, then twenty-four and forty-eight hours. Confocal images are shown in figure 93 in addition to average DCFDA expression over the three time points with and without injury. This was calculated from average optical intensity in a 2.2mm^2 area at the lesion edge (or a comparable location on the nanofibre aligned ellipse in control samples) using ImageJ on immunofluorescence images obtained. Plot profiles for the lesion edge are also included in early time points.

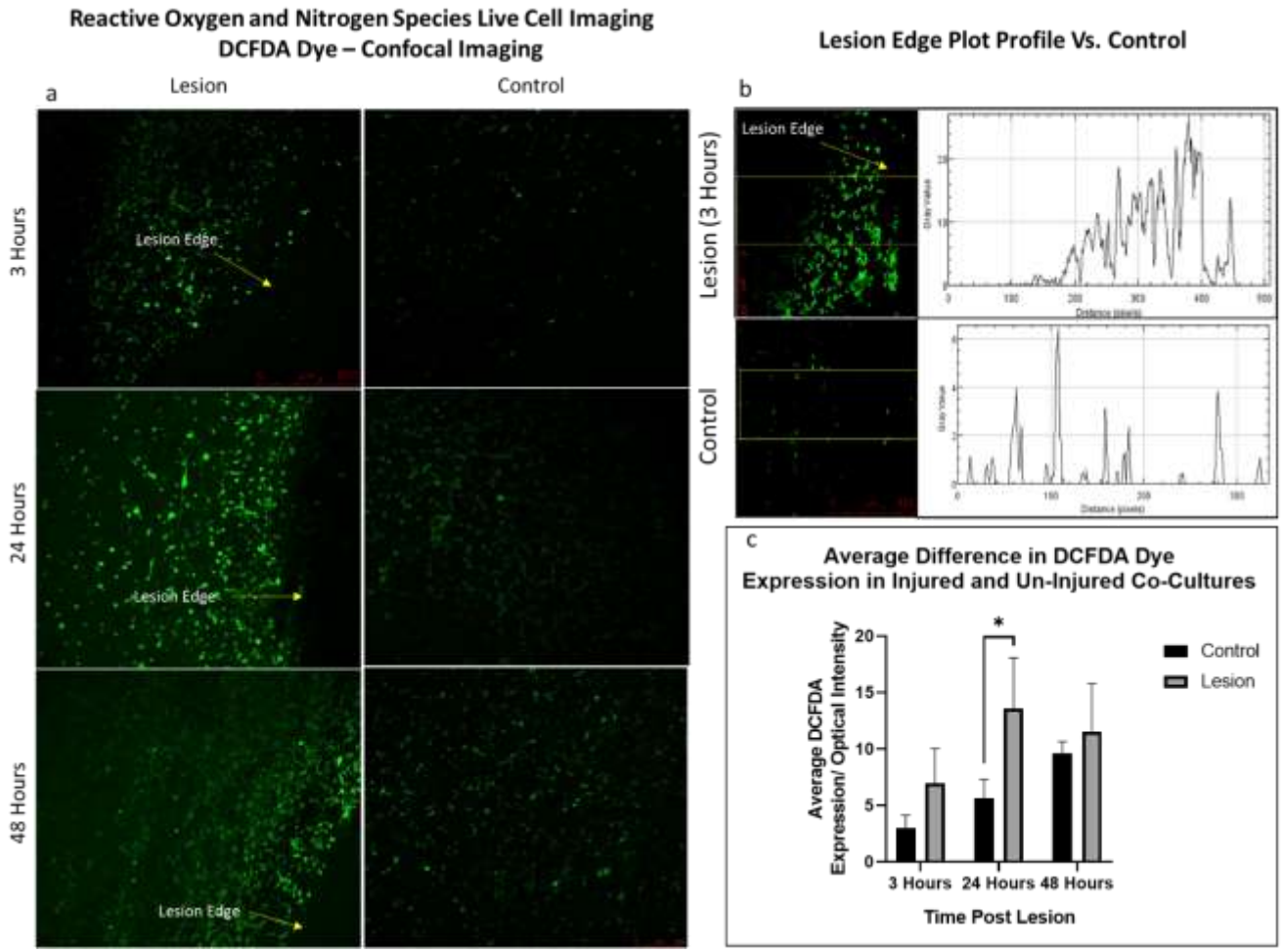

Figure 93. RONS expression in response to injury in a neuronal and glial co-culture. a. DCFDA dye assessing RONS in a mature co-culture of SH-SY5Y and U-87 MG cells three hours, twenty-four hours and forty-eight hours post lesion compared to a control (un-lesioned fibre). b. Plot profile comparison of the lesion edge at 0 and three hours post lesioning (plot profiles generated on ImageJ). c. Average DCFDA dye expression at each time point in control and lesioned samples. Quantification obtained by taking 5 random locations (in three samples) and calculating average optical intensity in a given area (2.2mm^2 in each case) for each time point. Significance was assessed using a two-way ANOVA with Sidak's multiple comparisons test with P<0.05 indicating significance (*).

Results showed an up-regulation of RONS after just three hours. This continued for up to seventy-two hours covered in this experiment. The expression of RONS was notably greater in all cases compared to control (significantly at twenty-four hours). Medium was not changed to ensure no RONS were lost. By forty-eight hours the expression of the control was also increasing, likely due to stress (though more experimentation would be required to show this), though populations still expressed notably less RONS than that of the injured samples. The *in vitro* up-regulation of RONS expression in response to injury provided encouraging supportive evidence as to the efficacy and relevance of this in vitro model.

11.5 GFAP Up-Regulation

As mentioned earlier, activation of glia in response to injury occurs in the acute and sub-acute phases of SCI *in vivo*. Following 'activation', certain proteins are up-regulated, which eventually leads to astroglial scar formation into the chronic phase of SCI. One such protein is GFAP. Evidence that this is up-regulated following SCI has been shown in vivo (Brenner 2014, Gomes et al. 1999). It was essential to provide evidence that glia in co-culture on nanofibre were experiencing this activation post lesioning.

To quantify GFAP expression, western blot analysis was used. It was known that GFAP is up-regulated to an extent during natural astrocyte differentiation (Lee, Y. et al. 2006). Therefore, to assess the marked increase in GFAP expression in response to injury, GFAP expression was tracked over the seven days that cells were matured, and the seven days post injury. For this, 25,000 SH-SY5Y and 25,000 U-87 MG cells were first seeded on aligned, 10wt% PAN and left to attach for twenty-four hours in a CO_2 incubator. Cells were then differentiated using low serum DMEM f-12 and retinoic acid treatment for seven days. The 'jig' was used to injure the co-culture and at this point, three hours was left before quantifying the first 'post-injury' time-point. Vinculin was used as a housekeeping protein. Results are shown in figure 94 in both the visual blots generated and densitometry data.

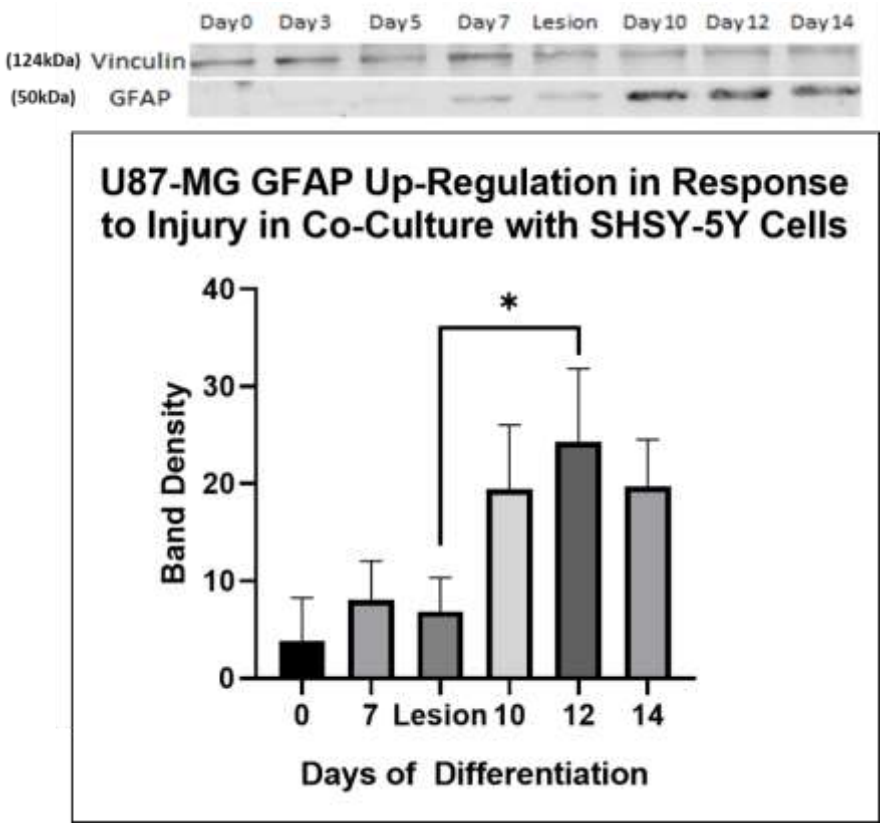

Figure 94. Western blot analysis of GFAP expression in a co-culture of SH-SY5Y and U-87 MG cells as cells were matured over seven days, injured, and then monitored over the subsequent seven days. Images of probed blots indicated band intensities at each time point and the graph indicates quantified densitometry. Significance was assessed using a one-way ANOVA with Sidak's multiple comparisons test with $P<0.05$ indicating significance (*).

The data yielded from this experiment indicated an average up-regulation of GFAP following the lesion, maintained from days ten to fourteen. This up-regulation was significant at day twelve. The initial on-average (but not statistically significant) down-regulation of GFAP was likely the product of initial cell death in the first few hours. A gradual increase in GFAP up-regulation was noted as expected between days zero and seven over normal differentiation. Results indicated that the *in vitro* model likely did provide evidence that GFAP was up-regulated in glial cells within a co-culture on nanofibre in response to transection injury, but significantly so only at five days post-injury. It was possible however that GFAP up-regulation was actioned significantly in sub-populations of cells within three days of injury and so the follow-up experiment sought to understand this visually.

The reason that days seven to fourteen of 'control' (un-lesioned) cultures were not also analysed with western blot was based on observations that U-87 MG cells were reaching maturity and literature indicated that GFAP expression had begun to peak (Qiu et al. 2012). It was therefore assumed that GFAP had peaked by this point and this became the control group. However, if the resources and time allowed, the control group would have been also continued through to fourteen days – this is something that could be

considered for future work. The same reasoning was used for the following supportive immunofluorescence experiment.

In combination with data obtained in western blots above, immunofluorescence staining was used to image lesion edges in co-cultures from day seven of differentiation post-injury. This immunofluorescence panel is shown in figure 95, illustrating SH-SY5Y cells stained with anti-βIII Tubulin primary antibody with red Alexa Fluor 568 secondary antibody staining and U-87 MG cells stained with anti-GFAP primary antibody with Alexa Fluor 532 secondary antibody staining. The experimental set up was identical and run in parallel to that described above. It was deemed important that visualisation of this process accompanied any functional Western Blot analysis data obtained. Using ImageJ, it was possible to quantify the GFAP expression by ensuring all images were taken with the same settings. Three images per time point were selected and a measurement of GFAP expression according to mean fluorescence of a given area in the GFAP channel only quantified. Results are shown in figure 95.

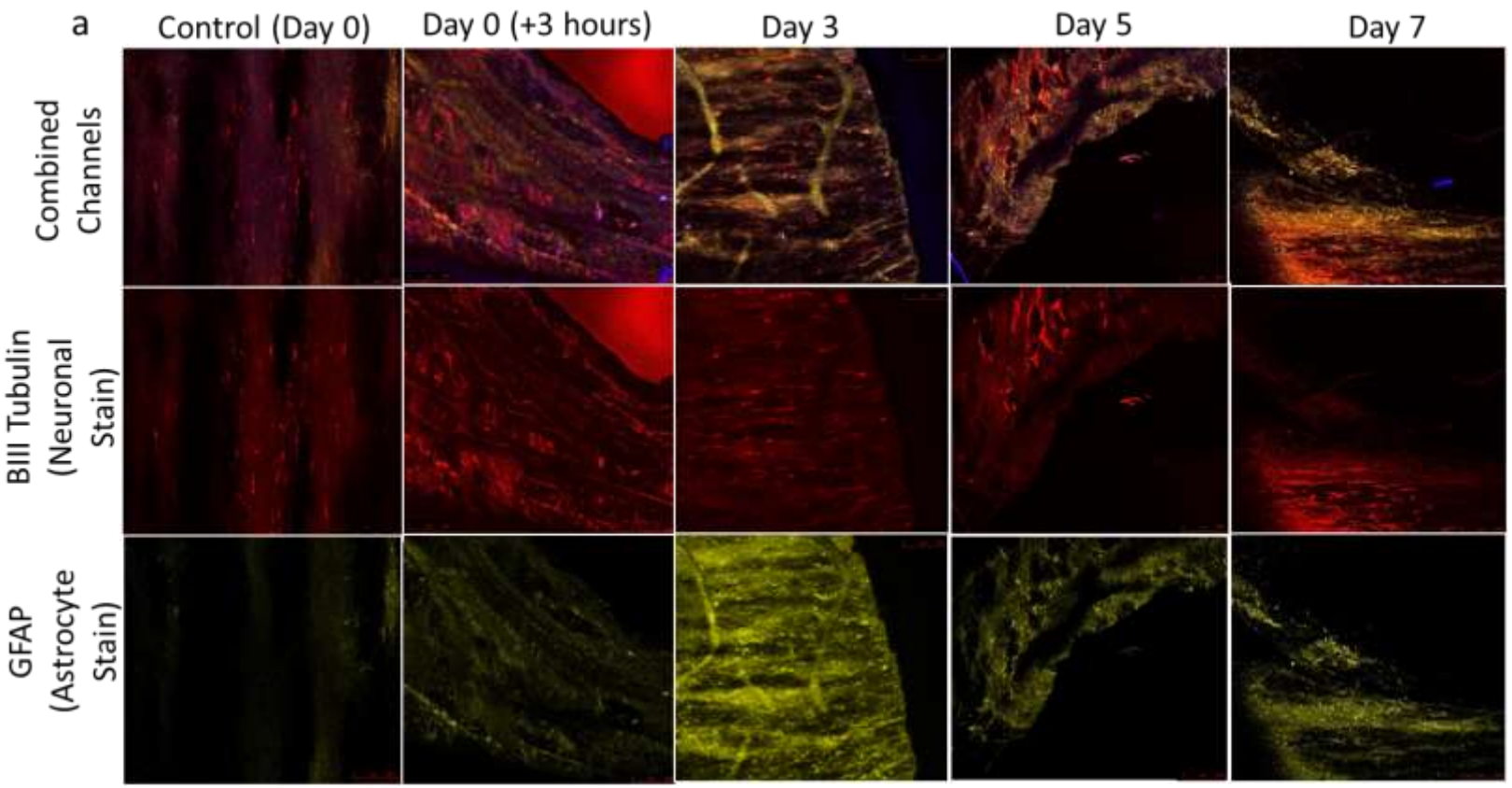
a
Control (Day 0)
Day 0 (+3 hours)
Day 3
Day 5
Day 7
Combined Channels
BIII Tubulin (Neuronal Stain)
GFAP (Astrocyte Stain)

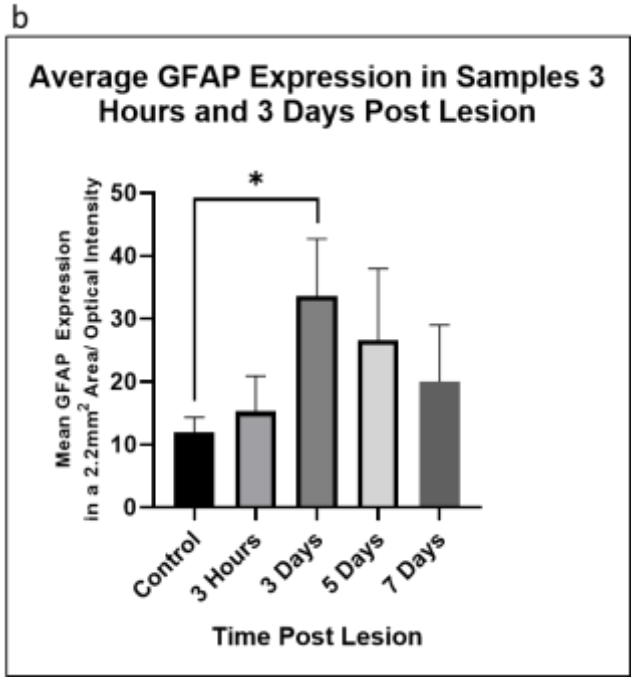

Figure 95. Immunofluorescence imaging/quantification of a neuronal and glial co-culture before and after injury. a. Immunofluorescence images showing a mature co-culture of SH-SY5Y and U-87 mg cells having been differentiated from seven days. Primary anti-βIII Tubulin antibody with secondary red Alexa Fluor 568 antibody stained neuronal cells and primary anti-GFAP with secondary yellow Alexa Fluor 532 antibody stained glial cells. Channels are shown overlaid and individually over the seven days post injury. b. Average GFAP expression as calculated using ImageJ to assess average optical intensity in a given area (2.2mm^2) in triplicate samples at the lesion edge. Significance was assessed using a one-way ANOVA with Tukey's multiple comparisons test with P<0.05 indicating significance (*).

Immunofluorescence imaging showed a notable increase in mean GFAP expression between the first two time points. When quantified across three samples using ImageJ, this up-regulation was shown to be significant between three hours and three days only. On average, GFAP expression did seem to gradually decrease from day three until day seven visually, though not significantly. It was for this reason that functional western blotting was required in combination to provide clarity. In every case, the differentiation process was shown to be effective in that neuronal axons were elongated.

The limitation of this experiment was in chance – it was ensured that wherever possible a representative snapshot of the lesion edge (or control) was obtained in every case. However, the quantification of GFAP expression was at the mercy of the locations selected for imaging. Only day zero control (seven days of differentiation) was included as glia (and neurons) were considered fully mature. In future experiments if time and finances allowed, the controls could be extended to day fourteen.

11.6 Modelling Treatment of SCI

Using layering, it was possible to experiment with the idea of 'treating' the SCI modelled with a nanofibre treatment layer. The concept here was to assess the effect on the SCI on patching the lesion, but also to understand cellular behaviour in the treatment layer. It was hoped that this would provide the *in vitro* model with evidence to suggest that it could be used to trial treatments as well as understand pathology.

Initially, immunofluorescence imaging was used to assess neuronal migration from the lesion edge into a top layer of nanofibre. The primary goal of the nanofibre 'treatment' was in theory to act as a bridge to navigate surviving neurons across an injured region. Therefore, tracking neuronal migration not only into the treatment patch but also across it was paramount. In each case, 25,000 SH-SY5Y and 25,000 U-87 MG cells were first seeded on aligned, 10wt% PAN and left to attach for twenty-four hours in a CO_2 incubator. Cells were then differentiated using low serum DMEM f-12 and retinoic acid treatment for seven days. Having injured the fibre, an aligned, 10wt% (1ml deposition) top nanofibre layer was added three hours post injury. This was for several reasons. Firstly, the first experimental time point in the lesion alone was chosen to be three hours. Secondly, in vivo, a human SCI is very rarely treated immediately. Lastly, purely experimentally speaking, layering after three hours ensured that any cells on the top layer of nanofibre were not there because of cells being disturbed into the medium and simply floating there. Cells were stained with anti-neurofilament antibodies and imaged at three hours, three days, five days and seven-days post lesioning using am SP8 confocal microscope. Results are shown in figure 96.

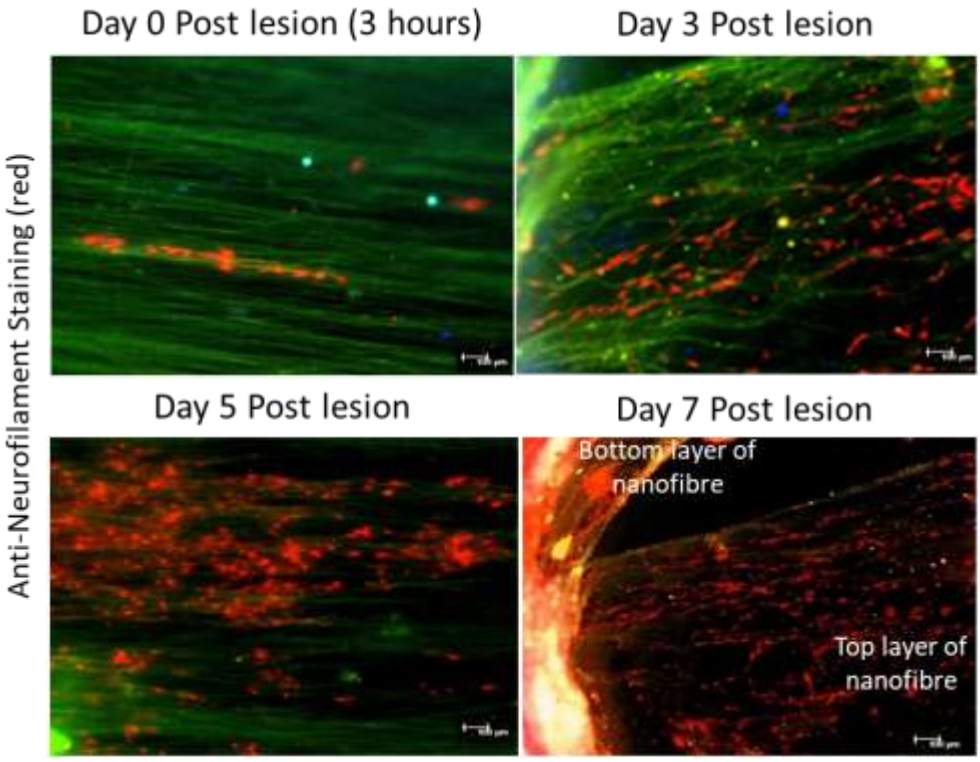

Figure 96. Immunofluorescence images showing neurofilament-stained SH-SY5Y cells on the top-layer of PAN on a bridge layer over the seven days post injury. This bridge layer traverses an injured coculture of mature SH-SY5Y and U-87 MG cells (matured for seven days). Fibre runs left to right in each case.

The images obtained suggested that a gradual neuronal migration was evident. Cells seemed to migrate unidirectionally from the bottom layer across the aligned top layer of fibre according to the physical cues provided by this top layer. It had already been discerned that PAN as a top layer mediated neuronal migration well (see chapter 8.2). It was however hypothesised that a certain amount of glia migration may have occurred also. In a separate experiment, sharing the same experimental design, anti-GFAP primary antibody (and yellow Alexa Fluor 532 secondary antibody) staining was carried out on the resident cells to track glial migration from an injured co-culture into a top PAN layer. It was hypothesised that providing a layer into which cells could migrate could mediate migration of activated glia. In effect, this could provide a means of displacing activated glial cells and potential scar tissue. The immunofluorescence images in figure 97 present this anti-GFAP antibody-stained top layer.

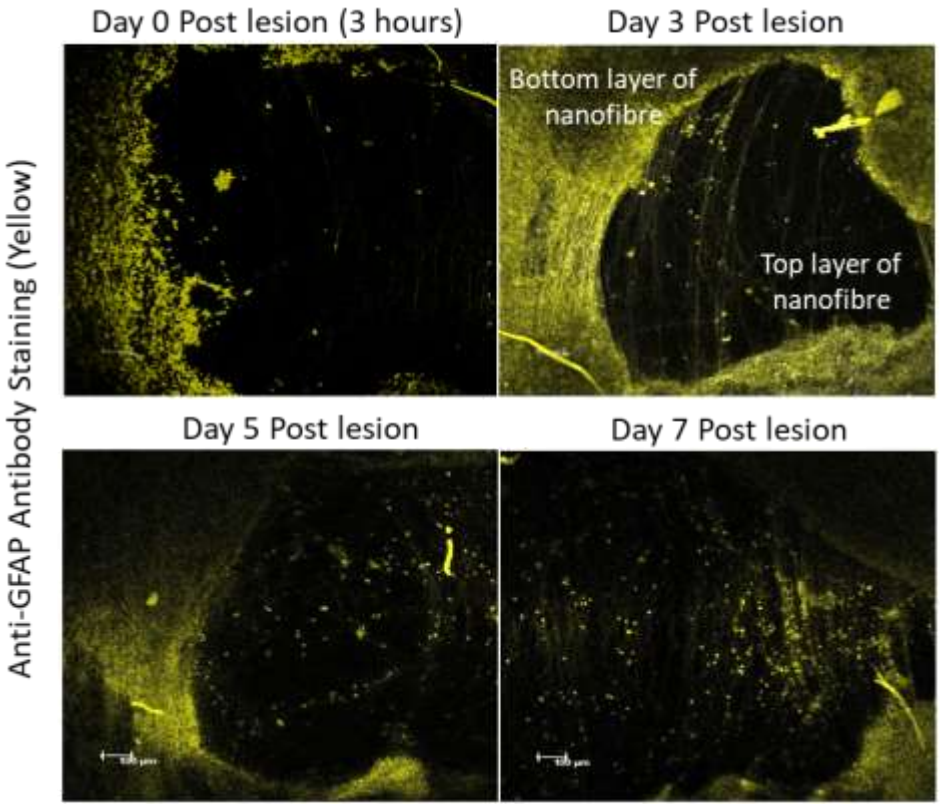

Figure 97. Immunofluorescence images showing anti-GFAP primary antibody (and yellow Alexa Fluor 532 secondary antibody) stained U-87 MG cells on the top-layer of PAN on a bridge layer over the seven days post injury. This bridge layer traverses an injured coculture of mature SH-SY5Y and U-87 MG cells (matured for seven days prior to injury and lamination) also stained with anti-GFAP antibody (in yellow). Fibre runs top to bottom in each case.

Interestingly, images showed consistency with both Western Blot and ImageJ data obtained above. A few visual observations were made. A notable increase in GFAP expression was seen at the lesion edge at day three post lesion. Visually, there was a steep gradient in GFAP expression at three hours and more so at three days. The presence of a top layer seemed to lead to migration of GFAP expressing cells into the layer. This in turn reduced the GFAP gradient seen at the lesion edge. Results supported the hypothesised idea that activated glia could be extracted from an in vitro lesion site using nanofibre.

Having established that both neurons and glia underwent migration into the treatment patch, it was important to understand overall cellular migration. Overall migration was tracked using DAPI nuclear stained counts into the top layer. This data was extracted from the same experiment as that in figure 96 (Neurofilament stained bridges) and thus shares the same experimental design. Imaging in addition to quantification is shown in figure 98. In combination, a multi-channel image of the distribution of neurons and glia at seven days post layering was included which was carried out in a separate, identically designed experiment. This gave an idea as to the distribution of neuronal and glial populations that had undergone migration into this top layer. All results are shown in figure 98.

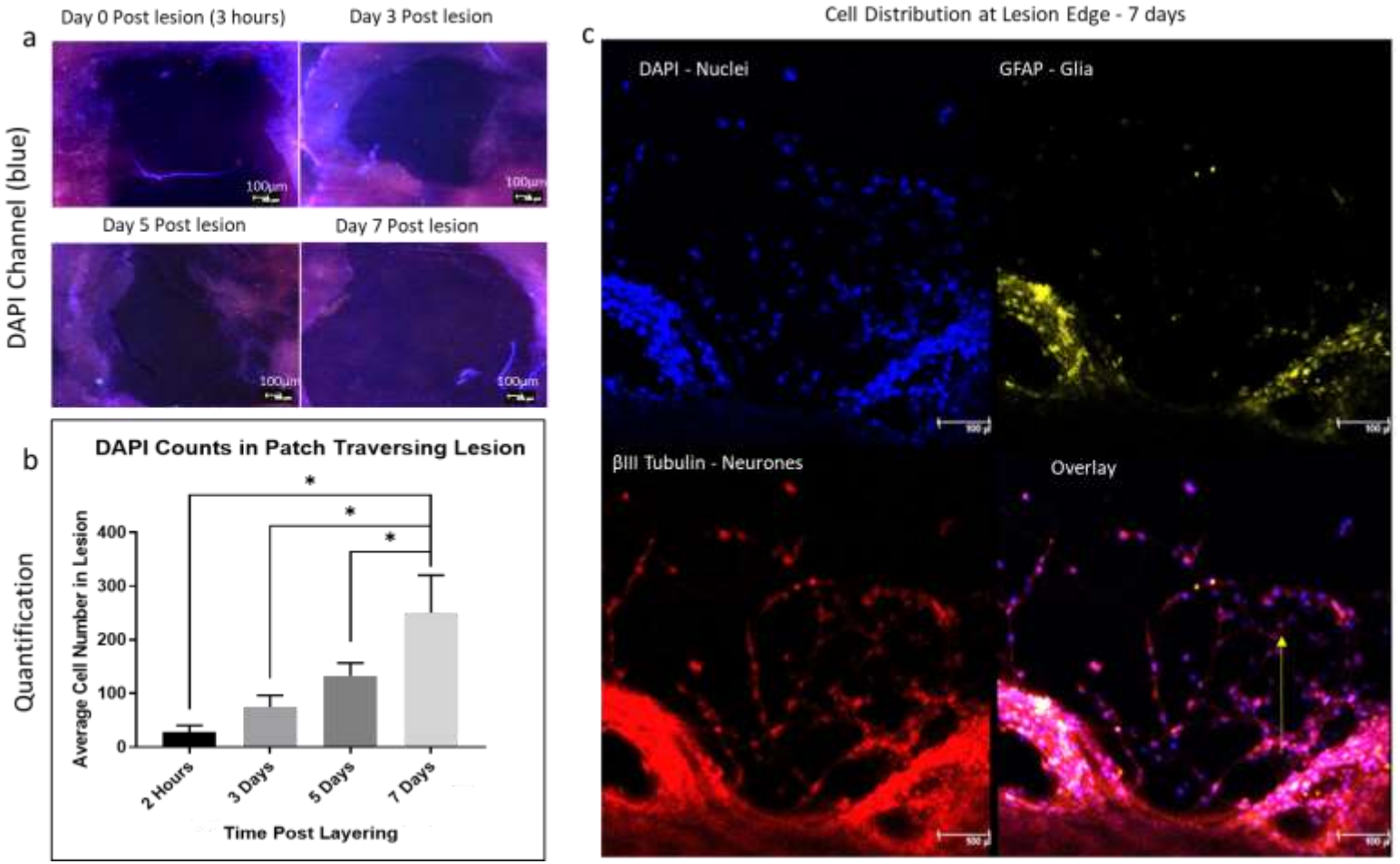

Figure 98. Distribution of neuronal and glial cells at the lesion edge. a. Fluorescence images showing DAPI-stained SH-SY5Y and U-87 MG cells on the top-layer of PAN on a bridge layer over the seven days post injury. This bridge layer traverses an injured coculture of mature SH-SY5Y and U-87 MG cells (matured for seven days prior to injury). Fibre runs left to right. b. Quantified overall nuclei count of all cells that had migrated onto the top layer of nanofibre. c. Immunofluorescence images showing anti-βIII Tubulin primary antibody (and red Alexa Fluor 568 secondary antibody) stained SH-SY5Y cells and primary anti-GFAP primary antibody (and yellow Alexa Fluor 532 secondary antibody) stained U-87MG cells at the lesion edge at seven days post injury (blue indicates DAPI nuclear staining). The yellow arrow denotes migration direction of all cells. Significance was assessed using a one-way ANOVA with Sidak's multiple comparisons test with $P<0.05$ indicating significance (*).

Results showed a steadily increasing nuclei count on the top nanofibre layer post lesion over seven days (significantly more cells were shown at day seven compared to all other days). It could be visually seen that cells tended to migrate from the two ends of the nanofibre bridge which was interesting though perhaps unsurprising. Although some insight could be gained from the cellular distribution, the overall cell count did not conclusively establish individual cell population behaviour in the co-culture.

An additional follow up experiment aimed to carry out more in depth staining for the cellular contents of this top layer was designed. This experimental design was identical again to that of the previous set; 25,000 SH-SY5Y and 25,000 U-87 MG cells were seeded in co-culture and matured for seven days prior to injury. Three hours post injury, a layer of PAN was introduced as before. SH-SY5Y cells were stained with anti-βIII Tubulin primary antibody (and red secondary Alexa Fluor 568 antibody) and U-87 MG with primary anti-GFAP antibody (and yellow Alexa Fluor 532 secondary antibody) for immunofluorescence imaging. To follow up on an observation made in chapter 8 which suggested that soaking a top layer of nanofibre in medium in which differentiating glia had been cultured (to maturity) significantly increased overall neuronal migration, as an additional parameter, control layers were compared to top layers soaked in glial conditioned medium. Cellular migration was tracked using confocal imaging and overall cellular viability (as quantified using the CellTiter-Glo® assay) compared. Results are shown in figure 99.

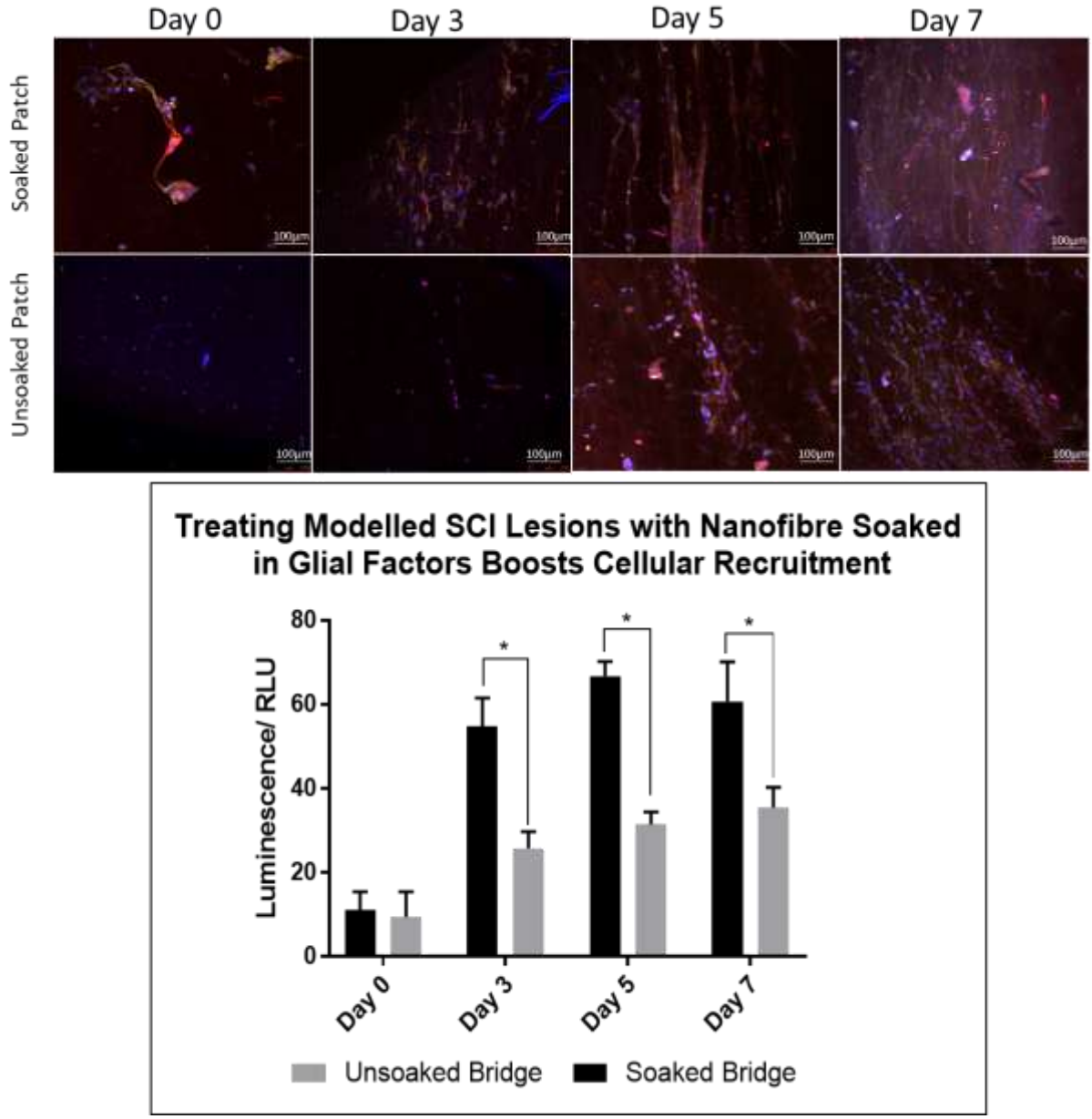

Figure 99. Neural and glial migration into treatment layers of nanofibre. a. Immunofluorescence image depicting anti-βIII Tubulin primary antibody (and red Alexa Fluor 568 secondary antibody) stained SH-SY5Y cells and primary anti-GFAP antibody (and yellow Alexa Fluor 532 secondary antibody) stained U-87 MG cells on the top layer of the SCI model from three hours to seven days post injury. Images were compared in patches (PAN top layers) that were soaked in glial conditioned medium or not. b. CellTiter-Glo® assay showing overall cellular viability in the top layer of PAN with and without soaking the PAN in glial conditioned medium in the seven days post layering. Significance was assessed using a one-way ANOVA with Sidak's multiple comparisons test with P<0.05 indicating significance (*).

Assessing of the immunofluorescence images indicated both neuronal and glial cell migration was evident in comparable numbers. This did not change when soaking in glial conditioned medium. Glia cell numbers were perhaps visibly slightly higher, but no significance could be allocated to this. Looking at the CellTiter-Glo® assay data however, there were significantly greater cellular viability from day three to seven in total when top layers were soaked in glial conditioned medium. This evidence further supported the indirect co-

culture hypothesis presented in previous chapters. It also provided an opportunity to test the model created for its ability to investigate different treatment options.

In addition to the data obtained on neuronal-glial distribution, it was hypothesised that if glial migration was occurring into this top layer, perhaps some evidence of astrogliosis may also be identified. This was the case as shown in the immunofluorescence images shown in figure 100 (stained as before). If activated astrocytes could be extracted from a lesion, this may provide some method of reducing the negative effects of scar tissue in SCI.

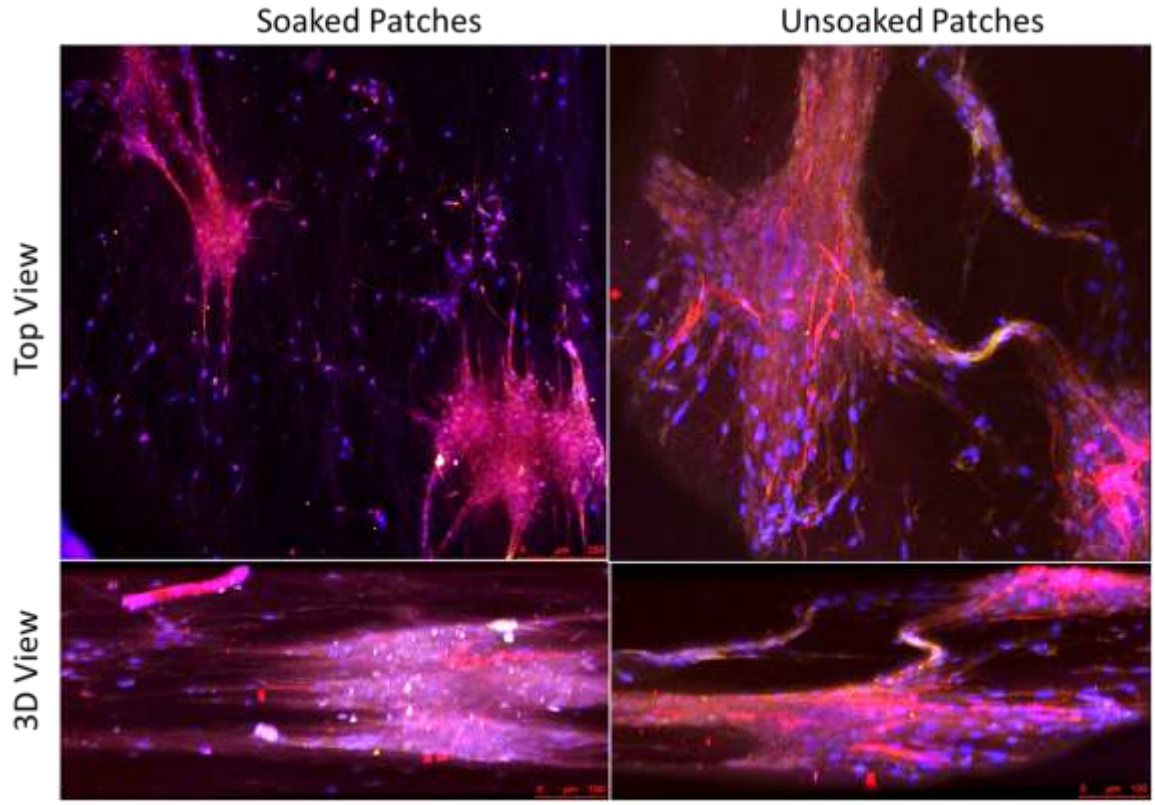

Figure 100. Comparison of the cellular content of top-layers of nanofibre (with and without glial conditioned medium soaking) placed on top of an injured co-culture layer. Immunofluorescence images show SH-SY5Y cells which were stained with anti-βIII Tubulin primary antibody (and red Alexa Fluor 568 secondary antibody) and U-87 MG cells which were stained with primary anti-GFAP antibody (and secondary yellow Alexa Fluor 532 antibody). The images show top and 3D views of glial clumping on the top layer – attributed to potential astrogliosis evidence seen in the top layer of PAN layered onto the SCI model below.

Clumps of glia were seen in which neurons were clearly present. These neuronal extensions did not seem to always penetrate the glial clump – as would be expected if this effect was indeed astrogliosis. It was possible that the cells were simply existing in direct co-culture though the morphological 'clumped' appearance in which cells deviated greatly from nanofibre alignment cues did suggest astrogliosis. This effect was seen in both soaked and un-soaked patches alike. If combined with the gel-based interface developed earlier, it is possible that a scaffold could in the future be designed to encourage glial migration and therefore focus on activated glial cell extraction from the injury site. This could perhaps be an

alternative to direct neuronal rerouting. Future work could be carried out to characterise this astrogliosis further.

The final experiment carried out sought to test the *in vitro* model further, using both chemical and physical treatment. Notably, more optimisation steps are required to assess dosing, though here, clinical-grade corticosteroids were used at a physiological human adult dose. The chosen compound was fluocinolone acetonide, which is primarily used in dermatology to relieve skin inflammation, but it is also used to treat chronic diabetic macular oedema (Massa et al. 2019). Nanofibre was manufactured harbouring said clinical grade corticosteroids. Specifically, the clinically recommended dose (0.025% or 0.25mg per gram of polymer) of corticosteroid was spun into the randomly aligned, 1ml 10wt% PAN nanofibre by mixing with the polymer pre-spinning. As before, a co-culture of SH-SY5Y cells and U-87 MG cells were seeded at 25,000 cells each and matured for seven days with low serum DMEM f-12 and retinoic acid treatment. The co-culture was then injured and for twenty-four hours treated (laminated) with either undoped randomly aligned PAN, or with corticosteroid-doped PAN. Using DCFDA dye, the RONS were imaged at the end of this process. The results are shown in figure 101 in combination with a quantification carried out by taking the average fluorescence intensity from five replicate samples using ImageJ.

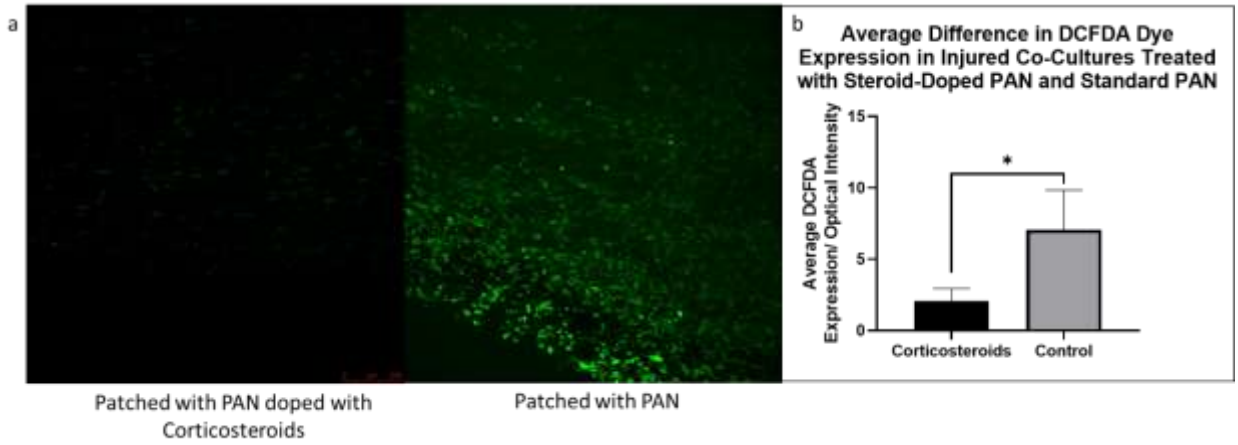

Figure 101. a. DCFDA dye fluorescence showing RONS expression in a co-culture of injured (mature) SH-SY5Y and U-87 MG cells having been layered with undoped PAN or PAN doped with clinical grade corticosteroids (fluocinolone acetonide). b. Average DCFDA fluorescence in a given area (2.2mm^2) with and without steroid treatment as calculated by assessing average optical intensity using ImageJ. Significance was assessed using a two-tailed, parametric, unpaired t-test with Welch's correction with a P-value of <0.05 (*).

There was a notable visual difference in DCFDA fluorescence at the standard microscope settings. This difference was shown to be significant using ImageJ analysis of images taken using confocal microscopy. In future investigations, the dose included in the PAN when spun and the treatment time could be modified. However, this experiment provided a good preliminary example of how the in vitro model can be potentially used to test a spectrum of physical and chemical treatments for SCI.

11.7 Discussion

In summary, an in vitro, clonal cell-based SCI model was created by maturing a co-culture of SH-SY5Y and U-87 MG cells for seven days on aligned 10wt% PAN and then injuring by scalpel, guided by a jig. The model demonstrated widespread cell death in both cell lines and up-regulation of RONS as demonstrated by DCFDA dye. Astrocyte 'activation' was demonstrated by up-regulation of GFAP as shown using western blot analysis and immunofluorescence staining. By layering with a top layer of 10wt% PAN, neuronal and glial cell migration was noted, demonstrating the potential for neuronal re-routing and extraction of activated glia (two separate potential treatments). It is possible that introducing some form of glial cell-displacing layer around the outside of the prosthesis could add an extra layer of engineerable complexity to the resultant prosthesis design. Some astrogliosis was noted on the top treatment layer. By doping the top layer of PAN nanofibre doped with clinical grade corticosteroids, some evidence was provided that suggested oxygen radical scavenging was possible in the injury below. This was demonstrated by reduced RONS expression following DCFDFA dye staining.

Considering the overall aims of this investigation, inter-layer migration provided an opportunity to create an injury and model physical nanofibre-based treatment. In creating this model, prosthesis designs could be tested in the future in addition to other chemical treatments for example like corticosteroid or ABC chondroitinase treatments common for SCI. Though unexpected, this line of investigation provided an interesting, potentially commercial concept which could be taken forward in the future. The fact that it was cell line-based was beneficial as shown in industry as it was simple and avoided the need for animal tissue or animal testing.

Assessing the literature, *in vitro* models for disease are a trend that's growing with the aim to reduce reliance on animal models (Luder Ripoli et al. 2019). The majority of SCI models appear to be animal-model based, with rats forming the basis of most of these models. For example, partial transection injury has been recreated in animal (similar to the injury specification used here) by the You et al group, who showed that following partial transection, the majority of recovery occurs within 3 weeks in vivo (You et al. 2003). The Boomkamp et al group aimed to move away from animal models by carrying out a 'cut' on dissociated rat embryonic spinal cord cells on an astrocyte monolayer. The group showed that multiple hallmarks of SCI could be generated with this simple model, including demyelination, infiltration of microglia, neurite density reduction and reactive astrocytes (Boomkamp et al. 2012). The Weightman et al group used aligned PLA nanofibre in combination with rat spinal tissue slices to show outgrowth and alignment of astrocytes and neurons into the nanofibre bridge (Weightman et al. 2014). This study was very informative and presented data on gliosis, cellular infiltration, neuronal outgrowth and migration into layers of nanofibre that were in-line with the findings of this chapter. The aim of this chapter was to build on the evidence provided in this study and other in vitro trials, such as the Blomkamp et al group, advancing them further

by avoiding the use of animal tissue slices and instead using human cells. General assessment of the literature suggested that a relevant, reproducible model for SCI is needed and still holds potential for novel approaches to the challenge, one such novel approach was presented in this chapter.

12.1 Prosthesis Design

Clonal SH-SY5Y and U-87 MG cell lines were utilised in the development of the proposed prosthesis design. In the future, in place of resident U-87 MG cells, mesenchymal stem cells (MSCs) could be utilised as some evidence has been seen showing that undifferentiated MSCs mediate the recovery of neurons well (Ropper et al. 2017). Using this new cellular population would require further material optimisation steps, however having developed the prosthesis design first in two clonal cell populations, the optimisation process has been established. Making use of a stem cell population would allow future in vivo testing of this design, as the resident support population would not be of cancerous (glioblastoma) origin. A good source of clinical a grade material could come from cord tissue from example from which it is possible to obtain MSCs.

Another therapeutic direction involves the use of autologous Olfactory Ensheathing Cells (OECs). These cells have been shown to mediate the continuous axonal extension and topographic targeting (guidance) of neurons within the olfactory system (Yao et al. 2018). OECs are macroglia that could be (and have been) harvested from the olfactory bulbs of the patient in need of SCI treatment and re-introduced with some success (Tabakow et al. 2013). This was shown in clinical trials by the Raisman group in the Spinal Repair Unit in UCL. In collaboration with this group, preliminary work has shown that it is possible to produce cellularised membranes from electrospun nanofibre and OEC populations. Figure 102a presents preliminary SEM images of OECs on aligned PAN nanofibre. Cells had been first subject to dehydration and gold coating prior to imaging. Figure 102b perhaps more clearly shows immunofluorescence images taken on a confocal microscope using a panoramic function to capture the long extensions formed by OECs across the length of the aligned nanofibre network. Cells were seeded at 50,000 cells per scaffold by the researcher at the Spinal Repair Unit, and the details of culture time, maturation and staining protocols have not been disclosed.

Figure 102: a. SEM imaging displaying OECs on PAN nanofibre following dehydration and gold coating prior to imaging. b. Immunofluorescence imaging showing OECs imaged with panoramic confocal analysis. Image from Raisman Group, Spinal Repair Unit, University College London, UK.

Results showed that OECs appeared to follow the unidirectional physical cues provided by the aligned PAN nanofibre. It was hypothesised that introducing OECs into humans with scaffold guidance may boost the efficiency of neuronal regeneration neuronal guidance would be enhanced even further. It is possible that aligned nanofibre would not be needed for this purpose, though observing the aligned channels formed by the glia in figure 102 suggested that aligned fibre could perhaps maximise efficiency of any neuronal recovery (Tabakow et al. 2013).

The clonal cell line-based prosthesis structure could be tested in combination with the proposed gel-fibre interface. This is unlikely to be in vivo on account of the cancerous cells in use, though part of this investigation involved the development of an in vitro SCI model capable of testing nanofibre based designs. This confluent layer of injured (or un-injured) SH-SY5Y and U-87 MG cells could allow early-stage testing particularly in understanding how well neuronal axons migrate into and extend across the prosthesis from an outside mixed population of cells. The presence of a glial support layer has already shown the potential to enhance axonal extension – future work which measures the recruitment of axons from glial scar regions of the spinal cord injury model and then the unidirectional extension of the axons through the prosthesis would be pertinent.

In testing the efficacy of the cryo-milled fibre + gel interface, it was mentioned in chapter 10 that in the development of the gel-fibre interface, undifferentiated SH-SY5Y cells were used initially. In future work, fully differentiated neurons should be used to understand the migratory behaviour of mature axons through the proposed interface. Introducing gels into nanofibre systems has been approached in a number of ways in this investigation. Dispensing gel on to nanofibre has been shown to be possible by mixing and pipetting it on directly, as has mixing in cryo-milled fibre into the gel-forming components, but electrospray has evidenced potential in a more controlled deposition. A future investigation into functionality of deposited collagen for example could be useful in developing a more refined, patterned nanofibre structure and in engineering a functioning prosthesis-SCI interface.

It was seen that the indirect presence of a glial population (even when just the media was used), provided long term neuronal viability support, migratory up-regulation and axon elongation. In future work, an investigation as to the identity of the factors exocytosed by glial cells would be of interest. This is likely to be a factor such as NT-3, as suggested by literature (Ji et al. 2015). Time of flight Mass Spectrometry would be a good candidate for this assessment. If these exocytosed factors could be successfully identified it is possible that they could be introduced to the nanofibre system directly (pre-spun or electrosprayed for example) and be used to for example better control migratory/extensional behaviour through the prosthesis on a nano-scale.

Though many of the prosthesis design parameters have been developed in this investigation, some specifications are outstanding. For the prosthesis to be used in vivo, the remaining polyester supportive sheets upon which nanofibre was spun should either be removed or replaced with a material suitable for transplant. Steps have been taken to develop this idea, using the barrier layer as the supportive layer, though more work would be required to action this. Further, it is logical that some form of encapsulating layer could prove beneficial for several functions. Specifically, effective deployment of a prosthesis would likely be enhanced if the prosthesis was protected with an encapsulating layer. Secondly, this layer could serve to minimise any influx of damaging unwanted activated glia or microglia into the 'safe-haven' that is the prosthesis. Finally, some evidence in this investigation suggested that astroglial scar tissue, or at least activated glial cells, could be 'displaced' by providing a layer of nanofibre into which they migrate. It follows that using a semi-porous random nanofibre layer (perhaps non-welded to recruit activated glia away from the injury) to encapsulate the laminated layers of fibre within it could be an effective way of achieving all three of these functions. As part of future work, an investigation into the use of vascular endothelial growth factor (VEGF) for example could be conducted in its ability to recruit blood vessels to vascularise the prosthesis (at least the outer encapsulating membrane). VEGF could potentially be introduced early in the electrospinning process or by electrospray.

12.2 SCI Modelling

In chapter 10, the basis of a SCI model founded on nanofibre based co-cultures was described. Using clonal cell lines in 3D as a model was a novel concept, in that it provided structural relevance but also simplicity, and avoids animal tissue or animal modelling. To further test this model, further chemical treatments for SCI could be employed. A corticosteroid (fluocinolone acetonide) was used at adult physiological dose to assess its ability to scavenge oxygen radicals post injury. Though some evidence was shown through DCFDA imaging, further experimentation with varying dose is needed in future work. In addition, other chemical treatments such as ABC chondroitinase enzymes, which are known to break down scar tissue, could be tested for example in their ability to dissociate the astrogliosis that was evidenced in the chapter above (Bradbury et al. 2002). Crucially, in the future, nanofibre-based treatments could be tested using this model. It would provide an opportunity to test not only the prosthesis ability to redirect neurons over a SCI lesion, but also restrict access of activated glia from the injury using a gel.

Further layers of complexity could be added to the model. Specifically, placing the injured scaffolds in a hypoxic chamber could further recreate aspects of SCI seen in vivo. Further, microglia could be added as a third population pre-injury - the HMC3 line for example (Dello Russo et al. 2018). In this way an even more complex view of SCI could be recreated in vitro with cell lines only, requiring no animal tissue or testing.

12.3 Commercialisation

As part of the research carried out in this project, a commercialisation element was also investigated. Specifically, enrolment into the Innovate UK Innovation to Commercialisation Scheme (ICURE) was successfully acquired for work carried out in this project. Training on business planning, networking and pitching a commercial entity born out of this investigation was carried out. Three months of market intelligence was carried out globally, assessing the commercial viability of nanofibre-based vitro modelling of a variety of tissue types (including spinal cord) that have been established within the research group.

Feedback was positive with evidence from close to 100 meaningful conversations in Europe, the USA and China from distributors, CEOs of biotech companies, business incubators and catapults. Feedback was that the concept of a complex, in vitro, truly 3D model was one that had commercial interest. With a little more investigation in proving efficacy of some of the other models, this could become a marketable product family. Specifically, an array of developed in-vitro, nanofibre based models could form the basis of a contract drugs testing organisation, with an aim to grow into a specialist CRO (contract research organisation) in time. Research suggested that 60% of all drug development is out-sourced to CROs. Introducing a non-animal-based model which provides accuracy and tissue relevant data (because it is both human and in 3D) has the potential to accelerate the drug development processes and reduce the number of drugs that make it through to animal trials simply by identifying unsuitable candidates early.

With a multitude of high-profile business links established, it is important that this commercialisation concept is carried forward. Already a non-disclosure agreement (NDA) has been formed with a local CRO in Nottingham and talks have been established to develop a working relationship. It is hoped that with working directly with existing CROs, this concept can move from the research space into the commercial space quickly. Focussing on this commercialisation process is paramount and filing for patents/ required IP protection is of interest to the group.

13 Discussion

The purpose of this research was to optimise acellular and cellularised nanofibre based tissue scaffold technologies which can be configured to form an implantable prosthesis for the repair of SCI. Numerous scaffold technologies exist in the context of tissue engineering, however owing to the physiology of the spinal cord white matter, it was decided that aligned nanofibre electrospinning was an appropriate option. This research group has facilitated development of the rotating-drum electrospinning technology and technique. Carrying out optimisation steps showed this electrospinning technique to be dynamic and thus customisable to multiple cell types (even simultaneously in layer form). Specifically, changing numerous system and process parameters, for example weight percentage of polymer, it was possible to manufacture nanofibre with varied physical properties such as material, fibre diameter, pore size, scaffold thickness, hydrophobicity and post-manufacture modifications. In this way, it was possible to engineer bio-inert, aligned and random nanofibre scaffolds suitable for culture of the cellular populations in question. It was shown that the scaffolds were suitable for cell culture in that they could be effectively sterilised, physically handled and could be the subject of standard cell culture analysis techniques/assays. Crucially, if in future work cellular populations of interest were to change, optimisation steps could be carried out to engineer a new scaffold suitable to the resident cells.

Within this investigation, development of a human SCI prosthesis required choosing appropriate subject cellular populations for research. Initially, human SH-SY5Y neuroblastoma and U87 glioblastoma cells (ATCC, USA) offered a robust, easily sourced, animal-free solution. The advantage that experimenting with these cells had over starting with stem cells directly was that the populations could be differentiated into distinct neuronal and glial populations without maturing into a spectrum of daughter cell phenotypes. In this way, nanofibre scaffolds could be better engineered to cellular sub-types that suited cell type requirements. This was shown to be important, for example with the finding that the hydrophilicity of PAN doped with Jeffamine showed improved long-term viability, metabolic activity and morphology in the glial populations. Differentiation protocols for the cell lines were developed and cellular behaviour assessed over this differentiation. It was for this reason that once nanofibre design parameters had been perfected to each individual cell type, standard cell culture assays (western blotting, MTT assays etc) were adapted to 3D cell culture. Assessing viability, metabolic activity and morphological characteristics (such as axon length as a product of differentiation, it was shown that on these 3D scaffolds, cells could be cultured and matured effectively. Having understood these lessons, stem-cell based research could start in the future, however skipping these key optimisation steps would be limiting.

It was decided that this treatment option would not introduce new neurons but to encourage re-growth and re-routing of surviving neurons into and across the prosthesis. Within this investigation it was decided that a supportive glial (astrocyte) population may support this process and so within a prosthesis, these

cells would be resident. Lessons learnt during the cellular optimisation process dictated that neuronal and glial populations performed better both metabolically and morphologically on materials with different hydrophobicity's. As a result, the multi-layer design concept was born. It was not expected that bringing multiple layers of nanofibre together would lead to inter-layer migration, though this controllable event proved useful in this investigation. It was quickly established that in a prosthesis, a layer of neurons and glia brought into proximity caused extensive migration. This process was characterised, and it was eventually concluded that neuronal cells not in direct contact with a glial population benefitted in long term viability and axonal elongation as much as those in contact. Layers needed to be brought together but separated by a form of porous barrier to prevent migration between layers. It is pertinent to note that aspects of inter-layer migration were deemed useful in modelling prosthesis designs for example. Multiple porous barriers were screened for their effect on neuronal and glial viability, attachment affinity and migration limitation. It was concluded that a welded 10wt% PAN + 5% Jeffamine nanofibre (with 1-hour of DMF welding) was likely the most effective barrier in a prosthesis containing a layer of glia providing indirect support to the axons of a layer of neurons (on their relevant materials) through said barrier (shown in both long-term viability and axon length).

Having identified layering with a porous barrier as a potentially effective design, attention was turned to developing an interface which allowed cells to be selectively introduced into the nanofibre scaffolds. This was important as in vivo, neuronal cells were needed inside the prosthesis without the resident activated glial cells present within the injury. Making use of inter-layer migration, gels were placed in between layers to try to understand the change in cellular migration with these interfaces. It was discerned that an interface constructed of 3mg/ml collagen I, rat tail and 0.0002g/ml cryo-fractured PAN nanofibre may be the candidate material that best encouraged neuronal cellular migration whilst limiting glial migration, though more conclusive evidence would be needed before conclusions could be made. In future experiments this could be tested in combination with the proposed prosthesis design.

Inter-layer migration provided one more unexpected discovery in the form of an in vitro SCI model. Co-culturing both neuronal and glial cells on PAN and maturing for the requisite time frame provided mature neuronal-glial 3D tissue. This could be injured, and certain hallmarks of SCI recreated in vitro. It was interesting that this could be recreated using these accessible human cell lines and a technique that was reproducible in-house. The model could be treated physically with nanofibre to show neuronal re-routing across a created lesion. Alternative treatments for example in extraction of activated glial tissue were also shown as well as early-phase data showing oxygen radical scavenging could be carried out. This concept proved to have commercial potential and so a publication has been written, and commercial leads are also being followed up.

13.1 Summation of Findings – Real World Perspective

During this investigation, the on-going consideration was how the prosthesis design would take shape based on the results obtained as a real-world human treatment. Engineering a personalised prosthesis was a concept that was developed early on. However, during this investigation it was established that using electrospinning and lamination of multiple cellular and acellular layers, a prosthesis could be manufactured bespoke to requirements. In summary, the likely best prosthesis design based on the evidence from this study was one that incorporates layered regions of aligned nanofibre capable of encouraging neuronal ingrowth and axonal elongation, and random fibre (harbouring a supportive cellular population) separated by physical porous barriers (such as welded nanofibre). The supportive population could be mature astrocytes, or else immature mesenchymal stem cells or even OECs used by collaborators in UCL. This three-part unit would in effect form a subunit that could be repeated to manufacture a scaffold which matches the requirements of the injury in question (based on size). One of the findings of this investigation was the potential dispersion of astrogliosis and activated glia using nanofibre. It follows that in the design of the prosthesis, perhaps a surrounding layer (or two) of nanofibre could coat the layered prosthesis design to absorb any activated glia or even scar as it forms but prevent it from entering the prosthesis inside. 'Plugging' the ends of this prosthesis could be gel-cryo-milled fibre mixes which regulate the selective entrance of regenerating white matter axons and neuronal cell bodies if present (some may be) into the prosthesis, whilst limiting the access of activated glia. Figure 103 summarises the suggested prosthesis design presented in the abstract.

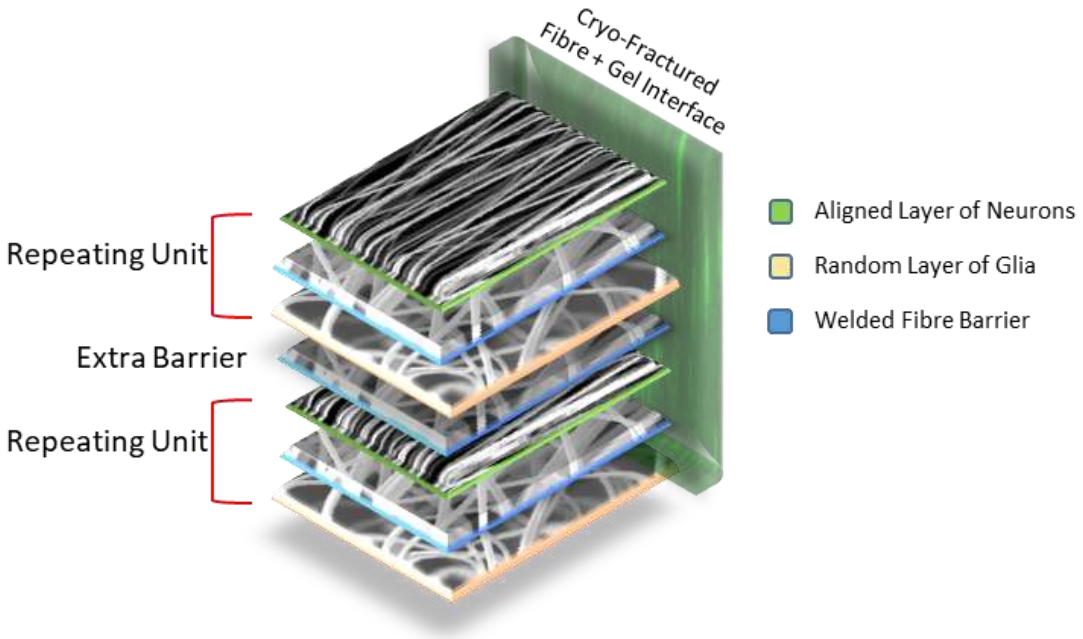

Figure 103: Diagrammatic depiction of the proposed prosthesis design to maximise neuronal recovery whilst minimising the damaging effects of scar tissue formation.

As depicted in figure 103, the lamination concept used in this investigation in combination with a nanofibre-based outer layer could both treat the spinal cord injury site and provide a means of efficiently re-routing surviving axons (and cell bodies) of the white matter across the damage, whilst limiting access to activated glia and scar. The ends of the aligned nanofibre layers could be manufactured longer such that they extend into the gel interface, picking up maximum neuronal cell/axonal traffic. If the external PAN + 5% Jeffamine case was made from welded fibre it would have certain rigidity and its properties would also allow it to serve as a protective capsule. Though more work needs to be done on establishing the outer-layer and on deployment of such a prosthesis design, the core of the research required has been established in this investigation using clonal cell lines.

Limitations of this study were largely rooted in the use of clonal cell lines. Certainly, to generate a prosthesis suitable for in vivo trials, a stem cell-based population (or OEC population) will be used in future work.

14 Conclusion

In conclusion, this inter-disciplinary project provided the basis for future development of electrospun nanofibre-based prosthesis manufacture for the treatment of SCI. Within this investigation, frameworks aimed at testing for the optimum nanofibre-based treatment have been established using clonal cell lines, but which could be developed further with incorporation of stem cells in future investigations. A nanofibre-based multi-layer design has been suggested as a potential for future testing in addition to a gel-based system aimed at mediating neuronal migration into the prosthesis whilst limiting glial migration. Spinal cord injury could be a treatable condition, and it is hoped that this work will pave the way to a mainstream treatment pathway that will become accessible to all.

15 References

1. ABDEL-MAGUID, T.E. and BOWSHER, D., 1985. The grey matter of the dorsal horn of the adult human spinal cord, including comparisons with general somatic and visceral efferent cranial nerve nuclei. *Journal of Anatomy*, Oct, vol. 142, pp. 33-58 ISSN 0021-8782; 0021-8782.

2. ABDEL-MAGUID, T.E. and BOWSHER, D., 1984. Classification of neurons by dendritic branching pattern. A categorisation based on Golgi impregnation of spinal and cranial somatic and visceral afferent and efferent cells in the adult human. *Journal of Anatomy*, Jun, vol. 138 (Pt 4), no. Pt 4, pp. 689-702 ISSN 0021-8782; 0021-8782.

3. ADIGUN, O.O. and VARACALLO, M., 2018. Anatomy, Back, Spinal Cord. In: *StatPearls* Treasure Island (FL): StatPearls Publishing LLC,Jan DOI NBK537004 [bookaccession].

4. AGUDELO-GARCIA, P.A., DE JESUS, J.K., WILLIAMS, S.P., NOWICKI, M.O., CHIOCCA, E.A., LIYANARACHCHI, S., LI, P.K., LANNUTTI, J.J., JOHNSON, J.K., LAWLER, S.E. and VIAPIANO, M.S., 2011a. Glioma cell migration on three-dimensional nanofiber scaffolds is regulated by substrate topography and abolished by inhibition of STAT3 signaling. *Neoplasia (New York, N.Y.)*, Sep, vol. 13, no. 9, pp. 831-840 ISSN 1476-5586; 1476-5586.

5. AGUDELO-GARCIA, P.A., DE JESUS, J.K., WILLIAMS, S.P., NOWICKI, M.O., CHIOCCA, E.A., LIYANARACHCHI, S., LI, P.K., LANNUTTI, J.J., JOHNSON, J.K., LAWLER, S.E. and VIAPIANO, M.S., 2011b. Glioma cell migration on three-dimensional nanofiber scaffolds is regulated by substrate topography and abolished by inhibition of STAT3 signaling. *Neoplasia (New York, N.Y.)*, Sep, vol. 13, no. 9, pp. 831-840 ISSN 1476-5586; 1476-5586.

6. AHUJA, C.S., NORI, S., TETREAULT, L., WILSON, J., KWON, B., HARROP, J., CHOI, D. and FEHLINGS, M.G., 2017. Traumatic Spinal Cord Injury-Repair and Regeneration. *Neurosurgery*, Mar 1, vol. 80, no. 3S, pp. S9-S22 ISSN 1524-4040; 0148-396X. DOI 10.1093/neuros/nyw080 [doi].

7. AL-ENIZI, A.M., ZAGHO, M.M. and ELZATAHRY, A.A., 2018. Polymer-Based Electrospun Nanofibers for Biomedical Applications. *Nanomaterials (Basel, Switzerland)*, 20180420, Apr 20, vol. 8, no. 4, pp. 10.3390/nano8040259 ISSN 2079-4991; 2079-4991. DOI E259 [pii].

8. ALI, F. and DUBLIN, A.B., 2018. Anatomy, Back, Anterior Spinal Artery. In: *StatPearls* Treasure Island (FL): StatPearls Publishing LLC,Jan DOI NBK532963 [bookaccession].

9. ALLEN, M., BJERKE, M., EDLUND, H., NELANDER, S. and WESTERMARK, B., 2016. Origin of the U87MG glioma cell line: Good news and bad news. *Science Translational Medicine*, Aug 31, vol. 8, no. 354, pp. 354re3 ISSN 1946-6242; 1946-6234. DOI 10.1126/scitranslmed.aaf6853 [doi].

10. ALLSOPP, T.E., MCLUCKIE, J., KERR, L.E., MACLEOD, M., SHARKEY, J. and KELLY, J.S., 2000. Caspase 6 activity initiates caspase 3 activation in cerebellar granule cell apoptosis. *Cell*

Death and Differentiation, Oct, vol. 7, no. 10, pp. 984-993 ISSN 1350-9047; 1350-9047. DOI 10.1038/sj.cdd.4400733 [doi].

11. ALVAREZ-PEREZ, M.A., GUARINO, V., CIRILLO, V. and AMBROSIO, L., 2010. Influence of gelatin cues in PCL electrospun membranes on nerve outgrowth. *Biomacromolecules*, Sep 13, vol. 11, no. 9, pp. 2238-2246 ISSN 1526-4602; 1525-7797. DOI 10.1021/bm100221h [doi].

12. ANTOINE, E.E., VLACHOS, P.P. and RYLANDER, M.N., 2014. Review of collagen I hydrogels for bioengineered tissue microenvironments: characterization of mechanics, structure, and transport. *Tissue Engineering.Part B, Reviews*, 20140722, Dec, vol. 20, no. 6, pp. 683-696 ISSN 1937-3376; 1937-3368. DOI 10.1089/ten.TEB.2014.0086 [doi].

13. ARAB-BAFRANI, Z., SHAHBAZI-GAHROUEI, D., ABBASIAN, M. and FESHARAKI, M., 2016. Multiple MTS Assay as the Alternative Method to Determine Survival Fraction of the Irradiated HT-29 Colon Cancer Cells. *Journal of Medical Signals and Sensors*, Apr-Jun, vol. 6, no. 2, pp. 112-116 ISSN 2228-7477; 2228-7477.

14. BARKER, D.A., BOWERS, D.T., HUGHLEY, B., CHANCE, E.W., KLEMBCZYK, K.J., BRAYMAN, K.L., PARK, S.S. and BOTCHWEY, E.A., 2013. Multilayer cell-seeded polymer nanofiber constructs for soft-tissue reconstruction. *JAMA Otolaryngology-- Head & Neck Surgery*, Sep, vol. 139, no. 9, pp. 914-922 ISSN 2168-619X; 2168-6181. DOI 10.1001/jamaoto.2013.4119 [doi].

15. BEACHLEY, V. and WEN, X., 2009. Effect of electrospinning parameters on the nanofiber diameter and length. *Materials Science & Engineering.C, Materials for Biological Applications*, Apr 30, vol. 29, no. 3, pp. 663-668 ISSN 1873-0191; 0928-4931. DOI 10.1016/j.msec.2008.10.037 [doi].

16. BEILKE, M.C., ZEWE, J.W., CLARK, J.E. and OLESIK, S.V., 2013. Aligned electrospun nanofibers for ultra-thin layer chromatography. *Analytica Chimica Acta*, 20121129, Jan 25, vol. 761, pp. 201-208 ISSN 1873-4324; 0003-2670. DOI 10.1016/j.aca.2012.11.028 [doi].

17. BHATTARAI, S.R., BHATTARAI, N., YI, H.K., HWANG, P.H., CHA, D.I. and KIM, H.Y., 2004. Novel biodegradable electrospun membrane: scaffold for tissue engineering. *Biomaterials*, Jun, vol. 25, no. 13, pp. 2595-2602 ISSN 0142-9612; 0142-9612. DOI S0142961203007816 [pii].

18. BIEDLER, J.L., HELSON, L. and SPENGLER, B.A., 1973. Morphology and growth, tumorigenicity, and cytogenetics of human neuroblastoma cells in continuous culture. *Cancer Research*, Nov, vol. 33, no. 11, pp. 2643-2652 ISSN 0008-5472; 0008-5472.

19. BIEDLER, J.L., ROFFLER-TARLOV, S., SCHACHNER, M. and FREEDMAN, L.S., 1978. Multiple neurotransmitter synthesis by human neuroblastoma cell lines and clones. *Cancer Research*, Nov, vol. 38, no. 11 Pt 1, pp. 3751-3757 ISSN 0008-5472; 0008-5472.

20. BLOOMFIELD, I.G., JOHNSTON, I.H. and BILSTON, L.E., 1998. Effects of proteins, blood cells and glucose on the viscosity of cerebrospinal fluid. *Pediatric Neurosurgery*, May, vol. 28, no. 5, pp. 246-251 ISSN 1016-2291; 1016-2291. DOI pne28246 [pii].

21. BOMSTEIN, Y., MARDER, J.B., VITNER, K., SMIRNOV, I., LISAEY, G., BUTOVSKY, O., FULGA, V. and YOLES, E., 2003. Features of skin-coincubated macrophages that promote recovery from spinal cord injury. *Journal of Neuroimmunology*, Sep, vol. 142, no. 1-2, pp. 10-16 ISSN 0165-5728; 0165-5728. DOI S0165572803002601 [pii].

22. BONNEFONT-ROUSSELOT, D., COLLIN, F., JORE, D. and GARDES-ALBERT, M., 2011. Reaction mechanism of melatonin oxidation by reactive oxygen species in vitro. *Journal of Pineal Research*, 20110118, Apr, vol. 50, no. 3, pp. 328-335 ISSN 1600-079X; 0742-3098. DOI 10.1111/j.1600-079X.2010.00847.x [doi].

23. BOOIJ, J.C., BAAS, D.C., BEISEKEEVA, J., GORGELS, T.G. and BERGEN, A.A., 2010. The dynamic nature of Bruch's membrane. *Progress in Retinal and Eye Research*, 20090910, Jan, vol. 29, no. 1, pp. 1-18 ISSN 1873-1635; 1350-9462. DOI 10.1016/j.preteyeres.2009.08.003 [doi].

24. BOOMKAMP, S.D., RIEHLE, M.O., WOOD, J., OLSON, M.F. and BARNETT, S.C., 2012. The development of a rat in vitro model of spinal cord injury demonstrating the additive effects of Rho and ROCK inhibitors on neurite outgrowth and myelination. *Glia*, 20111202, Mar, vol. 60, no. 3, pp. 441-456 ISSN 1098-1136; 0894-1491. DOI 10.1002/glia.22278 [doi].

25. BORISOFF, J.F., CHAN, C.C., HIEBERT, G.W., OSCHIPOK, L., ROBERTSON, G.S., ZAMBONI, R., STEEVES, J.D. and TETZLAFF, W., 2003. Suppression of Rho-kinase activity promotes axonal growth on inhibitory CNS substrates. *Molecular and Cellular Neurosciences*, Mar, vol. 22, no. 3, pp. 405-416 ISSN 1044-7431; 1044-7431. DOI S1044743102000325 [pii].

26. BRACKEN, M.B., SHEPARD, M.J., COLLINS, W.F.,Jr, HOLFORD, T.R., BASKIN, D.S., EISENBERG, H.M., FLAMM, E., LEO-SUMMERS, L., MAROON, J.C. and MARSHALL, L.F., 1992. Methylprednisolone or naloxone treatment after acute spinal cord injury: 1-year follow-up data. Results of the second National Acute Spinal Cord Injury Study. *Journal of Neurosurgery*, Jan, vol. 76, no. 1, pp. 23-31 ISSN 0022-3085; 0022-3085. DOI 10.3171/jns.1992.76.1.0023 [doi].

27. BRADBURY, E.J., KHEMANI, S., VON, R., King, PRIESTLEY, J.V. and MCMAHON, S.B., 1999. NT-3 promotes growth of lesioned adult rat sensory axons ascending in the dorsal columns of the spinal cord. *The European Journal of Neuroscience*, Nov, vol. 11, no. 11, pp. 3873-3883 ISSN 0953-816X; 0953-816X. DOI ejn809 [pii].

28. BRADBURY, E.J., MOON, L.D., POPAT, R.J., KING, V.R., BENNETT, G.S., PATEL, P.N., FAWCETT, J.W. and MCMAHON, S.B., 2002. Chondroitinase ABC promotes functional recovery after spinal cord injury. *Nature*, Apr 11, vol. 416, no. 6881, pp. 636-640 ISSN 0028-0836; 0028-0836. DOI 10.1038/416636a [doi].

29. BRADL, M. and LASSMANN, H., 2010. Oligodendrocytes: biology and pathology. *Acta Neuropathologica*, 20091022, Jan, vol. 119, no. 1, pp. 37-53 ISSN 1432-0533; 0001-6322. DOI 10.1007/s00401-009-0601-5 [doi].

30. BRENNER, M., 2014. Role of GFAP in CNS injuries. *Neuroscience Letters*, 20140206, Apr 17, vol. 565, pp. 7-13 ISSN 1872-7972; 0304-3940. DOI 10.1016/j.neulet.2014.01.055 [doi].

31. BRUSTLE, O., JONES, K.N., LEARISH, R.D., KARRAM, K., CHOUDHARY, K., WIESTLER, O.D., DUNCAN, I.D. and MCKAY, R.D., 1999. Embryonic stem cell-derived glial precursors: a source of myelinating transplants. *Science (New York, N.Y.)*, Jul 30, vol. 285, no. 5428, pp. 754-756 ISSN 0036-8075; 0036-8075. DOI 7707 [pii].

32. BUIRA, S.P., ALBASANZ, J.L., DENTESANO, G., MORENO, J., MARTIN, M., FERRER, I. and BARRACHINA, M., 2010. DNA methylation regulates adenosine A(2A) receptor cell surface expression levels. *Journal of Neurochemistry*, 20091210, Mar, vol. 112, no. 5, pp. 1273-1285 ISSN 1471-4159; 0022-3042. DOI 10.1111/j.1471-4159.2009.06538.x [doi].

33. BUNGE, R.P., PUCKETT, W.R., BECERRA, J.L., MARCILLO, A. and QUENCER, R.M., 1993. Observations on the pathology of human spinal cord injury. A review and classification of 22 new cases with details from a case of chronic cord compression with extensive focal demyelination. *Advances in Neurology*, vol. 59, pp. 75-89 ISSN 0091-3952; 0091-3952.

34. BURNS, A.S., MARINO, R.J., KALSI-RYAN, S., MIDDLETON, J.W., TETREAULT, L.A., DETTORI, J.R., MIHALOVICH, K.E. and FEHLINGS, M.G., 2017. Type and Timing of Rehabilitation Following Acute and Subacute Spinal Cord Injury: A Systematic Review. *Global Spine Journal*, 20170905, Sep, vol. 7, no. 3 Suppl, pp. 175S-194S ISSN 2192-5682; 2192-5682. DOI 10.1177/2192568217703084 [doi].

35. CADDY, K.W. and HERRUP, K., 1991. The fine structure of the Purkinje cell and its afferents in lurcher chimeric mice. *The Journal of Comparative Neurology*, Mar 15, vol. 305, no. 3, pp. 421-434 ISSN 0021-9967; 0021-9967. DOI 10.1002/cne.903050306 [doi].

36. CAI, Y., LI, J., ZHANG, Z., CHEN, J., ZHU, Y., LI, R., CHEN, J., GAO, L., LIU, R. and TENG, Y., 2017. Zbtb38 is a novel target for spinal cord injury. *Oncotarget*, Jul 11, vol. 8, no. 28, pp. 45356-45366 ISSN 1949-2553; 1949-2553. DOI 10.18632/oncotarget.17487 [doi].

37. CAPLAN, A.I., 2007. Adult mesenchymal stem cells for tissue engineering versus regenerative medicine. *Journal of Cellular Physiology*, Nov, vol. 213, no. 2, pp. 341-347 ISSN 0021-9541; 0021-9541. DOI 10.1002/jcp.21200 [doi].

38. CAPOGROSSO, M., MILEKOVIC, T., BORTON, D., WAGNER, F., MORAUD, E.M., MIGNARDOT, J.B., BUSE, N., GANDAR, J., BARRAUD, Q., XING, D., REY, E., DUIS, S., JIANZHONG, Y., KO, W.K., LI, Q., DETEMPLE, P., DENISON, T., MICERA, S., BEZARD, E., BLOCH, J. and COURTINE, G., 2016. A brain-spine interface alleviating gait deficits after spinal cord injury in primates. *Nature*, Nov 10, vol. 539, no. 7628, pp. 284-288 ISSN 1476-4687; 0028-0836. DOI 10.1038/nature20118 [doi].

39. CARLSON, G.D. and GORDEN, C., 2002. Current developments in spinal cord injury research. *The Spine Journal : Official Journal of the North American Spine Society*, Mar-Apr, vol. 2, no. 2, pp. 116-128 ISSN 1529-9430; 1529-9430. DOI S1529943001000298 [pii].

40. CHAN, S.L. and MATTSON, M.P., 1999. Caspase and calpain substrates: roles in synaptic plasticity and cell death. *Journal of Neuroscience Research*, Oct 1, vol. 58, no. 1, pp. 167-190 ISSN 0360-4012; 0360-4012. DOI 10.1002/(SICI)1097-4547(19991001)58:13.0.CO;2-K [pii].

41. CHEN, A., XU, X.M., KLEITMAN, N. and BUNGE, M.B., 1996. Methylprednisolone administration improves axonal regeneration into Schwann cell grafts in transected adult rat thoracic spinal cord. *Experimental Neurology*, Apr, vol. 138, no. 2, pp. 261-276 ISSN 0014-4886; 0014-4886. DOI S0014-4886(96)90065-5 [pii].

42. CHEN, B.K., KNIGHT, A.M., MADIGAN, N.N., GROSS, L., DADSETAN, M., NESBITT, J.J., ROONEY, G.E., CURRIER, B.L., YASZEMSKI, M.J., SPINNER, R.J. and WINDEBANK, A.J., 2011. Comparison of polymer scaffolds in rat spinal cord: a step toward quantitative assessment of combinatorial approaches to spinal cord repair. *Biomaterials*, 20110730, Nov, vol. 32, no. 32, pp. 8077-8086 ISSN 1878-5905; 0142-9612. DOI 10.1016/j.biomaterials.2011.07.029 [doi].

43. CHEN, Y., TANG, Y., VOGEL, L.C. and DEVIVO, M.J., 2013. Causes of spinal cord injury. *Topics in Spinal Cord Injury Rehabilitation*, Winter, vol. 19, no. 1, pp. 1-8 ISSN 1082-0744; 1082-0744. DOI 10.1310/sci1901-1 [doi].

44. CHENG, H., CAO, Y. and OLSON, L., 1996. Spinal cord repair in adult paraplegic rats: partial restoration of hind limb function. *Science (New York, N.Y.)*, Jul 26, vol. 273, no. 5274, pp. 510-513 ISSN 0036-8075; 0036-8075.

45. CHENG, H., HUANG, Y.C., CHANG, P.T. and HUANG, Y.Y., 2007. Laminin-incorporated nerve conduits made by plasma treatment for repairing spinal cord injury. *Biochemical and Biophysical Research Communications*, 20070418, Jun 15, vol. 357, no. 4, pp. 938-944 ISSN 0006-291X; 0006-291X. DOI S0006-291X(07)00747-4 [pii].

46. CHERIYAN, T., RYAN, D.J., WEINREB, J.H., CHERIYAN, J., PAUL, J.C., LAFAGE, V., KIRSCH, T. and ERRICO, T.J., 2014. Spinal cord injury models: a review. *Spinal Cord*, 20140610, Aug, vol. 52, no. 8, pp. 588-595 ISSN 1476-5624; 1362-4393. DOI 10.1038/sc.2014.91 [doi].

47. CHEW, S.Y., MI, R., HOKE, A. and LEONG, K.W., 2007. Aligned Protein-Polymer Composite Fibers Enhance Nerve Regeneration: A Potential Tissue-Engineering Platform. *Advanced Functional Materials*, vol. 17, no. 8, pp. 1288-1296 ISSN 1616-301X; 1616-301X. DOI 10.1002/adfm.200600441 [doi].

48. CHEW, S.Y., WEN, Y., DZENIS, Y. and LEONG, K.W., 2006. The role of electrospinning in the emerging field of nanomedicine. *Current Pharmaceutical Design*, vol. 12, no. 36, pp. 4751-4770 ISSN 1873-4286; 1381-6128.

49. CHINNOCK, P. and ROBERTS, I., 2005. Gangliosides for acute spinal cord injury. *The Cochrane Database of Systematic Reviews*, 20050418, Apr 18, vol. (2):CD004444. doi, no. 2, pp. CD004444 ISSN 1469-493X; 1361-6137. DOI 10.1002/14651858.CD004444.pub2 [doi].

50. CHOI, D.W. and ROTHMAN, S.M., 1990. The role of glutamate neurotoxicity in hypoxic-ischemic neuronal death. *Annual Review of Neuroscience*, vol. 13, pp. 171-182 ISSN 0147-006X; 0147-006X. DOI 10.1146/annurev.ne.13.030190.001131 [doi].

51. CHROBAK, K.M., POTTER, D.R. and TIEN, J., 2006. Formation of perfused, functional microvascular tubes in vitro. *Microvascular Research*, May, vol. 71, no. 3, pp. 185-196 ISSN 0026-2862; 0026-2862. DOI S0026-2862(06)00021-5 [pii].

52. CHUNG, K. and COGGESHALL, R.E., 1983. Numbers of axons in lateral and ventral funiculi of rat sacral spinal cord. *The Journal of Comparative Neurology*, Feb 10, vol. 214, no. 1, pp. 72-78 ISSN 0021-9967; 0021-9967. DOI 10.1002/cne.902140107 [doi].

53. CHVATAL, S.A., KIM, Y.T., BRATT-LEAL, A.M., LEE, H. and BELLAMKONDA, R.V., 2008. Spatial distribution and acute anti-inflammatory effects of Methylprednisolone after sustained local delivery to the contused spinal cord. *Biomaterials*, 20080205, Apr, vol. 29, no. 12, pp. 1967-1975 ISSN 0142-9612; 0142-9612. DOI 10.1016/j.biomaterials.2008.01.002 [doi].

54. COLEMAN, W.P., BENZEL, D., CAHILL, D.W., DUCKER, T., GEISLER, F., GREEN, B., GROPPER, M.R., GOFFIN, J., MADSEN, P.W.,3rd, MAIMAN, D.J., ONDRA, S.L., ROSNER, M., SASSO, R.C., TROST, G.R. and ZEIDMAN, S., 2000. A critical appraisal of the reporting of the National Acute Spinal Cord Injury Studies (II and III) of methylprednisolone in acute spinal cord injury. *Journal of Spinal Disorders*, Jun, vol. 13, no. 3, pp. 185-199 ISSN 0895-0385; 0895-0385.

55. CUELLO, A.C., STEPHENS, P.H., TAGARI, P.C., SOFRONIEW, M.V. and PEARSON, R.C., 1986. Retrograde changes in the nucleus basalis of the rat, caused by cortical damage, are prevented by exogenous ganglioside GM1. *Brain Research*, Jun 25, vol. 376, no. 2, pp. 373-377 ISSN 0006-8993; 0006-8993. DOI 0006-8993(86)90202-7 [pii].

56. CURTIS, E., MARTIN, J.R., GABEL, B., SIDHU, N., RZESIEWICZ, T.K., MANDEVILLE, R., VAN GORP, S., LEERINK, M., TADOKORO, T., MARSALA, S., JAMIESON, C., MARSALA, M. and CIACCI, J.D., 2018. A First-in-Human, Phase I Study of Neural Stem Cell Transplantation for Chronic Spinal Cord Injury. *Cell Stem Cell*, Jun 1, vol. 22, no. 6, pp. 941-950.e6 ISSN 1875-9777; 1875-9777. DOI S1934-5909(18)30232-7 [pii].

57. DA FONSECA, A.C., MATIAS, D., GARCIA, C., AMARAL, R., GERALDO, L.H., FREITAS, C. and LIMA, F.R., 2014. The impact of microglial activation on blood-brain barrier in brain diseases. *Frontiers in Cellular Neuroscience*, 20141103, Nov 3, vol. 8, pp. 362 ISSN 1662-5102; 1662-5102. DOI 10.3389/fncel.2014.00362 [doi].

58. DAFNY, N., 2000. **Chapter 3: Anatomy of the Spinal Cord**. In: McGovern Medical School, The University of Texas ed., *Neuroscience Online* Online: McGovern Medical School.

59. DAS, A., BANIK, N.L. and RAY, S.K., 2008. Retinoids induced astrocytic differentiation with down regulation of telomerase activity and enhanced sensitivity to taxol for apoptosis in human glioblastoma T98G and U87MG cells. *Journal of Neuro-Oncology*, 20071107, Mar, vol. 87, no. 1, pp. 9-22 ISSN 0167-594X; 0167-594X. DOI 10.1007/s11060-007-9485-1 [doi].

60. DAVIES, S.J., GOUCHER, D.R., DOLLER, C. and SILVER, J., 1999. Robust regeneration of adult sensory axons in degenerating white matter of the adult rat spinal cord. *The Journal of Neuroscience : The Official Journal of the Society for Neuroscience*, Jul 15, vol. 19, no. 14, pp. 5810-5822 ISSN 1529-2401; 0270-6474.

61. DEDA, H., INCI, M.C., KUREKCI, A.E., KAYIHAN, K., OZGUN, E., USTUNSOY, G.E. and KOCABAY, S., 2008. Treatment of chronic spinal cord injured patients with autologous bone marrow-derived hematopoietic stem cell transplantation: 1-year follow-up. *Cytotherapy*, vol. 10, no. 6, pp. 565-574 ISSN 1477-2566; 1465-3249. DOI 10.1080/14653240802241797 [doi].

62. DELLO RUSSO, C., CAPPOLI, N., COLETTA, I., MEZZOGORI, D., PACIELLO, F., POZZOLI, G., NAVARRA, P. and BATTAGLIA, A., 2018. The human microglial HMC3 cell line: where do we stand? A systematic literature review. *Journal of Neuroinflammation*, 20180910, Sep 10, vol. 15, no. 1, pp. 259-018-1288-0 ISSN 1742-2094; 1742-2094. DOI 10.1186/s12974-018-1288-0 [doi].

63. DENG, Y., JIANG, C., LI, C., LI, T., PENG, M., WANG, J. and DAI, K., 2017. 3D printed scaffolds of calcium silicate-doped beta-TCP synergize with co-cultured endothelial and stromal cells to promote vascularization and bone formation. *Scientific Reports*, 20170717, Jul 17, vol. 7, no. 1, pp. 5588-017-05196-1 ISSN 2045-2322; 2045-2322. DOI 10.1038/s41598-017-05196-1 [doi].

64. DING, Y., KASTIN, A.J. and PAN, W., 2005. Neural plasticity after spinal cord injury. *Current Pharmaceutical Design*, vol. 11, no. 11, pp. 1441-1450 ISSN 1381-6128; 1381-6128.

65. DODZIUK, H., 2016. Applications of 3D printing in healthcare. *Kardiochirurgia i Torakochirurgia Polska = Polish Journal of Cardio-Thoracic Surgery*, 20160930, Sep, vol. 13, no. 3, pp. 283-293 ISSN 1731-5530; 1731-5530. DOI 10.5114/kitp.2016.62625 [doi].

66. DUBREUIL, C.I., WINTON, M.J. and MCKERRACHER, L., 2003. Rho activation patterns after spinal cord injury and the role of activated Rho in apoptosis in the central nervous system. *The Journal of Cell Biology*, 20030714, Jul 21, vol. 162, no. 2, pp. 233-243 ISSN 0021-9525; 0021-9525. DOI 10.1083/jcb.200301080 [doi].

67. ELLIOTT DONAGHUE, I., TATOR, C.H. and SHOICHET, M.S., 2016. Local Delivery of Neurotrophin-3 and Anti-NogoA Promotes Repair After Spinal Cord Injury. *Tissue Engineering.Part A*, 20160505, May, vol. 22, no. 9-10, pp. 733-741 ISSN 1937-335X; 1937-3341. DOI 10.1089/ten.TEA.2015.0471 [doi].

68. ENCINAS, M., IGLESIAS, M., LIU, Y., WANG, H., MUHAISEN, A., CENA, V., GALLEGO, C. and COMELLA, J.X., 2000. Sequential treatment of SH-SY5Y cells with retinoic acid and brain-derived neurotrophic factor gives rise to fully differentiated, neurotrophic factor-

dependent, human neuron-like cells. *Journal of Neurochemistry*, Sep, vol. 75, no. 3, pp. 991-1003 ISSN 0022-3042; 0022-3042.

69. EVANIEW, N. and DVORAK, M., 2016. Cochrane in CORR1: Steroids for Acute Spinal Cord Injury (Review). *Clinical Orthopaedics and Related Research*, Jan, vol. 474, no. 1, pp. 19-24 ISSN 1528-1132; 0009-921X. DOI 10.1007/s11999-015-4601-6 [doi].

70. FAN, D., AKKARAJU, G.R., COUCH, E.F., CANHAM, L.T. and COFFER, J.L., 2011. The role of nanostructured mesoporous silicon in discriminating in vitro calcification for electrospun composite tissue engineering scaffolds. *Nanoscale*, 20101125, Feb, vol. 3, no. 2, pp. 354-361 ISSN 2040-3372; 2040-3364. DOI 10.1039/c0nr00550a [doi].

71. FEHLINGS, M.G., TATOR, C.H. and LINDEN, R.D., 1989. The effect of nimodipine and dextran on axonal function and blood flow following experimental spinal cord injury. *Journal of Neurosurgery*, Sep, vol. 71, no. 3, pp. 403-416 ISSN 0022-3085; 0022-3085. DOI 10.3171/jns.1989.71.3.0403 [doi].

72. FEHLINGS, M.G., VACCARO, A., WILSON, J.R., SINGH, A., W CADOTTE, D., HARROP, J.S., AARABI, B., SHAFFREY, C., DVORAK, M., FISHER, C., ARNOLD, P., MASSICOTTE, E.M., LEWIS, S. and RAMPERSAUD, R., 2012. Early versus delayed decompression for traumatic cervical spinal cord injury: results of the Surgical Timing in Acute Spinal Cord Injury Study (STASCIS). *PloS One*, 20120223, vol. 7, no. 2, pp. e32037 ISSN 1932-6203; 1932-6203. DOI 10.1371/journal.pone.0032037 [doi].

73. FIELDS, R.D., 2008. White matter in learning, cognition and psychiatric disorders. *Trends in Neurosciences*, 20080605, Jul, vol. 31, no. 7, pp. 361-370 ISSN 0166-2236; 0166-2236. DOI 10.1016/j.tins.2008.04.001 [doi].

74. FUHRMANN, T., TAM, R.Y., BALLARIN, B., COLES, B., ELLIOTT DONAGHUE, I., VAN DER KOOY, D., NAGY, A., TATOR, C.H., MORSHEAD, C.M. and SHOICHET, M.S., 2016. Injectable hydrogel promotes early survival of induced pluripotent stem cell-derived oligodendrocytes and attenuates longterm teratoma formation in a spinal cord injury model. *Biomaterials*, 20160101, Mar, vol. 83, pp. 23-36 ISSN 1878-5905; 0142-9612. DOI 10.1016/j.biomaterials.2015.12.032 [doi].

75. FUJIMOTO, J.G., PITRIS, C., BOPPART, S.A. and BREZINSKI, M.E., 2000. Optical coherence tomography: an emerging technology for biomedical imaging and optical biopsy. *Neoplasia (New York, N.Y.)*, Jan-Apr, vol. 2, no. 1-2, pp. 9-25 ISSN 1522-8002; 1476-5586.

76. GARG, K. and BOWLIN, G.L., 2011. Electrospinning jets and nanofibrous structures. *Biomicrofluidics*, 20110330, Mar 30, vol. 5, no. 1, pp. 13403 ISSN 1932-1058; 1932-1058. DOI 10.1063/1.3567097 [doi].

77. GAVIRIA, M., PRIVAT, A., D'ARBIGNY, P., KAMENKA, J., HATON, H. and OHANNA, F., 2000. Neuroprotective effects of a novel NMDA antagonist, Gacyclidine, after experimental contusive spinal cord injury in adult rats. *Brain Research*, Aug 25, vol. 874, no. 2, pp. 200-209 ISSN 0006-8993; 0006-8993. DOI S0006899300025816 [pii].

78. GIOVANINI, M.A., REIER, P.J., ESKIN, T.A., WIRTH, E. and ANDERSON, D.K., 1997. Characteristics of human fetal spinal cord grafts in the adult rat spinal cord: influences of lesion and grafting conditions. *Experimental Neurology*, Dec, vol. 148, no. 2, pp. 523-543 ISSN 0014-4886; 0014-4886. DOI S0014-4886(97)96703-0 [pii].

79. GOMES, F.C., PAULIN, D. and MOURA NETO, V., 1999. Glial fibrillary acidic protein (GFAP): modulation by growth factors and its implication in astrocyte differentiation. *Brazilian Journal of Medical and Biological Research = Revista Brasileira De Pesquisas Medicas E Biologicas*, May, vol. 32, no. 5, pp. 619-631 ISSN 0100-879X; 0100-879X.

80. GONZENBACH, R.R. and SCHWAB, M.E., 2008. Disinhibition of neurite growth to repair the injured adult CNS: focusing on Nogo. *Cellular and Molecular Life Sciences : CMLS*, Jan, vol. 65, no. 1, pp. 161-176 ISSN 1420-682X; 1420-682X. DOI 10.1007/s00018-007-7170-3 [doi].

81. GRAY, C.W. and PATEL, A.J., 1992. Characterization of a neurotrophic factor produced by cultured astrocytes involved in the regulation of subcortical cholinergic neurons. *Brain Research*, Mar 6, vol. 574, no. 1-2, pp. 257-265 ISSN 0006-8993; 0006-8993. DOI 0006-8993(92)90825-T [pii].

82. GRODECKI, J., SHORT, A.R., WINTER, J.O., RAO, S.S., WINTER, J.O., OTERO, J.J., LANNUTTI, J.J. and SARKAR, A., 2015. Glioma-astrocyte interactions on white matter tract-mimetic aligned electrospun nanofibers. *Biotechnology Progress*, 20150626, Sep-Oct, vol. 31, no. 5, pp. 1406-1415 ISSN 1520-6033; 1520-6033. DOI 10.1002/btpr.2123 [doi].

83. HALL, E.D. and BRAUGHLER, J.M., 1993. Free radicals in CNS injury. *Research Publications - Association for Research in Nervous and Mental Disease*, vol. 71, pp. 81-105 ISSN 0091-7443; 0091-7443.

84. HANNA-MITCHELL, A.T., O'LEARY, D., MOBARAK, M.S., RAMER, M.S., MCMAHON, S.B., PRIESTLEY, J.V., KOZLOVA, E.N., ALDSKOGIUS, H., DOCKERY, P. and FRAHER, J.P., 2008. The impact of neurotrophin-3 on the dorsal root transitional zone following injury. *Spinal Cord*, 20080610, Dec, vol. 46, no. 12, pp. 804-810 ISSN 1362-4393; 1362-4393. DOI 10.1038/sc.2008.57 [doi].

85. HANSEBOUT, C.R., SU, C., REDDY, K., ZHANG, D., JIANG, C., RATHBONE, M.P. and JIANG, S., 2012. Enteric glia mediate neuronal outgrowth through release of neurotrophic factors. *Neural Regeneration Research*, Oct 5, vol. 7, no. 28, pp. 2165-2175 ISSN 1673-5374; 1673-5374. DOI 10.3969/j.issn.1673-5374.2012.028.001 [doi].

86. HUARD, J.M., YOUNGENTOB, S.L., GOLDSTEIN, B.J., LUSKIN, M.B. and SCHWOB, J.E., 1998. Adult olfactory epithelium contains multipotent progenitors that give rise to neurons and non-neural cells. *The Journal of Comparative Neurology*, Nov 2, vol. 400, no. 4, pp. 469-486 ISSN 0021-9967; 0021-9967. DOI 10.1002/(SICI)1096-9861(19981102)400:43.0.CO;2-8 [pii].

87. HUFF, T. and VARACALLO, M., 2018. Neuroanatomy, Cerebrospinal Fluid. In: *StatPearls* Treasure Island (FL): StatPearls Publishing LLC,Jan DOI NBK470578 [bookaccession].

88. HUNTSMAN, C., 2019. *JEFFAMINE® ED-2003 Polyetheramine.* Huntsman. Available from: http://www.huntsman.com/performance_products/Media%20Library/a_MC348531CFA3EA9A2E040EBCD2B6B7B06/Products_MC348531D0B9FA9A2E040EBCD2B6B7B06/Amines_MC348531D0BECA9A2E040EBCD2B6B7B06/Polyetheramines%20%20%20JE_MC348531D0E07A9A2E040EBCD2B6B7B06/Diamine%20products_MC348531D0EA1A9A2E040EBCD2B6B7B06/files/jeffamine_ed_2003_us_2_08.pdf.

89. IFKOVITS, J.L., SUNDARARAGHAVAN, H.G. and BURDICK, J.A., 2009. Electrospinning fibrous polymer scaffolds for tissue engineering and cell culture. *Journal of Visualized Experiments : JoVE*, 20091021, Oct 21, vol. (32). pii: 1589. doi, no. 32, pp. 10.3791/1589 ISSN 1940-087X; 1940-087X. DOI 10.3791/1589 [doi].

90. IN VIVO, T., 2019. ***Science of SCI: Pathophysiology of Chronic SCI.*** In Vivo Therapeutics. Available from: http://www.invivotherapeutics.com/research-clinical-development/science-of-sci/pathophysiology-of-chronic-sci/.

91. INNALA, M., RIEBE, I., KUZMENKO, V., SUNDBERG, J., GATENHOLM, P., HANSE, E. and JOHANNESSON, S., 2014. 3D culturing and differentiation of SH-SY5Y neuroblastoma cells on bacterial nanocellulose scaffolds. *Artificial Cells, Nanomedicine, and Biotechnology*, 20130729, Oct, vol. 42, no. 5, pp. 302-308 ISSN 2169-141X; 2169-1401. DOI 10.3109/21691401.2013.821410 [doi].

92. JAHANI, H., KAVIANI, S., HASSANPOUR-EZATTI, M., SOLEIMANI, M., KAVIANI, Z. and ZONOUBI, Z., 2012. The effect of aligned and random electrospun fibrous scaffolds on rat mesenchymal stem cell proliferation. *Cell Journal*, 20120613, Spring, vol. 14, no. 1, pp. 31-38 ISSN 2228-5806; 2228-5806.

93. JAIN, A., BETANCUR, M., PATEL, G.D., VALMIKINATHAN, C.M., MUKHATYAR, V.J., VAKHARIA, A., PAI, S.B., BRAHMA, B., MACDONALD, T.J. and BELLAMKONDA, R.V., 2014. Guiding intracortical brain tumour cells to an extracortical cytotoxic hydrogel using aligned polymeric nanofibres. *Nature Materials*, 20140216, Mar, vol. 13, no. 3, pp. 308-316 ISSN 1476-1122; 1476-1122. DOI 10.1038/nmat3878 [doi].

94. JAMMALAMADAKA, U. and TAPPA, K., 2018. Recent Advances in Biomaterials for 3D Printing and Tissue Engineering. *Journal of Functional Biomaterials*, 20180301, Mar 1, vol. 9, no. 1, pp. 10.3390/jfb9010022 ISSN 2079-4983; 2079-4983. DOI E22 [pii].

95. JANKOWSKA, E., 2001. Spinal interneuronal systems: identification, multifunctional character and reconfigurations in mammals. *The Journal of Physiology*, May 15, vol. 533, no. Pt 1, pp. 31-40 ISSN 0022-3751; 0022-3751. DOI PHY_11989 [pii].

96. JI, W., ZHANG, X., JI, L., WANG, K. and QIU, Y., 2015. Effects of brainderived neurotrophic factor and neurotrophin3 on the neuronal differentiation of rat adiposederived stem cells. *Molecular Medicine Reports*, 20150720, Oct, vol. 12, no. 4, pp. 4981-4988 ISSN 1791-3004; 1791-2997. DOI 10.3892/mmr.2015.4099 [doi].

97. JONES, L.L., OUDEGA, M., BUNGE, M.B. and TUSZYNSKI, M.H., 2001. Neurotrophic factors, cellular bridges and gene therapy for spinal cord injury. *The Journal of Physiology*, May 15, vol. 533, no. Pt 1, pp. 83-89 ISSN 0022-3751; 0022-3751. DOI PHY_11990 [pii].

98. JOOSTEN, E.A. and GRIBNAU, A.A., 1989. Astrocytes and guidance of outgrowing corticospinal tract axons in the rat. An immunocytochemical study using anti-vimentin and anti-glial fibrillary acidic protein. *Neuroscience*, vol. 31, no. 2, pp. 439-452 ISSN 0306-4522; 0306-4522. DOI 0306-4522(89)90386-2 [pii].

99. JU, G., WANG, J., WANG, Y. and ZHAO, X., 2014. Spinal cord contusion. *Neural Regeneration Research*, Apr 15, vol. 9, no. 8, pp. 789-794 ISSN 1673-5374; 1673-5374. DOI 10.4103/1673-5374.131591 [doi].

100. KADOYA, K., LU, P., NGUYEN, K., LEE-KUBLI, C., KUMAMARU, H., YAO, L., KNACKERT, J., POPLAWSKI, G., DULIN, J.N., STROBL, H., TAKASHIMA, Y., BIANE, J., CONNER, J., ZHANG, S.C. and TUSZYNSKI, M.H., 2016. Spinal cord reconstitution with homologous neural grafts enables robust corticospinal regeneration. *Nature Medicine*, 20160328, May, vol. 22, no. 5, pp. 479-487 ISSN 1546-170X; 1078-8956. DOI 10.1038/nm.4066 [doi].

101. KARMAKAR, S., BANIK, N.L. and RAY, S.K., 2008. Combination of all-trans retinoic acid and paclitaxel-induced differentiation and apoptosis in human glioblastoma U87MG xenografts in nude mice. *Cancer*, Feb 1, vol. 112, no. 3, pp. 596-607 ISSN 0008-543X; 0008-543X. DOI 10.1002/cncr.23223 [doi].

102. Kenhub., 2019. ***Ascending and Descending Tracts of the Spinal Cord***. KenHub. Available from: https://www.kenhub.com/en/library/anatomy/ascending-and-descending-tracts-of-the-spinal-cord.

103. KHAN, F.A., ALMOHAZEY, D., ALOMARI, M. and ALMOFTY, S.A., 2018. Impact of nanoparticles on neuron biology: current research trends. *International Journal of Nanomedicine*, 20180509, May 9, vol. 13, pp. 2767-2776 ISSN 1178-2013; 1176-9114. DOI 10.2147/IJN.S165675 [doi].

104. KHAZAEI, M., AHUJA, C.S. and FEHLINGS, M.G., 2017. Induced Pluripotent Stem Cells for Traumatic Spinal Cord Injury. *Frontiers in Cell and Developmental Biology*, 20170119, Jan 19, vol. 4, pp. 152 ISSN 2296-634X; 2296-634X. DOI 10.3389/fcell.2016.00152 [doi].

105. KHWANRAJ, K., PHRUKSANIYOM, C., MADLAH, S. and DHARMASAROJA, P., 2015. Differential Expression of Tyrosine Hydroxylase Protein and Apoptosis-Related Genes in Differentiated and Undifferentiated SH-SY5Y Neuroblastoma Cells Treated with MPP(.). *Neurology Research International*, 20151108, vol. 2015, pp. 734703 ISSN 2090-1852; 2090-1860. DOI 10.1155/2015/734703 [doi].

106. KIDOAKI, S., KWON, I.K. and MATSUDA, T., 2005. Mesoscopic spatial designs of nano- and microfiber meshes for tissue-engineering matrix and scaffold based on newly devised multilayering and mixing electrospinning techniques. *Biomaterials*, Jan, vol. 26, no. 1, pp. 37-46 ISSN 0142-9612; 0142-9612. DOI 10.1016/j.biomaterials.2004.01.063 [doi].

107. KIJANSKA, M. and KELM, J., 2004. In vitro 3D Spheroids and Microtissues: ATP-based Cell Viability and Toxicity Assays. In: G.S. SITTAMPALAM, N.P. COUSSENS, K. BRIMACOMBE, A. GROSSMAN, M. ARKIN, D. AULD, C. AUSTIN, J. BAELL, B. BEJCEK, J.M.M. CAAVEIRO, T.D.Y. CHUNG, J.L. DAHLIN, V. DEVANARYAN, T.L. FOLEY, M. GLICKSMAN, M.D. HALL, J.V. HAAS, J. INGLESE, P.W. IVERSEN, S.D. KAHL, S.C. KALES, M. LAL-NAG, Z. LI, J. MCGEE, O. MCMANUS, T. RISS, J. TRASK OJ, J.R. WEIDNER, M.J. WILDEY, M. XIA and X. XU eds., *Assay Guidance Manual* Bethesda (MD): DOI NBK343426 [bookaccession].

108. KIM, J.I., HWANG, T.I., AGUILAR, L.E., PARK, C.H. and KIM, C.S., 2016. A Controlled Design of Aligned and Random Nanofibers for 3D Bi-functionalized Nerve Conduits Fabricated via a Novel Electrospinning Set-up. *Scientific Reports*, 20160329, Mar 29, vol. 6, pp. 23761 ISSN 2045-2322; 2045-2322. DOI 10.1038/srep23761 [doi].

109. KOBRINE, A.I., DOYLE, T.F. and MARTINS, A.N., 1975. Autoregulation of spinal cord blood flow. *Clinical Neurosurgery*, vol. 22, pp. 573-581 ISSN 0069-4827; 0069-4827.

110. KOFFLER, J., ZHU, W., QU, X., PLATOSHYN, O., DULIN, J.N., BROCK, J., GRAHAM, L., LU, P., SAKAMOTO, J., MARSALA, M., CHEN, S. and TUSZYNSKI, M.H., 2019. Biomimetic 3D-printed scaffolds for spinal cord injury repair. *Nature Medicine*, 20190114, Feb, vol. 25, no. 2, pp. 263-269 ISSN 1546-170X; 1078-8956. DOI 10.1038/s41591-018-0296-z [doi].

111. KOVALEVICH, J. and LANGFORD, D., 2013. Considerations for the use of SH-SY5Y neuroblastoma cells in neurobiology. *Methods in Molecular Biology (Clifton, N.J.)*, vol. 1078, pp. 9-21 ISSN 1940-6029; 1064-3745. DOI 10.1007/978-1-62703-640-5_2 [doi].

112. KREUTER, J., RAMGE, P., PETROV, V., HAMM, S., GELPERINA, S.E., ENGELHARDT, B., ALYAUTDIN, R., VON BRIESEN, H. and BEGLEY, D.J., 2003. Direct evidence that polysorbate-80-coated poly(butylcyanoacrylate) nanoparticles deliver drugs to the CNS via specific mechanisms requiring prior binding of drug to the nanoparticles. *Pharmaceutical Research*, Mar, vol. 20, no. 3, pp. 409-416 ISSN 0724-8741; 0724-8741.

113. KUMAR, A.A., KUMAR, S.R., NARAYANAN, R., ARUL, K. and BASKARAN, M., 2009. Autologous bone marrow derived mononuclear cell therapy for spinal cord injury: A phase I/II clinical safety and primary efficacy data. *Experimental and Clinical Transplantation : Official Journal of the Middle East Society for Organ Transplantation*, Dec, vol. 7, no. 4, pp. 241-248 ISSN 2146-8427; 1304-0855.

114. KURAKHMAEVA, K.B., DJINDJIKHASHVILI, I.A., PETROV, V.E., BALABANYAN, V.U., VORONINA, T.A., TROFIMOV, S.S., KREUTER, J., GELPERINA, S., BEGLEY, D. and ALYAUTDIN, R.N., 2009. Brain targeting of nerve growth factor using poly(butyl cyanoacrylate) nanoparticles. *Journal of Drug Targeting*, Sep, vol. 17, no. 8, pp. 564-574 ISSN 1029-2330; 1026-7158. DOI 10.1080/10611860903112842 [doi].

115. KWON, B.K., OXLAND, T.R. and TETZLAFF, W., 2002. Animal models used in spinal cord regeneration research. *Spine*, Jul 15, vol. 27, no. 14, pp. 1504-1510 ISSN 1528-1159; 0362-2436. DOI 00007632-200207150-00005 [pii].

116. LANNES, N., EPPLER, E., ETEMAD, S., YOTOVSKI, P. and FILGUEIRA, L., 2017. Microglia at center stage: a comprehensive review about the versatile and unique residential macrophages of the central nervous system. *Oncotarget*, 20171211, Dec 11, vol. 8, no. 69, pp. 114393-114413 ISSN 1949-2553; 1949-2553. DOI 10.18632/oncotarget.23106 [doi].

117. LEDEEN, R.W., 1978. Ganglioside structures and distribution: are they localized at the nerve ending?. *Journal of Supramolecular Structure*, vol. 8, no. 1, pp. 1-17 ISSN 0091-7419; 0091-7419. DOI 10.1002/jss.400080102 [doi].

118. LEE, H., MCKEON, R.J. and BELLAMKONDA, R.V., 2010. Sustained delivery of thermostabilized chABC enhances axonal sprouting and functional recovery after spinal cord injury. *Proceedings of the National Academy of Sciences of the United States of America*, 20091102, Feb 23, vol. 107, no. 8, pp. 3340-3345 ISSN 1091-6490; 0027-8424. DOI 10.1073/pnas.0905437106 [doi].

119. LEE, J.Y., CHOI, S.Y., OH, T.H. and YUNE, T.Y., 2012. 17beta-Estradiol inhibits apoptotic cell death of oligodendrocytes by inhibiting RhoA-JNK3 activation after spinal cord injury. *Endocrinology*, 20120614, Aug, vol. 153, no. 8, pp. 3815-3827 ISSN 1945-7170; 0013-7227. DOI 10.1210/en.2012-1068 [doi].

120. LEE, Y., SU, M., MESSING, A. and BRENNER, M., 2006. Astrocyte heterogeneity revealed by expression of a GFAP-LacZ transgene. *Glia*, May, vol. 53, no. 7, pp. 677-687 ISSN 0894-1491; 0894-1491. DOI 10.1002/glia.20320 [doi].

121. LENTING, K., VERHAAK, R., TER LAAN, M., WESSELING, P. and LEENDERS, W., 2017. Glioma: experimental models and reality. *Acta Neuropathologica*, 20170110, Feb, vol. 133, no. 2, pp. 263-282 ISSN 1432-0533; 0001-6322. DOI 10.1007/s00401-017-1671-4 [doi].

122. LI, D., OUYANG, G., MCCANN, J.T. and XIA, Y., 2005. Collecting electrospun nanofibers with patterned electrodes. *Nano Letters*, May, vol. 5, no. 5, pp. 913-916 ISSN 1530-6984; 1530-6984. DOI 10.1021/nl0504235 [doi].

123. LI, H., ZHU, C., XUE, J., KE, Q. and XIA, Y., 2017. Enhancing the Mechanical Properties of Electrospun Nanofiber Mats through Controllable Welding at the Cross Points. *Macromolecular Rapid Communications*, 20170310, May, vol. 38, no. 9, pp. 10.1002/marc.201600723. Epub 2017 Mar 10 ISSN 1521-3927; 1022-1336. DOI 10.1002/marc.201600723 [doi].

124. LI, J., ZHANG, L., CHU, Y., NAMAKA, M., DENG, B., KONG, J. and BI, X., 2016. Astrocytes in Oligodendrocyte Lineage Development and White Matter Pathology. *Frontiers in Cellular Neuroscience*, 20160510, May 10, vol. 10, pp. 119 ISSN 1662-5102; 1662-5102. DOI 10.3389/fncel.2016.00119 [doi].

125. LI, Y., FIELD, P.M. and RAISMAN, G., 1998. Regeneration of adult rat corticospinal axons induced by transplanted olfactory ensheathing cells. *The Journal of Neuroscience : The Official Journal of the Society for Neuroscience*, Dec 15, vol. 18, no. 24, pp. 10514-10524 ISSN 0270-6474; 0270-6474.

126. LIANG, C., YANG, L. and GUO, S., 2015. All-trans retinoic acid inhibits migration, invasion and proliferation, and promotes apoptosis in glioma cells in vitro. *Oncology Letters*, 20150415, Jun, vol. 9, no. 6, pp. 2833-2838 ISSN 1792-1074; 1792-1074. DOI 10.3892/ol.2015.3120 [doi].

127. LIM, F. and SUN, A.M., 1980. Microencapsulated islets as bioartificial endocrine pancreas. *Science (New York, N.Y.)*, Nov 21, vol. 210, no. 4472, pp. 908-910 ISSN 0036-8075; 0036-8075.

128. LIMA, D. and COIMBRA, A., 1986. A Golgi study of the neuronal population of the marginal zone (lamina I) of the rat spinal cord. *The Journal of Comparative Neurology*, Feb 1, vol. 244, no. 1, pp. 53-71 ISSN 0021-9967; 0021-9967. DOI 10.1002/cne.902440105 [doi].

129. LIU, R., WANG, Z., GOU, L. and XU, H., 2015. A cortical astrocyte subpopulation inhibits axon growth in vitro and in vivo. *Molecular Medicine Reports*, 20150429, Aug, vol. 12, no. 2, pp. 2598-2606 ISSN 1791-3004; 1791-2997. DOI 10.3892/mmr.2015.3702 [doi].

130. LOANE, D.J. and KUMAR, A., 2016. Microglia in the TBI brain: The good, the bad, and the dysregulated. *Experimental Neurology*, 20150903, Jan, vol. 275 Pt 3, pp. 316-327 ISSN 1090-2430; 0014-4886. DOI S0014-4886(15)30079-0 [pii].

131. LOMAS, A.J., WEBB, W.R., HAN, J., CHEN, G.Q., SUN, X., ZHANG, Z., EL HAJ, A.J. and FORSYTH, N.R., 2013. Poly (3-hydroxybutyrate-co-3-hydroxyhexanoate)/collagen hybrid scaffolds for tissue engineering applications. *Tissue Engineering.Part C, Methods*, 20130214, Aug, vol. 19, no. 8, pp. 577-585 ISSN 1937-3392; 1937-3384. DOI 10.1089/ten.TEC.2012.0457 [doi].

132. LOPES, F.M., SCHRODER, R., DA FROTA, M.L.,Jr, ZANOTTO-FILHO, A., MULLER, C.B., PIRES, A.S., MEURER, R.T., COLPO, G.D., GELAIN, D.P., KAPCZINSKI, F., MOREIRA, J.C., FERNANDES MDA, C. and KLAMT, F., 2010. Comparison between proliferative and neuron-like SH-SY5Y cells as an in vitro model for Parkinson disease studies. *Brain Research*, 20100407, Jun 14, vol. 1337, pp. 85-94 ISSN 1872-6240; 0006-8993. DOI 10.1016/j.brainres.2010.03.102 [doi].

133. LOSEY, P. and ANTHONY, D.C., 2014. Impact of vasculature damage on the outcome of spinal cord injury: a novel collagenase-induced model may give new insights into the mechanisms involved. *Neural Regeneration Research*, Oct 15, vol. 9, no. 20, pp. 1783-1786 ISSN 1673-5374; 1673-5374. DOI 10.4103/1673-5374.143422 [doi].

134. LU, D., GAO, Y., LUO, C., LU, S., WANG, Q., XU, X., SUN, S., WANG, C. and LONG, M., 2015. Selectivity of biopolymer membranes using HepG2 cells. *Regenerative Biomaterials*, 20150209, Mar, vol. 2, no. 1, pp. 21-29 ISSN 2056-3418; 2056-3426. DOI 10.1093/rb/rbu018 [doi].

135. LUDER RIPOLI, F., BUETTNER, M. and BLEICH, A., 2019. Alternative methods to replace or reduce animal models in biomedical research. *Altex*, vol. 36, no. 1, pp. 141-142 ISSN 1868-596X; 1868-596X. DOI 10.14573/altex.1812171 [doi].

136. MALLETT, A.G. and KORBUTT, G.S., 2009. Alginate modification improves long-term survival and function of transplanted encapsulated islets. *Tissue Engineering.Part A*, Jun, vol. 15, no. 6, pp. 1301-1309 ISSN 1937-335X; 1937-3341. DOI 10.1089/ten.tea.2008.0118 [doi].

137. MASSA, H., NAGAR, A.M., VERGADOS, A., DADOUKIS, P., PATRA, S. and PANOS, G.D., 2019. Intravitreal fluocinolone acetonide implant (ILUVIEN(R)) for diabetic macular oedema: a literature review. *The Journal of International Medical Research*, 20181216, Jan, vol. 47, no. 1, pp. 31-43 ISSN 1473-2300; 0300-0605. DOI 10.1177/0300060518816884 [doi].

138. MATTHEWS, J.A., WNEK, G.E., SIMPSON, D.G. and BOWLIN, G.L., 2002. Electrospinning of collagen nanofibers. *Biomacromolecules*, Mar-Apr, vol. 3, no. 2, pp. 232-238 ISSN 1525-7797; 1525-7797. DOI bm015533u [pii].

139. MCCLELLAN, P. and LANDIS, W.J., 2016. Recent Applications of Coaxial and Emulsion Electrospinning Methods in the Field of Tissue Engineering. *BioResearch Open Access*, 20160801, Aug 1, vol. 5, no. 1, pp. 212-227 ISSN 2164-7844; 2164-7844. DOI 10.1089/biores.2016.0022 [doi].

140. MCDONALD, J.W., 1999. Repairing the damaged spinal cord. *Scientific American*, Sep, vol. 281, no. 3, pp. 64-73 ISSN 0036-8733; 0036-8733.

141. MCDONALD, J.W., LIU, X.Z., QU, Y., LIU, S., MICKEY, S.K., TURETSKY, D., GOTTLIEB, D.I. and CHOI, D.W., 1999. Transplanted embryonic stem cells survive, differentiate and promote recovery in injured rat spinal cord. *Nature Medicine*, Dec, vol. 5, no. 12, pp. 1410-1412 ISSN 1078-8956; 1078-8956. DOI 10.1038/70986 [doi].

142. MCMURTREY, R.J., 2014. Patterned and functionalized nanofiber scaffolds in three-dimensional hydrogel constructs enhance neurite outgrowth and directional control. *Journal of Neural Engineering*, 20141031, Dec, vol. 11, no. 6, pp. 066009-2560/11/6/066009. Epub 2014 Oct 31 ISSN 1741-2552; 1741-2552. DOI 10.1088/1741-2560/11/6/066009 [doi].

143. MIEKISIAK, G., LATKA, D., JARMUZEK, P., ZALUSKI, R., URBANSKI, W. and JANUSZ, W., 2019. Steroids in Acute Spinal Cord Injury: All But Gone Within 5 Years. *World Neurosurgery*, 20181024, Feb, vol. 122, pp. e467-e471 ISSN 1878-8769; 1878-8750. DOI S1878-8750(18)32379-9 [pii].

144. MITA, R., COLES, J.E., GLUBRECHT, D.D., SUNG, R., SUN, X. and GODBOUT, R., 2007. B-FABP-expressing radial glial cells: the malignant glioma cell of origin?. *Neoplasia (New York, N.Y.)*, Sep, vol. 9, no. 9, pp. 734-744 ISSN 1476-5586; 1476-5586.

145. MONGA, V., MEENA, C.L., KAUR, N. and JAIN, R., 2008. Chemistry and biology of thyrotropin-releasing hormone (TRH) and its analogs. *Current Medicinal Chemistry*, vol. 15, no. 26, pp. 2718-2733 ISSN 0929-8673; 0929-8673.

146. MOSKOWITZ, P.F., SMITH, R., PICKETT, J., FRANKFURTER, A. and OBLINGER, M.M., 1993. Expression of the class III beta-tubulin gene during axonal regeneration of rat dorsal root ganglion neurons. *Journal of Neuroscience Research*, Jan, vol. 34, no. 1, pp. 129-134 ISSN 0360-4012; 0360-4012. DOI 10.1002/jnr.490340113 [doi].

147. MURILLO, J.R., GOTO-SILVA, L., SANCHEZ, A., NOGUEIRA, F.C.S., DOMONT, G.B. and JUNQUEIRA, M., 2017. Quantitative proteomic analysis identifies proteins and pathways related to neuronal development in differentiated SH-SY5Y neuroblastoma cells. *EuPA Open Proteomics*, 20170623, Jun 23, vol. 16, pp. 1-11 ISSN 2212-9685; 2212-9685. DOI 10.1016/j.euprot.2017.06.001 [doi].

148. MYERS, T.A., NICKERSON, C.A., KAUSHAL, D., OTT, C.M., HONER ZU BENTRUP, K., RAMAMURTHY, R., NELMAN-GONZALEZ, M., PIERSON, D.L. and PHILIPP, M.T., 2008. Closing the phenotypic gap between transformed neuronal cell lines in culture and untransformed neurons. *Journal of Neuroscience Methods*, 20080710, Sep 15, vol. 174, no. 1, pp. 31-41 ISSN 0165-0270; 0165-0270. DOI 10.1016/j.jneumeth.2008.06.031 [doi].

149. NAS, K., YAZMALAR, L., SAH, V., AYDIN, A. and ONES, K., 2015. Rehabilitation of spinal cord injuries. *World Journal of Orthopedics*, 20150118, Jan 18, vol. 6, no. 1, pp. 8-16 ISSN 2218-5836; 2218-5836. DOI 10.5312/wjo.v6.i1.8 [doi].

150. NGUYEN, L.H., GAO, M., LIN, J., WU, W., WANG, J. and CHEW, S.Y., 2017. Three-dimensional aligned nanofibers-hydrogel scaffold for controlled non-viral drug/gene delivery to direct axon regeneration in spinal cord injury treatment. *Scientific Reports*, 20170207, Feb 7, vol. 7, pp. 42212 ISSN 2045-2322; 2045-2322. DOI 10.1038/srep42212 [doi].

151. NÓGRÁDI, A. and VRBOVÁ, G., 2000. Anatomy and Physiology of the Spinal Cord. In: *Madame Curie Bioscience* Austin: Landes Bioscience DOI 2000.

152. ORR, S.B., CHAINANI, A., HIPPENSTEEL, K.J., KISHAN, A., GILCHRIST, C., GARRIGUES, N.W., RUCH, D.S., GUILAK, F. and LITTLE, D., 2015. Aligned multilayered electrospun scaffolds for rotator cuff tendon tissue engineering. *Acta Biomaterialia*, 20150614, Sep, vol. 24, pp. 117-126 ISSN 1878-7568; 1742-7061. DOI 10.1016/j.actbio.2015.06.010 [doi].

153. OUDEGA, M. and HAGG, T., 1996. Nerve growth factor promotes regeneration of sensory axons into adult rat spinal cord. *Experimental Neurology*, Aug, vol. 140, no. 2, pp. 218-229 ISSN 0014-4886; 0014-4886. DOI S0014-4886(96)90131-4 [pii].

154. PARK, J., LIM, E., BACK, S., NA, H., PARK, Y. and SUN, K., 2010. Nerve regeneration following spinal cord injury using matrix metalloproteinase-sensitive, hyaluronic acid-based biomimetic hydrogel scaffold containing brain-derived neurotrophic factor. *Journal of Biomedical Materials Research.Part A*, Jun 1, vol. 93, no. 3, pp. 1091-1099 ISSN 1552-4965; 1549-3296. DOI 10.1002/jbm.a.32519 [doi].

155. PASPALA, S.A., MURTHY, T.V., MAHABOOB, V.S. and HABEEB, M.A., 2011. Pluripotent stem cells - a review of the current status in neural regeneration. *Neurology India*, Jul-Aug, vol. 59, no. 4, pp. 558-565 ISSN 0028-3886; 0028-3886. DOI 10.4103/0028-3886.84338 [doi].

156. PERALE, G., GIORDANO, C., BIANCO, F., ROSSI, F., TUNESI, M., DANIELE, F., CRIVELLI, F., MATTEOLI, M. and MASI, M., 2011. Hydrogel for cell housing in the brain and in the spinal cord. *The International Journal of Artificial Organs*, Mar, vol. 34, no. 3, pp. 295-303 ISSN 1724-6040; 0391-3988. DOI 5ABCED5A-E53E-4103-9359-BCFD0AD02925 [pii].

157. PERALE, G., ROSSI, F., SUNDSTROM, E., BACCHIEGA, S., MASI, M., FORLONI, G. and VEGLIANESE, P., 2011. Hydrogels in spinal cord injury repair strategies. *ACS Chemical Neuroscience*, 20110504, Jul 20, vol. 2, no. 7, pp. 336-345 ISSN 1948-7193; 1948-7193. DOI 10.1021/cn200030w [doi].

158. PIRES, L.R. and PEGO, A.P., 2015. Bridging the lesion-engineering a permissive substrate for nerve regeneration. *Regenerative Biomaterials*, 20150810, Sep, vol. 2, no. 3, pp. 203-214 ISSN 2056-3418; 2056-3426. DOI 10.1093/rb/rbv012 [doi].

159. PONTEN, J. and MACINTYRE, E.H., 1968. Long term culture of normal and neoplastic human glia. *Acta Pathologica Et Microbiologica Scandinavica*, vol. 74, no. 4, pp. 465-486 ISSN 0365-5555; 0365-5555.

160. PRESGRAVES, S.P., AHMED, T., BORWEGE, S. and JOYCE, J.N., 2004. Terminally differentiated SH-SY5Y cells provide a model system for studying neuroprotective effects of dopamine agonists. *Neurotoxicity Research*, vol. 5, no. 8, pp. 579-598 ISSN 1029-8428; 1029-8428.

161. PRITCHARD, C.D., SLOTKIN, J.R., YU, D., DAI, H., LAWRENCE, M.S., BRONSON, R.T., REYNOLDS, F.M., TENG, Y.D., WOODARD, E.J. and LANGER, R.S., 2010. Establishing a model spinal cord injury in the African green monkey for the preclinical evaluation of biodegradable polymer scaffolds seeded with human neural stem cells. *Journal of Neuroscience Methods*, 20100226, May 15, vol. 188, no. 2, pp. 258-269 ISSN 1872-678X; 0165-0270. DOI 10.1016/j.jneumeth.2010.02.019 [doi].

162. PRITCHARD, E.M. and KAPLAN, D.L., 2011. Silk fibroin biomaterials for controlled release drug delivery. *Expert Opinion on Drug Delivery*, 20110401, Jun, vol. 8, no. 6, pp. 797-811 ISSN 1744-7593; 1742-5247. DOI 10.1517/17425247.2011.568936 [doi].

163. PURVES, D., AUGUSTINE, G. and FITZPATRICK, D., 2001. **Motor Neuron-Muscle Relationships**. In: Sunderland (MA) and Sinauer Associates eds., ***Neuroscience. 2nd edition***2nd ed.Sinauer Associates.

164. PUSKAR, Z., POLGAR, E. and TODD, A.J., 2001. A population of large lamina I projection neurons with selective inhibitory input in rat spinal cord. *Neuroscience*, vol. 102, no. 1, pp. 167-176 ISSN 0306-4522; 0306-4522. DOI S0306-4522(00)00445-0 [pii].

165. QIU, B., SUN, X., ZHANG, D., WANG, Y., TAO, J. and OU, S., 2012. TRAIL and paclitaxel synergize to kill U87 cells and U87-derived stem-like cells in vitro. *International Journal of Molecular Sciences*, 20120720, vol. 13, no. 7, pp. 9142-9156 ISSN 1422-0067; 1422-0067. DOI 10.3390/ijms13079142 [doi].

166. RALSTON, H.J.,3rd, 1982. The fine structure of laminae IV, V, and VI of the Macaque spinal cord. *The Journal of Comparative Neurology*, Dec 20, vol. 212, no. 4, pp. 425-434 ISSN 0021-9967; 0021-9967. DOI 10.1002/cne.902120409 [doi].

167. RAY, S.K., SAMANTARAY, S., SMITH, J.A., MATZELLE, D.D., DAS, A. and BANIK, N.L., 2011. Inhibition of cysteine proteases in acute and chronic spinal cord injury.

Neurotherapeutics : The Journal of the American Society for Experimental NeuroTherapeutics, Apr, vol. 8, no. 2, pp. 180-186 ISSN 1878-7479; 1878-7479. DOI 10.1007/s13311-011-0037-1 [doi].

168. RENE HUDSON, B., COOK, C. and GOODE, A., 2008. Identifying myelopathy caused by thoracic syringomyelia: a case report. *The Journal of Manual & Manipulative Therapy*, vol. 16, no. 2, pp. 82-88 ISSN 1066-9817; 1066-9817. DOI 10.1179/106698108790818512 [doi].

169. RESTREPO, A., SMITH, C.A., AGNIHOTRI, S., SHEKARFOROUSH, M., KONGKHAM, P.N., SEOL, H.J., NORTHCOTT, P. and RUTKA, J.T., 2011. Epigenetic regulation of glial fibrillary acidic protein by DNA methylation in human malignant gliomas. *Neuro-Oncology*, 20101112, Jan, vol. 13, no. 1, pp. 42-50 ISSN 1523-5866; 1522-8517. DOI 10.1093/neuonc/noq145 [doi].

170. RIANJANU, A., ROTO, R., JULIAN, T., HIDAYAT, S.N., KUSUMAATMAJA, A., SUYONO, E.A. and TRIYANA, K., 2018. Polyacrylonitrile Nanofiber-Based Quartz Crystal Microbalance for Sensitive Detection of Safrole. *Sensors (Basel, Switzerland)*, 20180410, Apr 10, vol. 18, no. 4, pp. 10.3390/s18041150 ISSN 1424-8220; 1424-8220. DOI E1150 [pii].

171. ROCHE, R. and YALCINKAYA, F., 2019. Electrospun Polyacrylonitrile Nanofibrous Membranes for Point-of-Use Water and Air Cleaning. *ChemistryOpen*, 20190124, Jan 24, vol. 8, no. 1, pp. 97-103 ISSN 2191-1363; 2191-1363. DOI 10.1002/open.201800267 [doi].

172. ROPPER, A.E., THAKOR, D.K., HAN, I., YU, D., ZENG, X., ANDERSON, J.E., ALJUBOORI, Z., KIM, S.W., WANG, H., SIDMAN, R.L., ZAFONTE, R.D. and TENG, Y.D., 2017. Defining recovery neurobiology of injured spinal cord by synthetic matrix-assisted hMSC implantation. *Proceedings of the National Academy of Sciences of the United States of America*, 20170117, Jan 31, vol. 114, no. 5, pp. E820-E829 ISSN 1091-6490; 0027-8424. DOI 10.1073/pnas.1616340114 [doi].

173. ROSS, R.A., SPENGLER, B.A. and BIEDLER, J.L., 1983. Coordinate morphological and biochemical interconversion of human neuroblastoma cells. *Journal of the National Cancer Institute*, Oct, vol. 71, no. 4, pp. 741-747 ISSN 0027-8874; 0027-8874.

174. ROWLAND, J.W., HAWRYLUK, G.W., KWON, B. and FEHLINGS, M.G., 2008. Current status of acute spinal cord injury pathophysiology and emerging therapies: promise on the horizon. *Neurosurgical Focus*, vol. 25, no. 5, pp. E2 ISSN 1092-0684; 1092-0684. DOI 10.3171/FOC.2008.25.11.E2 [doi].

175. SAEED, Y., REHMAN, A., XIE, B., XU, J., HONG, M., HONG, Q. and DENG, Y., 2015. Astroglial U87 Cells Protect Neuronal SH-SY5Y Cells from Indirect Effect of Radiation by Reducing DNA Damage and Inhibiting Fas Mediated Apoptotic Pathway in Coculture System. *Neurochemical Research*, 20150705, Aug, vol. 40, no. 8, pp. 1644-1654 ISSN 1573-6903; 0364-3190. DOI 10.1007/s11064-015-1642-x [doi].

176. SAFRONOV, B.V., WOLFF, M. and VOGEL, W., 2000. Excitability of the soma in central nervous system neurons. *Biophysical Journal*, Jun, vol. 78, no. 6, pp. 2998-3010 ISSN 0006-3495; 0006-3495. DOI S0006-3495(00)76838-X [pii].

177. SALTER, M.W. and BEGGS, S., 2014. Sublime microglia: expanding roles for the guardians of the CNS. *Cell*, Jul 3, vol. 158, no. 1, pp. 15-24 ISSN 1097-4172; 0092-8674. DOI 10.1016/j.cell.2014.06.008 [doi].

178. SAMANTARAY, S., SMITH, J.A., DAS, A., MATZELLE, D.D., VARMA, A.K., RAY, S.K. and BANIK, N.L., 2011. Low dose estrogen prevents neuronal degeneration and microglial reactivity in an acute model of spinal cord injury: effect of dosing, route of administration, and therapy delay. *Neurochemical Research*, 20110525, Oct, vol. 36, no. 10, pp. 1809-1816 ISSN 1573-6903; 0364-3190. DOI 10.1007/s11064-011-0498-y [doi].

179. SEMB, H., 2005. Human embryonic stem cells: origin, properties and applications. *APMIS : Acta Pathologica, Microbiologica, Et Immunologica Scandinavica*, Nov-Dec, vol. 113, no. 11-12, pp. 743-750 ISSN 0903-4641; 0903-4641. DOI APMapm_312 [pii].

180. SHARMA, H.S., 2008. New perspectives for the treatment options in spinal cord injury. *Expert Opinion on Pharmacotherapy*, Nov, vol. 9, no. 16, pp. 2773-2800 ISSN 1744-7666; 1465-6566. DOI 10.1517/14656566.9.16.2773 [doi].

181. SHI, Z., LOU, M., ZHAO, Y., ZHANG, Q., CUI, D. and WANG, K., 2013. Effect of all-trans retinoic acid on the differentiation of U87 glioma stem/progenitor cells. *Cellular and Molecular Neurobiology*, 20130713, Oct, vol. 33, no. 7, pp. 943-951 ISSN 1573-6830; 0272-4340. DOI 10.1007/s10571-013-9960-5 [doi].

182. SHIPLEY, M.M., MANGOLD, C.A., KUNY, C.V. and SZPARA, M.L., 2017. Differentiated Human SH-SY5Y Cells Provide a Reductionist Model of Herpes Simplex Virus 1 Neurotropism. *Journal of Virology*, 20171114, Nov 14, vol. 91, no. 23, pp. 10.1128/JVI.00958-17. Print 2017 Dec 1 ISSN 1098-5514; 0022-538X. DOI e00958-17 [pii].

183. SHIPLEY, M.M., MANGOLD, C.A. and SZPARA, M.L., 2016. Differentiation of the SH-SY5Y Human Neuroblastoma Cell Line. *Journal of Visualized Experiments : JoVE*, 20160217, Feb 17, vol. (108):53193. doi, no. 108, pp. 53193 ISSN 1940-087X; 1940-087X. DOI 10.3791/53193 [doi].

184. SILVA, N.A., SOUSA, N., REIS, R.L. and SALGADO, A.J., 2014. From basics to clinical: a comprehensive review on spinal cord injury. *Progress in Neurobiology*, 20131120, Mar, vol. 114, pp. 25-57 ISSN 1873-5118; 0301-0082. DOI 10.1016/j.pneurobio.2013.11.002 [doi].

185. SOFRONIEW, M.V. and VINTERS, H.V., 2010. Astrocytes: biology and pathology. *Acta Neuropathologica*, 20091210, Jan, vol. 119, no. 1, pp. 7-35 ISSN 1432-0533; 0001-6322. DOI 10.1007/s00401-009-0619-8 [doi].

186. SRNEC, R., DIVIN, R., SKORIC, M., SNASIL, R., KRBEC, M. and NECAS, A., 2018. Use of the Peptigel with Nanofibres in the Bone Defects Healing. *Acta Chirurgiae Orthopaedicae Et Traumatologiae Cechoslovaca*, vol. 85, no. 5, pp. 359-365 ISSN 0001-5415; 0001-5415.

187. STOKES, B.T., 1992. Experimental spinal cord injury: a dynamic and verifiable injury device. *Journal of Neurotrauma*, Summer, vol. 9, no. 2, pp. 129-31; discussion 131-4 ISSN 0897-7151; 0897-7151. DOI 10.1089/neu.1992.9.129 [doi].

188. STOKOLS, S., SAKAMOTO, J., BRECKON, C., HOLT, T., WEISS, J. and TUSZYNSKI, M.H., 2006. Templated agarose scaffolds support linear axonal regeneration. *Tissue Engineering*, Oct, vol. 12, no. 10, pp. 2777-2787 ISSN 1076-3279; 1076-3279. DOI 10.1089/ten.2006.12.2777 [doi].

189. SYKOVA, E., HOMOLA, A., MAZANEC, R., LACHMANN, H., KONRADOVA, S.L., KOBYLKA, P., PADR, R., NEUWIRTH, J., KOMRSKA, V., VAVRA, V., STULIK, J. and BOJAR, M., 2006. Autologous bone marrow transplantation in patients with subacute and chronic spinal cord injury. *Cell Transplantation*, vol. 15, no. 8-9, pp. 675-687 ISSN 0963-6897; 0963-6897.

190. SZUCS, P., ODEH, F., SZOKOL, K. and ANTAL, M., 2003. Neurons with distinctive firing patterns, morphology and distribution in laminae V-VII of the neonatal rat lumbar spinal cord. *The European Journal of Neuroscience*, Feb, vol. 17, no. 3, pp. 537-544 ISSN 0953-816X; 0953-816X. DOI 2484 [pii].

191. TABAKOW, P., JARMUNDOWICZ, W., CZAPIGA, B., FORTUNA, W., MIEDZYBRODZKI, R., CZYZ, M., HUBER, J., SZAREK, D., OKUROWSKI, S., SZEWCZYK, P., GORSKI, A. and RAISMAN, G., 2013. Transplantation of autologous olfactory ensheathing cells in complete human spinal cord injury. *Cell Transplantation*, vol. 22, no. 9, pp. 1591-1612 ISSN 1555-3892; 0963-6897. DOI 10.3727/096368912X663532 [doi].

192. TABATA, H., 2015. Diverse subtypes of astrocytes and their development during corticogenesis. *Frontiers in Neuroscience*, 20150407, Apr 7, vol. 9, pp. 114 ISSN 1662-4548; 1662-453X. DOI 10.3389/fnins.2015.00114 [doi].

193. TASCIOTTI, E., CABRERA, F.J., EVANGELOPOULOS, M., MARTINEZ, J.O., THEKKEDATH, U.R., KLOC, M., GHOBRIAL, R.M., LI, X.C., GRATTONI, A. and FERRARI, M., 2016. The Emerging Role of Nanotechnology in Cell and Organ Transplantation. *Transplantation*, Aug, vol. 100, no. 8, pp. 1629-1638 ISSN 1534-6080; 0041-1337. DOI 10.1097/TP.0000000000001100 [doi].

194. TEO, W.E., INAI, R. and RAMAKRISHNA, S., 2011. Technological advances in electrospinning of nanofibers. *Science and Technology of Advanced Materials*, 20110112, Jan 12, vol. 12, no. 1, pp. 013002 ISSN 1468-6996; 1468-6996. DOI 10.1088/1468-6996/12/1/013002 [doi].

195. TEO, W.E. and RAMAKRISHNA, S., 2006. A review on electrospinning design and nanofibre assemblies. *Nanotechnology*, 20060630, Jul 28, vol. 17, no. 14, pp. R89-R106 ISSN 1361-6528; 0957-4484. DOI 10.1088/0957-4484/17/14/R01 [doi].

196. TODD, A.J. and LEWIS, S.G., 1986. The morphology of Golgi-stained neurons in lamina II of the rat spinal cord. *Journal of Anatomy*, Dec, vol. 149, pp. 113-119 ISSN 0021-8782; 0021-8782.

197. TODD, A.J. and SPIKE, R.C., 1993. The localization of classical transmitters and neuropeptides within neurons in laminae I-III of the mammalian spinal dorsal horn. *Progress in Neurobiology*, Nov, vol. 41, no. 5, pp. 609-645 ISSN 0301-0082; 0301-0082. DOI 0301-0082(93)90045-T [pii].

198. TORCHILIN, V.P., 2000. Drug targeting. *European Journal of Pharmaceutical Sciences : Official Journal of the European Federation for Pharmaceutical Sciences*, Oct, vol. 11 Suppl 2, pp. S81-91 ISSN 0928-0987; 0928-0987. DOI S0928098700001664 [pii].

199. TOSETTI, P., TAGLIETTI, V. and TOSELLI, M., 1998. Functional changes in potassium conductances of the human neuroblastoma cell line SH-SY5Y during in vitro differentiation. *Journal of Neurophysiology*, Feb, vol. 79, no. 2, pp. 648-658 ISSN 0022-3077; 0022-3077. DOI 10.1152/jn.1998.79.2.648 [doi].

200. TOY, D. and NAMGUNG, U., 2013. Role of glial cells in axonal regeneration. *Experimental Neurobiology*, 20130627, Jun, vol. 22, no. 2, pp. 68-76 ISSN 1226-2560; 1226-2560. DOI 10.5607/en.2013.22.2.68 [doi].

201. TRAN, P.A. and WEBSTER, T.J., 2013. Understanding the wetting properties of nanostructured selenium coatings: the role of nanostructured surface roughness and air-pocket formation. *International Journal of Nanomedicine*, 20130520, vol. 8, pp. 2001-2009 ISSN 1178-2013; 1176-9114. DOI 10.2147/IJN.S42970 [doi].

202. TSUJI, O., MIURA, K., OKADA, Y., FUJIYOSHI, K., MUKAINO, M., NAGOSHI, N., KITAMURA, K., KUMAGAI, G., NISHINO, M., TOMISATO, S., HIGASHI, H., NAGAI, T., KATOH, H., KOHDA, K., MATSUZAKI, Y., YUZAKI, M., IKEDA, E., TOYAMA, Y., NAKAMURA, M., YAMANAKA, S. and OKANO, H., 2010. Therapeutic potential of appropriately evaluated safe-induced pluripotent stem cells for spinal cord injury. *Proceedings of the National Academy of Sciences of the United States of America*, 20100706, Jul 13, vol. 107, no. 28, pp. 12704-12709 ISSN 1091-6490; 0027-8424. DOI 10.1073/pnas.0910106107 [doi].

203. USHIKU, C., SUDA, K., MATSUMOTO, S., KOMATSU, M., TAKAHATA, M., IWASAKI, N. and MINAMI, A., 2017. Dural penetration caused by a vertebral bone fragment in a lumbar burst fracture: a case report. *Spinal Cord Series and Cases*, 20170112, Jan 12, vol. 3, pp. 16040 ISSN 2058-6124; 2058-6124. DOI 10.1038/scsandc.2016.40 [doi].

204. VALIZADEH, A. and MUSSA FARKHANI, S., 2014. Electrospinning and electrospun nanofibres. *IET Nanobiotechnology*, Jun, vol. 8, no. 2, pp. 83-92 ISSN 1751-8741; 1751-8741. DOI 10.1049/iet-nbt.2012.0040 [doi].

205. VARMA, A.K., DAS, A., WALLACE, G.,4th, BARRY, J., VERTEGEL, A.A., RAY, S.K. and BANIK, N.L., 2013. Spinal cord injury: a review of current therapy, future treatments, and basic science frontiers. *Neurochemical Research*, 20130306, May, vol. 38, no. 5, pp. 895-905 ISSN 1573-6903; 0364-3190. DOI 10.1007/s11064-013-0991-6 [doi].

206. VASILE, F., DOSSI, E. and ROUACH, N., 2017. Human astrocytes: structure and functions in the healthy brain. *Brain Structure & Function*, 20170309, Jul, vol. 222, no. 5, pp. 2017-2029 ISSN 1863-2661; 1863-2653. DOI 10.1007/s00429-017-1383-5 [doi].

207. VASITA, R. and KATTI, D.S., 2006. Nanofibers and their applications in tissue engineering. *International Journal of Nanomedicine*, vol. 1, no. 1, pp. 15-30 ISSN 1176-9114; 1176-9114.

208. VAWDA, R., WILCOX, J. and FEHLINGS, M., 2012. Current stem cell treatments for spinal cord injury. *Indian Journal of Orthopaedics*, Jan, vol. 46, no. 1, pp. 10-18 ISSN 1998-3727; 0019-5413. DOI 10.4103/0019-5413.91629 [doi].

209. VILLA, F., MARENGO, M. and DE CONINCK, J., 2018. A new model to predict the influence of surface temperature on contact angle. *Scientific Reports*, 20180425, Apr 25, vol. 8, no. 1, pp. 6549-018-24828-8 ISSN 2045-2322; 2045-2322. DOI 10.1038/s41598-018-24828-8 [doi].

210. VISMARA, I., PAPA, S., ROSSI, F., FORLONI, G. and VEGLIANESE, P., 2017. Current Options for Cell Therapy in Spinal Cord Injury. *Trends in Molecular Medicine*, 20170812, Sep, vol. 23, no. 9, pp. 831-849 ISSN 1471-499X; 1471-4914. DOI S1471-4914(17)30123-5 [pii].

211. VOGELAAR, C.F., 2016. Extrinsic and intrinsic mechanisms of axon regeneration: the need for spinal cord injury treatment strategies to address both. *Neural Regeneration Research*, Apr, vol. 11, no. 4, pp. 572-574 ISSN 1673-5374; 1673-5374. DOI 10.4103/1673-5374.180740 [doi].

212. WAKE, H. and FIELDS, R.D., 2011. Physiological function of microglia. *Neuron Glia Biology*, Feb, vol. 7, no. 1, pp. 1-3 ISSN 1741-0533; 1740-925X. DOI 10.1017/S1740925X12000166 [doi].

213. WALHOVD, K.B., JOHANSEN-BERG, H. and KARADOTTIR, R.T., 2014. Unraveling the secrets of white matter--bridging the gap between cellular, animal and human imaging studies. *Neuroscience*, 20140706, Sep 12, vol. 276, pp. 2-13 ISSN 1873-7544; 0306-4522. DOI 10.1016/j.neuroscience.2014.06.058 [doi].

214. WALL, J.T., XU, J. and WANG, X., 2002. Human brain plasticity: an emerging view of the multiple substrates and mechanisms that cause cortical changes and related sensory dysfunctions after injuries of sensory inputs from the body. *Brain Research.Brain Research Reviews*, Sep, vol. 39, no. 2-3, pp. 181-215 DOI S0165017302001923 [pii].

215. WANG, C.Y., ZHANG, K.H., FAN, C.Y., MO, X.M., RUAN, H.J. and LI, F.F., 2011. Aligned natural-synthetic polyblend nanofibers for peripheral nerve regeneration. *Acta Biomaterialia*, 20100916, Feb, vol. 7, no. 2, pp. 634-643 ISSN 1878-7568; 1742-7061. DOI 10.1016/j.actbio.2010.09.011 [doi].

216. WANG, F., NI, J., WANG, X., XIE, B., FENG, C., ZHAO, S., SAEED, Y., QING, H. and DENG, Y., 2015. Salsolinol Damaged Neuroblastoma SH-SY5Y Cells Induce Proliferation of Human Monocyte THP-1 Cells Through the mTOR Pathway in a Co-culture System. *Neurochemical Research*, 20150315, May, vol. 40, no. 5, pp. 932-941 ISSN 1573-6903; 0364-3190. DOI 10.1007/s11064-015-1547-8 [doi].

217. WANG, H., MA, J., TAN, Y., WANG, Z., SHENG, C., CHEN, S. and DING, J., 2010. Amyloid-beta1-42 induces reactive oxygen species-mediated autophagic cell death in U87 and SH-SY5Y cells. *Journal of Alzheimer's Disease : JAD*, vol. 21, no. 2, pp. 597-610 ISSN 1875-8908; 1387-2877. DOI 10.3233/JAD-2010-091207 [doi].

218. WANG, Y.F., FAN, Z.K., CAO, Y., YU, D.S., ZHANG, Y.Q. and WANG, Y.S., 2011. 2-Methoxyestradiol inhibits the up-regulation of AQP4 and AQP1 expression after spinal cord injury. *Brain Research*, 20101116, Jan 25, vol. 1370, pp. 220-226 ISSN 1872-6240; 0006-8993. DOI 10.1016/j.brainres.2010.11.016 [doi].

219. WEBB, A.A., NGAN, S. and FOWLER, J.D., 2010. Spinal cord injury I: A synopsis of the basic science. *The Canadian Veterinary Journal = La Revue Veterinaire Canadienne*, May, vol. 51, no. 5, pp. 485-492 ISSN 0008-5286; 0008-5286.

220. WEIGHTMAN, A.P., PICKARD, M.R., YANG, Y. and CHARI, D.M., 2014. An in vitro spinal cord injury model to screen neuroregenerative materials. *Biomaterials*, 20140129, Apr, vol. 35, no. 12, pp. 3756-3765 ISSN 1878-5905; 0142-9612. DOI 10.1016/j.biomaterials.2014.01.022 [doi].

221. WENGER, N., MORAUD, E.M., RASPOPOVIC, S., BONIZZATO, M., DIGIOVANNA, J., MUSIENKO, P., MORARI, M., MICERA, S. and COURTINE, G., 2014. Closed-loop neuromodulation of spinal sensorimotor circuits controls refined locomotion after complete spinal cord injury. *Science Translational Medicine*, Sep 24, vol. 6, no. 255, pp. 255ra133 ISSN 1946-6242; 1946-6234. DOI 10.1126/scitranslmed.3008325 [doi].

222. WHO., 2019. *Highest rate of Spinal Cord Injury Pie Chart.* Available from: ://www.who.int/mediacentre/factsheets/fs384/en/.

223. WIESE, S., KARUS, M. and FAISSNER, A., 2012. Astrocytes as a source for extracellular matrix molecules and cytokines. *Frontiers in Pharmacology*, 20120626, Jun 26, vol. 3, pp. 120 ISSN 1663-9812; 1663-9812. DOI 10.3389/fphar.2012.00120 [doi].

224. WILCOX, B., MOBBS, R.J., WU, A.M. and PHAN, K., 2017. Systematic review of 3D printing in spinal surgery: the current state of play. *Journal of Spine Surgery (Hong Kong)*, Sep, vol. 3, no. 3, pp. 433-443 ISSN 2414-469X; 2414-4630. DOI 10.21037/jss.2017.09.01 [doi].

225. WON, J.S., NAM, H., LEE, H.W., HWANG, J.Y., NOH, Y.J., NAM, D.H., LEE, S.H. and JOO, K.M., 2018. In vivo distribution of U87MG cells injected into the lateral ventricle of rats with spinal cord injury. *PloS One*, 20180816, Aug 16, vol. 13, no. 8, pp. e0202307 ISSN 1932-6203; 1932-6203. DOI 10.1371/journal.pone.0202307 [doi].

226. WU, J.C., HUANG, W.C., CHEN, Y.C., TU, T.H., TSAI, Y.A., HUANG, S.F., HUANG, H.C. and CHENG, H., 2011. Acidic fibroblast growth factor for repair of human spinal cord injury: a clinical trial. *Journal of Neurosurgery.Spine*, 20110610, Sep, vol. 15, no. 3, pp. 216-227 ISSN 1547-5646; 1547-5646. DOI 10.3171/2011.4.SPINE10404 [doi].

227. WU, U.I., MAI, F.D., SHEU, J.N., CHEN, L.Y., LIU, Y.T., HUANG, H.C. and CHANG, H.M., 2011. Melatonin inhibits microglial activation, reduces pro-inflammatory cytokine levels, and rescues hippocampal neurons of adult rats with acute Klebsiella pneumoniae meningitis. *Journal of Pineal Research*, 20101109, Mar, vol. 50, no. 2, pp. 159-170 ISSN 1600-079X; 0742-3098. DOI 10.1111/j.1600-079X.2010.00825.x [doi].

228. WU, Y., WANG, L., GUO, B. and MA, P.X., 2017. Interwoven Aligned Conductive Nanofiber Yarn/Hydrogel Composite Scaffolds for Engineered 3D Cardiac Anisotropy. *ACS Nano*, 20170607, Jun 27, vol. 11, no. 6, pp. 5646-5659 ISSN 1936-086X; 1936-0851. DOI 10.1021/acsnano.7b01062 [doi].

229. XICOY, H., WIERINGA, B. and MARTENS, G.J., 2017. The SH-SY5Y cell line in Parkinson's disease research: a systematic review. *Molecular Neurodegeneration*, 20170124, Jan 24, vol. 12, no. 1, pp. 10-017-0149-0 ISSN 1750-1326; 1750-1326. DOI 10.1186/s13024-017-0149-0 [doi].

230. XIE, J., MACEWAN, M.R., LI, X., SAKIYAMA-ELBERT, S.E. and XIA, Y., 2009. Neurite outgrowth on nanofiber scaffolds with different orders, structures, and surface properties. *ACS Nano*, May 26, vol. 3, no. 5, pp. 1151-1159 ISSN 1936-086X; 1936-0851. DOI 10.1021/nn900070z [doi].

231. XU, C.Y., INAI, R., KOTAKI, M. and RAMAKRISHNA, S., 2004. Aligned biodegradable nanofibrous structure: a potential scaffold for blood vessel engineering. *Biomaterials*, Feb, vol. 25, no. 5, pp. 877-886 ISSN 0142-9612; 0142-9612. DOI S0142961203005933 [pii].

232. XU, J., HUANG, G., ZHANG, K., SUN, J., XU, T., LI, R., TAO, H. and XU, W., 2014. Nrf2 activation in astrocytes contributes to spinal cord ischemic tolerance induced by hyperbaric oxygen preconditioning. *Journal of Neurotrauma*, 20140711, Aug 1, vol. 31, no. 15, pp. 1343-1353 ISSN 1557-9042; 0897-7151. DOI 10.1089/neu.2013.3222 [doi].

233. XU, X.M., GUENARD, V., KLEITMAN, N. and BUNGE, M.B., 1995. Axonal regeneration into Schwann cell-seeded guidance channels grafted into transected adult rat spinal cord. *The Journal of Comparative Neurology*, Jan 2, vol. 351, no. 1, pp. 145-160 ISSN 0021-9967; 0021-9967. DOI 10.1002/cne.903510113 [doi].

234. YANG, F., MURUGAN, R., WANG, S. and RAMAKRISHNA, S., 2005. Electrospinning of nano/micro scale poly(L-lactic acid) aligned fibers and their potential in neural tissue engineering. *Biomaterials*, May, vol. 26, no. 15, pp. 2603-2610 ISSN 0142-9612; 0142-9612. DOI S0142-9612(04)00856-7 [pii].

235. YANG, Z. and WANG, K.K., 2015. Glial fibrillary acidic protein: from intermediate filament assembly and gliosis to neurobiomarker. *Trends in Neurosciences*, 20150511, Jun, vol. 38, no. 6, pp. 364-374 ISSN 1878-108X; 0166-2236. DOI 10.1016/j.tins.2015.04.003 [doi].

236. YAO, R., MURTAZA, M., VELASQUEZ, J.T., TODOROVIC, M., RAYFIELD, A., EKBERG, J., BARTON, M. and ST JOHN, J., 2018. Olfactory Ensheathing Cells for Spinal Cord Injury: Sniffing Out the Issues. *Cell Transplantation*, 20180608, Jun, vol. 27, no. 6, pp. 879-889 ISSN 1555-3892; 0963-6897. DOI 10.1177/0963689718779353 [doi].

237. YIU, G. and HE, Z., 2006. Glial inhibition of CNS axon regeneration. *Nature Reviews.Neuroscience*, Aug, vol. 7, no. 8, pp. 617-627 ISSN 1471-003X; 1471-003X. DOI nrn1956 [pii].

238. YOU, S.W., CHEN, B.Y., LIU, H.L., LANG, B., XIA, J.L., JIAO, X.Y. and JU, G., 2003. Spontaneous recovery of locomotion induced by remaining fibers after spinal cord transection in adult rats. *Restorative Neurology and Neuroscience*, vol. 21, no. 1-2, pp. 39-45 ISSN 0922-6028; 0922-6028.

239. YU, L. and DING, J., 2008. Injectable hydrogels as unique biomedical materials. *Chemical Society Reviews*, 20080611, Aug, vol. 37, no. 8, pp. 1473-1481 ISSN 0306-0012; 0306-0012. DOI 10.1039/b713009k [doi].

240. YU, L., SHAO, Z., XU, L. and WANG, M., 2017. High Throughput Preparation of Aligned Nanofibers Using an Improved Bubble-Electrospinning. *Polymers*, 20171129, Nov 29, vol. 9, no. 12, pp. 10.3390/polym9120658 ISSN 2073-4360; 2073-4360. DOI E658 [pii].

241. YU, Y., MENG, D., MAN, L. and WANG, X., 2016. The Interactions Between Aligned Poly(L-Lactic Acid) Nanofibers and SH-SY5Y Cells In Vitro. *Journal of Nanoscience and Nanotechnology*, Jun, vol. 16, no. 6, pp. 6407-6413 ISSN 1533-4880; 1533-4880.

242. YUAN, Y.M. and HE, C., 2013. The glial scar in spinal cord injury and repair. *Neuroscience Bulletin*, 20130716, Aug, vol. 29, no. 4, pp. 421-435 ISSN 1995-8218; 1995-8218. DOI 10.1007/s12264-013-1358-3 [doi].

243. ZABLOCKA, A., MITKIEWICZ, M., MACALA, J. and JANUSZ, M., 2015. Neurotrophic Activity of Cultured Cell Line U87 is Up-Regulated by Proline-Rich Polypeptide Complex and Its Constituent Nonapeptide. *Cellular and Molecular Neurobiology*, 20150405, Oct, vol. 35, no. 7, pp. 977-986 ISSN 1573-6830; 0272-4340. DOI 10.1007/s10571-015-0192-8 [doi].

244. ZHANG, L., MA, Z., SMITH, G.M., WEN, X., PRESSMAN, Y., WOOD, P.M. and XU, X.M., 2009. GDNF-enhanced axonal regeneration and myelination following spinal cord injury is mediated by primary effects on neurons. *Glia*, Aug 15, vol. 57, no. 11, pp. 1178-1191 ISSN 1098-1136; 0894-1491. DOI 10.1002/glia.20840 [doi].

245. ZHANG, N., YIN, Y., XU, S.J., WU, Y.P. and CHEN, W.S., 2012. Inflammation & apoptosis in spinal cord injury. *The Indian Journal of Medical Research*, Mar, vol. 135, pp. 287-296 ISSN 0971-5916; 0971-5916. DOI IndianJMedRes_2012_135_3_287_95602 [pii].

246. ZHANG, W.Y., DE ALMEIDA, P.E. and WU, J.C., 2008. Teratoma formation: A tool for monitoring pluripotency in stem cell research. In: *StemBook* Cambridge (MA): Wendy Y. Zhang, Patricia E. de Almeida, and Joseph C. Wu DOI NBK133287 [bookaccession].

247. ZHANG, X., YANG, S., YU, B., TAN, Q., ZHANG, X. and CONG, H., 2018. Advanced Modified Polyacrylonitrile Membrane with Enhanced Adsorption Property for Heavy Metal Ions. *Scientific Reports*, 20180119, Jan 19, vol. 8, no. 1, pp. 1260-018-19597-3 ISSN 2045-2322; 2045-2322. DOI 10.1038/s41598-018-19597-3 [doi].

248. ZHAO, J., JIANG, W.J., SUN, C., HOU, C.Z., YANG, X.M. and GAO, J.G., 2013. Induced pluripotent stem cells: origins, applications, and future perspectives. *Journal of Zhejiang University.Science.B*, Dec, vol. 14, no. 12, pp. 1059-1069 ISSN 1862-1783; 1673-1581. DOI 10.1631/jzus.B1300215 [doi].

249. ZHENG, J., YAN, X., LI, M.M., YU, G.F., ZHANG, H.D., PISULA, W., HE, X.X., DUVAIL, J.L. and LONG, Y.Z., 2015. Electrospun Aligned Fibrous Arrays and Twisted Ropes: Fabrication, Mechanical and Electrical Properties, and Application in Strain Sensors. *Nanoscale Research Letters*, 20151209, Dec, vol. 10, no. 1, pp. 475-015-1184-9. Epub 2015 Dec 9 ISSN 1931-7573; 1556-276X. DOI 10.1186/s11671-015-1184-9 [doi].

250. ZORNER, B., BACHMANN, L.C., FILLI, L., KAPITZA, S., GULLO, M., BOLLIGER, M., STARKEY, M.L., ROTHLISBERGER, M., GONZENBACH, R.R. and SCHWAB, M.E., 2014. Chasing central nervous system plasticity: the brainstem's contribution to locomotor recovery in rats with spinal cord injury. *Brain : A Journal of Neurology*, 20140415, Jun, vol. 137, no. Pt 6, pp. 1716-1732 ISSN 1460-2156; 0006-8950. DOI 10.1093/brain/awu078 [doi].

251. ZORNER, B. and SCHWAB, M.E., 2010. Anti-Nogo on the go: from animal models to a clinical trial. *Annals of the New York Academy of Sciences*, Jun, vol. 1198 Suppl 1, pp. E22-34 ISSN 1749-6632; 0077-8923. DOI 10.1111/j.1749-6632.2010.05566.x [doi].

Acknowledgements

Director of Studies Professor Bob Stevens

Secondary Supervisor Dr. Luigi De Girolamo

Third Supervisor Dr. Alan Hargreaves

Prof. Daqing Li from UCL

Dr. Jorge Bernardino de la Serna from Didcot RAL

Mr Joseph Chemmarapally and Dr Michael Cripps for their friendship and support